ROLE OF SILICON CARBIDE ADDITIVES IN REDUCING DEWAXING TIME AND MOULD CRACK IN INVESTMENT CASTING USING MICROWAVE-ASSISTED HEATING

AHMED OMAR ASWAYE AMHAMED

UNIVERSITI TEKNOLOGI MALAYSIA

UNIVERSITI TEKNOLOGI MALAYSIA
DECLERATION OF THESIS

Author's full name	:	AHMED OMAR ASWAYE AMHAMED			
Student's Matric No.	:	PKM203029	Academic Session	:	2024/2025-2
Date of Birth	:	18 NOVEMBER 1982	UTM Email	:	ahmedaswaye@graduate.utm.my
Thesis Title	:	ROLE OF SILICON CARBIDE ADDITIVES IN REDUCING DEWAXING TIME AND MOULD CRACK IN INVESTMENT CASTING USING MICROWAVE-ASSISTED HEATING			

I declare that this thesis is classified as:

☒ **OPEN ACCESS** — I agree that my report to be published as a hard copy or made available through online open access.

☐ **RESTRICTED** — Contains restricted information as specified by the organization/institution where research was done.
(The library will block access for up to three (3) years)

☐ **CONFIDENTIAL** — Contains confidential information as specified in the Official Secret Act 1972)

(If none of the options are selected, the first option will be chosen by default)

I acknowledged the intellectual property in the thesis belongs to Universiti Teknologi Malaysia, and I agree to allow this to be placed in the library under the following terms :

1. This is the property of Universiti Teknologi Malaysia
2. The Library of Universiti Teknologi Malaysia has the right to make copies for the purpose of only.
3. The Library of Universiti Teknologi Malaysia is allowed to make copies of this thesis for academic exchange.

Signature of Student:

Signature : Ahmed

Full Name: AHMED OMAR ASWAYE AMHAMED
Date : 26 MAY 2025

Approved by Supervisor(s)

Signature of Supervisor I:	Signature of Supervisor II:
Full Name of Supervisor I WAN FAHMIN FAIZ WAN ALI	Full Name of Supervisor II IZMAN BIN SUDIN
Date : 26 MAY 2025	Date : 26 MAY 2025

NOTES : If the thesis is CONFIDENTIAL or RESTRICTED, please attach with the letter from the organization with period and reasons for confidentiality or restriction

"We hereby declare that we have read this thesis and in our opinion, this thesis is sufficient in terms of scope and quality for the award of the degree of Doctor of Philosophy in Mechanical Engineering"

Signature : _____

Name of Supervisor I : WAN FAHMIN FAIZ WAN ALI

Date : 26 MAY 2025

Signature : _____

Name of Supervisor II : IZMAN BIN SUDIN

Date : 26 MAY 2025

Signature : _____

Name of Supervisor III : NAJLAA' NAZIHAH BINTI MAS'OOD

Date : 26 MAY 2025

Pengesahan Peperiksaan

Tesis ini telah diperiksa dan diakui oleh:

Nama dan Alamat Pemeriksa Luar : Prof. Madya. Ir. Dr. Mohd Shukor bin Salleh
Fakulti Teknologi dan Kejuruteraan Industri dan Pembuatan
Universiti Teknikal Malaysia Melaka
76100 Durian Tunggal, Melaka

Nama dan Alamat Pemeriksa Dalam : Prof. Madya. Ir. Ts. Dr. Mohd Azlan Suhaimi
Fakulti Kejuruteraan Mekanikal
Universiti Teknologi Malaysia
81310 UTM, Johor Bahru, Johor

Nama Penyelia Lain (jika ada) :

Disahkan oleh Timbalan Pendaftar di Fakulti:

Tandatangan :

Nama :

Tarikh :

ROLE OF SILICON CARBIDE ADDITIVES IN REDUCING DEWAXING TIME AND MOULD CRACK IN INVESTMENT CASTING USING MICROWAVE-ASSISTED HEATING

AHMED OMAR ASWAYE AMHAMED

A thesis submitted in fulfilment of the
requirements for the award of the degree of
Doctor of Philosophy

Faculty of Mechanical Engineering
Universiti Teknologi Malaysia

MAY 2025

DECLARATION

I declare that this thesis *"Role of silicon carbide additives in reducing dewaxing time and mould crack in investment casting using microwave-assisted heating"* is the result of my own research except as cited in references. This thesis has not been accepted for any degree and is not concurrently submitted in candidature of any other degree.

Signature : ……..

Name: : AHMED OMAR ASWAYE AMHAMED

Date: : 26 MAY 2025

ACKNOWLEDGEMENT

In preparing this thesis, I was in contact with many people, researchers, academicians, and practitioners. They have contributed towards my understanding and thoughts. In particular, I wish to express my sincere appreciation to my dedicated thesis supervisor, Ir. Ts. Dr. Wan Fahmin Faiz Wan Ali, Professor Dr. Izman Bin Sudin, and Dr. Najlaa Nazihah Binti Mas'ood, for encouragement, guidance, criticism, and friendship. Without their continued support and interest, this thesis would not have been the same as presented here. I would like to take this opportunity to express my deepest appreciation to the technical staff of the foundry lab, whose support and assistance have been invaluable throughout my research.

I am immensely thankful to my parents, who have been my constant source of strength, support, and inspiration. Their sacrifices, prayers, and belief in my potential have motivated me through every step of this journey. I am also profoundly grateful to my wife, Thuraya Mohammed, whose patience, understanding, and encouragement have supported me throughout this journey. Her steadfast belief and love have made this accomplishment possible. Not to forget my beloved children, whose cheerfulness has been a source of joy and motivation. Finally, my heartfelt thanks go to my brothers and sisters, who have offered unwavering support throughout my studies. May Allah reward all of you in the Hereafter. Above all, I thank Allah the Almighty for His grace, mercy, compassion, and guidance.

ABSTRACT

Mould cracking and dewaxing time are among the most critical issues affecting the economic efficiency of investment casting (IC), as they increase the likelihood of rework, costs, and production time. Despite numerous attempts to address these constraints, balancing production speed with economic performance in modern investment casting remains an ongoing challenge. Therefore, there is a pressing need to make appropriate modifications to the mould, wax, and heating methods to address these issues. This study aims to investigate the effects of silicon carbide (SiC) addition on dewaxing time and the dielectric, physical, thermal, and mechanical properties of the mould in two different waxes under microwave hybrid heating. In the first stage of this study, patterns were created using HYFILL B289 MOD S wax and SIVUCH L1203 wax. For the mould fabrication stage, stucco (Al_2O_3-SiO_2) was mixed with SiC, a material with high microwave absorbance, in varying amounts (0, 1, 2.5, 5, and 7.5 wt.%) to enhance microwave absorption and improve the thermal properties of the green moulds. This modified stucco was applied to the mould's coarse backup layers (3^{rd} to 6^{th}) by dip-coating in slurry followed by stuccoing. The thermal expansion of the waxes and the standard green ceramic mould was evaluated. The modified green moulds underwent various characterization, including assessments of dielectric properties, thermal conductivity, density, porosity, and flexural strength. Dewaxing tests were then conducted at various microwave powers (300, 450, 600, and 850 W) to determine the most effective power for the dewaxing process. The findings revealed that adding SiC demonstrated a pivotal role in enhancing the hybrid heating process. In particular, the electrical insulation properties improved significantly, increasing by 11-folds, 12-folds, and 15-folds at SiC contents of 2.5, 5, and 7.5 wt.%, respectively. The thermal conductivity also increased by 40%, 49%, and 59% at these SiC concentrations. The density and flexural strength of the modified green moulds were also increased while their porosity was reduced. The 600 W microwave power was determined to be the most feasible for the dewaxing process due to its efficiency and safety. The improvement in dielectric and thermal properties resulted in a 62% reduction in dewaxing time at 7.5wt.% SiC compared to direct microwave heating of standard mould, and an 84% reduction compared to traditional electric firing furnace heating, contributed to up to 75% energy savings. Furthermore, statistical analysis (ANOVA) showed that the addition of SiC was the most significant factor, contributing to a 96% reduction in dewaxing time. A comparison of the thermal expansion behaviours of the two waxes revealed that HYFILL B289 MOD S wax exhibited a thermal expansion three times higher than that of SIVUCH L1203 wax, which negatively affected the integrity of the mould shell structure. Strain gauge tests further confirmed crack formation in HYFILL B289 MOD S moulds. In contrast, SIVUCH L1203 wax demonstrated better compatibility with the ceramic shell's thermal expansion, outperforming HYFILL B289 MOD S in producing crack-free ceramic investment moulds. This study revealed that combining SiC-assisted microwave hybrid heating with compatible thermal expansion between the wax and the ceramic mould offers an efficient and effective approach for rapid dewaxing and defect-free moulds. This approach presents a promising alternative to conventional heating methods and is well-suited for rapid, energy-efficient, and environmentally friendly investment casting.

ABSTRAK

Retakan acuan dan masa penyahlilinan merupakan antara isu paling kritikal yang menjejaskan kecekapan ekonomi dalam proses penuangan lilin (IC) kerana ia meningkatkan kemungkinan kerja semula, kos, dan masa pengeluaran. Walaupun pelbagai usaha telah dilakukan untuk menangani kekangan ini, menyeimbangkan kelajuan pengeluaran dengan prestasi ekonomi dalam penuangan lilin moden masih menjadi cabaran berterusan. Oleh itu, terdapat keperluan mendesak untuk melakukan pengubahsuaian yang sesuai pada acuan, lilin, dan kaedah pemanasan untuk menangani isu-isu ini. Kajian ini bertujuan untuk menyiasat kesan penambahan silikon karbida (SiC) terhadap masa penyahlilinan serta sifat dielektrik, fizikal, haba, dan mekanikal acuan menggunakan dua jenis lilin yang berbeza di bawah pemanasan hibrid gelombang mikro. Pada peringkat pertama kajian ini, corak telah dihasilkan menggunakan lilin HYFILL B289 MOD S dan SIVUCH L1203. Untuk peringkat pembuatan acuan, bahan *stucco* (Al_2O_3-SiO_2) dicampurkan dengan SiC, iaitu bahan yang mempunyai kadar serapan gelombang mikro yang tinggi, dalam pelbagai kepekatan (0, 1, 2.5, 5, dan 7.5 wt.%) untuk meningkatkan penyerapan gelombang mikro dan memperbaiki sifat haba acuan hijau. *Stucco* yang telah diubah suai ini digunakan pada lapisan sandaran kasar acuan (lapisan ke-3 hingga ke-6) melalui kaedah celupan dalam buburan diikuti dengan penaburan *stucco*. Pengembangan haba lilin dan acuan seramik hijau piawai telah dinilai. Acuan hijau yang diubah suai ini kemudiannya melalui pelbagai pencirian, termasuk penilaian sifat dielektrik, kekonduksian haba, ketumpatan, keliangan, dan kekuatan lenturan. Ujian penyahlilinan dijalankan pada pelbagai kuasa gelombang mikro (300, 450, 600, dan 850 W) bagi menentukan kuasa yang paling berkesan untuk proses ini. Hasil kajian menunjukkan bahawa penambahan SiC memainkan peranan penting dalam meningkatkan proses pemanasan hibrid. Secara khusus, sifat penebatan elektrik meningkat dengan ketara, masing-masing sebanyak 11, 12, dan 15 kali ganda pada kepekatan SiC sebanyak 2.5, 5, dan 7.5 wt.%. Kekonduksian haba turut meningkat sebanyak 40%, 49%, dan 59% pada kepekatan yang sama. Ketumpatan dan kekuatan lenturan acuan hijau yang diubah suai juga meningkat manakala keliangannya menurun. Kuasa gelombang mikro 600 W didapati paling sesuai untuk proses penyahlilinan kerana kecekapan dan keselamatannya. Peningkatan dalam sifat dielektrik dan haba membawa kepada pengurangan masa penyahlilinan sebanyak 62% kepada 7.5 wt.% SiC berbanding pemanasan gelombang mikro langsung pada acuan piawai, dan sebanyak 84% berbanding pemanasan relau elektrik tradisional. Ini sekali gus menyumbang kepada penjimatan tenaga sehingga 75%. Selain itu, analisis statistik (ANOVA) menunjukkan bahawa penambahan SiC merupakan faktor paling signifikan, menyumbang kepada pengurangan masa penyahlilinan sebanyak 96%. Perbandingan tingkah laku pengembangan haba antara kedua-dua jenis lilin menunjukkan bahawa lilin HYFILL B289 MOD S mengalami pengembangan haba tiga kali ganda lebih tinggi daripada lilin SIVUCH L1203, yang mana memberi kesan negatif terhadap keutuhan struktur kulit acuan. Ujian tolok regangan turut mengesahkan pembentukan retakan pada acuan menggunakan HYFILL B289 MOD S. Sebaliknya, lilin SIVUCH L1203 menunjukkan keserasian yang lebih baik dengan pengembangan haba kulit seramik, sekali gus menghasilkan acuan seramik tuangan lilin yang bebas retak. Kajian ini membuktikan bahawa gabungan pemanasan hibrid gelombang mikro yang dibantu SiC dengan keserasian pengembangan haba antara lilin dan acuan seramik menawarkan pendekatan yang cekap dan berkesan untuk penyahlilinan pantas serta acuan bebas kecacatan. Pendekatan ini merupakan alternatif yang menjanjikan kepada kaedah pemanasan konvensional dan sangat sesuai untuk proses penuangan lilin yang pantas, cekap tenaga, dan mesra alam.

TABLE OF CONTENTS

LIST OF TABLES

LIST OF FIGURES

LIST OF ABBREVIATIONS

AL_2O_3	-	Alumina (Aluminium oxide)
AL	-	Aluminum
ASTM	-	American Standard for Testing Materials
CB	-	Carbon black
CFAs	-	Crossed field amplifiers
DMH	-	Direct microwave heating
DTA	-	Differential thermal analysis
DTG	-	Derivative thermogravimetric
EDX	-	Energy dispersive x-ray
FTIR	-	Fourier transform infrared spectroscopy
IC	-	Investment casting
MHH	-	Microwave hybrid heating
MW	-	Microwave
NA	-	Not Applicable
SEM	-	Scanning electron microscopy
SiC	-	Silicon carbide
SiO_3	-	Silicate
TD	-	Theoretical Density
TGA	-	Thermogravimetric analysis
TWTs	-	Travelling wave tubes

LIST OF SYMBOLS

A	-	Cross-section area (m^2)
B	-	Magnetic flux density (C/m^2)
c	-	The velocity of light (m/s)
c_p	-	Specific heat of water (J/kg K)
D	-	Electric flux density (W/m^2)
D_M	-	Inner diameter of the mould (m)
D_S	-	Outer diameter of the wax pattern (m)
dp	-	Penetration depth (mm)
E	-	Electric field intensities (V/m)
Ei	-	Electromagnetic radiation energy (W)
$F(x)$	-	Failure probability
F_{max}	-	Fracture load applied (N)
ƒ	-	Frequency (Hz)
H	-	Magnetic field intensities (A/m)
h	-	Sample thickness (m)
h_{air}	-	Convection heat transfer coefficient of air (W/m^2 K)
k	-	Thermal conductivity (W/m.K)
L	-	Sample length (m)
m	-	Sample mass (kg)
$\dot{m}$	-	Mass flow rate of water (kg/s)
NA	-	Not applicable
P	-	Apparent porosity (%)
P_{abs}	-	Microwave energy absorbed (W/m^3)
P_b	-	Pressure value at bursting point (MPa)
P_e	-	Electronic polarization
P_i	-	Ionic polarization
P_m	-	Molecular polarization
P_{MW}	-	Microwave power (W/m^3)
P_S	-	Surface polarization
$P(\sigma)$	-	Failure probability at the strength σ

Q_1	-	Heat required to melt the wax by furnace (J)
Q_2	-	Heat required to melt the wax by microwave (J)
Q_i	-	Heat supply to the furnace's interior (J)
Q_{L1}	-	Energy losses from the furnace chamber walls (J)
Q_{L2}	-	Heat losses from the mould surface (J)
Q_{LH}	-	Latent heat of wax melting (J)
Q_r	-	Heat required to raise the moulds' temperature from T_a to T_i (J)
Q_w	-	Heat required to melt out the wax pattern (J)
q	-	Conduction heat transfer (J/s)
$R(\sigma)$	-	Weibull reliability at the strength σ
r_i	-	Internal radius of the spherical shell sample (m)
S	-	Shell thickness (m)
T	-	Temperature ($^\circ$C)
T_a	-	Ambient temperature ($^\circ$C)
T_i	-	Furnace internal temperature ($^\circ$C)
T_m	-	Temperature of wax melting ($^\circ$C)
T_s	-	Sample surface temperature ($^\circ$C)
$tan\ \delta$	-	Loss tangent
$tan\ \delta\varepsilon$	-	Dielectric loss tangents
$tan\ \delta\mu$	-	Magnetic loss tangents
t	-	Time (sec)
V	-	Kinematic viscosity (m^2/s)
V_D	-	Actual volume of the die cavity (m^3)
w	-	Sample width (m)
μ	-	Magnetic permeability (H/m)
μ^*	-	Complex permeability
μ'	-	Magnetic permeability
μ''	-	Magnetic loss factor
μ_r'	-	Relative magnetic constant
$\mu_r^{"}$	-	Relative magnetic loss factor
ε^*	-	Complex permittivity of material (F/m)
ε'	-	Dielectric constant

$\varepsilon^{“}$	-	Loss factor
ε_r'	-	Relative dielectric constant
$\varepsilon_r^{"}$	-	Relative dielectric loss factor
ΔP	-	Pressure difference (N/m^2)
λ	-	Wavelength
α	-	Thermal expansion coefficients
η	-	Dynamic viscosity of Air at ambient temperature ($N.s/m^2$)
σ	-	Electrical conductivity of a material (Siemens/m)
σ_h	-	Stress value at the bursting point (MPa)
σ_{max}	-	Flexural strength (MPa)
ρ	-	Bulk density (g/cm^3)
ω	-	Angular frequency (1/s)

LIST OF APPENDICES

CHAPTER 1

INTRODUCTION

1.1 Research Background

Investment casting (IC), also known as lost wax casting, has evolved from a specialized technique in the mid-20th century into a globally significant manufacturing method, particularly for applications requiring high dimensional accuracy and complex geometries (Lehmhus, 2022). Among various casting methods, such as sand casting, die casting, and centrifugal casting, investment casting stands out for its ability to produce components with exceptional dimensional precision, intricate details, near-net shapes, and minimal post-processing (Dejene et al., 2023). A classic example is the production of turbine blades in aerospace engines, where complex cooling channels and aerodynamic profiles demand the precision and repeatability that IC provides (Dong et al., 2024). Despite its advantages, IC is often associated with higher costs and longer lead times compared to conventional casting methods. To address these challenges, recent advancements have focused on integrating additive manufacturing (AM) for rapid wax pattern production, enhancing design flexibility and reducing production time (Prakash et al., 2021). Furthermore, sustainable practices such as recyclable ceramic slurries and energy-efficient heating methods are gaining momentum, aligning IC with modern eco-friendly manufacturing trends (Lee et al., 2020; Pérez-Conesa et al., 2022).

Bae et al. (2019) clarified that ceramic investment casting shells must have several critical properties. These include; i) adequate strength to withstand generated stresses from the cast alloy after solidification, ii) good thermal stability for accurate dimensions, iii) moderate or minimal reactivity with alloying components, and iv) open porosity to enhance suitable air permeability. Furthermore, good thermal conductivity is required to ensure appropriate cooling of the cast metal from the ceramic wall. Many researchers have been working toward improving these properties. Some researchers have observed that sacrificial pore formation agents (PFAs) such as

charcoal, rice husk, walnut shell, seeds, different polymers, and ammonium carbonate could be added to the ceramic slurry before creating the shell to increase the permeability dramatically (Kanyo et al., 2020). Unfortunately, increased permeability sometimes comes at the expense of shell strength, which lowers the load-bearing capability of the mould (Kline et al., 2010). However, more layers were added to make a thicker shell to compensate for the decreased green and fired shell strengths. However, extra coating counteracts the sacrificial pore process, reducing permeability, cooling rate, and collapsibility (Lü et al., 2016b). Researchers tweaked a ceramic slurry binder to optimize the shell strength without adding layers by adding a latex-based liquid polymer. While this alteration has enhanced the mould's green strength, it has also reduced its fired strength (Tamta and Karunakar, 2019). Organic fiber additives, such as nylon, have been utilized to improve the mould strength of cast aluminium alloys. The capacity of a hybrid fiber made of aluminium silicate and polypropylene to simultaneously improve green strength, fire strength, and shell permeability has been discovered, but controlling the orientation of the fibers has proven problematic (Lü et al., 2016b). Many recent investigations have focused on substituting fiber reinforcements with powder additives to overcome the limitations of fiber addition. Unfortunately, research has shown that improving both flexural strength and permeability with a single constituent is challenging, as increases in one generally come at the expense of the other (Wisniewski et al., 2020).

Cracking of green ceramic mould shells is one of the predominant problems encountered during the dewaxing process of investment casting. It is thought that 80% of cracks in made moulds originate during dewaxing (interface of shell and wax), with the remaining 20% probably the result of handling (Raza, 2015; Lee, 2016). The mismatch of thermal expansion coefficients between the green ceramic mould shell and the wax pattern is a major cause of cracking during dewaxing; when the coefficient of thermal expansion of the wax is higher than that of the shell, the fragile structures is exposed to intense thermal stresses, resulting in shell fracturing (Mishra and Ranjana, 2010; Singh et al., 2021b; Mukhtarkhanov et al., 2024). Accordingly, researchers believe that wax with a high melting point is another problem because it takes longer to transform from a solid phase to a liquid. During this phase, it gradually expands and negatively affects the shell. The other mechanisms that may involve in

shell cracking include inconsistent shelling processes (poor green strength), excessively high liquid wax viscosities, low green shell mould permeability, inconsistent wax blends, intricate geometry in the mould and insufficient gates for liquid wax flow (Lee, 2016; Kanyo et al., 2020). Therefore, extensive research has sought to diminish or eliminate these issues.

Wax removal from the ceramic mould shell is a critical stage in the investment casting process, as it directly impacts the integrity and quality of the final casting. While it is widely accepted that heating the ceramic shell enables molten wax to flow out, the process must be rapid to minimize wax expansion and avoid cracking or dimensional distortion. Traditional methods, such as autoclave and flash fire dewaxing, remain common but have notable drawbacks. The autoclave method often produces impure wax mixed with condensate and dirt, making recovery and reuse difficult, and it frequently leaves residual wax within the shell, making the process inefficient and time-consuming (Pattnaik et al., 2012). Flash fire dewaxing, introduced to address these issues, carries a significantly higher operational cost, rendering it less favorable for widespread adoption (Luján et al., 2025). Due to these limitations, researchers have explored alternative technologies to reduce energy consumption, processing time, and environmental impact (Badanova et al., 2021; Mahrabi et al., 2016), with microwave heating showing particular promise. Compared to conventional methods, microwave processing offers faster heating rates, shorter cycle times, and improved mechanical and metallurgical outcomes (Gude et al., 2013; Goyal et al., 2022). However, its effectiveness is strongly influenced by the dielectric properties of the ceramic materials. While high-loss ceramics like silicon carbide absorb microwave energy efficiently, low-loss materials such as alumina are poorly responsive at standard industrial frequencies (2.45 GHz), limiting the effectiveness of direct microwave heating (DMH). This observation aligns with the findings of Brum et al. (2009) and Rani and Karunakar (2013), who demonstrated that direct microwave heating of ceramics using a household microwave oven is a viable approach, but it introduces other challenges. Chief among these is non-uniform heating, which induces thermal stress and increases the risk of ceramic cracking. In addition, uneven electromagnetic field distribution and hot-spot formation continue to pose significant

limitations to direct microwave heating of ceramics, often resulting in inconsistent heating and prolonged processing times (Klinger et al., 2018; Meng et al., 2018).

Owing to the limitations of direct microwave heating, hybrid microwave heating (MHH) technology has been developed. Hybrid heating can be categorized into two types: one that combines conventional heating with direct microwave heating (e.g., induction or infrared), and another that uses microwave susceptors (Zhang et al., 2024). The effectiveness of the microwave dewaxing process largely depends on the dielectric properties of the mould materials or patterns. Incorporating a microwave susceptor into the mould-making materials can enhance their microwave absorption, thereby improving the overall efficiency of the dewaxing process. The susceptor provides two functions during microwave hybrid heating: changing the temperature of the material from room temperature to critical temperature by heat conduction method, reducing energy waste at high temperatures, and reducing the risk of thermal shocks (Bhattacharya and Basak, 2017). This allows the use of susceptors, which can substantially reduce dewaxing time and energy consumption. These basic findings align with the work of Yahaya et al. (2016), who added activated charcoal to the stucco, which was prepared to build the outer layers of the mould shell. The dielectric loss factor increased, while the density and strength of both green and fired moulds decreased. However, Gill et al. (2021) proposed a method for dewaxing by incorporating carbon black (CB) as a microwave susceptor in a low-density polyethylene-paraffin wax composition used for creating patterns. Increasing the CB concentration increased the melting temperature and reduced the melting time of the pattern wax. However, it also led to increased agglomeration of the wax blends. A recent study by the same researcher replaced carbon black with polyaniline, and almost the same results were obtained with regard to reducing the dewaxing time; however, surface defects and cracks appeared in wax blends with polyaniline concentrations above 5 wt.% (Gill et al., 2022). Finally, as noted, these attempts did not consider the wax contamination, nor were the characteristics of the ceramic mould reported, besides the limited weight of the tested wax sample, 10g only. Pérez-Conesa et al. (2022) evaluated the use of a susceptor composed of 25% titanium oxide (TiO_2), 25% graphite, and 50% colloidal silica applied to the outer surface of the wax pattern for microwave-assisted dewaxing of ceramic shell moulds at 2200 W. The results

demonstrated that the technique is viable, achieving a surface temperature exceeding 200 ºC, which enabled complete dewaxing in a short time. However, the study faced drawbacks such as wax burning, the appearance of hotspots, and ceramic shell ignitions. By going deeper and understanding the properties and interactions of microwaves, it is possible to choose the most suitable susceptor that helps absorb electromagnetic waves and makes the heating process of the casting mould as quick as possible while avoiding any distortions and achieving the optimum investment.

1.2 Problem Statement

Removing wax from the internal cavity of the green ceramic mould structure is one of the most critical and final stages of ceramic shell manufacturing in the investment casting (IC) process. This stage carries the highest possibility of ceramic shell cracking. Although autoclave and flash dewaxing methods have been widely approved traditional methods in investment casting, they present several drawbacks. These include extended dewaxing times, high energy consumption, reduced green strength of the mould, internal scab formation, wax burn, and the release of environmental pollutants (Brum et al., 2009; Prasad, 2012; Vaghela et al., 2023). Another promising method to overcome such a drawback is microwave heating. However, overcoming certain obstacles is necessitated for its effective application, particularly in processing ceramic and poor-microwave-absorbing materials, including zirconia, silica, alumina, and MgO (Klinger et al., 2018; Meng et al., 2018; Vaghela et al., 2023). To address these limitations, Microwave Hybrid Heating (MHH) has been developed. This method involves doping the ceramic structure with high microwave-absorbing additives, known as susceptors, to enhance its dielectric properties and promote uniform heating.

The success of MHH depends heavily on the dielectric characteristics of the additives and microwave power (Hong et al., 2021; Zhang et al., 2024). In turn, these additives directly influence the physical, thermal, and mechanical properties of the ceramic mould shell (Pattnaik, 2017b). Thus, the optimal selection of the additive, along with microwave power is critical for achieving efficient and defect-free

dewaxing process. Despite MHH potential, limited studies have investigated using the MHH technique for dewaxing the IC process and have revealed persistent drawbacks. For example, although the incorporation of activated charcoal into stucco layers by Yahaya et al. (2016) reduced dewaxing time and energy consumption, the resulting moulds suffered from low green strength, increased porosity, and moisture absorption, ultimately leading to shell cracking. Similarly, efforts by Gill et al. (2021) to enhance microwave absorption using carbon black in LDPE-paraffin wax blends successfully reduced melt flow time but introduced wax agglomeration and polarity issues. Subsequent substitution of carbon black with polyaniline (Gill et al., 2022) continued to produce surface defects and cracking in the wax blends, while issues of wax contamination remained unaddressed. Pérez-Conesa et al. (2022) demonstrated rapid dewaxing using a TiO_2-graphite susceptor combination; however, this approach caused wax burning, hotspot formation, shell ignition, and subsequent cracking. Furthermore, most existing approaches require high microwave power levels (700–1100 W), which raises concerns regarding energy efficiency, safety, and scalability. Therefore, in this study, SiC, which was not previously reported for investment casting, was used as a reinforcer for microwave-assisted heating due to its multiple advantages over earlier susceptors. SiC exhibits high microwave absorption efficiency even at moderate power levels, significantly reducing the risk of hotspots, thermal runaway and energy consumption. It also possesses exceptional thermal stability, superior mechanical strength, strong chemical resistance, and a well-established track record in high-temperature applications (Chiu et al., 2010; Peng et al., 2013; Singh et al., 2024). Unlike carbon-based or metallic additives, SiC does not contribute to wax contamination, does not degrade under thermal stress, and promotes uniform heating due to its stable dielectric behaviour. This offering a safer, cleaner, and more energy-efficient alternative to conventional and previously attempted methods.

For a successful dewaxing process, IC waxes must exhibit key characteristics, including a low melting point, low thermal expansion, and low viscosity. It is also essential to ensure that the wax's expansion pressure does not create critical tensile stress in the shell (Lee, 2016; Tewo et al., 2019; Mukhtarkhanov et al., 2024). Consequently, accurately estimating the shell’s mechanical strength and the expansion pressure from the side of wax is essential for predicting and mitigating failure risks.

This study also suggested a new wax pattern type (SIVUCH L1203 wax) with acceptable physical and thermal properties has the potential to replace the current HYFILL B289 MOD S wax. However, its performance has not been evaluated and reported in the literature. Hence, the finding of Al_2O_3-SiO_3/SiC modified moulds with SIVUCH L1203 wax patterns is expected to create opportunities for entry into actual industry practices, where they can be more thoroughly evaluated through implementation in modern manufacturing methods.

1.3 Research Questions

This study sought to answer three main questions which are:

i. What is the influence of adding different percentages of SiC (wt.%) on the dielectric, physical, morphological, thermal, and mechanical properties of modified green moulds compared to standard green moulds?
ii. What are the feasible range of microwave power and the significant factors balancing efficiency in time for the dewaxing process in standard and modified green ceramic moulds with different types of wax?
iii. How does the dewaxing process in standard green ceramic moulds compare to that in modified green ceramic moulds regarding crack formation and energy efficiency?

1.4 Research Objectives

The main objective of this research was to obtain investment casting moulds without shell cracking defects and reduced processing time by employing microwave hybrid heating technology. The specific objectives were as follows:

i. To evaluate the influence of different percentages of SiC (wt.%) as a microwave-absorbing additive on enhancing the dielectric, physical, thermal, and

mechanical properties of modified green ceramic moulds compared to standard moulds.

ii. To determine the feasible microwave power range and significant factors affecting the dewaxing process in standard and modified green ceramic moulds, balancing efficiency in time with different types of wax.

iii. To compare the performance of the dewaxing process in standard and modified green ceramic moulds in terms of crack formation and energy efficiency.

1.5 Scopes of the Research

Achieving the objectives of this study requires recognizing the following scopes:

i. Thermal and chemical properties of the two types of wax pattern materials were evaluated using a dilatometer, Thermogravimetric Analysis (TGA), Differential Thermal Analysis (DTA), and Fourier Transform Infrared (FTIR), respectively.

ii. Patterns were moulded using two different types of wax: the traditional investment casting wax (HYFILL B289 MOD S) and the newer alternative wax (SIVUCH L1203).

iii. Ceramic mould shell materials were made of slurry and backup stucco, consisting of seven layers only.

iv. Silicon carbide (SiC) particles (700-800 μm) were added into the four backup stucco layers from 3 to 6, with varied percentages of 1, 2.5, 5, and 7.5 wt.% to become modified ceramic moulds.

v. Dewaxing process was evaluated at various microwave powers of 300, 450, 600, and 850 W, with a frequency of 2.45 GHz, using a modified multi-mode applicator Samsung microwave oven (model MS28F303TFK).

vi. The dewaxing performance of standard and modified green ceramic moulds was compared in terms of dewaxing time, the incidence of cracks, and energy consumption.

1.6 Significance of Research

This research significantly contributes to adding new understanding to materials science and advanced manufacturing by exploring the effect of silicon carbide (SiC) additions on the dielectric, thermal, and mechanical properties of ceramic moulds. It provides new insights into the application of microwave hybrid heating (MHH) in investment casting, a technique that remains underexplored in the context of dewaxing. The study also highlights the importance of wax type compatibility, particularly the role of SIVUCH L1203 wax, in ensuring structural integrity during the heating process. The research addresses key limitations in the traditional investment casting process, specifically the prolonged dewaxing time, high energy consumption, and reduced green strength of ceramic moulds due to unsuitable additives and conventional heating methods. By incorporating SiC as a microwave susceptor and optimizing the wax-mould compatibility, the study demonstrates a significant improvement in mould performance and process efficiency. The optimized process reduces defects, enhances heating uniformity, and improves the mechanical stability of green moulds, offering a more robust and consistent manufacturing approach. This research provides a viable and scalable solution for industries seeking cost-effective and sustainable solutions, especially in countries that still rely on wax casting in many sectors where time and energy are paramount. Furthermore, this research contributes to global sustainability efforts by introducing energy-efficient and eco-friendly alternatives to conventional heating methods, aligning with the goals of advancing sustainable industrial practices. It also reflects a commitment to innovation and problem-solving in advanced manufacturing.

1.7 Thesis Organization

This thesis is organized into five chapters. Chapter 1 provides an introduction to the study, including a background review and the problem statement. It addresses the drawbacks of the dewaxing process in investment casting, particularly concerning dewaxing time and shell cracking. Additionally, it outlines the study's objectives, scope, significance, and research contributions. Chapter 2 reviews the relevant

literature in this research, which is divided into two main sections. The first section includes the investment casting, which begins with a description of the investment casting process, pattern-making materials, and the different dewaxing techniques. Lastly, the effects of ceramic shell fabrication and additives on mould properties are reviewed. The section ends by discussing the developments and optimizations of ceramic shells in investment casting. The second section includes microwave material processing, which begins with a discussion of the principle of microwave heating and the basics of the materials' interaction with microwaves. This section also reviews the techniques of direct and hybrid microwave heating. Chapter 3 presents the research methodology used in detail. It includes the materials, lab procedures, and analytical methods used to achieve the research goals. Chapter 4 discusses and Analysis the results of this study, divided into three main sections. The first section examines the properties of wax patterns and green ceramic moulds, focusing on their dielectric, physical, thermal, and mechanical characteristics. The second section addresses the dewaxing test results. The third section evaluates the energy saving in the dewaxing stage using microwave hybrid heating. Finally, Chapter 5 includes the full conclusion of this work and offers some recommendations for future research.

CHAPTER 2

LITERATURE REVIEW

2.1 Introduction

This chapter presented the fundamental principles of investment casting, including pattern technologies and the dewaxing process using both conventional and non-conventional techniques. It also discussed ceramic mould-making methods and the effects of various additives on mould properties. Furthermore, recent developments and optimizations of ceramic shells in investment casting are summarized accordingly. The principles of microwave heating were highlighted, along with the mechanisms of material polarization and the key parameters influencing the microwave heating process. The chapter also covered the dielectric and magnetic properties of materials that govern their interaction with microwaves, as well as the influence of microwave penetration depth on heating efficiency. In addition, both direct and hybrid heating of materials using microwaves were discussed.

2.2 Investment Casting Process (IC)

In investment casting, two methods are used based on the type of mould used. The first method, known as the thick block moulds method, involves pouring refractory ceramic around a wax pattern assembly. However, this method has a significant drawback: the resulting cast metal is encased in an extremely thick ceramic shell, which acts as an insulator. This insulation impedes cooling and often leads to poor metallurgical structures. Conversely, the second method, referred to as the shell moulds method or investment shell, involves creating a ceramic slurry that is applied in multiple layers, typically consisting of five to eight around "investing" a wax assembly (Williams and Okonek, 2018; Beeley and Smart, 2023).

Over the past two centuries, investment casting has evolved into the most modern and adaptable of all metal casting techniques, renowned for minimizing material waste, energy consumption, and subsequent machining requirements. Consequently, it has gained prominence in industries such as dental, orthopedic, aerospace, and automotive. Investment casting is particularly suited for manufacturing parts with complex shapes, offering advanced capabilities that produce components with exceptional surface smoothness and high dimensional accuracy. However, the process requires following various precise stages to design and create the appropriate workpieces that achieve the final product specifications. Kalpakjian (1997) briefly demonstrated the six basic processes required in manufacturing and investment casting using a ceramic shell, as shown in Figure 2.1.

i. Creating a master Pattern: A pattern of the desired workpiece is typically made from wax, plastic or polystyrene as pattern materials. This can be achieved by carving from a wax block by hand, injecting molten wax into a metallic die, or utilizing a 3D printer. To enhance productivity, similar patterns are grouped and connected to a central wax sprue, forming a tree-like structure (Badanova et al., 2022).
ii. Apply investment materials (Shell Molding): The ceramic mould is constructed by alternately coating and stuccoing to achieve the desired thickness. Initially, a pattern or cluster of patterns is dipped into a ceramic or fine refractory slurry, then drained to ensure a uniform coating. This prime coat, often using delicate materials, preserves fine details of the mould. The slurry typically contains colloidal silica or ethyl silicate binder mixed with zirconium silicate, alumina, or other refractory powders. Subsequently, the pattern or cluster is covered with a layer of fine stucco by dipping into a fluidized bed, using a rainfall sander with dry flour, or by manual sprinkling. This process may be repeated with coarser stucco to build the necessary mould thickness to withstand casting stresses. The final mould assembly is then left to dry for 18-48 hours (Kumar and Karunakar, 2021).
iii. Wax Removal: Wax patterns are eliminated by heating inside an oven or with steam in a specialized oven, and can also be removed by burning.

iv. Mould Casting: After wax removal, the remaining shell forms a hollow cavity that precisely mirrors the required product shape. This cavity is filled with molten metal or another liquid material and is left to cool and solidify.

v. Removing the ceramic Shell: The shell is removed using mechanical or chemical methods to reveal the final solidified product.

vi. Inspection and finishing: The final cast part undergoes inspection, and any detected imperfections are corrected**.**

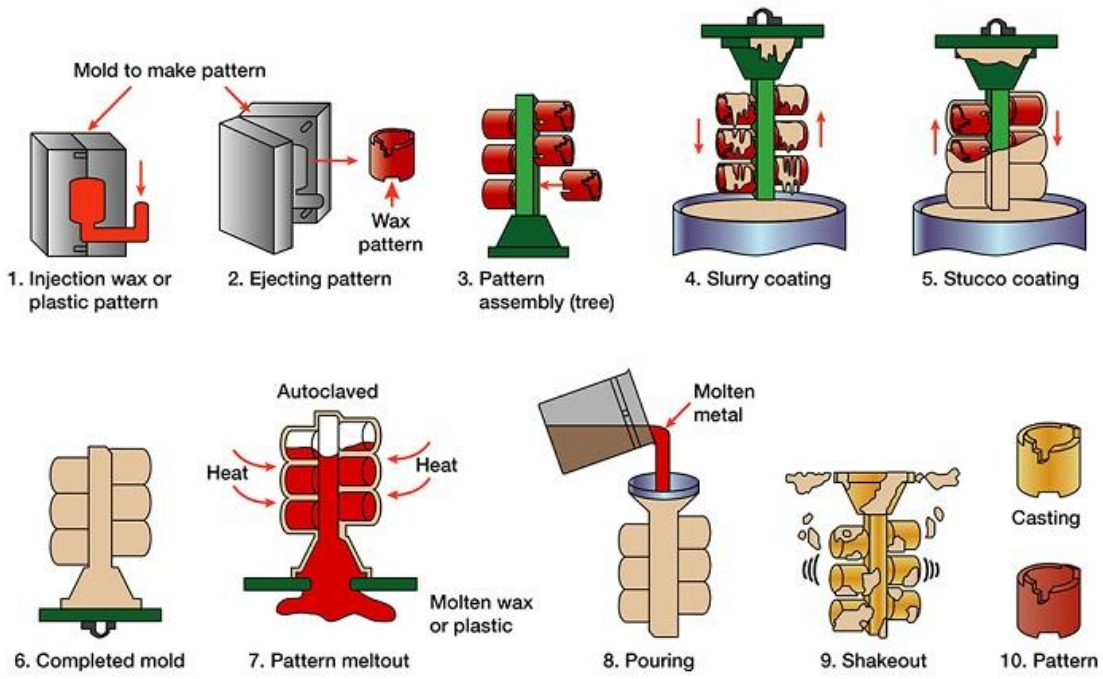

Figure 2.1 Schematic illustration of investment casting process (Engineering Product Design, 2022)

2.2.1 Pattern Technology

Pattern is a principal part of the investment casting process, often featuring complex geometries or specific attributes that present challenges in casting. This design strategy allows researchers to evaluate the impact of various process variables on the quality of the final product (Pattnaik et al., 2012). The geometry of the final cast part, including its dimensional accuracy, surface quality, and intricate details, is inherently linked to the characteristics of the original pattern used in casting.

Consequently, selecting the appropriate material for constructing the pattern is crucial (Tamta and Karunakar, 2021). Additionally, understanding the thermal behavior of the pattern material and choosing a suitable thermal expansion coefficient are essential to prevent large thermal stresses that can cause the ceramic shell to break during the heating process. Therefore, pattern preparation is one of the most crucial steps in the investment casting stages (Everhart et al., 2013).

Wax is the most commonly used material for creating patterns in investment casting (IC); however, recent advancements in rapid prototyping using additive manufacturing have introduced other materials such as plastics, polymers, polystyrene, ice, and frozen mercury (Pattnaik et al., 2012; Shah et al., 2023). In general, Tamta and Karunakar (2021) have summarized the properties of these pattern materials which crucially influence dimensional accuracy and surface quality. These include:

- Ash content: minimizing the ash content in the pattern material can significantly reduce gas porosity defects.
- Coefficient of thermal expansion: a low coefficient of thermal expansion in the pattern material is critical, as it helps mitigate its expansion during pattern removal and thereby reduces the risk of mould cracking.
- Viscosity: high viscosity in the pattern material can lead to the formation of flow lines and knit lines on the pattern surface, damaging the surface finish of the cast part. Conversely, very low viscosity allows the material to fill into the tooling gap, which may trap gases. Thus, a moderate viscosity is essential to balance these concerns and achieve optimal casting results.

The size and shape of the wax pattern are extremely important to the success of the investment casting process. Researchers often select wax patterns with specific shapes and dimensions that exemplify the types of parts produced using this method, in order to thoroughly investigate the wax investment casting process. These patterns are typically designed with complex geometries or specific features known to present challenges in casting, enabling researchers to assess the impact of process variables on the quality of the final product (Pattnaik et al., 2012). When conducting research and experiments, it is essential to ensure that the design is both simple and efficient to

facilitate the acquisition of accurate and consistent data. This often requires minimizing resource utilization, streamlining measuring instruments, and focusing on reducing material usage (Kumar and Bhardwaj, 2015).

2.2.1.1 Wax Patterns

Despite the wide range of pattern materials available, waxes (or wax blends) are still the material of choice for pattern manufacturing since they are affordable and their qualities can be easily adjusted with additives to suit a variety of needs. The low melting points and melt viscosities of waxes also make them popular because they make it easier to combine, inject, assemble into a tree, and remove from thin ceramic shell moulds without cracking (Prasad, 2012). Researchers have explored various types of waxes, including petroleum-based, mineral, animal, and vegetable waxes (Szabó et al., 2022). However, purely natural or synthetic waxes often have a high thermal expansion coefficient, which can lead to shell cracking during the dewaxing process. Moreover, these waxes are prone to excessive shrinkage, resulting in dimensional inaccuracies in the final cast product (Tewo et al., 2019; Tamta and Karunakar, 2021).

As investment casting technology advances, there is a corresponding need for improvements in pattern properties to reduce manufacturing costs and enhance productivity. Consequently, numerous intensive investigations have been conducted to identify the most critical properties of pattern wax. The key findings from these investigations have been summarized by Bemblage and Karunakar (2011) and Tamta and Karunakar (2021) as follows:

- The pattern wax should exhibit minimal thermal expansion to ensure the accuracy of the shape's dimensions.
- The melting point should be sufficiently low to facilitate easy release from the mould during the dewaxing process, which typically occurs below ambient temperature.

- In its molten state, the wax should possess moderate viscosity, enabling it to fill even the smallest cavities within the die.
- At room temperature, the wax must be robust enough to resist breakage during handling.
- Pattern wax should exhibit low shrinkage characteristics and a short solidification time to maintain dimensional integrity.
- The pattern material should contain lower ash (less than 0.05%) to ensure a clean ceramic shell is produced.
- The wax must be compatible with the ceramic mould materials used in the casting process.
- Used wax should be environmentally friendly; it should not emit harmful or carcinogenic compounds upon burning.
- It can be reusable if possible.

Numerous efforts have been made to modify the properties of pattern wax to satisfy various requirements. In lost wax investment casting, petroleum-based waxes like microcrystalline and paraffin wax are being widely utilized because of their better surface finish, dimensional accuracy, chemical stability, and acceptable flow control. These waxes are often blended to leverage the complementary properties of each (Czarnecka-Komorowska et al., 2020). Common additives to the wax matrix include resins, plastics, antioxidants, fillers, and dyes, which enhance specific characteristics (Prasad, 2012). Some efforts highlighted the crucial role of each component in achieving strong dimensional control in pattern waxes. For instance, resins are added to increase the strength of the wax body (Pattnaik and Sutar, 2021), while fillers help produce more consistent patterns (Fleckenstein, 2017). Further, the polymeric substance is used as a filler to improve the thermal and mechanical behaviour of wax patterns owing to their wide range of attractive characteristics including low density, low coefficient of friction, transparency, and satisfactory toughness (Harsha, 2011). Cerita™ 29-51, an unfilled wax blend currently used in industry, consists of 70% paraffin wax, microcrystalline wax, a proprietary polymer, and synthetic hydrocarbon resin (Sabau and Viswanathan, 2003).

Other research by Surendran et al. (2022) revealed that the addition of powdered soybeans as a filler material to waxes improves their properties by decreasing shrinkage and improving tensile strength and surface roughness. Subsequent studies by Rahman Khan et al. (2024) revealed that additives such as palmitic acid and cross-linked polyvinylpyrrolidone further enhance pattern attributes, including thermal expansion coefficient, tensile strength, surface roughness, and viscosity. However, despite the widespread use of both natural and synthetic waxes, numerous researchers have identified limitations that hinder their application in manufacturing complex metal parts. Consequently, future developments in pattern technology should focus on reducing lead times and enhancing the physical, mechanical, thermal, and rheological properties of waxes (Tewo et al., 2019).

2.2.1.2 Plastic Patterns

Numerous studies have explored the use of plastic as an alternative pattern material to wax, owing to its stability and cost-effectiveness (Prasad, 2012). Furthermore, plastic patterns offer enhanced resistance to the breakage or deformation commonly experienced with wax in the fabrication of metal parts featuring thin, intricate geometries, such as delicate airfoils (Shah et al., 2023). However, challenges persist; the intricate mechanism of plastic injection, significant thermal expansion during heating, and elevated ash content restrict the broader adoption of plastic patterns (Prasad, 2012; Tewo et al., 2019).

2.2.1.3 Ice Patterns

The ice cast process represents a unique and environmentally friendly freeform production technology that generates 3D ice patterns directly from CAD models, offering an alternative to traditional wax patterns in investment casting. This method not only simplifies the manufacturing process but also accelerates the production cycle (Hodgir et al., 2022). Moreover, ice, being more readily available than wax, reduces the overall cost of materials and minimizes environmental impact. Notably, ice's

propensity to shrink upon melting significantly lowers the risk of mould fractures (Huang et al., 2007).

Rapid freeze prototyping is employed to fabricate ice patterns, allowing for a comparative analysis of dimensional variability and the surface quality of castings against those produced using wax patterns. While the surface finish of items created with ice patterns surpasses those made with wax, the wax patterns achieve superior dimensional accuracy in the final cast parts (Hodgir et al., 2022).

2.2.1.4 Other Pattern Materials

Pattern materials, including naphthalene and paradichlorobenzene, are employed alongside urea-based patterns. These urea patterns provide a significant advantage, facilitating effortless removal from ceramic shell moulds without inflicting damage. This is achieved through their ability to dissolve easily in water or other aqueous solutions (Viswanathan et al., 2008).

2.2.2 Wax Pattern-making and Improvement

Patterns are typically created by injecting a specific grade of wax, either in liquid or semisolid form, into a metal die shaped to the desired configuration (Tewo et al., 2019). Solid injection, which is employed to minimize shrinkage and enhance strength, can require high injection pressures, sometimes up to 10.3 MPa, depending on the wax injection machinery and the wax components, with temperatures ranging from 43 to 77 °C. In contrast, liquid waxes necessitate lower pressures and higher temperatures during the injection process (Viswanathan et al., 2008). When liquid wax is introduced into the die solely by gravity, significant shrinkage may occur, altering its dimensions.

Rapid investment casting (RIC), leveraging additive manufacturing (AM) technologies, has recently gained prominence within the investment casting industry.

This rise in popularity is attributed to its capacity for swift pattern production without the necessity for tooling. Moreover, the adoption of AM for pattern making facilitates the integration of more sophisticated design methodologies, such as topology optimization (TO), enhancing the precision and functionality of the castings (Richard and Kwok, 2019; Ripetskiy et al., 2023).

In the rapid fabrication of tooling for investment casting processes, Rapid Investment Casting (RIC) involving pattern creation is categorized into two approaches: (i) direct additive manufacturing (AM) of patterns and (ii) indirect AM of patterns. The direct AM route encompasses a variety of rapid prototyping (RP) processes, including fused deposition modeling (FDM), stereolithography apparatus (SLA), laminated object manufacturing (LOM), selective laser sintering (SLS), and 3D Printing (3DP). Conversely, indirect methods typically involve RTV vacuum casting. Each approach uniquely differs in terms of geometry, materials, quality, and costs, offering distinct advantages and limitations (Pal and Ravi, 2007).

Recent advancements have been made in wax formulations to enhance their properties for investment casting. Numerous studies have shown that blending a base wax with other types of waxes and materials imparts essential characteristics to the original wax. This results in a pattern wax that ideally suits the specific requirements of investment casting foundries, particularly in the development aspects of the casting process (Czarnecka-Komorowska et al., 2020; Kumar and Karunakar, 2022; Venkat et al., 2020). Table 2.1 provides a summary of prior research on enhancements in wax materials used for investment casting patterns. These wax blends have been effectively proven to serve as excellent pattern materials, offering a balance of desirable qualities at a reduced cost.

Table 2.1 Survey review of wax improvements through material additions

Pattern preparation	Additives materials	Effect of additives	Reference
14%Paraffine, 7%Microcystalline, 40% polyethylene terephthalate, resins	5%–50% polyethylene terephthalate	- Improved the properties of pattern material	(Guinn, 2002)
A blend of three types of waxes	50% paraffin wax Thank you for your email. 30% bees wax Thank you for your email. 20% montan wax	- Least shrinkage (1.05mm). - Good surface roughness (1.04 µm) - Injection temp (68 ˚C) - Holding time (9min) - Die temp (46 ˚C) - Injection time (10s) - Injection force (490N)	(Singh et al., 2006; Bemblage and Karunakar, 2011)
70% Paraffin wax	20% stearin + 10% polyethylene wax	- Reduced the shrinkage capacity. - Increased hardness	(Karwiński et al., 2011)
Change the composition of petroleum wax (mass percent)	35%–65% paraffin wax + 25%–55% solid chlorinated polyphenyl +5%–15% montan wax+ 0.1%–5% stearic acid	- Improved the pattern material	(Rani and Karunakar, 2013)
80% paraffin wax	8% beeswax + 8% carnauba wax + 4% montan wax	- decrease melting point to 42.6 ˚C - decrease congealing point to 40.3 ˚C - Ash content was 0.16%	(Shivappa et al., 2014)
Coconut oil-based hybrid (COBH)	Mix coconut oil with Microcrystalline wax.	- COBH has a lower melting point ranging (42 ˚C -47 ˚C) compared to traditional wax blend (65 ˚C- 71˚C). - Accuracy level of 95%. - Improved surface quality - Lesser shrinkage. - Pattern hardness increased.	(Tamta and Karunakar, 2021)
Paraffin– LDPE wax (Low-density polyethylene)	1.5 wt.% of carbon black (CB)	- Increase in thermal stability - reduce melt flow time of wax by 71.9%; microwave was used for the dewaxing process	(Gill et al., 2021)

2.2.3 Effect of Additives on Pattern Waxes Properties

Waxes are composed of carbon atoms arranged in straight chains, while some materials used as fillers or resins feature carbon atoms in ring structures. The properties of waxes, such as melting point, hardness, viscosity, and solubility, are influenced by the length of these carbon chains. Typically, shorter chains are associated with lower melting points and reduced hardness, whereas longer chains result in higher melting points and increased hardness (Defonseka, 2019). During heating, wax transitions through several stages before it becomes completely liquid. Initially, gradual heating softens the solid wax, transforming it into a semi-plastic and then a fully plastic state. Further heating produces a semi-liquid consistency, and ultimately, upon complete melting, the wax attains a Newtonian liquid state. This gradual transition occurs as the short-chain fractions melt first, with the longer chains subsequently melting at increasing temperatures until the fully liquid state is achieved (Tewo et al., 2019).

When wax cools, the opposite effect occurs, and its expansion/contraction characteristics are influenced by its components. Like other materials, wax expands when heated and contracts when cooled; however, its rate of expansion relative to metals is notably higher. The rates of expansion and contraction span a temperature range from approximately 20 $^{\circ}$C to the melting point and are non-uniform, varying across the temperature spectrum according to the wax's structural composition (Andrianov et al., 2019). As the wax begins to cool, the short-chain fractions soften even at lower temperatures, causing an initial increase in the expansion curve. This curve then steepens as higher molecular crystalline fractions begin to transform, and subsequently, it rises more gradually as it approaches the liquid state. Conversely, non-crystalline resins exhibit a consistent expansion pattern from the onset of heating until they reach the liquid phase. This consistent behavior is one reason why some resins are blended with wax to diminish its crystalline structure, thereby moderating its capacity for expansion and contraction (Williams and Okonek, 2018).

The base wax used in investment casting patterns primarily consists of paraffin, a hydrocarbon characterized by long, unbranched chains. This paraffin is predominantly derived from the distillation of crude oil. It is favored in casting

techniques for its lower cost and melting point, which significantly influence the mechanical properties of the waxes at room temperature. Conversely, microcrystalline waxes, a blend of solid, purified hydrocarbons, contain branched chains, saturated microcrystalline hydrocarbons, as well as monocyclic and polycyclic compounds, and normal alkanes. These waxes are distinguished by their higher molecular weight, typically containing between 41 to 50 carbon atoms. Unlike paraffin waxes, microcrystalline waxes possess a less defined, smaller crystalline structure, offering different performance characteristics (Zbigniew et al., 2019).

Waxes composed of paraffin, microcrystalline, natural or synthetic wax, and potentially polymeric materials are commonly referred to as base waxes or unfilled waxes. To control and mitigate the expansion and contraction in wax patterns, fillers, and resins are often added, with their content varying from 10% to 50% of the total formulation (Rutto, 2011; Prasad, 2012). Typically, waxes include the following additives within these ranges: Waxes (30-70%), Resins (20-60%), Plastics (1-20%), and Other additives (0-5%) (Srinivasan, 2012). Moreover, the careful selection of components in a wax mixture is crucial for reducing the incidence of defects such as hardness, elasticity, core breakage, wall displacement, non-fill, flow lines, and poor surface finish. The formulation should be optimized to minimize the risk of one type of defect without increasing the probability of others. Economic considerations are also vital, as industrial production must remain cost-effective (Czarnecka-Komorowska et al., 2020). Among the main materials that are added to the base wax include microcrystalline, fillers, and resins.

2.2.3.1 Microcrystalline

Microcrystalline waxes, known for their high degree of plasticity, enhance the durability of wax blends. Available in hard, non-sticky, soft, and sticky variations, these waxes also feature elevated melting points and are commonly blended with paraffin wax (Srinivasan, 2012). However, blending microcrystalline with paraffin wax to create patterns for investment casting introduces several potential disadvantages that warrant careful consideration:

i. Increase dewaxing time: Microcrystalline wax has a higher melting point than paraffin wax, and blending the two can make it harder to achieve the desired melting temperature for the pattern, potentially complicating the dewaxing process (Zbigniew et al., 2019).
ii. Reduced flexibility: Although microcrystalline wax enhances the strength and durability of the pattern, it may also decrease its flexibility. This reduction in flexibility can make it more difficult to remove the pattern from the mould, potentially causing cracks or distortions in the final casting (Kääriäinen et al., 2020).
iii. Increased volumetric expansion: High crystallinity waxes typically show higher volumetric expansion. The degree to which wax molecules are arranged in a crystalline structure is known as crystallinity. As the wax is heated, the molecules begin to move more freely, causing the crystalline structure to break down and resulting in volumetric expansion (Kim et al., 2015).

2.2.3.2 Fillers

Powdered solids, known as fillers, classify pattern waxes as either filled or unfilled. Fillers, possessing a higher melting point than base wax and being insoluble in it, lead to reduced shrinkage during the solidification of the mixture. The extent of this reduction in shrinkage is directly proportional to the quantity of fillers used (Srinivasan, 2012).

The utilization of fillers is increasingly vital as they enhance the properties of the original mixtures. Fillers contribute to improvements in tensile and compressive strength, thermal and dimensional stability, hardness, density, surface quality, chemical resistance, and dielectric strength. They also mitigate the shrinkage, abrasion, thermal shock resistance, absorption, and wear of the model's material (Rutto, 2011). Organic fillers are particularly valued for their minimal residual ash upon burning, unimpaired surface quality due to their low molecular structure, and the minimal phase separation during heating, facilitated by their similar specific weight to waxes (Yuan et al., 2012). Commonly developed and utilized fillers include spherical

polystyrene, thermosetting plastic particles, hollow carbon microspheres, silica, isophthalic acids, organic acids, soybean flour, polymers, and glass (Bemblage and Karunakar, 2011; Rydzkowski et al., 2020).

2.2.3.3 Resins

Incorporating plastics into waxes can mitigate the occurrence of surface cavitation caused by solidification shrinkage to a considerable extent. However, the addition of resins and fillers leads to an even more significant reduction in surface cavitation. Moreover, including resins not only lowers the melting point and thermal expansion of the wax but also enhances its strength. Suitable resins for this purpose encompass coal tar resins, various rosin derivatives, hydrocarbon resins derived from petroleum, and natural resins from sources like dammar, Burgundy Pitch, and terpene(Srinivasan, 2012). When integrating resins into pattern waxes, it is crucial to account for their wide range of softening points and differing viscosities at various temperatures. Additionally, incorporating certain resins can enhance the flexibility of casting pattern waxes, thereby making them more adaptable for crafting complex and detailed patterns (Singh et al., 2018).

Dammar resin, which is a natural product from the bark of some trees in the family Dipterocarpaceae, finds application in numerous uses. Some of these include use in folk medicine, as a painting varnish, and in the production of many products such as adhesives (Martha et al., 2021). In the realm of lost wax casting, dammar resin is frequently added to pattern wax to enhance its flow, reduce shrinkage, improve durability. Furthermore, the inclusion of dammar resin in wax has resulted in more precise and detailed castings (Babalola, 2014). Additionally, dammar resin possesses physical and thermal properties that make it an ideal component in pattern wax, contributing to:

- Thermal conductivity: According to Mills et al. (2006), dammar gum can be used as an additional component to enhance the thermal performance and conductivity of composite phase change materials during their preparation.

Although dammar gum has a lower latent heat compared to tallow and beeswax, its thermal conductivity is significantly higher (Umar et al., 2018).

- Reduction in crystalline structure: The level of crystallinity within wax can significantly affect its thermal expansion, which may be influenced by shear during wax injection. It has been observed that higher crystallinity leads to greater volumetric expansion. The addition of certain resins can effectively reduce the crystalline structure, thereby minimizing the expansion and contraction of the wax (Beeley and Smart, 2008).
- Availability: Natural dammar resin is obtained from shrubs belonging to the Caesalpiniaceae and Dipterocarpaceae families and other families categorized under the genus Dammar. These plants are native to Malaysia, Indonesia, and the East Indies (Martha et al., 2021).

2.2.4 Dewaxing Process Review

The wax removal process is a critical intermediate stage in investment casting. Following the shell-building process, the wax pattern must be extracted from the mould interior to create the required cavity. Typically, the dewaxing method involves heating the ceramic shell, allowing the molten wax to flow out of the mould (Pattnaik et al., 2012). However, in many investment casting operations, the pattern removal process is fraught with challenges, as the mould shell is subjected to significant pressure, leading to cracking. This pressure results from the rapid expansion of the wax, which often occurs when the mould is heated slowly. Therefore, during the dewaxing process, the mould should be heated rapidly from the outside toward the inside. Consequently, the wax layer in contact with the ceramic shell melts quickly before the rest of the pattern has a chance to heat substantially. This strategy provides free space for expansion as the remaining wax heats up (Viswanathan et al., 2008). The molten wax, after being cleaned to remove any process impurities, is often reused in new designs, depending on the level of contamination.

Figure 2.2 summarizes the mechanisms that occur during the dewaxing process, highlighting the stages of heat transfer and their interaction with the properties of ceramic mould and wax. These stages occur sequentially during investment casting and play a crucial role in determining the success of the dewaxing process. Any imbalance in these mechanisms can lead to defects, such as mould cracking. Therefore, careful control of the thermal and material properties throughout the process is essential to minimize the risk of such defects.

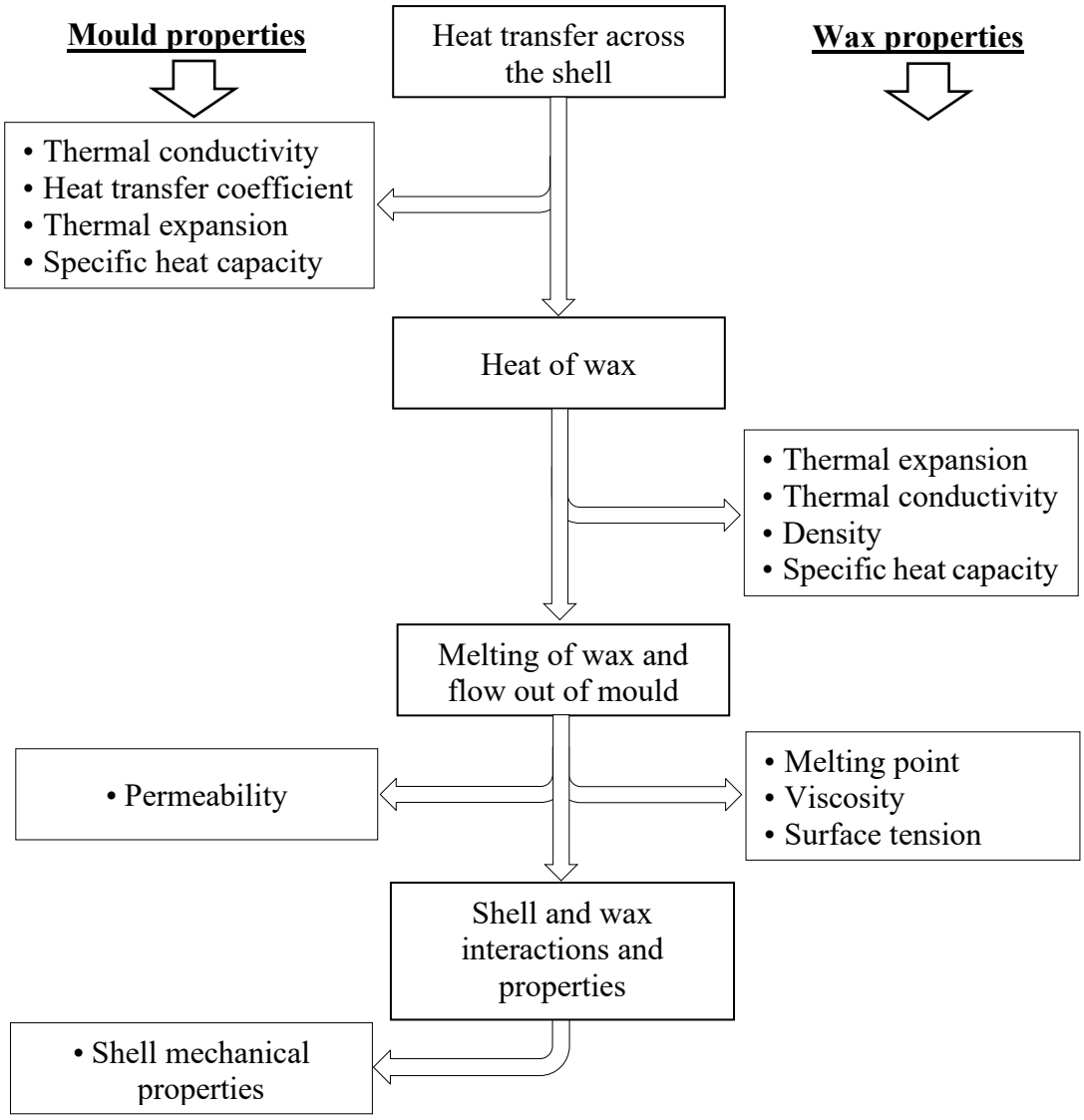

Figure 2. 2 The mechanisms occur during the dewaxing process

Several methods have been developed to melt out pattern wax during the investment casting process, whether conventional or non-conventional techniques. The conventional techniques include: autoclave dewaxing, hot liquid dewaxing, flash-fried dewaxing, and reverse solidification. However, only autoclave dewaxing and high-temperature flash dewaxing have become widely adopted. Hot liquid dewaxing has also found favor among smaller businesses seeking to reduce capital expenditures (Viswanathan et al., 2008; Beeley and Smart, 2023). On the other hand, non-conventional techniques employ electromagnetic radiation, such as microwave dewaxing, for the removal of wax.

2.2.4.1 Autoclave Dewaxing Technique

The autoclave dewaxing process is regarded as the most reliable technique in investment casting, primarily due to its ability to provide uniform heating which reduces stress on the material. In this method, the ceramic moulds containing the wax patterns are positioned on a sliding tray and heated by steam at high temperatures and pressure within an autoclave heating chamber. Saturated steam, typically ranging from 550 to 620 kPa, is utilized, and a steam accumulator is often included to deliver rapid and high pressure(Viswanathan et al., 2008). The schematic of an autoclave is illustrated in Figure 2.3. During this process, the wax typically mixes with the steam condensate, making its recovery challenging and costly. Furthermore, most autoclaves do not completely remove the wax, and the systems are costly to install and maintain. Additionally, operating the boiler is considered relatively risky due to the high pressure of the steam generated, approximately 9 bar, suggesting that while autoclave dewaxing is effective, it may not always be the optimal choice for investment casting (Foster, 1994; Gill et al., 2022).

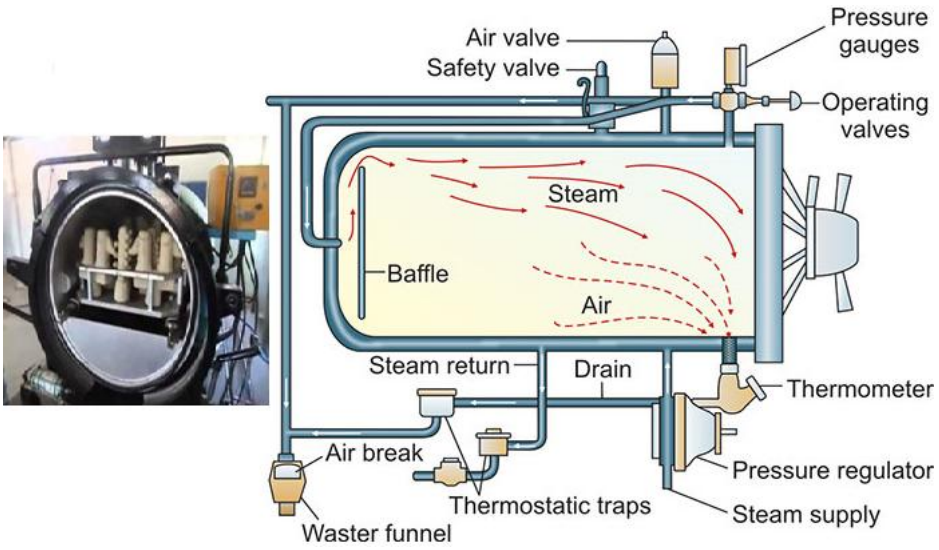

Figure 2.3 Schematic diagram of an autoclave system (VeteranKey, 2016)

2.2.4.2 Flash Fired Dewaxing Technique

In this method, the shell moulds are placed at predetermined cup locations on the load bed, as illustrated in Figure 2.4. Before placing the set into the furnace, the temperature must be set between 870 to 1095°C, depending on the specific requirements of the process. Wax can be removed from the furnace as soon as it melts, facilitated by most furnaces having an open bottom (Viswanathan et al., 2008). As the wax drips to the furnace bottom, it often ignites due to the availability of oxygen and the high temperatures involved. While the flames can be quickly extinguished with water, this method poses a greater risk of damage compared to wax melted in an autoclave. Moreover, recovering the wax can be challenging and costly. To mitigate wax contamination issues, inert, non-aqueous gases such as CO_2 or N_2 are recommended for the flame extinguishing process instead of water (Foster, 1994; Luján et al., 2025).

Compared to the autoclave method, the flash-fired technique places less stress on the moulds and simplifies wax recovery (Foster, 1994). However, this method has not been widely adopted in the investment casting industry due to its high operating costs and the intense combustion of wax at high temperatures (Pattnaik et al., 2012).

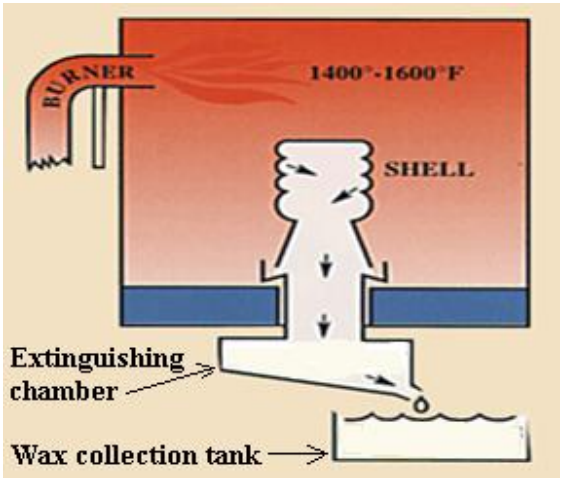

Figure 2.4 Schematic diagram of flash fire dewaxing process (Yahaya, 2016)

2.2.4.3 Dewaxing Techniques Using Electromagnetic Radiation

The usage of microwave heating in industrial processes has been rapidly expanding because of the benefits related to achieving time and energy savings, minimizing environmental effects, volumetric and selective material heating, and improving product quality (Zhang et al., 2024). Some wax compounds used in the investment casting process have varying dielectric properties, which allow them to be heated through microwave absorption (Pattnaik et al., 2012).

A preliminary experimental study was conducted to evaluate and compare the chemical and structural properties, as well as the recyclability, of modeling wax after multiple dewaxing cycles using both autoclave and microwave processing methods. Additionally, the study explored the feasibility of replacing the autoclave with a microwave oven for wax removal, as reported by Brum et al. (2009). A conventional microwave oven (Sanyo) operating at 2.45 GHz and 1100 watts under atmospheric pressure (1 atm) and reaching a maximum temperature of 120 °C was used. Under these conditions, 500 g of wax was completely melted within 20 minutes. The results demonstrate the technical viability of using a microwave oven as an alternative to the autoclave for dewaxing, highlighting the microwave's advantages in preserving wax

purity and maintaining its chemical and structural integrity even after repeated processing cycles.

A similar study was reported by Rani and Karunakar (2013), in which they used a wax blend composed of paraffin, microcrystalline, and carnauba with different mixing percentages. The mixtures were heated in a domestic microwave oven at 2.45GHz and 1100 Watts for 15 minutes. After 10 repeated dewaxing cycles, the results showed that the percentage of linear shrinkage and volumetric shrinkage for each cycle was gradually increased. Another study was done to see the wax behavior of infrared dewaxing. The wax was placed into a home infrared oven and heated for 30 minutes at 215 THz. The wax can withstand a maximum temperature of 110 $^{\circ}$C. The linear and volumetric shrinkage was also found to increase after ten cycles of repeated dewaxing (Rani et al., 2014). Although both methods showed a gradual change in wax shrinkage, the studies found that microwave and infrared dewaxing caused minimal physical and chemical changes. This preserved the structural and chemical integrity of the wax and allowed it to be reused without the need for purification after multiple remelting cycles.

Through the above literature survey, microwaves have been widely exploited for the dewaxing process. However, none of these researchers considered the mould behaviors during this process. Yahaya et al. (2016) Investigating activated charcoal in ceramic shells has significantly affected the process under hybrid heating. It was found that an increased percentage of activated charcoal obtained from oil palm shells has decreased the dewaxing time by about 37.5%. Mixing 25% of activated charcoal was found to be the optimum quantity that should be added to the coarse stucco and applied from layer 3 to layer 6 in order to achieve an almost crack-free shell. Furthermore, the porosity of the shell was improved. However, the strength and density of the shell decreased.

Despite the reduction in dewaxing time with the incorporation of carbon black (CB) (Gill et al., 2021), the amount of wax tested was minimal (10 g), and the issue of wax contamination remains unresolved. Gill et al. (2022) used polyaniline as a microwave susceptor instead of CB in the wax blend and found that incorporating 10%

polyaniline effectively reduced dewaxing time. However, the mechanical properties of the wax decreased, and surface defects and cracks appeared in blends with polyaniline concentrations above 5 wt.%. Pérez-Conesa et al. (2022) assessed a susceptor blend of 25% TiO_2, 25% graphite, and 50% colloidal silica for microwave-assisted dewaxing of ceramic moulds at 2200 W. While the method effectively achieved temperatures over 200 °C, enabling rapid dewaxing and ceramic shell integrity, it also resulted in issues such as wax burning, hotspots, and shell ignitions. Table 2.2 summarizes several improvements in dewaxing time using microwave hybrid heating.

Table 2.2 Dewaxing time reduction using microwave hybrid heating due to the modification of ceramic mould shell compositions or wax pattern blends

Susceptor material	The susceptor was added to:	The Operating Conditions (Domestic Microwave)	Percentage reduction in dewaxing time compared to standard conditions (%)	Reference
Activated charcoal	Ceramic mould shell	2.45GHz, 700 W	37.5%	(Yahaya et al., 2016)
Carbon black	Pattern wax blend	2.45 GHz, 900 W	71.9%	(Gill et al., 2021)
Polyaniline	Pattern wax blend	2.45 GHz, 900 W	72.7%	(Gill et al., 2022)
Titanium oxide (TiO_2)	Ceramic mould shell	2.45GHz, 1100 W	-	(Pérez-Conesa et al., 2022)

* For reductions of 71.9% and 72.7%, the test sample size was only 10 grams.

Based on the evidence presented, it can be stated that utilizing microwave technology for the dewaxing process in investment casting has several advantages compared to traditional methods. Firstly, microwaves have the ability to penetrate the mould deeply, leading to more uniform heating while preserving the physical and chemical properties of wax. Secondly, the process is faster, reducing the overall processing time and enhancing productivity. Thirdly, microwave technology enables selective wax heating, leaving the ceramic mould unaffected, which is not feasible with other techniques. Finally, microwaves are more eco-friendly since they use less

energy and do not emit harmful substances (Barba and D'amore, 2012; Bhattacharya and Basak, 2017; El Khaled et al., 2018; Luján et al., 2025).

2.2.5 Ceramic Shell Building

Ceramic shell mould is a crucial part of the investment casting process after creating the wax pattern. It is a hollow shell that includes the shape and dimensions of the part to be cast or produced. The shell comprises several layers between five and fifteen, depending on the mould's strength requirements (Beeley and Smart, 2008). The construction of the ceramic mould is schematically shown in Figure 2.5. The mould-making process goes through some stages. First, the slurry, composed of a fine refractory powder capable of withstanding high temperatures without deforming or breaking, is mixed with a colloidal binder. Next, a wax pattern is dipped into the slurry, and before the coating dries, the surface is sprinkled with coarse stucco. The mould is then systematically re-dipped into the slurry and coated with stucco until the desired shell thickness is achieved. Each layer must fully dry before the next one is applied (Beeley and Smart, 2008; Pattnaik and Sutar, 2022).

The mould's primary (face) layer is responsible for all the details of the pattern, including its smooth surface and dimensions. The bonding agent gives bonding strength to the mould structure. The coarse stucco particles aid in: (i) stopping the slurry from running off or pulling away, (ii) providing bonding between coating layers, (iii) building mould thickness quickly, and (iv) preventing the mould from cracking (Viswanathan et al., 2008).

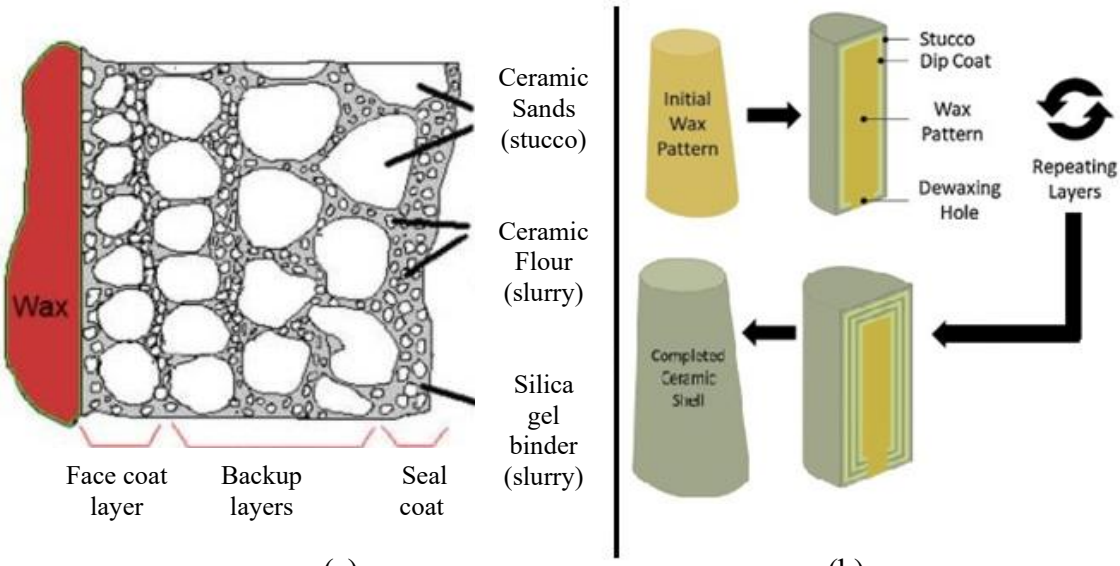

Figure 2.5 Schematic diagram of; (a) the ceramic mould construction (Neto et al., 2017). (b) the dipping and stuccoing process, repeated to form a layered shell [adapted from a diagram by Kanyo et al. (2020)]

During the shell construction process, the green and residual burned strength of the ceramic shell plays an essential role in preventing shell failure or rupture. Thus, to achieve a successful casting, both the physical and mechanical properties of the shell must be taken into consideration (Venkat et al., 2021). Jones and Yuan (2003) and Kumar and Karunakar (2021) summarized the most important requirements that must be met in the ceramic shell as follows:

- Sufficient green strength, green strength protects against strains caused by the thermal behaviour during dewaxing.
- Sufficient fired strength to resist the high thermal shock during metal pouring.
- High chemical stability to avoid interaction between the mould and the molten metal.
- Sufficient mould permeability helps eliminate the gases formed during the casting process through wall mould.
- Sufficient thermal conductivity allows for enough thermal transmission through the mould wall and, as a result, for the metal to cool.

- Low thermal expansion to keep the required mould dimensions from changing; it may happen if the mould is stretched.

Although this requirement list is valid in most casting cases, the ceramic shell needs to meet additional requirements in some circumstances, such as casting superalloys (Pattnaik et al., 2012). For instance, an Al_2O_3–Al_2O_3 ceramic shell shows less interaction with nickel-based superalloys compared to the Al_2O_3–SiO_2 shell (Varfolomeev and Shcherbakova, 2021). Incorporating needle coke into the ceramic slurry enhances permeability, which helps reduce porosity defects in cast parts and allows for improved control over the internal structure of the shell (Kumar and Karunakar, 2021). Moreover, using ceramic materials with additives such as glass fibers and metal powders can enhance mechanical strength and microstructural integrity in superalloy castings (Rakoczy et al., 2019).

2.2.5.1 Refractory Powder of Ceramic Mould

The quality of the ceramic shell depends on the slurry and shell materials, as well as the process used to construct the shell. Investment casting slurry typically consists of refractory powder, liquid binder and sometimes other additives. Surfactants and defoaming agents are critical additives in investment casting slurries, enhancing fluidity and minimizing air entrapment, which can lead to defects. For example, quaternary ammonium salts (QAS) are effective surfactants that can stabilize turbulent flows and reduce drag in various fluids (Naseri et al., 2018). While silicones help reduce foam formation (Pattnaik et al., 2012). Several materials are used as refractory powder and stucco. The most common refractories are silica, zirconium silicates, alumina and aluminium silicates. Other refractories, such as graphite, zirconia and yttria, have also been added, particularly for casting reactive alloys; however, graphite may cost (Viswanathan et al., 2008).

Silica can be created by heating the natural sand to a glass-like and then solidified followed by crushing and filtering to produce stucco particles. Moulds made from silica exhibit high thermal shock resistance due to their extremely low thermal

expansion coefficient. Additionally, silica-based shell material can be chemically removed by exposing it to molten sodium hydroxide or a strong caustic solution, where silica undergoes a chemical reaction that breaks it down into soluble silicates. This process provides a precise method for removing residual ceramic material from complex casting sections that are difficult to clean in other ways (Viswanathan et al., 2008).

Zircon is coarse enough to be used for stuccoing backup coatings, though it is often reserved for prime coats. Its key advantages are its high refractoriness and resistance to wetting by molten metals. Alumina is extracted from bauxite ore using the Bayer process. It is less reactive toward many alloys and more refractory than silica. Therefore, its main application is in superalloy casting. (Davis, 1996). Aluminium silicates often contain mullite ($Al_2O_3.2SiO_2$) with some free silica, typically present as silica glass. They are created by calcining fireclays to produce mullite containing 72% alumina and free silica in varying amounts (Prasad, 2012).

2.2.5.2 Binder Systems

In ceramic processing, binder systems provide a ceramic bond between the refractory particles. These binders, typically organic or inorganic compounds, hold the fine refractory particles together during forming and drying processes, allowing the ceramic structure to maintain its shape before firing. Upon firing, the binders decompose, leaving behind a stable ceramic bond that enhances the mechanical strength and integrity of the material (Sarkar, 2020).

The typical binders used in casting technology are sodium silicate, hydrolyzed ethyl silicate, and colloidal silica. For many years, colloidal silica has been used widely to produce good-quality investment castings due to its excellent bonding properties. The colloidal silica is produced by removing sodium ions from sodium silicate via ion exchange. However, the main drawback of using this binder is due to the poor drying process. The bonding properties of ethyl silicate are improved through hydrolysis in the presence of ethyl alcohol as an exchange solvent, with hydrochloric acid used as a

catalyst in the process. Ammonia is then added as an alkali to further enhance the process and accelerate drying. The ethyl silicate compound dries much faster than colloidal silica; however, it is more expensive and poses higher fire and environmental risks. Therefore, its usage in casting technology has decreased rapidly (Viswanathan et al., 2008). More refractory binders have been developed due to directed solidification and single-crystal processes at higher temperatures or when using reactive superalloys. (Prasad, 2012).

Furthermore, it cannot ignore that many factors influence the choice of the type of binder when making a ceramic mould, including the mould size, pre-heat and fire temperatures, method of mould formation and type of metal being cast (Beeley and Smart, 2023).

2.2.6 Development of Ceramic Mould Shell in Investment Casting

The ceramic mould shell is a crucial element in the investment casting process. Among the problems faced by casting producers are dimensional accuracy, low green strength or fired strength of the shell, rougher surface, and longer production time. Identifying the ideal specification for these parameters is necessary to acquire good casting quality (Clancy et al., 2022). By directly modifying the ceramic slurry before the investment casting process, it is feasible to enhance the qualities of a ceramic mould shell significantly (Kumar and Karunakar, 2021).

In the investment casting process, the permeability of the ceramic mould is one of the greatest challenges besides its strength. In order to improve the permeability, the filler materials were added to the ceramic shell to improve bending strength and permeability (Kumar and Karunakar, 2019). It was also found that the green strength of ceramic mould can be improved by mixing organic polymers with colloidal silica (Wiśniewski, 2021). Although green strength is improved, however, the fired mould strength is likely to suffer due to the decomposition of organic polymers during firing, which can weaken the structure of the ceramic shell. In addition, organic polymers are costly and will affect the overall production cost. Other methods to improve the

permeability of the ceramic mould shell by incorporate the organic or synthetic fibers into ceramic slurries. However, the addition of fibers is only acceptable for casting non-ferrous alloys. These fibers were burned and evaporated, leaving certain pores inside the ceramic mould shell to pass hot gases (Yuan and Jones, 2003). The findings demonstrated that using fibers in the ceramic shell slurry enhanced the shell thickness by 15%. The fiber-modified system also has a higher bearing capacity, and its fired permeability increased greatly. Alternatively, the use of natural such as cattail fibers also have been found to improve the green bending strength by 44%; the permeability increased with sufficient strength in fired mould (Lü et al., 2016a).

The synthetic fibers such as zirconia fibers in an alumina matrix improved the bending strength by 61% compared to the abovementioned natural fibers. Moreover, it has achieved more than 27% of porosity after fired (Chen et al., 2016; Zhu et al., 2019). Yahaya et al. (2016) recorded that the green and fired porosity were 16.455 %, and 22.412%, respectively.

It is also noted that sacrificial pore formation agents (PFAs) can be added to the ceramic slurry to increase the mould permeability (Kline et al., 2010). PFAs are frequently found in both inorganic substances like ammonium carbonate and organic materials, including carbon, walnut shell, rice husk, seeds, and polymers (Kline et al., 2010). However, the acquired permeability using PFAs have negatively affects the strength of the ceramic mould (Kline, 2010). The permeability of the ceramic mould was found improved when adding sawdust particles to the slurry of secondary coats, however, reduced mould's strength (Pattnaik et al., 2017). Similar patterned was found in mould when camphor was added to the conventional slurry (Tamta and Karunakar, 2014). In another study, the green and fired strength ceramic mould were enhanced by adding nano-alumina to the conventional slurry. However, the mould permeability was reduced by adding nano alumina (Tamta and Karunakar, 2019). Table 2.3 summarized different materials that have been utilized in the construction of the mould, and the effect of these combinations on the green and fired strength of the mould.

Table 2.3 Effect of additives materials on the mechanical strength of modified mould shell

The additive material used during ceramic mould fabrication	Heating method	Mechanical strength of green mould shell	Fired strength relative to the standard mould	Reference
Aluminium silicate fiber & polypropylene fiber	Hot water	Increased 35.7%	Decreased	(Lü et al., 2016b)
Activated charcoal	Domestic microwave (2.45GHz & 700 W)	Decreased	Decreased	(Yahaya et al., 2016)
Sawdust	Microwave	Increased	Decreased	(Pattnaik, 2017a)
Nano alumina	Flash fire	Increased 45%	Increased 52%	(Tamta and Karunakar, 2019)
Fine polyethylene wax powder	Microwave	Increased 33%	Increased 3%	(Pattnaik and Sutar, 2022)

The use of reactive alloys has significantly affected the mould-molten material interaction. This is a big obstacle because of their rapid reaction in their molten state with ceramic mould walls. During casting, these alloys are very reactive to refractory oxides, resulting in defects in the characteristics of cast parts. This may be due to their thermodynamic characteristics and chemical compatibility (Hao et al., 2020).

2.2.7 Shell Cracking During Dewaxing Process

Removing wax from the shell is a crucial step in investment casting. However, it can also cause the shell to crack. About 80% of these cracks occur during dewaxing, while the remaining 20% are caused by handling (Snyder et al., 2003; Lee, 2016). The primary cause of shell cracking is believed to be the expansion of wax during the pressure increase stage. This is because, during heating in the autoclave, the wax expands faster than the ceramic shells, leading to a pressure buildup in the shell mould cavity (Pattnaik et al., 2012; Lee, 2016). Accordingly, the permeability of the shell plays a crucial role in enabling steam to penetrate the shell for efficient heat transfer and allowing the mould to relieve pressure (O'sullivan et al., 2021). However, wax is

known to permeate into the mould, but there are still limitations to its flow that can result in incomplete infiltration and potential defects. Kumar and Karunakar (2021) suggested that wax infiltration into the ceramic shell during autoclaving is constrained by the colloidal silica network, which binds the filler and stucco particles together. Lee (2016) indicated that only the base wax is capable of penetrating the primary coat, while the filler particles are filtered out and prevented from entering the fine colloidal silica network.

Thermal expansion in wax is influenced by its crystallinity, as Richards and Mascreen (2003) noted. They observed that crystallinity in wax fluctuates due to shear forces during wax injection, with increased crystallinity leading to greater volumetric expansion, especially when it reaches its melting point. In contrast, Beeley and Smart (2008) demonstrated that adding specific resins can reduce the crystalline structure, thereby minimizing expansion and contraction. Their findings also indicated that resin exhibits a linear thermal expansion with temperature (Figure 2.6). This indicates that resin expands steadily and predictably with rising temperatures without sharp changes in expansion rates. Furthermore, combining resin with a homogenous crystalline material produced an intermediate thermal expansion curve, represented in Figure 2.6 as 'wax.' Additionally, the researchers discovered that thicker sections of wax expand at a slower rate than thinner sections, possibly due to the higher shear forces experienced by thinner sections, which may promote greater crystallinity (Li et al., 2021).

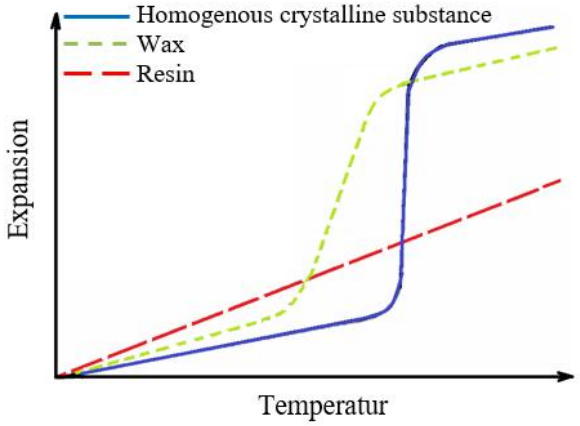

Figure 2.6 Comparison of the expansion behavior of a pure crystalline substance, resin, and wax (a mixture of crystalline and resin components) (Beeley and Smart, 2008)

The primary coat of the mould plays a crucial role in determining the overall permeability of the mould (Pattnaik and Sutar, 2022). Whitehouse and Dahlin (2008) further emphasized that in a mould system consisting of a single primary coat followed by six backup layers, the primary coat alone can account for up to 50% of the mould's total permeability. Their study also demonstrated that wax viscosity significantly influences shell integrity, where higher viscosity results in a slower dewaxing rate and an increased probability of cracking.

Several other mechanisms have been proposed as contributors to ceramic shell cracking, such as insufficient green strength, inconsistency in the wax blend, inadequate gates for liquid wax flow, the excessively high viscosity of the liquid wax, and complicated mould geometry (Lee, 2016). However, a number of studies have shown that the green strength of the mould decreases with increasing moisture content, whether during mould preparation or autoclave heating (Freitag et al., 2017; Yuan et al., 2005). Another key factor is the thermal conductivity of wax. Higher thermal conductivity results in the formation of a thicker wax layer during, prior to reaching the softening point. This thicker layer expands more, increasing the likelihood of shell cracking (Grzeskowiak et al., 2015). Additionally, an investigation has examined the relationship between temperature, the duration of pattern removal, and ceramic shell performance in investment casting by Gebelin and Jolly (2003), they found that as the temperature during pattern removal increased suddenly, the length of cracks in the ceramic shell also increased.

The issue of reduced shell strength is made worse in the corners and leading edges of the mould design, where the thickness of the shell is less than that of the flat sections due to a decrease in surface area. The decrease in surface area results in a lower stucco volume density at these edges, as shown in Figure 2.7, which increases the likelihood of crack propagation in areas of the mould that are already under stress (Kline, 2010; Tamta and Karunakar, 2019). Correspondingly, Richards and Mascreen (2003) discovered that thinner sections of shells have a higher wax expansion rate than thicker sections. This could be attributed to the increased shear experienced by the wax in thinner sections, leading to more crystalline formation. This finding highlights why shells are more prone to cracking at sharp edges. Other investigation was done by

Komaragiri et al. (2013) to understand how pattern geometry affects shell cracking. The researchers found that patterns with rounded corners tend to cause shell cracking lower than patterns with sharp corners. Additionally, their study confirmed that thick shells are more capable of withstanding the pressure caused by pattern expansion during firing than thin shells.

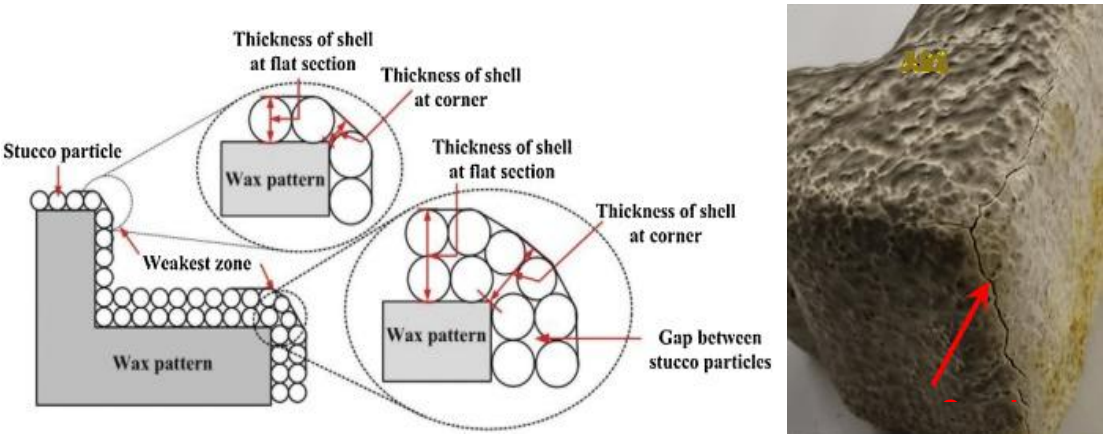

(a) (b)

Figure 2.7 (a) Schematic depicts the surface retention along flat sections and sharp edges (reproduced from reference (Tamta and Karunakar, 2019)). (b) serious shell cracking on the surface edge (Fedorov et al., 2022)

Various heating methods can be affected the mould shell cracking during the dewaxing process. Autoclave heating, for example, raises the moisture content of the mould, which in turn promotes cracking. In contrast, direct microwave heating can cause uneven temperature distribution, leading to the formation of plasma and hot spots. These hot spots generate significant thermal stress within the ceramic material, ultimately resulting in crack formation (Dąbrowska et al., 2018).

2.3 Theory and Background of Microwave Heating

Microwave heating is quickly becoming a popular and useful tool in different technological and scientific disciplines. Unlike traditional heating, microwave heating involves converting energy from electromagnetic radiation to thermal energy rather than heat transmission. The microwave energy is delivered directly to the substance

through molecular interaction with the electromagnetic field. Volumetric heating occurs when microwaves penetrate materials and disperse energy, producing heat across their volume. In addition to volumetric heating, microwave heating has a range of benefits which will be referred to later in this chapter. Understanding the fundamentals of microwave interactions is necessary for better application of microwave technology.

2.3.1 Fundamentals of Microwave Heating

Microwave is an unparalleled heat source that is widely used in various technological and scientific fields, for example; food industry and processing, radio astronomy, medical treatments, treatment of medical waste, domestic purposes, sintering of metals and ceramics and many other physical and chemical fields especially in recent years (Guo et al., 2017; Chandrasekaran et al., 2012). Electromagnetic radiation is a type of energy that moves through free space in a wave-like pattern from 300 MHz to 300 GHz, as shown in Figure 2.8. The waves consist of equally electric (E) and magnetic (B) fields that are orthogonal to each other, as shown in Figure 2.9 (Ling et al., 2016).

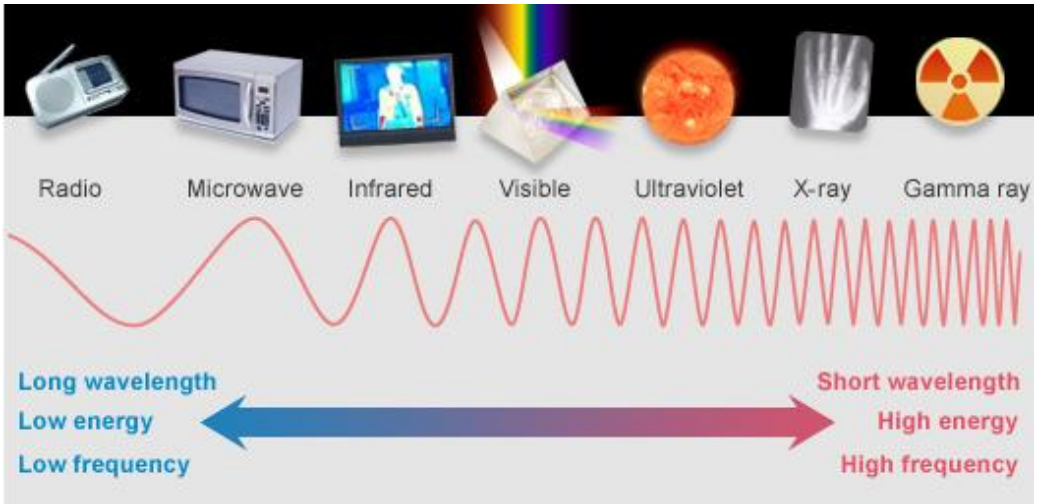

Figure 2.8 The electromagnetic spectrum (Butcher, 2016)

For industrial applications, including plastic manufacture, rubber extrusion, treatment of ceramics, food processing etc, the most widely utilized frequencies are 0.915 GHz (λ= 32.7cm) and 2.45 GHz (λ= 12.2cm) (Torgovnikov and Vinden, 2009). However, microwave energy is generated by converting electrical energy, with a conversion efficiency of about 50% for 2450 MHz and 85% for 915 MHz (Gupta and Sharma, 2011). In addition, microwave furnaces with tunable frequencies ranging from 0.9 to 18 GHz have recently been created for material processing (Brodie, 2012).

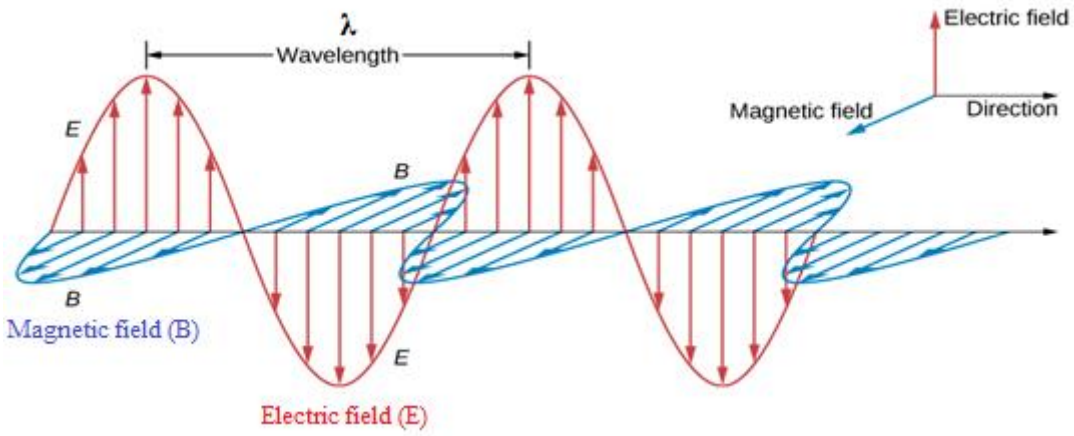

Figure 2.9 Plane of electromagnetic waves (Ling et al., 2016)

Microwaves behave similarly to light waves; they change direction while passing through one dielectric material to another. It can be reflected by metallic objects, absorbed by materials with specific dielectric properties, or transmitted without considerable absorption via other dielectric materials. However, it depends greatly on the nature of the material (Bansal and Vasudev, 2022). Therefore, a material can be classified in one of the following three types (Fernández et al., 2011), as shown in Figure 2.10.

i. Insulator (transparent): the material where microwaves pass through without any loss of energy.
ii. Conductor (reflective): the material that completely reflects the microwave, thus is difficult to penetrate.

iii. Absorber (dielectric): the materials that absorb the highest amount of microwave energy.

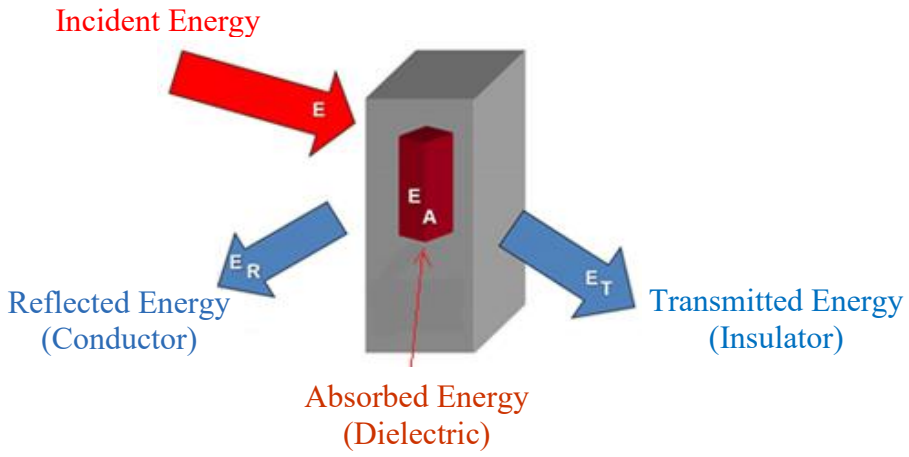

Figure 2.10 Reflection, Absorption, and Transmission of microwave radiation

The fundamental relationship between electromagnetic radiation energy (Ei), wavelength (λ), and frequency (v) is defined by Equation (2.1) (Sindhu, 2006).

$$Ei = hv = \frac{hc}{\lambda} \tag{2.1}$$

Where h is Planck's constant, c is the velocity of light (3.8 x 10^8 m.s^{-1}).

Infrared radiation primarily induces bond vibrations, whereas microwave radiation causes molecular rotation. The energy of microwave photons at the commonly used frequency for microwave heating systems (2.45 GHz, corresponding to a wavelength of 12.24 cm) is approximately 0.00001 eV. This energy is significantly lower than the strength required to break hydrogen bonds and is also much weaker than the energy associated with Brownian motion. Consequently, the energy absorbed from microwaves is incapable of breaking chemical bonds in materials (Stuerga, 2006).

2.3.2 Mechanisms of Material's Polarization

Microwave heating operates through energy transfer at the molecular level, relying on the dielectric properties of materials to achieve effective heating. This process occurs through the interaction of high-frequency electromagnetic radiation with the material, which is why it is commonly referred to as dielectric heating. Specifically, dielectric heating arises from the interaction between the electric field component of the electromagnetic waves and the dipoles within the material, as illustrated in Figure 2.11. Furthermore, the polarization mechanisms underlying this process can be categorized into four fundamental divisions, as detailed by Das and Banik (2021):

- dipolar/ molecular polarization P_m (rotation of dipoles)
- ionic conduction P_i (ionic polarization)
- electronic polarization P_e (atomic polarization)
- interfacial polarization P_S (surface polarization)

Microwave dielectric heating operates based on two primary mechanisms: dipolar polarization and ionic conduction. In the dipolar polarization mechanism, dipoles within the material respond to external electric waves by rotating to align with the direction of the electric field. However, under a high-frequency electric field, the dipoles cannot fully adjust to the rapid oscillations. This inability to keep pace results in dielectric heating, which arises from dielectric loss and molecular friction. Materials such as water and oil exemplify this phenomenon, where internal friction leads to volumetric heating (Das and Banik, 2021).

In the conduction mechanism, ionic polarization occurs due to dissolved or dissociated charged particles. These particles oscillate back and forth under the influence of the microwave electric field, thereby generating an electric current. The oscillatory motion causes the charged particles to collide with surrounding atoms or molecules, resulting in electrical resistance. This resistance leads to internal molecular friction, which subsequently produces volumetric heating and heat energy within the material. These two mechanisms; dipolar polarization and ionic conduction, typically

operate simultaneously during microwave heating. This interplay is particularly significant in systems where a conducting material is dispersed within a non-conducting medium (Horikoshi et al., 2012; Das and Banik, 2021).

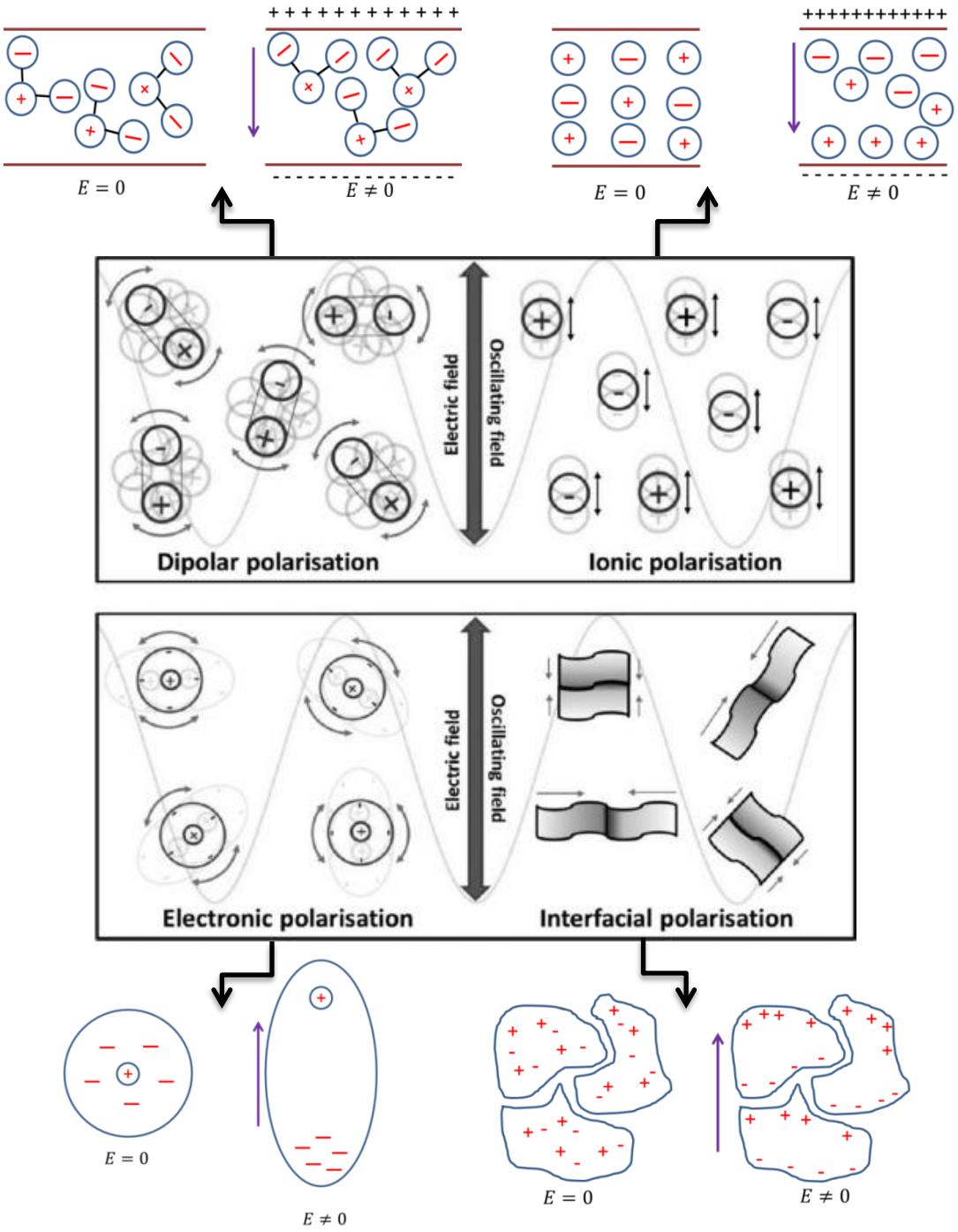

Figure 2.11 Schematic representation of the four divisions of polarization mechanisms [modified from Das and Banik (2021)]

In the third mechanism, neutral atoms become polarized, causing a shift in the electrons and their center relative to the nucleus, resulting in the formation of a dipole moment. The fourth mechanism involves polarization due to charge accumulation on the material's contact surface. Collectively, the net polarization (P) of a dielectric substance is determined by the combined contributions of all these mechanisms, as expressed in Equation (2.2) (Das and Banik, 2021).

$$P = P_e + P_i + P_m + P_S \tag{2.2}$$

Where; P_e is the electronic polarization, P_i is the ionic conduction, P_m is the molecular polarization, and P_S is the surface polarization.

2.3.3 Parameters Affecting Microwave-based Heating Processes

Loharkar et al. (2019) identified four critical parameters that significantly influence microwave heating: (i) the dielectric and magnetic properties of the materials, (ii) the heating mechanisms, (iii) the load subjected to microwave heating, and (iv) the heating applicators and the variables governing these parameters. Adequate knowledge of these parameters and the variables compared is necessary for controlling and optimising the microwave processing of materials. As microwaves are electromagnetic radiation, the heating is largely governed by the dielectric and magnetic properties of the materials. These parameters and their interrelations are illustrated in Figure 2.12.

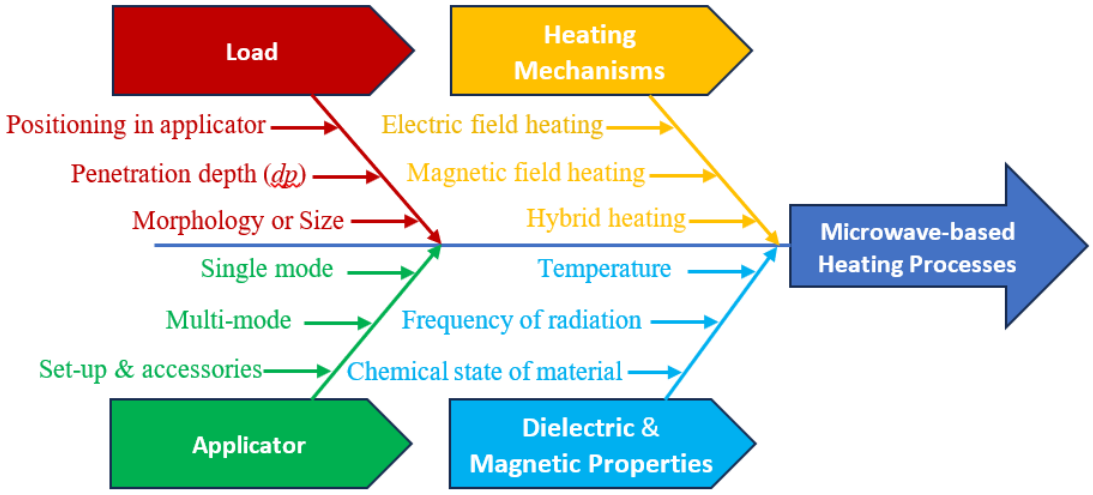

Figure 2.12 Parameters that affect microwave-based heating processes (Loharkar et al., 2019)

The microwave heating process is fundamentally governed by the interaction of electromagnetic fields with the dielectric and magnetic properties of materials, which are defined by complex permittivity (ε*) and permeability (μ*); their real parts represent energy storage, while the imaginary parts indicate energy dissipation as heat. The efficiency of this heating largely depends on the dielectric and magnetic loss tangents (tan δε and tan δμ), with materials exhibiting high loss tangents being more effective absorbers of microwave energy. These properties are influenced by factors such as temperature, frequency, and composition (Loharkar et al., 2019). Heating mechanisms occur through electric and magnetic field interactions: electric field heating involves dipolar polarization, ionic conduction, and the Maxwell–Wagner effect, while magnetic field heating includes eddy current losses, hysteresis, and magnetic resonance. For poorly absorbing materials, microwave hybrid heating (MHH) using susceptors like SiC or graphite enhances heating efficiency by initiating conduction-based heating (Miyata et al., 2023). The load itself, which refers to the material being processed, affects microwave absorption based on its size, shape, placement within the applicator, and penetration depth. Optimal load design ensures uniform heating, while powders and porous structures improve coupling due to higher surface areas; poor placement can cause uneven heating, particularly in multi-mode cavities (Loharkar et al., 2019). Applicator design also plays a key role, with single-mode applicators offering precise, uniform heating suitable for smaller loads, and

multi-mode applicators enabling larger-scale processing but with less uniformity. Accessories such as stirrers, rotating platforms, gas inlets, and vacuum systems further aid in enhancing performance (Zheng et al., 2023).

Among all influencing factors, material properties play a crucial role in determining the energy absorption potential in an electromagnetic field. Therefore, understanding material property-microwave electromagnetic property relations and interaction phenomena are essential to effective microwave processing. The following sections briefly discuss the mathematical model for estimating power absorption, the significance of governing equations in applicator design, and the key concepts underlying microwave-material interactions:

2.3.3.1 Maxwell's Equations

In microwave-material interactions, Maxwell's Equations (Equations 2.3–2.6) are used to describe the physics of the heating phenomenon (Equations 2.3–2.6) (Ayappa et al., 1991). These equations provide the foundational framework for understanding microwave propagation and its interaction with materials, and regulating the heating behavior. The key Maxwell's Equations relevant to this context are as follows:

$$\nabla . D = \nabla . (\varepsilon^* E) = \rho \tag{2.3}$$

$$\nabla . B = \nabla . (\mu H) = 0 \tag{2.4}$$

$$\nabla \times E = -\frac{\partial B}{\partial t} \tag{2.5}$$

$$\nabla \times H = J + \frac{\partial D}{\partial t} \tag{2.6}$$

Where; E is the electric field intensities (V/m), H is the magnetic field intensities (A/m), D is the electric flux density (W/m^2), B is the magnetic flux density (C/m^2), J denotes the current density (J=σE) , $\partial D/\partial t$ is the displacement current density, ε^* is the complex permittivity of material (F/m), and μ is the magnetic permeability (H/m).

It is essential to understand how the utilized electromagnetic fields interact with the material dielectric properties to know how the electromagnetic energy is transformed into heat inside the target material. To calculate the microwave power (P_{MW}) (W/m^3) transmitted across the material surface, the Poynting Vector Theorem, derived from Maxwell's equations, can be applied, as shown in Equation (2.7) (Thostenson and Chou, 1999).

$$P_{MW} = \sigma |E|^2 = 2\pi f \varepsilon'' E^2 \quad (2.7)$$

Where; σ is the conductivity of a material (Siemens/m), E= electric field intensity inside the material (V/m), f = frequency (Hz), ε''= loss factor. Equation (2.7) above shows that the ability of any material to absorb the microwave's power varies with each frequency, loss tangent, dielectric constant and electric field square (Meredith, 1998).

2.3.3.2 Dielectric and Magnetic Properties

Dielectric characteristics are among the most critical properties to consider when evaluating the effectiveness of microwave-induced heating, as they determine how a material interacts with electric fields. Therefore, a thorough understanding of a material's dielectric properties is essential. Additionally, microwave electromagnetism inherently causes electric and magnetic fields to interact with electrons, ions, or molecules at a finer level (Reeja-Jayan et al., 2012). The dielectric property that defines a material's heating ability is the complex permittivity (ε*), as described by Chandrasekaran et al. (2012). This property is mathematically expressed by Equation (2.8).

$$\varepsilon^* = \varepsilon' - j\varepsilon'' \quad (2.8)$$

Where; ε' is the dielectric constant determining a material's ability to absorb microwaves and store electric energy, ε'' is the dielectric loss factor representing the material's ability to convert absorbed energy into useful heat.

The magnetic field also plays a significant role in microwave heating, which should not be overlooked compared to heating driven by the electric field. However, limited research has focused on the effects of microwave heating on magnetic fields (Peng et al., 2012). Unlike dielectric materials, magnetic materials possess magnetic dipoles that interact with the alternating magnetic field, causing oscillation (Haimbaugh, 2015). In practice, magnetic loss is a critical factor in microwave heating, as discussed extensively by Mishra and Sharma (2016). Yoshikawa et al. (2006) investigated the effects of microwave interaction on iron particles and ferromagnetic materials. The complex permeability (μ*) is the crucial property determining the loss and storage of magnetic energy for magnetic materials. This property is mathematically defined in Equation (2.9) (National and Stein, 1994).

$$\mu^* = \mu' - j\mu'' \quad (2.9)$$

Where; μ' is the magnetic permeability, its ability of a material to magnetic energy, μ'' is called magnetic loss factor, its ability of a material to convert the magnetic energy to heat.

The process of storing energy and converting it into heat within a material depends on its dielectric properties, which include the dielectric constant (ε′) and the dielectric loss factor (ε″). The dielectric constant represents the material's ability to store energy in an electric field, while the dielectric loss factor refers to the energy dissipated as heat when the electric field is applied. Materials exhibiting a high dielectric constant have a greater ability to store electrical energy, while those with a low dielectric constant are less effective at energy storage. Whereas a smaller loss factor denotes less energy absorption, a larger loss factor shows that the material absorbs more energy and transforms it into heat. The loss factor is especially important

in the context of microwave heating since it dictates the conversion efficiency (Chen et al., 2004; Siores and Do Rego, 1995). Therefore, the dielectric properties of a material are critical in microwave processing, as they govern how effectively the material absorbs and converts microwave energy into thermal energy.

According to the literature, dielectric materials with a loss factor (ε'') below 0.01 exhibit minimal interaction with microwaves, resulting in poor heating performance (Sebastian et al., 2015; Yahaya, 2016). The loss tangent quantifies the ability of a material to convert electromagnetic energy into thermal energy ($\tan \delta$), which is defined by Equation (2.10) (Bhattacharya and Basak, 2016; Chen et al., 1993; Meredith, 1998).

$$tan\ \delta = \frac{\varepsilon''}{\varepsilon'} \tag{2.10}$$

As indicated by Equation (2.10), selecting an optimal combination of dielectric constant and dielectric loss is essential to achieve effective interaction between microwaves and the material. The dielectric properties of a material are influenced by factors such as composition, structure, and temperature. Moreover, these properties are further affected by variables, including temperature, frequency, purity, chemical conditions, and the manufacturing method (Gupta and Leong, 2008; Ramesh et al., 1999).

2.3.3.3 Microwave Penetration Depth

Microwave penetration depth (*dp*) measures the extent to which microwaves penetrate a material. It can also be defined as the distance from the material's surface where the microwave power reduces to 1/e (≈0.368) of its initial value (Bansal and Vasudev, 2022).The *dp* can be calculated using Equation (2.11) (Lv et al., 2018).

$$d_p = \frac{\sqrt{2}\,c}{\omega\ \sqrt{\varepsilon_r'\,\mu_r'}}\ \left[(1 + tan^2\,\delta\varepsilon\ tan^2\,\delta\mu + tan^2\,\delta\varepsilon + tan^2\,\delta\mu)^{1/2} + tan\,\delta\varepsilon\ tan\delta\mu - 1\right]^{-1/2} \quad (2.11)$$

$$tan\,\delta\varepsilon = \frac{\varepsilon_r''}{\varepsilon_r'} \quad , \quad tan\,\delta\mu = \frac{\mu_r''}{\mu_r'} \quad (2.12)$$

Where; c is the velocity of light, $c = 1/\sqrt{\varepsilon_0\,\mu_0}$ = 3×10^8 m/s, ω is the angular frequency $\omega = 2\pi f$ (s^{-1}), ε_r' is the relative dielectric constant, μ_r' is the relative magnetic constant, ε_r'' is the relative dielectric loss factor, μ_r'' is the relative magnetic loss factor, and $tan\delta\varepsilon$, $tan\,\delta_\mu$ are the dielectric and magnetic loss tangents.

The penetration depth of microwaves (*dp*) is inversely related to frequency and the effective dielectric and magnetic loss factors. In other words, at a fixed frequency, materials with a high capability to convert microwave energy into heat generally exhibit a low penetration depth. Conversely, materials with a low loss tangent (tan δ) tend to have greater penetration depths. However, certain materials with exceptionally low loss factors, such as high-purity quartz glass and non-polar substances, are nearly transparent to microwaves, allowing them to pass through with minimal energy loss. Nevertheless, when the penetration depth is significantly smaller than the sample diameter, the penetration of microwave energy is restricted, leading to uneven heating. To ensure effective microwave heating, the penetration depth should ideally be comparable to the sample's dimensions (Bansal and Vasudev, 2022).

In the case of materials that solely interact with an electric field ($\mu_r'' = 0$), the Equation (2.11) of penetration depth can be reduced as Equation (2.13) (Peng et al., 2010).

$$d_p = \frac{\sqrt{2}\,c}{\omega\left[\varepsilon'(\sqrt{1+(tan\delta\varepsilon)^2}-1\right]^{1/2}} \quad (2.13)$$

The penetration depth is important for quantifying microwave interactions with materials, and it is used to classify materials as; (i) reflectors or opaque material, (ii) transparent material and (iii) absorbent material.

Variations in the strength of the electric (E) and magnetic (H) fields across the thickness of a material result in distinct microwave absorption capabilities among different materials. As the electric loss factor increases, the strength of the E and H fields decreases. Moreover, the energy absorption per unit volume of a material rises with an increase in the loss factor; however, penetration depth correspondingly decreases. The energy absorption per unit volume reaches its maximum when the loss factor attains a critical value. The amount of energy absorbed per unit volume and the penetration depth are strongly influenced by the material's molecular structure. Both parameters decrease as the efficiency of energy conversion within the material diminishes. Conductive metals, such as bulk metals, exhibit the highest dielectric loss factor, resulting in significant microwave reflectance. However, despite this high reflectance, the power absorption (P) remains minimal (Mishra and Sharma, 2016).

Reflectors are materials characterized by exceptionally shallow penetration depths, with metals being the most common example, as shown in Table 2.4. In such materials, electrons tend to concentrate at surfaces and edges due to the penetration of electromagnetic waves. This accumulation of kinetic energy can lead to ionization and breakdown in the surrounding area. Consequently, significant heat and energy are generated during this discharge process, resulting in localized "hot spots." This energy release manifests as arcing or plasma formation (El Khaled et al., 2018). Conversely, transparent materials, which are low-loss materials with exceptionally large penetration depths ($\tan \delta\varepsilon \leq 0.01$), allow microwaves to pass through with minimal absorption. Typical examples of such materials include alumina, fused quartz, Teflon, and polystyrene, which have penetration depths exceeding 500 mm at 2.45 GHz, as illustrated in Table 2.4. The third category comprises highly lossy materials with penetration depths of a few centimeters ($\tan \delta\varepsilon \geq 0.1$). This category of materials easily absorbs microwaves, transforming the energy into heat; among these materials are SiC, carbon and water (Bhattacharya and Basak, 2016).

Microwave heating is increasingly considered for high-temperature processing applications due to its ability to deliver rapid, volumetric, and selective heating. However, its direct application to the investment casting (IC) process, particularly during the dewaxing and shell firing stages, requires careful evaluation of material compatibility, energy absorption mechanisms, and geometric constraints. In investment casting, the ceramic moulds used are typically poor microwave absorbers due to their low dielectric loss (Li et al., 2022). However, wax materials typically exhibit low dielectric loss, making them also poor absorbers. This limitation necessitates the use of microwave susceptors, such as SiC, graphite and carbon materials. These susceptors are incorporated into the shell structure to enhance coupling with microwave energy, efficiently absorb microwaves, generate heat, and transfer it to surrounding low-loss materials via conduction. This mechanism accelerates dewaxing and firing by enabling localized heating at the wax–shell interface, improving process uniformity and reducing cycle times (Pérez-Conesa et al., 2022). The microwave penetration depth must ideally match the thickness of the mould shell to ensure efficient and uniform heating during dewaxing. If the *dp* is too small, energy is absorbed only at the surface, leading to non-uniform heating; if too large, microwaves may pass through the material with insufficient energy deposition (Gamit and Chudasama, 2020).

Limited studies have demonstrated the benefits and challenges of using microwave hybrid heating (MHH) in IC process. For example, Yahaya et al. (2016) incorporated activated carbon into ceramic shells and achieved improved microwave absorption and uniform heating. Similarly, Pérez-Conesa et al. (2022) reported that the addition of TiO_2–graphite enhanced the ceramic shell's ability to couple with microwave energy. Therefore, microwave heating is highly applicable to the IC process when the material properties and heating mechanisms are properly understood and optimized. Enhancing the dielectric properties of the mould and aligning the microwave penetration depth with the shell geometry are key to maximizing heating efficiency and process performance.

Table 2.4 Typical examples of microwave materials categorized as reflectors, transparent, and absorbing, including their penetration depth and loss tangent values at room temperature

Reflector		Microwave transparent			Microwave absorber			Reference
Bulk metal	*dp* (mm)	Material	*Tan δε*	*dp* (mm)	Material	*tan δε*	*dp* (mm)	
Al[1]	0.0017	Alumina[1]	0.001	126	SiC[1]	0.37	19.3	[1](Gupta and Leong, 2008; Balanis, 2012)
Cu[1]	0.0013	Fused quartz[1]	0.0003	757.3	Water[1]	0.15	30	[2](Greenacre, 1998)
Au[1]	0.0015	Borosilicate glass[1]	0.0012	150.7	Carbon Black (20 μm)[3]	0.23	57.5	[3](Hotta et al., 2011)
Zr[1]	0.0067	Teflon[1]	0.0004	564	Graphite Powder (20–80 μm)[3]	0.36 - 0.67	13.4 - 20.9	[4](Atwater and Wheeler Jr, 2003; Atwater and Wheeler Jr, 2004)
Ag[1]	0.0013	Mullite[1]	0.0015	102	Activated Carbon[4]	0.31- 0.9	7- 34.3	[5](Wu et al., 2008; Pickles, 2009)
Note: Most values were obtained at a frequency of 2.45 GHz		Yttria stabilized zirconia[2]	0.0011	>50	Charcoal[5]	0.14 - 0.38	60 -110	[6](Hong et al., 2014)
		Polystyrene[1]	0.0003	762	Carbon Fibers[6]	0.45 - 0.5	5 - 7	[7](Lin et al., 2007)
		Silicon[1]	<0.012	>39.6	Carbon Nanotube[7]	1.11	2	

2.4 Microwave Furnace

A microwave furnace is an electric device that heats items/ materials by exposing them to high-frequency electromagnetic waves called microwaves. The equipment of typical industrial microwave heating as presented in Figure 2.13. Basically, the microwave heating system has three major components; microwave source (generator), transmission lines (waveguides), and applicator. The capacity to build these components and combine them into an efficient system for processing materials necessitates knowledge and comprehension of electromagnetic theory (Thostenson and Chou, 1999).

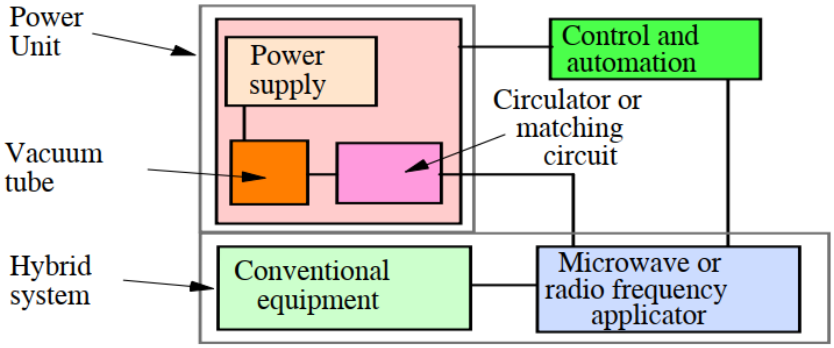

Figure 2.13 Main components of industrial microwave (Metaxas and Meredith, 1993)

Typically, the acceleration of charges generates electromagnetic radiation. To achieve the high power and frequency necessary for microwave heating, most microwave sources rely on vacuum tubes. Various types of vacuum tubes, such as magnetrons, traveling wave tubes (TWTs), power grid tubes, crossed field amplifiers (CFAs), klystrons, and gyrotrons have been employed (Kenji et al., 1986; Gupta and Leong, 2008). Furthermore, a microwave applicator serves as the chamber that channels microwave radiation from the source to the target material. These applicators are classified into different types based on their field strengths, with monomode (single mode cavities) and multimode cavities being the most prevalent. The selection of an applicator type typically hinges on the specific materials requiring processing (Fidalgo Fernández and Menéndez Díaz, 2013).

2.4.1 Single-mode Applicators

In these systems, the applicator operates at a singular resonant mode of microwave frequency, typically illustrated in Figure 2.14 as a 2.45 GHz single-mode cavity. Such an arrangement affords precise control over microwave process parameters due to predictable field distribution across the load. Notably, the primary advantage of single-mode applicators is their rapid heating capability, among other benefits. However, a significant limitation is that they can only treat one vessel at a time, restricting throughput (Fidalgo Fernández and Menéndez Díaz, 2013).

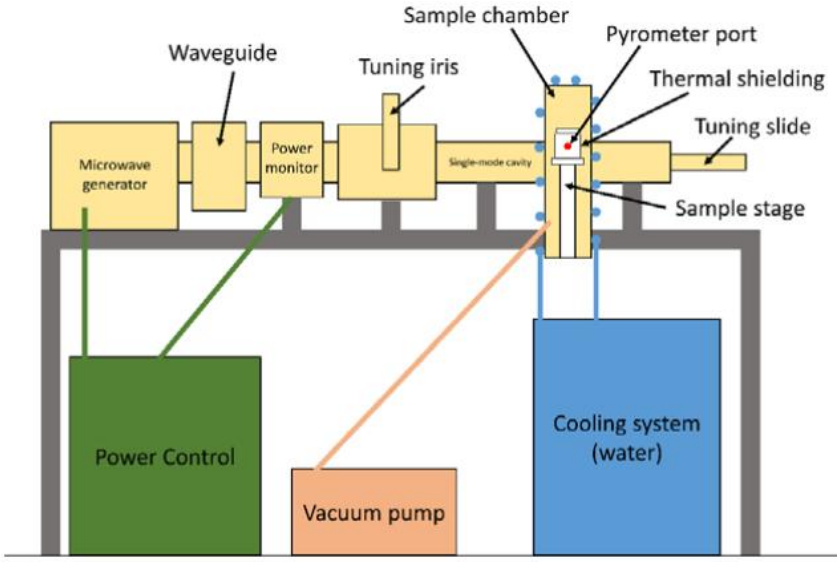

Figure 2.14 Schematic diagram 2.45GHz single-mode cavity microwave (Blair et al., 2018)

2.4.2 Multi-mode Applicators

Multi-mode microwave applicators, characterized by a broad cavity enclosed by conducting walls, facilitate the generation of multiple electric field modes due to reflections from the oven walls(E Wong and Gupta, 2006). This category encompasses both traditional simple microwave ovens and contemporary household models, as depicted in Figure 2.15. Moreover, these applicators offer reduced sensitivity to the placement or geometry of the product compared to single-mode applicators, making

them suitable for either batch or continuous flow processes and ideal for hybrid heating applications (National and Stein, 1994).

In these systems, the simultaneous presence of several modes creates multiple hot spots, thereby inducing significant chaos within the cavity. This chaos enhances the dispersion of radiation, consequently expanding the effective heating area. Accordingly, a multi-mode microwave heating system can contain several samples at the same time, unlike a single-mode system (Rana and Rana, 2014).

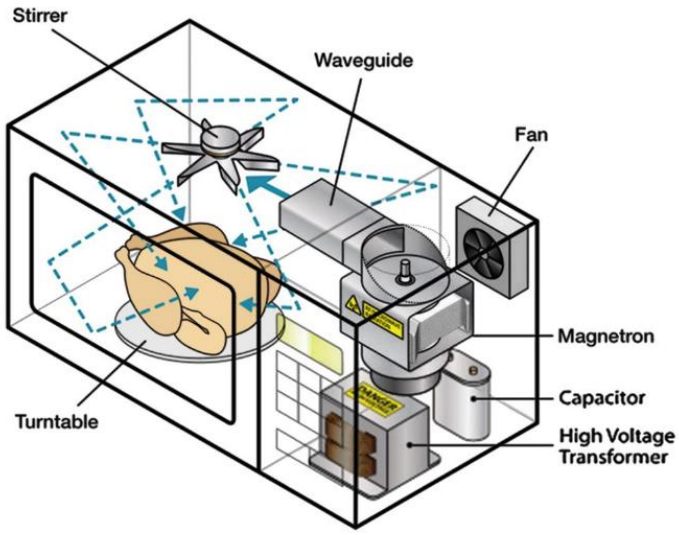

Figure 2.15 Schematic diagram of the multimode-household microwave oven (Paleotronic, 2020)

However, a major drawback of multi-mode apparatus is the uncontrolled heating of samples, leading to temperature inhomogeneity. To address this challenge and achieve more uniform heating at the prevalent microwave frequency of 2.45 GHz, several strategies have been employed:

- The introduction of a turntable to mitigate the effects of multiple hot spots (Tran, 1991).
- The use of mode stirrers (reflective fans) positioned near the waveguide to distribute energy more evenly (Tran, 1991).
- The application of hybrid heating techniques to enhance temperature uniformity (Janney et al., 1992).

2.5 Microwave Heating Techniques

Microwave heating began in the 1940s, about 75 years after James Clerk Maxwell developed the electromagnetic theory in 1864 (Sobol and Tomiyasu, 2002). Since its inception, extensive research has been conducted to investigate the application of microwaves in hybrid heating technologies, driven by benefits such as reduced processing times and significant cost and energy savings through quick and volumetric heating of materials. Studies indicate that microwave heating can achieve energy cost reductions exceeding 95% (Gao et al., 2020; Jie et al., 2019). This technique has been applied to a diverse range of materials, including ceramics, polymers, rubber, glass, semiconductors, metals, biomaterials, powders, chemicals, and wastes. Currently, microwave technology is prominently used in various industrial applications such as sintering, joining, melting, drying, chemical synthesis, and the treatment and recycling of sewage sludge, among others, employing both direct and indirect heating methods (Baghel, 2023).

Microwave technology is utilized extensively in both low and high-temperature processes due to its myriad benefits. Low-temperature applications include melting frozen foods, pasteurizing milk products, concentrating fruit juices, eradicating undesired microbes, removing moisture, various biomedical applications, and heating specific reactive systems. Conversely, high-temperature applications involve sintering ceramics and metals, melting metals and glass, and facilitating pyrolysis processes, etc. (Mehta et al., 2024). Despite these benefits, microwave heat processing faces significant challenges. These include the inefficient heating of materials that poorly absorb microwaves at room temperature and the weak interaction with low thermal conductivity materials. Moreover, microwave heating can lead to uneven heating and hotspots in some dielectric materials. As the dielectric loss of these materials increases with temperature, this can result in cracking and arcing, presenting substantial hurdles to application (Loharkar et al., 2019; Wu et al., 2022).

Microwave heating fundamentally relies on the material's or sample's capacity to absorb microwave radiation and convert it into heat. This method represents a novel and innovative approach to processing a broad spectrum of traditional industry

materials, as well as new materials that are unsuitable for conventional heating techniques. Furthermore, a significant advantage of microwave heating over traditional methods is that it reverses the direction of heat application-microwave energy heats materials from the inside out(Bhattacharya and Basak, 2016; Valverde et al., 2023).

In conventional thermal processing, thermal energy is externally sourced, allowing heat to flow inward from the surface to the core via conduction or convection, moving from hotter to colder regions as depicted in Figure 2.16(a). Consequently, the surface of the sample typically remains hotter than its center during traditional heating methods. Conversely, microwave thermal processing involves the microwave energy penetrating the sample and generating heat internally, starting at the core. This process is independent of surface heat transfer, resulting in the core maintaining a higher temperature than the surface. Figure 2.16(b) demonstrates this unique heat distribution within the material during microwave heating (Gupta and Leong, 2008; Mao et al., 2021). Consequently, the rapid and volumetric heating that originates internally within the material, without significantly increasing its surface temperature, is contingent upon the ability of microwaves to penetrate the material. The penetration depth of microwaves varies considerably among different materials and is affected by several factors including the material's dielectric and magnetic properties, the microwave frequency, its conductivity, and temperature (Mao et al., 2021).

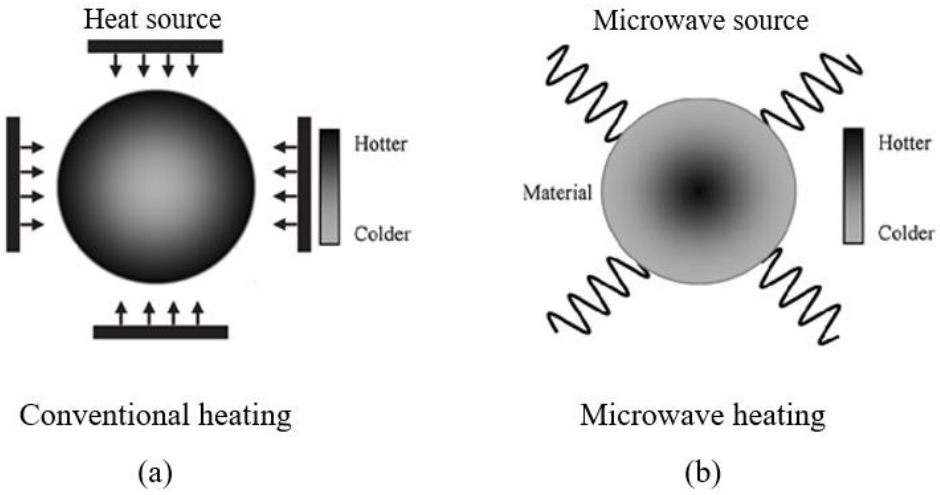

Figure 2.16 Comparison of heat distribution in materials (a) Conventional heating, and (b) Microwave heating (Gupta and Leong, 2008)

Generally, the microwave heating technique is categorized based on the type of material to be processed and its physical and mechanical properties. These categories are as follows: 1) Direct microwave heating (DMH), and 2) Microwave hybrid heating (MHH).

2.5.1 Direct Microwave Heating (DMH)

The direct microwave heating (DMH) technique is utilized for materials that possess sufficient skin depth for microwave absorption, allowing the process to be conveniently conducted at room temperature. This method is applicable to a range of materials, including ceramics, metallic powders, food products, composites, and semiconductors. The rapid interaction between the microwave energy and the material generates heat internally within the processed material. However, during microwave processing, the intrinsic temperature gradients can induce overheating and the formation of hotspots, potentially leading to thermal runaway (Shen et al., 2024). Such thermal instabilities may result in non-uniform material properties and cracking, as observed in materials like Al_2O_3, Fe_3O_4, ZrO_2, and SiO_2 when processed using this technique (Fliflet et al., 2000; Shen et al., 2024).

Several researchers have used Direct Microwave Heating (DMH) technology in the development of numerous applications in diverse areas, including cladding, coating, glazing, and sintering in surface engineering. However, for some ceramics, direct microwave sintering can be challenging due to uneven heating and control issues (Garnault et al., 2021). Generally, metal powders and carbides are efficiently heated in magnetic fields, while ceramics and most insulators respond better to electric fields (Cheng et al., 2002). For example, microwave sintering of nanocrystalline hydroxyapatite powder gel-cast has produced compacts with densities over 95%, grain sizes of 200-300 nm, and microhardness of 5.25GPa (Vijayan and Varma, 2002). Additionally, microwave treatment has successfully stabilized copper ions in heavy metal sludge (Hsieh et al., 2007). Using the DMH technique, molybdenum powder was sintered to 98% of the theoretical density with sub-micron grain sizes in less than five minutes, representing a significant reduction in time compared to the traditional

techniques requiring 10-20 hours (Chhillar et al., 2008). Moreover, microwave energy facilitated the production of SiC powder at lower temperatures and in shorter processing times than conventional methods (Ebadzadeh and Marzban-Rad, 2009). Furthermore, microwave heating has converted carbon into a susceptor or catalyst for chemical reactions, and direct heating has been used to sinter refractory metals like tungsten, rhenium, and molybdenum to densities over 98% of the theoretical density. The process has reduced processing time by 80% and has been very successful in sintering W-based alloys (Menéndez et al., 2010; Mondal et al., 2010).

The interaction of silicon and iron blends in independent microwave electric and magnetic fields was investigated by heating the mixtures within a single-mode cavity. It was found that in both electric and magnetic fields, an increase in iron content enhanced the absorption of microwave power. Consequently, the experiments consistently resulted in the formation of $FeSi_2$ and FeSi phases (Li et al., 2010). In a related advancement, Xie et al. (2011) developed an improved microwave welding procedure that facilitated the creation of a consistent carbon nanotube (CNT) coating on polyethylene (PE) substrates. This coating exhibited excellent electrical conductivity, and the interface between the CNT and PE was notably robust and durable.

The experimental study of the chemical behavior of iron ore (magnetite/hematite) in microwave electric and magnetic fields revealed that iron ore rapidly heats and effectively couples with the magnetic field, facilitating the reduction of the ore to metal ions (Kashimura et al., 2012). Microwave sintering of W-Ni alloys was conducted at 1450 $^{\circ}$C for durations of 5, 15, and 30 minutes. The optimal results were achieved after a 5-minute duration, yielding an alloy with a relative density close to 100% and a Vickers microhardness ranging from 370 to 440, while the average grain size was reduced to as small as 15μm (Zhou et al., 2012). Furthermore, a distinct study utilized Direct Microwave Heating (DMH) to synthesize nanostructured SiC powders from rice husk; this process employed a rapid carbothermal reduction reaction at 1500 $^{\circ}$C for merely 15 minutes (Li et al., 2013). In another experiment within a multimode microwave applicator, both pure and magnesia-doped alumina were sintered, demonstrating their capacity to absorb microwave energy and undergo

heating. While the microwave process had minimal impact on the densification of pure alumina, it significantly influenced the properties of magnesia-doped alumina (Żymełka et al., 2013).

In a recent study, bottom ash (BA) from a municipal solid waste incinerator (MSWI) was repurposed as the starting material for producing porous glass ceramics. Initially, the BA was milled and subsequently vitrified as a purification step. This process utilized Direct Microwave Heating (DMH) and sinter-crystallization at temperatures ranging from 800 to 900 $^{\circ}$C . The resulting material exhibited up to 70% porosity and demonstrated a compressive strength significantly exceeding 1 MPa (Flesoura et al., 2021).

In a comprehensive study focusing on the suitability of direct microwave heating for sintering ceramic materials, the research centered on sintering alumina and yttria-doped zirconia powder samples within a 2.45 GHz resonant cavity equipped with autonomous heat monitoring. Alumina and zirconia were selected for their representative microwave behaviours among ceramic materials, with alumina being mostly transparent and zirconia exhibiting varying degrees of absorbency. The limited conjugation capacity of alumina rendered its direct heating ineffective. In contrast, zirconia displayed dynamic coupling properties that changed significantly with temperature: it was poorly absorbent at low temperatures, became highly absorbent at intermediate temperatures, and ultimately reflective at the end of the sintering cycle (Garnault et al., 2021). These characteristics underscore the challenges of controlling direct heating, such as the formation of hot spots and plasma at high temperatures. The experimental and computational analysis concluded that direct microwave heating was not effective for achieving reliable and homogeneous sintering of traditional ceramics, explaining why susceptor-assisted heating is generally preferred.

In the context of dewaxing in investment casting, DMH has demonstrated the potential to significantly reduce processing time and energy consumption compared to conventional autoclave or flash fire methods. However, the effectiveness of DMH is highly dependent on the dielectric properties of the mould and wax materials. Most ceramic moulds used in IC (e.g., aluminosilicates) are poor microwave absorbers and

thus do not efficiently convert microwave energy into heat under direct exposure (Yahaya et al., 2016; Garnault et al., 2021). Similarly, many waxes have low dielectric loss tangents, making them nearly transparent to microwave energy. As a result, heating may be uneven, especially for complex geometries, leading to incomplete dewaxing or shell damage. Moreover, when penetration depth is much smaller than the sample size, DMH can cause localized overheating at the surface and insufficient heating within, producing thermal stress and non-uniform wax removal (El Khaled et al., 2018). This limitation restricts the scalability and consistency of DMH in industrial IC processes.

2.5.2 Microwave Hybrid Heating (MHH)

Although microwave heating offers numerous advantages over traditional methods, its successful implementation hinges on overcoming certain challenges. Particularly in ceramic processing, Direct Microwave Heating (DMH) often leads to thermal runaway, a form of thermal instability. This occurs when microwaves selectively heat localized areas on the surface of a substance, causing these spots to overheat and absorb more energy than cooler areas. Consequently, the slow heat exchange between these hot spots and the rest of the material underpins the principle of thermal runaway. The possibility of this behaviour is influenced by the material's dielectric constant. Uncontrolled heating not only adversely affects product quality but also reduces process repeatability (Bhattacharya and Basak, 2016). Moreover, the inherent temperature gradients that occur during volumetric heating may lead to severe temperature non-uniformities, resulting in non-uniform properties and cracking at high heating-up rates (Menezes et al., 2007).

A significant challenge associated with Direct Microwave Heating (DMH) is the slow heating of transparent materials to appropriate microwave processing temperatures. This extended warm-up period has two profound effects on microwave processing. It lowers the process efficiency in energy terms as well as enhances the possibility of plasma formation, which interferes with processes and produces instant discontinuities in heating patterns (Mishra and Sharma, 2016). To mitigate these

issues, various sintering studies have employed insulation to minimize temperature gradients. However, insulation may inadvertently contribute to temperature runaway (Shen et al., 2024). Consequently, the Microwave Hybrid Heating (MHH) technique has been developed to enhance the heating of materials with poor microwave absorption. This approach involves improving the dielectric properties of the material by doping it with high microwave-absorbing materials, known as susceptors. This strategy is effective in reducing the temperature gradients during the heating of materials with low thermal conductivity (Ngamkiatpaisan et al., 2023; Zhang et al., 2024).

Susceptors such as silicon carbide (SiC), carbon materials, alumina, and magnetite (Fe_3O_4) are lossy materials that are heated quickly by microwaves even at room temperature. The heating process involves three key stages: (i) the susceptor rapidly interacts with the microwaves, absorbing the energy and converting it into heat. Subsequently, (ii) this heat is transferred from the susceptor to the target sample through conventional heat transfer modes—conduction, convection, and radiation. As the temperature of the sample increases and reaches a critical threshold, it becomes increasingly lossy. Finally, (iii) at the critical temperature, the target sample begins absorbing radiation by direct interaction with the microwaves (Bhattacharya and Basak, 2016). According to the statistics reported by Samyal et al. (2022), as depicted in Figure 2.17, the highest usage rate of microwave processing until 2022 was in sintering applications, accounting for approximately 58%, while the lowest was in drilling applications, at 3%.

Microwave casting is one of the emerging fields which are yet to be studied in detail. In investment casting, the use of microwave hybrid heating (MHH) offers notable advantages not only for dewaxing but also for enhancing the structural integrity of ceramic moulds during thermal processing. Incorporating susceptors such as SiC into the mould shell layers promotes a more uniform distribution of microwave energy, helping to prevent common problems like localized overheating and shell cracking. This approach is especially beneficial for complex shapes or thick wax patterns, where conventional dewaxing methods often result in internal defects due to uneven heat distribution. Additionally, the high thermal conductivity of susceptors like

SiC enables faster heat transfer throughout the mould, speeding up the removal of residual wax and reducing overall processing time. Research has also shown that MHH improves energy efficiency by focusing heat generation precisely where it is needed, minimizing the thermal losses typically seen with conventional or direct microwave heating (DMH) techniques. In recent years, the use of microwave radiation for preparing metal-based materials for casting has gained significant attention. Gangwar et al. (2022)applied in-situ microwave-assisted casting to achieve bulk melting of AA-6063 alloy. Kaushal (2022) investigated microwave heating for the development of metal matrix composite (MMC) castings. Singh et al. (2021a) successfully employed microwave hybrid heating (MHH) to cost-effectively process nickel powder reinforced with alumina MMCs. Pal et al. (2022) effectively applied the MHH technique to produce iron-based MMCs with improved properties. Additionally, Kaushal et al. (2021) used microwave heating at 2.45 GHz and 900 W to fabricate Cu-Mo-based MMC castings, while Kumar et al. (2021) developed a hybrid aluminium MMC composed of aluminium and silicon carbide (SiC) using microwave irradiation.

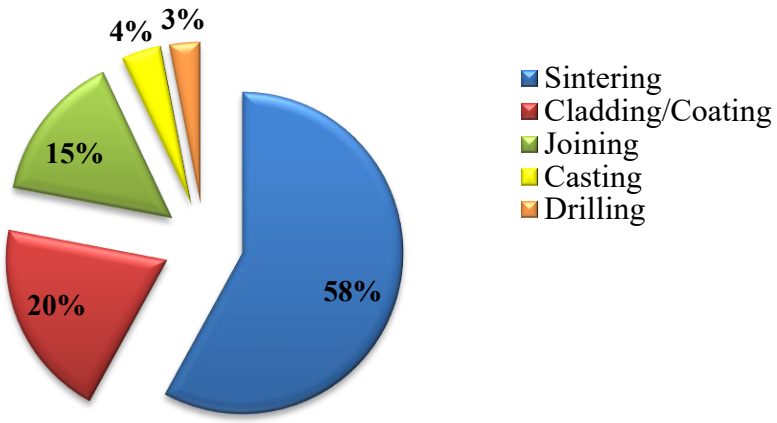

Figure 2.17 Microwave hybrid heating used in different applications (Samyal et al., 2022)

Due to the extensive body of research exploring the use of microwave hybrid heating in industrial applications, a selection of these studies is summarized in Table 2.5. These studies specifically focus on the application of the hybrid heating technique in ceramic sintering.

Table 2.5 Application of Microwave Hybrid Heating (MHH) on ceramic sintering in the body of the literature

Materials sintering	Process/ Operation conditions	Used Susceptor	Advantages	Reference
High purity alumina (99.97%)	2.45 GHz microwave	SiC lined enclosure around the sample	- 30 min hybrid sintering at 1500 °C - more than 95% TD (Theoretical Density)	(De et al., 1992)
Alumina, zirconia, ceria and their composites	980 W–2.45 GHz microwave	β-SiC powder (10 g)	- 95% TD was achieved in 35 min	(Ravi et al., 1997)
Pure mullite and zirconia doped mullite	980 W–2.45 GHz microwave	SiC powder	- At 1500 °C and 35 min, more than 90% TD achieved	(Ravi et al., 1998)
Alumina and zirconia (stabilized with yttria and/or ceria)	2.45 GHz microwave	SiC rods	- Avoided the crack formation and the crack free - At 100–200 °C lower than the conventional way	(Xie et al., 1999)
Yttria stabilized zirconia-alumina composites	2.45 GHz multimode oven	2 mm thick layer of α-SiC powder (80–300 μm)	- At 1200 °C, more than 95% TD during the 20 min - Reduced the cracking propensity	(Travitzky et al., 2000)
Alumina and zirconia (stabilized with yttria or ceria)		2 mm thick tubular SiC	- Successfully sintered in a 1.5–2 h compared to 6–8 h of a conventional way - free of plasma formation	(Zhao et al., 2000)
Si_3N_4 ceramics with (5 wt% Y_2O_3, 3.58 wt% Al_2O_3 and 1.42 wt% MgO)	28 GHz microwave	SiC	- Densify the ceramic pellets to 97% TD at 1300 °C	(Jones et al., 2001)
Nickel aluminate spinels ($NiAl_2O_4$)	2.45 GHz multimode cavity	SiC rods	- At 1400 °C in 15 min produced 95% dense ceramics (99% phase purity)	(Peelamedu et al., 2002)

Table 2.5 Application of Microwave Hybrid Heating (MHH) on ceramic sintering in the body of the literature (continued)

Materials sintering	Process/ Operation conditions	Used Susceptor	Advantages	Reference
MgO and yttria doped alumina tubes	2.45 GHz multimode microwave	SiC powder filled in two alumina crucibles as Fig 2.11(b)	- Successfully heated to 900 °C in 10 min. - Almost full density of alumina tubes	(Brosnan et al., 2003)
Mono-phasic β-sialon ceramics	Microwave (600 W)	SiC	- 98.7% TD in less than 60 min	(Panneerselvam and Rao, 2003)
Porcelain-based ceramics	Microwave	alumina cement	- Successfully heated to more than 1200 °C in less than 30 min - No crack or deformation	(Menezes et al., 2007)
Al_2O_3 (as raw material purity > 99.5%) Thank you for your email. MgO–Al_2O_3–SiO_2	2.45 GHz microwave, 0.5–2.7 kW	SiC plates around the sample	- Improved mechanical properties	(Huang et al., 2009)
8 mol% yttria-stabilized zirconia (8YZ)	2.45 GHz commercial multimode microwave	2 wt.% ZrO_2 doped Al_2O_3 cement	- Successfully sintered ceramics compared to the conventional	(Thridandapani et al., 2009)
Alumina – 3YSZ (3 mol% yttria-stabilized zirconia) nanocomposites	Multimode oven (1.8 kW)	SiC, ZrO_2 and AlN (enclosing sample within tubular)	- Raised the temperature to 1600 °C in just 15 min - more than 99% TD in 30–40 min	(Menezes et al., 2010) (Menezes and Kiminami, 2008)
Ti_2SC powders synthesized from Ti, C and S	2.45 GHz, 800 W Microwave	Put in a alumina crucible	- high purity Ti_2SC powders at 1100 °C for 3 min - Ti_2SC's synthesis temperature was about 500 °C lower than other way	(Guan, 2016)
Lead Zirconate Titanate (PZT)- bulk PZT elements	2.45 GHz, 1100 W Microwave	Carbon nanotubes (CNTs)	- Higher mechanical properties - Highest piezoelectric coefficient after sintering and poling	(Rezvani et al., 2022)

Two methods are commonly used to determine the position of the susceptor relative to the sample or material during hybrid heating. The first involves using separated external susceptors, while the second employs susceptors mixed with the material to be heated.

2.5.2.1 Separated Susceptor Method

In this method, an external susceptor, which may be a rod, powder, or tube, is used independently. This approach ensures that the chemical composition of the material or sample being heated is not mixed or altered, as shown in Figures 2.18(a-c)

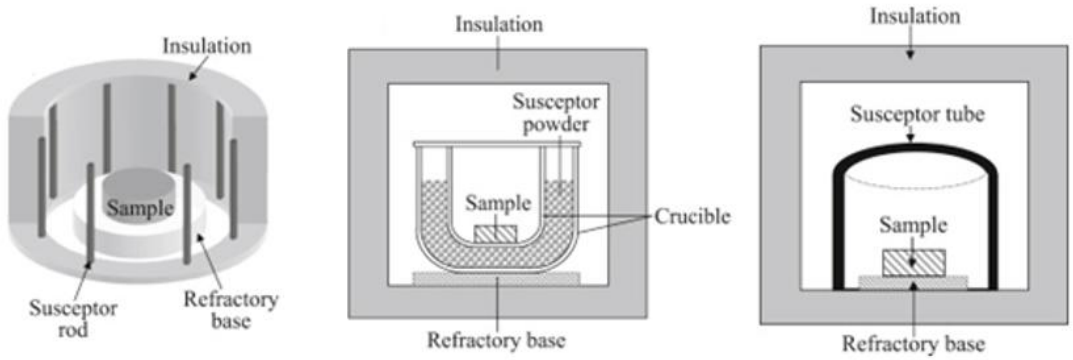

(a) (b) (c)

Figure 2.18 Schematic of the three external susceptors (a) rod, (b) powder, and (c) tubular (Tayier et al., 2022)

Figure 2.18(a) depicts six to eight susceptor rods made from high-loss materials such as SiC and $MoSi_2$, arranged in rod or bar forms to heat a standard semiconductor sample. While these susceptors may partially block microwaves, gaps between them can also lead to heat loss. For hybrid heating using susceptor powder, the typical method involves packing the powder around the sample within a two-crucible setup, as shown in Figure 2.18(b). Alternatively, embedding the sample within the susceptor powder facilitates direct heating, a technique that has been employed multiple times for synthesizing materials in the solid state. Common powders used as susceptors include SiC, carbon (C), and copper oxide (CuO). Figure 2.18(c) illustrates a typical hybrid heating design using a tubular susceptor. This configuration, while

widely used, has raised concerns due to the potential for significant microwave blockage posed by the enclosing susceptor tube. SiC and zirconia are the most frequently used materials for these tubular susceptors (Tayier et al., 2022).

Although this method offers the advantage of preserving the material's chemical composition, it is particularly suited for applications such as sintering and joining, where maintaining the integrity of the workpiece is critical (Masin et al., 2022; Zhang et al., 2024). However, in investment casting, when the susceptor is positioned separately from the ceramic mould, this approach can lead to less efficient and less uniform heating, especially for ceramics that are highly transparent to microwaves at low temperatures, such as alumina and zirconia. The ceramic may not reach the desired temperature quickly or evenly, leading to poor process control and potential defects (Garnault et al., 2021).

2.5.2.2 Mixed Susceptors Method

Mixed absorption techniques can be effectively utilized in composite or multi-phase materials where one phase is a low-absorbing (low-loss) material combined with another phase that is high-absorbing (high-loss), available in various forms such as slurry, dry powder, fiber, or nanotubes. During microwave processing of these composite materials, hybrid heating is particularly beneficial as it typically results in more uniform heating compared to traditional methods, provided that one of the phases possesses a significant loss factor. Without such a factor, the material will behave as a non-microwave absorbent. The microwave properties of composite materials, including dielectric loss factor, dielectric constant, penetration depth, powder size, and critical temperature, are determined by the concentration (weight percentage) of conductive reinforcements or susceptors within the matrix material. Optimal additive concentration is crucial for managing the underheating or overheating of the composite matrix (Mishra and Sharma, 2016; Vyzulin et al., 2021). Research has shown that any increase in additive content tends to enhance the microwave and conductivity properties of composites. For example, significant changes in these properties have

been documented in both ceramic matrix composites (CMCs) and polymer matrix composites (PMCs) (Vikulova et al., 2023; Wang et al., 2023b).

At normal temperature, the majority of electrically insulating ceramics, such as alumina, MgO, silica, and glasses, are transparent to microwaves. However, these materials begin to absorb and couple more efficiently with microwave radiation upon mixing with high-loss materials at a critical temperature (Tc). Conversely, SiC ceramics can absorb microwave energy more effectively even at room temperature due to their high dielectric properties. Thus, this phenomenon, known as mixed absorption, facilitates the process of hybrid heating or selective heating, as represented in Figure 2.19 (Borrell and Salvador, 2018; Fernández et al., 2011).

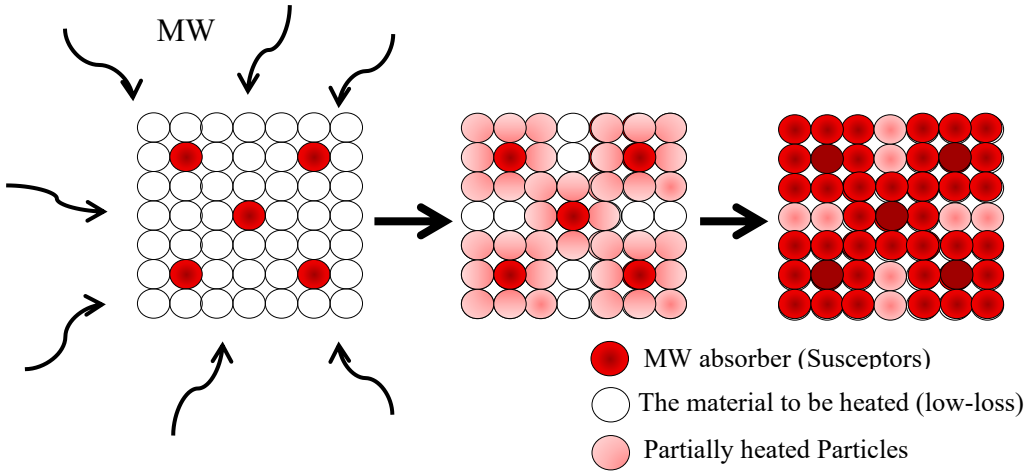

Figure 2.19 Schematic of the microwave heating process for low-loss materials using microwave susceptors

With a significant comprehension of microwave heating phenomenon, various applications of sintring, joining, cladding and coating using susceptor-assisted microwave hybrid heating have been reported in previous literatures. In a seminal study by Patterson et al. (2011), SiC powder was used to sinter a batch of 1 kg of silicon nitride (doped with 5% yttria and 5% alumina) using a 2.45 GHz microwave oven, resulting in ceramic pellets that achieved 97% of theoretical density while consuming only 22% of the energy required for traditional sintering. Similarly, Kim et al. (1997) reported that Si_3N_4 pellets reached over 95% theoretical density through 30 minutes of hybrid sintering at 1750 $^{\circ}$C, with additives of 12 and 8 wt.% SiC,

compared to traditional sintering methods, which failed to densify the ceramics beyond 90% theoretical density even at 1850 °C. Furthermore, Jones et al. (2001) demonstrated that incorporating SiC susceptors could significantly lower the sintering temperature for Si_3N_4 ceramics (with 5 wt.% Y_2O_3, 3.58 wt.% Al_2O_3, and 1.42 wt.% MgO) even under 28 GHz microwave processing. Menezes et al. (2007) explored the use of alumina as a susceptor to rapidly microwave sinter various types of porcelain bodies dental, electrical, and sanitary ware to temperatures exceeding 1200 °C in under 30 minutes, effectively avoiding the cracking or pyroplastic deformation typically associated with conventional firing at high rates. Additionally, Bai et al. (2013) leveraged microwave technology to fabricate graphene-based hybrid electrodes, using ethylene glycol as a solvent, microwave absorber, and reducing agent for various graphene-metal sulphides like ZnS, CdS, Ag_2S, and Cu_2S. Youn et al. (2014) further enhanced the microwave heating efficiency by using GR, a potent microwave absorber, to thermally reduce graphene oxide (GO) to GR within an MoS_2/GR composite, serving as an effective electrocatalyst for the hydrogen evolution reaction (HER). Zhou et al. (2016) reported that microwave curing of carbon fiber reinforced polymers (CFRPs) enhances adhesion at the fiber-matrix interface due to the selective heating of carbon fibers. Recent research by Pundhir et al. (2021) also highlights the influence of microwave power on the mechanical properties of high-density polyethylene (HDPE) composites reinforced with carbon nanotubes (CNTs), noting faster and more effective microwave coupling.

2.6 Summary

The literature review provided a comprehensive overview of the key processes involved in manufacturing ceramic mould shells for investment casting, including wax pattern-making and the dewaxing process. It also covered the development and optimization of ceramic shells within the investment casting process. Furthermore, the review explored the fundamentals of microwave heating, highlighting the mechanisms of material polarization and the critical parameters that influence microwave-based heating efficiency. It began with an exploration of the significance of materials' dielectric properties in assessing the practical effects of microwave-induced heating.

The review then addressed the limitations of direct microwave heating (DMH), such as thermal runaway and plasma generation, particularly when heating transparent materials like ceramics. To leverage the advantages of microwave heating, especially for materials that are poor microwave absorbers, the microwave hybrid heating process (MHH) was developed. This method enhances the dielectric properties of the material by doping it with high microwave-absorbing materials, known as susceptors. The literature indicates that the highest utilization of MHH has been in sintering applications, whereas its use in drilling and casting remains limited. Silicon carbide (SiC), in particular, has been widely used in sintering due to its excellent dielectric and thermal properties. However, studies focusing on the use of MHH in investment casting remain scarce, primarily due to the complex challenges associated with adapting this technique to mould fabrication and dewaxing. Moreover, while the incorporation of susceptors into mould materials can enhance microwave absorption, it also affects the mechanical and thermal behavior of the mould, depending on the type, quantity, and placement of the additive. Notably, there is currently no reported research on combining SiC with refractory ceramics to develop a hybrid ceramic shell specifically for investment casting applications. Such modified moulds are expected to demonstrate improved properties and faster dewaxing performance during microwave-assisted dewaxing.

CHAPTER 3

RESEARCH METHODOLOGY

3.1 Introduction

This chapter discusses the materials and methodology carried out in this research, aiming at reducing cracks and dewaxing time in the investment casting processes. It provides a detailed description of the procedures, experiments, and equipment used to analyse the dielectric, physical, thermal, and mechanical properties of green ceramic mould shell and wax pattern. The chapter also describes the dewaxing tests conducted using a modified domestic microwave. This chapter ends with evaluating the performance of standard and modified green ceramic moulds during the dewaxing process.

The research was conducted based on the objectives outlined in Chapter 1, as summarized in Figure 3.1. The experimental trials began with the fabricating of standard and modified green ceramic moulds, which contained varying weight percentages (0, 1, 2.5, 5, and 7.5 wt.%) of silicon carbide (SiC) and stucco. The thermal and chemical (FTIR) properties of waxes, as well as the dielectric, physical, thermal, and mechanical properties of green ceramic mould shells, were evaluated. Subsequently, the dewaxing performance of various wax types (HYFILL B289 MOD S and SIVUCH L1203) was examined using microwave hybrid heating at different power levels. The evaluation including dewaxing time, shell crack incidence, and energy consumption.

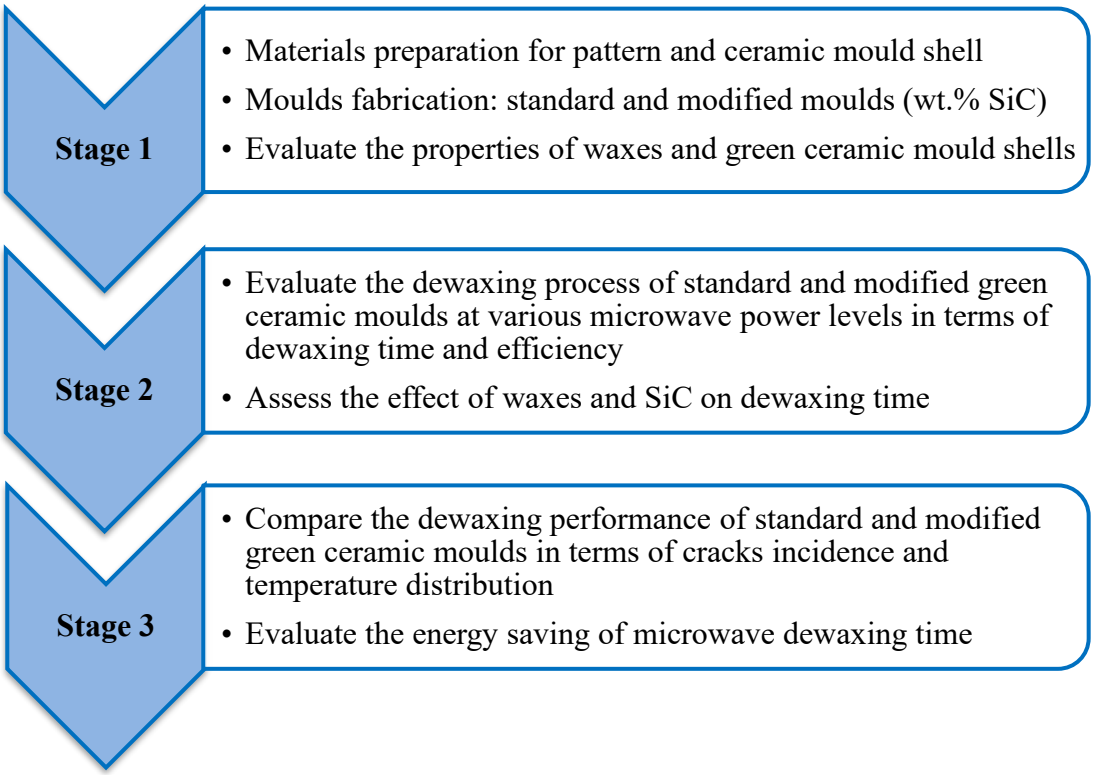

Figure 3.1 The overall experimental phases of research

3.2 Experimental Outline

The experimental outline of this research was divided into two stages. In Stage 1, the preliminary activities involved the characterization of materials for the wax patterns and ceramic moulds. The patterns were made using two types of wax and polystyrene. The polystyrene pattern facilitates the fabrication of green moulds, enabling easy pattern removal and the production of virgin ceramic shells without needing thermal intervention to assess their properties. Zirconium silicate (flour) was mixed with colloidal silica for the preparation of the ceramic slurry. This was followed by the fabrication of standard and modified ceramic moulds. For modified moulds, Stucco (700-800μm grain size) was mixed with various amounts of silicon carbide (SiC) (1, 2.5, 5, 7.5 wt.%). The ceramic moulds were created by dipping the wax pattern into the slurry and rainfalling the stucco on the slurry-coated cluster. The process of building each layer of the mould was followed by a controlled condition of

drying time and room temperature. The evaluation of the properties of the green ceramic mould shells was also included in this phase.

In Stage 2, microwave dewaxing processes of standard moulds were conducted. The effect of dewaxing time and microwave power on two different types of wax was investigated. Dewaxing processes were then performed on the modified moulds at the feasible power level to investigate further the effect of SiC on the dewaxing time and process efficiency of the two types of wax. This stage also included assessing the performance of the dewaxing process in standard and modified green ceramic moulds in terms of shell crack formation and microwave energy savings. The overall experimental activities are illustrated in Figure 3.2.

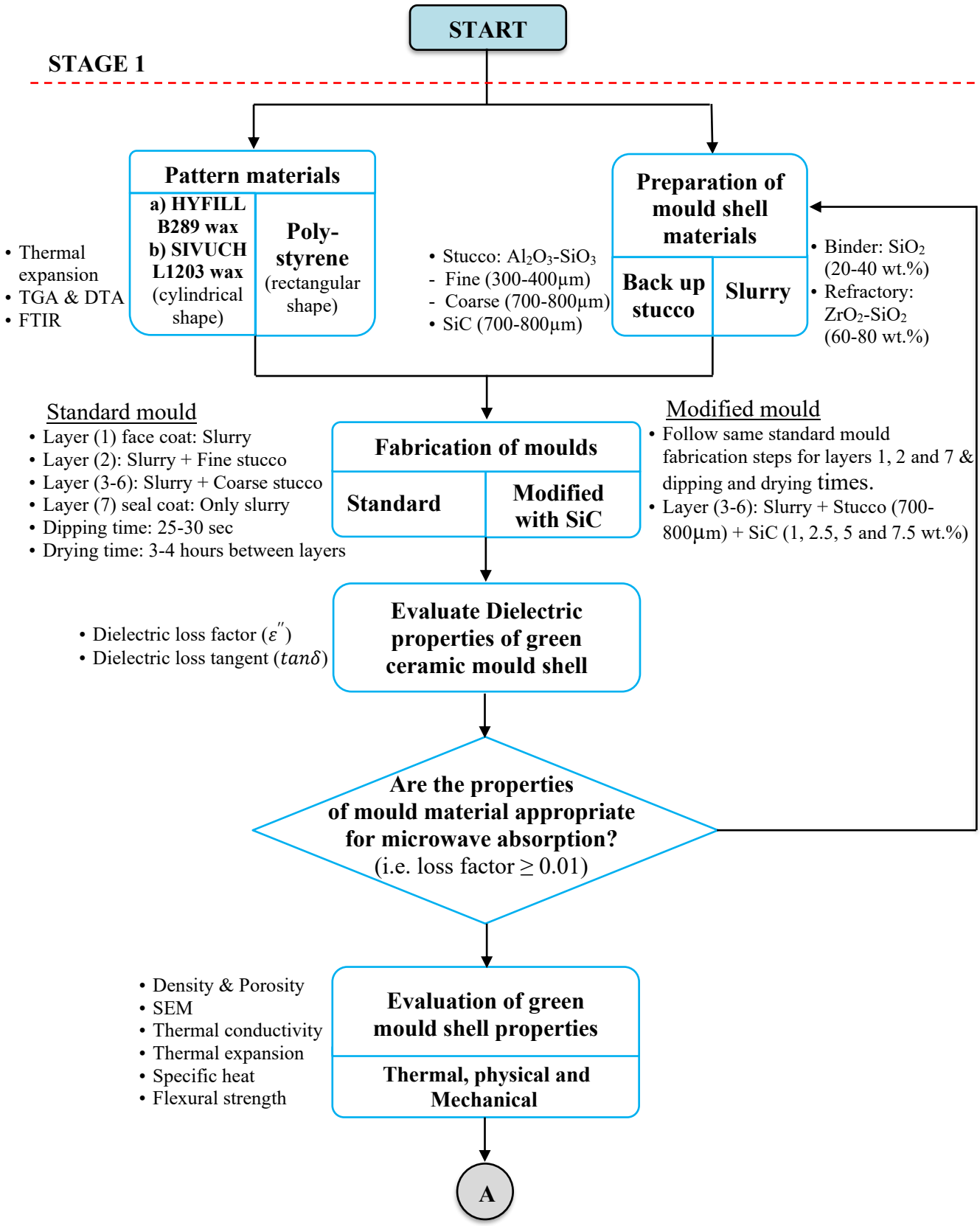

Figure 3.2 Overall flowchart of research methodology (cont….)

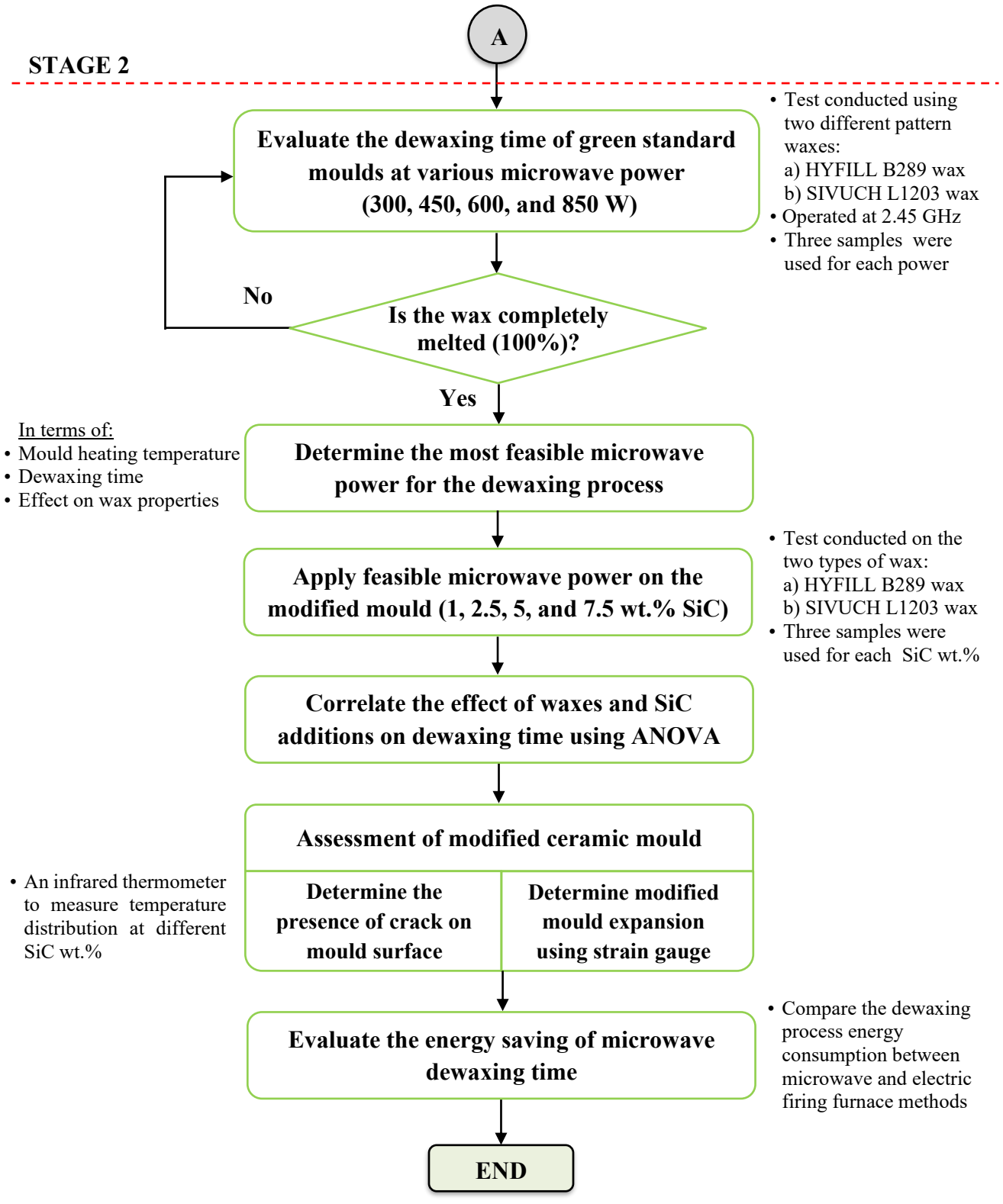

Figure 3.2 Overall flowchart of research methodology

3.3 Preparation and Fabrication of Investment Casting Mould

3.3.1 Geometry of Wax Patterns and Their Moulds

In this research, two different types of patterns were used, as shown in Figure 3.3. The rectangular pattern (Figure 3.3(a)) was made of polystyrene, while the cylindrical pattern was made of waxes (HYFILL B289 MOD S and SIVUCH L1203). Their respective shapes and moulds are also shown at the bottom of the figures. In the early stage of the experiment, the polystyrene pattern was used to fabricate green moulds, allowing for quick and easy pattern removal and enabling the production of virgin ceramic shells without requiring thermal intervention. At this stage, the virgin green mould shell was evaluated for its physical, morphological, thermal, and mechanical properties.

The cylindrical pattern features three varying diameter sizes, transitioning from a larger upper section to a smaller base through a 45° sloped edge. This design aims to investigate the behaviour of the ceramic mould during the dewaxing and metal casting process in terms of thermal and mechanical responses. The three-dimensional graduated cylindrical pattern comprised a base cylinder with dimensions of Ø40 mm × 45 mm (diameter × length), followed by a 5 mm long circular conical section connecting diameters of 40 mm and 50 mm, and ending with a cylinder measuring 50 mm in diameter and 60 mm in length, as illustrated in Fig. 3.3(a). The dimensions of the regular rectangular pattern are limited to 50mm × 30mm × 110mm (length, width, and height, respectively) is specifically designed for the cutting and preparation of samples used to evaluate the properties of green ceramic mould shells in various tests.

The selection of the stepped cylindrical pattern design to investigate the effects of wax pattern removal and the metal casting on the geometric shape of the ceramic mould was based on the study conducted by Razak (2017), which highlighted the in-situ melting technique. Furthermore, this approach facilitated the examination of how varying pattern sizes impact the behavior of the ceramic mould shell (Yahaya, 2016).

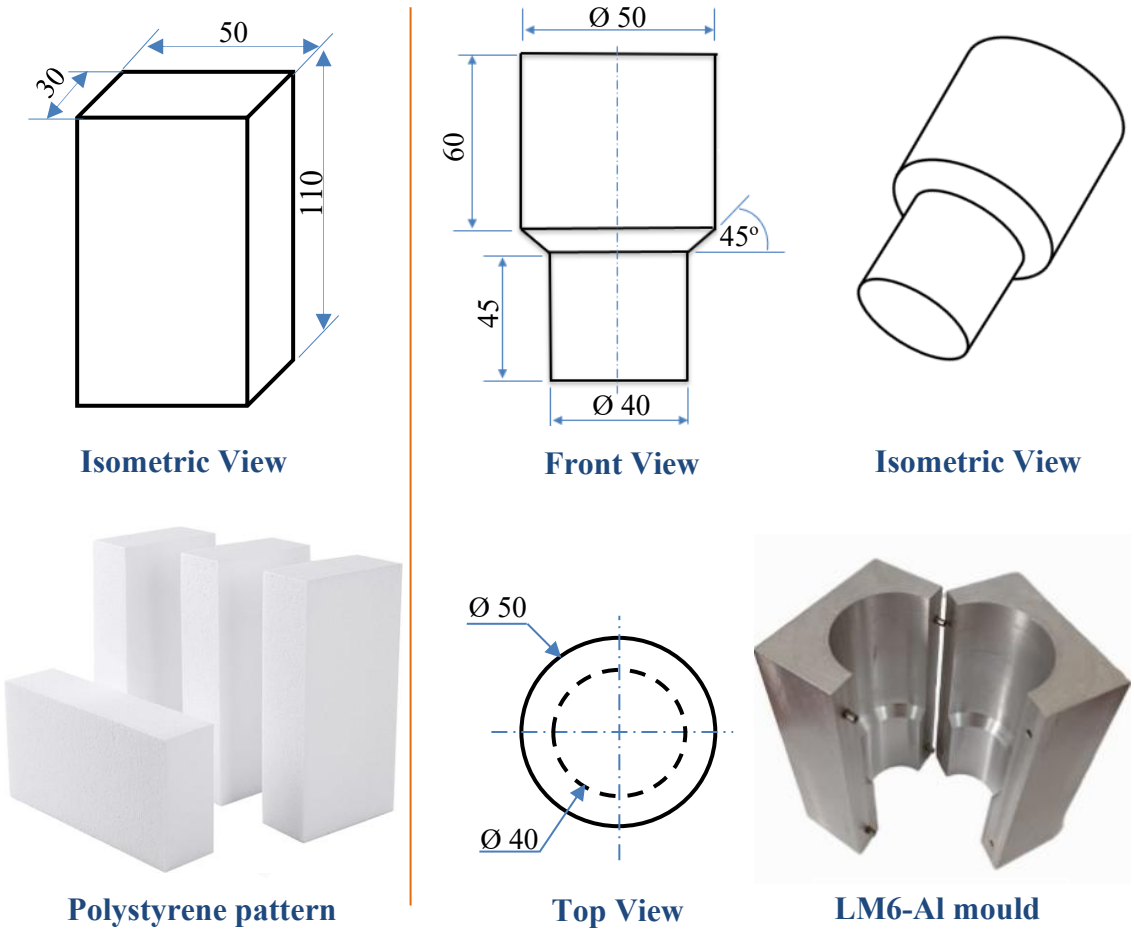

Figure 3.3 Geometry and dimensions of the two different types of patterns: (a) polystyrene rectangular shape pattern, and (b) cylindrical stepped shape pattern and its aluminium mould

3.3.2 Wax Pattern Materials

In this study, two different types of IC wax a) HYFILL B289 MOD S wax (REMET Co., LTD UK), and b) SIVUCH L1203 wax (LIANG LINN ENTERPRISE Co., Ltd Taiwan), were used to make the patterns, as shown in Figure 3.4. HYFILL B289 MOD S is a widely used wax designed for various applications and was conducted in previous studies (Suhasril, 2016; Yahaya, 2016; Razak, 2017). In contrast, SIVUCH L1203 is a newer product, characterized by a low melting point,

low thermal expansion, and low viscosity. The composition and properties of these waxes are presented in Table 3.1. Other properties of these waxes are given in Appendix A & B.

(a) (b)

Figure 3.4 Types of wax used in the study (a) HYFILL B289 MOD S, and (b) SIVUCH L1203 wax

Table 3.1 Elemental composition, physical and thermal properties of pattern waxes used

Property	HYFILL B289 MOD S wax	SIVUCH L1203 wax
Composition	Paraffin, microcrystalline, 30% polymers, 0.5% styrene and resins	40% paraffin, 27% dammar resin, 11% Eva polymer, 8% ceresin, 7% synthetic resin and 3% beeswax, 1% microcrystalline
Softening point range	67 to 71 °C	58 to 60 °C
Melting point range	70 to 84 °C	60 to 70 °C
Flash point	> 200 °C	> 210 °C
Viscosity (cP)	400 to 600 at 100 °C	300 to 340 at 70 °C
Ash content	-	0.002 (1000 °C /1hr)

The LM6-Aluminium die casting consists of two sections, allowing for the easy removal of wax patterns. LM6 was selected for its good machinability, smooth

surface finish, non-stick characteristic with wax, and high thermal conductivity for efficient heat dissipation from the wax (Parthiban et al., 2024; Liu and Xiong, 2024). During the pattern production process, the two die halves are securely clamped together by a press to ensure proper alignment and prevent any wax leakage. In the next step, the investment wax inside the container was heated until it completely melted, within 70 to 110 °C, using an electric hot plate (Cusimax 1500W). Once the wax had fully melted, it was poured into the die and allowed to solidify at room temperature. Subsequently, the wax pattern is removed after separating the die halves, as illustrated in Figure 3.5.

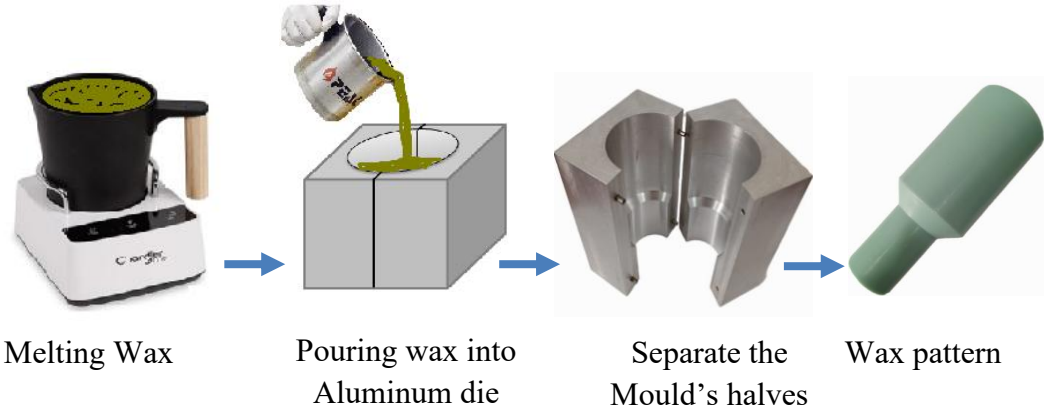

Figure 3.5 Wax pattern production steps

3.3.3 Ceramic Mould Shell Materials

The number of layers can range from a few to several, depending on the size, complexity and weight of the part being cast. The preparation of a ceramic shell underwent three consecutive stages. Initially, the slurry was made, followed by the preparation of stucco, and finally, the application of both slurry and stucco to the patterns.

3.3.3.1 Slurry Preparation Procedure

The ceramic slurry consists of a hardenable liquid binder and a refractory ceramic powder. Silica is a ceramic substance typically used to make binders. Table 3.2 shows the slurry components that were selected in this research.

Table 3.2 Refractory slurry composition materials

Selection criteria	Components of slurry		References
	Aqueous binder	Refractory ceramic powder	
Scientific name	Colloidal silica[1,2] SiO_2	Zirconium silicate[1,2] (zircon flour) ZrO_2-SiO_2	[1](Prasad, 2012) [2](Yahaya, 2016) [3](Pattnaik et al., 2012) [4](Dave and Kaila, 2014) [5](Nadolski et al., 2008)
Weight percentage %	(20-40%)[1]	(60-80%)[1]	
Size	N/A	(74μm)[2]	
The choice depends upon	• High bonding strength[3] • High stability[3] • Free of volatile organic compound[3] • No emit harmful gases during dewaxing & pouring stage[5]	• Availability[3] • Less cost[3] • Excellent casting surface[4] • Resists metal reaction[4] • Inertness and stability at high-temperature (resistance to thermal shock)[3]	

The slurry preparation process began by pouring 1500 milliliters of colloidal silica into a clean stainless-steel container. Next, zircon powder was gradually added to the container. The mixture was stirred slowly using the motor-driven mixer, as shown in Figure 3.6. The addition of zircon powder continued gradually until the desired viscosity was achieved. The slurry was stirred for two hours to prevent the refractory powder from settling out of suspension (Reddy et al., 1998; Vyas et al., 2020). The dipping-type Zahn viscometer is used to measure the required viscosity of the slurry. When the viscosity is high, larger orifice sizes are utilized. In contrast, cups with smaller orifice sizes are used when viscosity is low. This study used Zahn cup #4

to measure the slurry viscosity, as this size is commonly used in IC (Yahaya, 2016; Venkat et al., 2020). During the measurement process, the cup was filled by dipping it into the mixture and then pulling it out. When the cup was withdrawn, a stopwatch was started simultaneously and turned off when the first break was seen in the steady flow of the liquid (Abbas et al., 2010). The time passed was converted to kinematic viscosity according to Equation 3.1. Two control times for slurry viscosity were used: 20-22 seconds for the primary and seal coat and 25-27 seconds for the remaining layers (O'sullivan et al., 2021).

$$V = 14.8(t - 5) \tag{3.1}$$

Where V is kinematic viscosity ($m^2.s^{-1}$), t is efflux time (Zahn seconds).

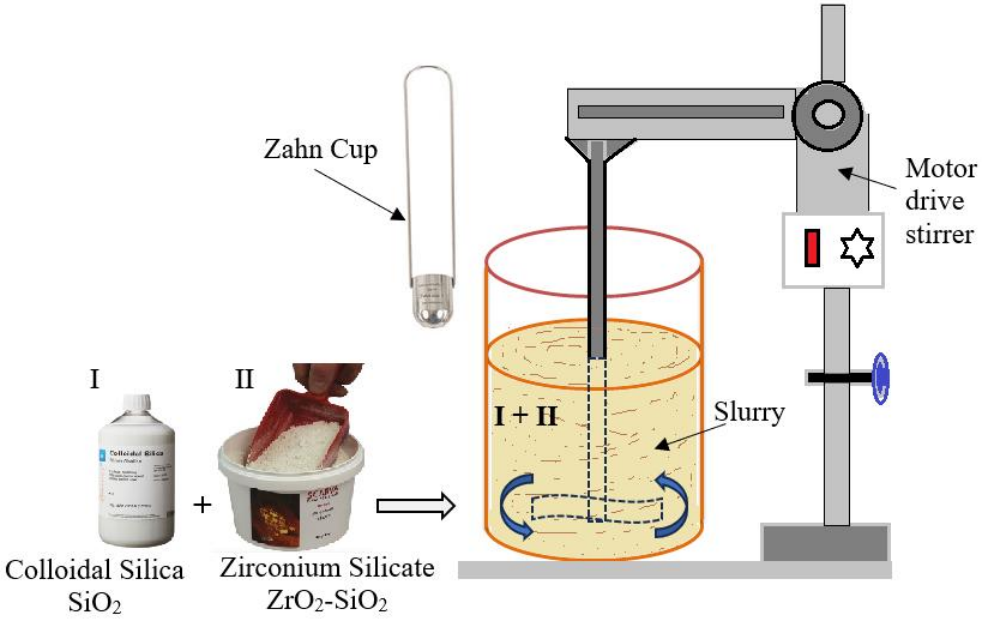

Figure 3.6 Schematic of ceramic slurry preparation using a motor-driven mixer with Zahn cup

3.3.3.2 Stucco Preparation Procedure

The stucco used in this research was aluminium-silicate (Al_2O_3-SiO_3). The stucco was prepared into two groups, i.e. one for standard and the other for modified moulds. The main difference between the two groups is in the third to sixth layers. For the modified mould, SiC was incorporated at varying percentages into the stucco across the four layers. Two types of stucco were used in ceramic mould shell fabrication, i.e. fine backup stucco (300 - 400µm) and coarse backup stucco (700 - 800µm). Figure 3.7 illustrates the fine and coarse backup stucco as well as SiC particles employed in the fabrication work. Figure 3.8 shows enlarged optical images of the above particles. Other properties of these particles are given in Appendix C & D.

Stucco
(Al_2O_3-SiO_3)

Fine backup stucco

- Particles size in range (300 - 400µm)
- Used for the second layer

Coarse backup stucco

- Particles size in range (700 – 800µm) + varying SiC contents (1, 2.5, 5 and 7.5 wt.%) in the same particles size
- Used from the third layer to the pre-final layer (3^{rd} – 6^{th})

(300 – 400µm) fine stucco Al_2O_3-SiO_3

(700 – 800µm) coarse stucco Al_2O_3-SiO_3

(700 – 800µm) SiC

Figure 3.7 Backup stuccos and SiC particles for ceramic mould shell fabrication

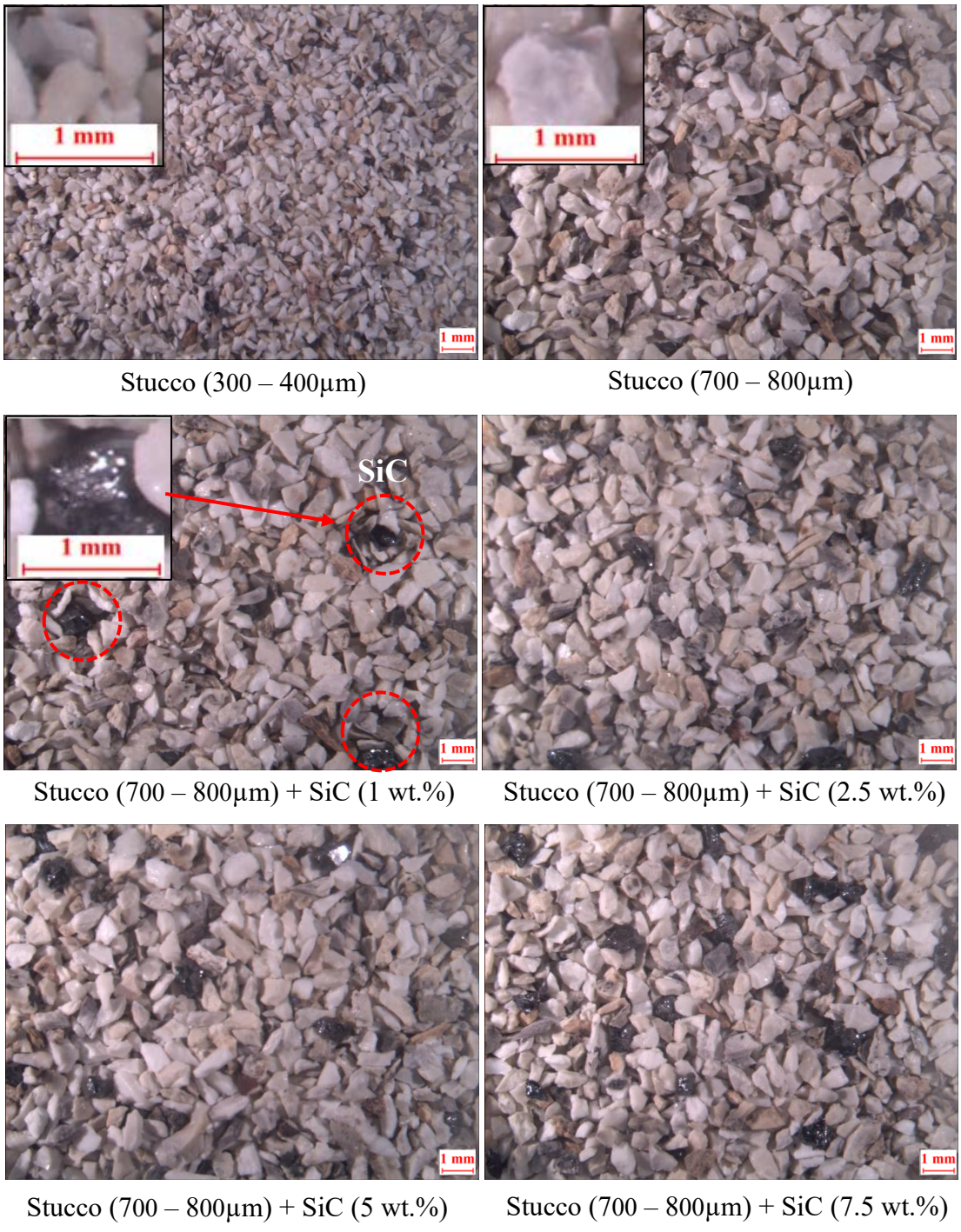

Stucco (300 – 400µm) Stucco (700 – 800µm)

Stucco (700 – 800µm) + SiC (1 wt.%) Stucco (700 – 800µm) + SiC (2.5 wt.%)

Stucco (700 – 800µm) + SiC (5 wt.%) Stucco (700 – 800µm) + SiC (7.5 wt.%)

Figure 3.8 Optical images of virgin and modified stucco with SiC at different percentages

3.3.3.3 Ceramic Mould Shell Fabrication Procedure

Once the wax pattern, slurry, fine and coarse stucco were prepared, the ceramic mould shell was ready for fabrication. The following steps were used to fabricate a standard ceramic mould shell:

Step 1: the wax pattern was dipped into the prepared ceramic slurry and gently moved for 25-30 seconds to ensure complete coating (Venkat et al., 2020).

Step 2: the coated wax pattern was lifted out from the slurry, and the sample was suspended over the slurry's container for one minute while being regularly rotated to ensure a uniform primer coat around the pattern. The sample was hung and allowed to dry for 4 hours (Venkat et al., 2021). At the end of this step, the first layer (primary layer) was completed but free of stucco. Due to the manual dip-coating process, minor variations in coating thickness were inevitable. However, meticulous attention was given to ensuring complete wetting during dip-coating, as the quality of the front coat and the bonding between coats hold significant importance for the final product.

Step 3: After the primary layer dried, the backup stucco (300- 400 μm) was added by dip-coating in slurry: An in-house fabricated vibration sieving machine was utilised for the stuccoing process to ensure uniform layer thickness, as illustrated in Figure 3.9 (a). The wax patterns were attached to a screw extension using a screw driller. A sufficient quantity of the stucco material was initially placed in the sieve with a mesh size of 600μm. Through the vibration of the sieving machine and the rotation of the wax pattern for 3 minutes, the stucco was completely applied to the sample. The mould was left to dry for 3 hours (Venkat et al., 2021).

Step 4: for the next four layers (third to sixth), the slurry was applied in the same method in the second layer, and then the coarse backup stucco (700 – 800 μm) was applied using the modified sieving machine (sieve mesh size of 1200μm), followed by drying process for 3 hours.

Step 5: in the seventh layer (seal coat), the mould was dipped into the slurry and allowed to dry without applying any stucco for 24 hours at 27-29 $^{\circ}$C before starting the dewaxing process (Zych and Snopkiewicz, 2011). Figure 3.10 summarizes the construction stages of the standard ceramic mould shell layers.

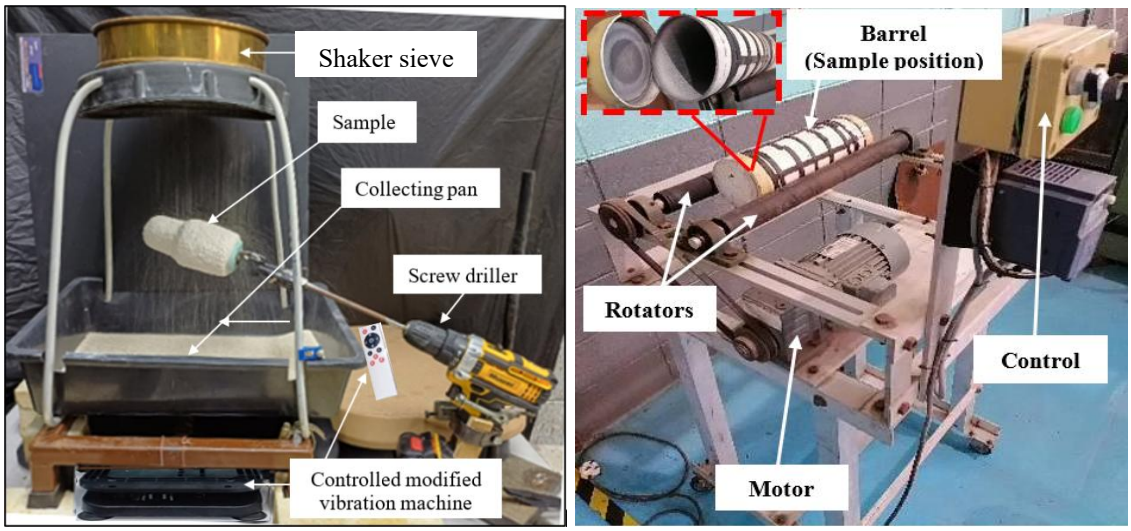

(a) (b)

Figure 3.9 An in-house fabricated (a) sieving machine utilized in the stuccoing process, and (b) mixing machine for preparing SiC particles ratio in coarse-stucco

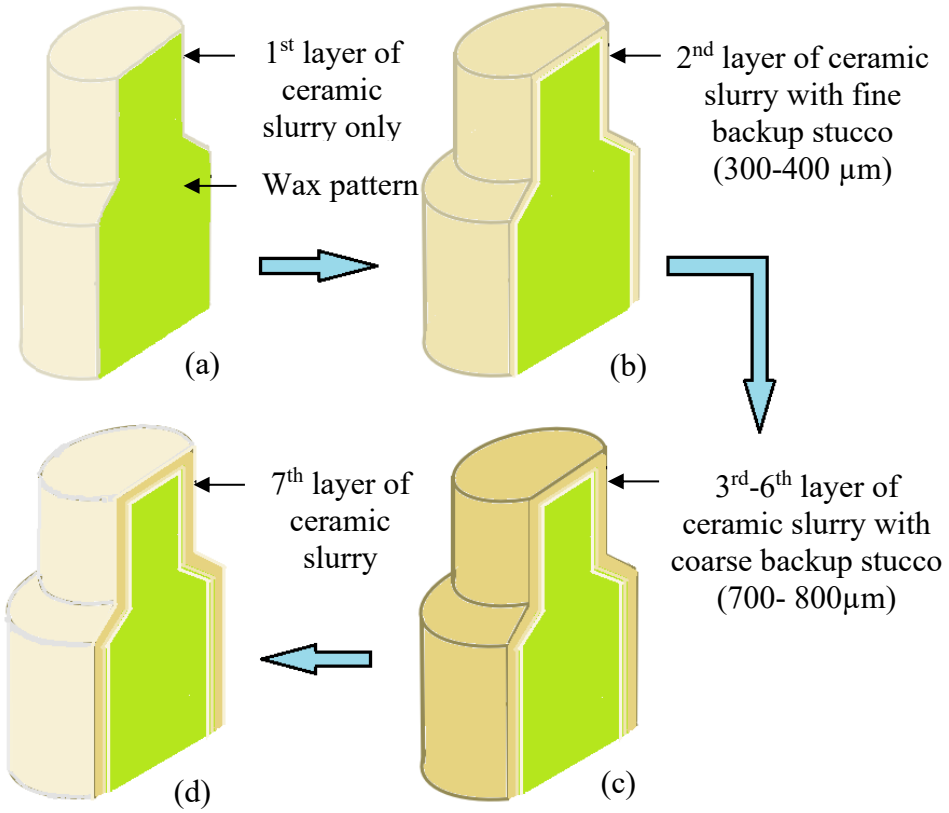

Figure 3.10 Schematic diagram of coating and stucco application stages

Similar fabrication steps were followed to fabricate a modified ceramic mould shell. However, prior to step three, SiC particles were mixed into coarse backup stucco at 1, 2.5, 5, and 7.5 wt.% using an in-house fabricated mixing machine, as shown in Figure 3.9 (b). These mixture ratios were applied in fabrication steps 3 to 6 using the same in-house fabricated sieving machine illustrated in Figure 3.9 (a).

Table 3.3 provides a detailed description of the fabrication of the ceramic mould shell in each layer. In a standard mould, no SiC particles were added to the stucco for layers 3 to 6. Additionally, Figure 3.11 presents a schematic diagram illustrating the alignment of the layers in the modified ceramic mould shell.

Table 3.3 Detail of the standard and modified ceramic mould shell fabrication

Layer No.	Slurry			Dipping time (sec)	Stucco	Dry time (hour)
	Composition		Viscosity (sec)			
	Powder	Binder				
1	ZrO_2-SiO_2 (74µm)	Colloidal silica	26-28	25-30	-	4
2	ZrO_2-SiO_2 (74µm)	Colloidal silica	20-22	25-30	Al_2O_3-SiO_3 (300-400 µm)	3
3 - 6	ZrO_2-SiO_2 (74µm)	Colloidal silica	20-22	25-30	Al_2O_3-SiO_3 (700-800 µm) + 1, 2.5, 5, 7.5 w.t % SiC (700-800 µm)	3
7	ZrO_2-SiO_2 (74µm)	Colloidal silica	26-28	25-30	-	24

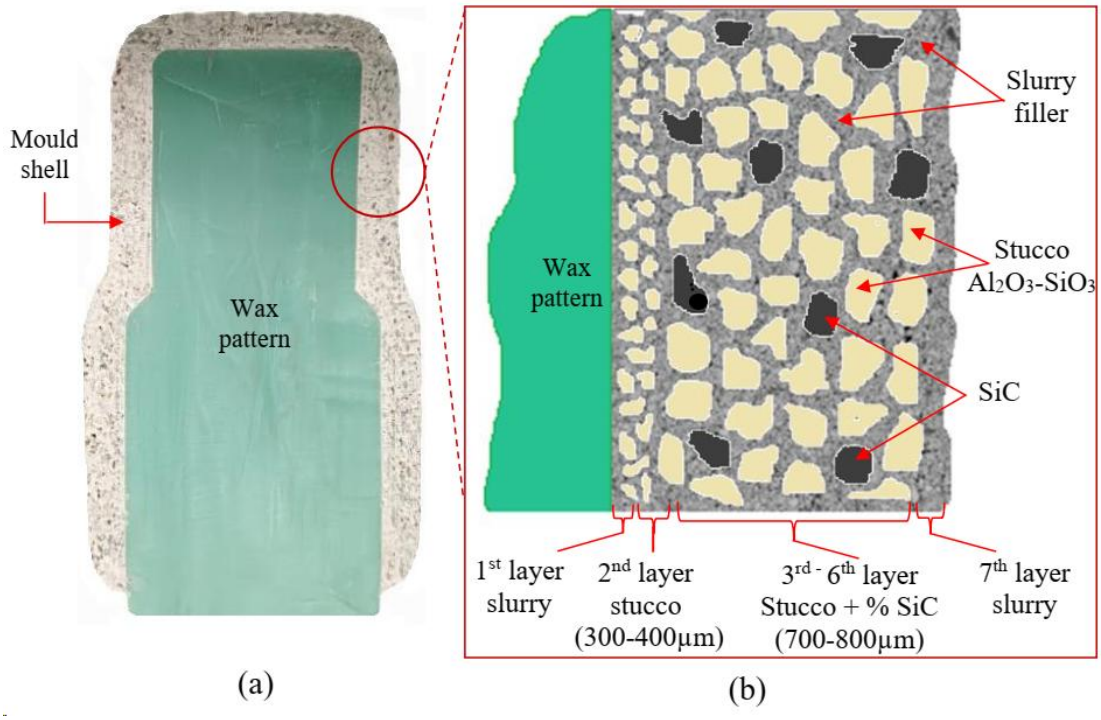

Figure 3.11 Schematic diagram of (a) ceramic mould cross-section, (b) close-up view of ceramic mould shell layer construction

3.4 Wax Properties Testing Procedure

3.4.1 Linear Thermal Expansion Test

The thermal expansion test was conducted to analyse the relationship between linear thermal expansion ($\Delta L/L_o$) and temperature for waxes and standard ceramic mould shell materials using a dilatometer (TMA 60H, Germany), as shown in Figure 3.12. The thermal behaviour of the waxes was tested in the range of 0-60 °C, while the mould was tested in the range of 0-600 °C. The test was carried out at a constant heating rate of 2 °C/min and a negligible load of 0.5N, with a nitrogen gas atmosphere flow of 100 ml/min. The dimensions of the tested samples were 4 × 4 × 10 mm, in regular cubic shapes. The selected temperature ranges reflect the practical application limits and thermal properties of wax and ceramic materials. One sample was tested for each. Waxes typically soften, melt, or exhibit their expansion around 60 °C (Sarcinella et al., 2024), while ceramics require higher temperatures to evaluate thermal expansion

related to their stability and thermal shock resistance. The thermal expansion coefficients (α) for waxes and moulds materials were calculated following Equation (3.2) (Ahrens, 1995).

$$\alpha = \frac{1}{L_o} \frac{\Delta L}{\Delta T} \tag{3.2}$$

Where L_o(mm) is the original length, ΔL(mm) is the change in length, and ΔT (K) is the temperature change.

Figure 3.12 Dilatometer (TMA 60H)

3.4.2 Thermogravimetric and Differential Thermal (TGA & DTA)

The thermogravimetric analysis test (TGA) was employed to measure the weight loss of two pattern wax types as a temperature function. TGA (Mettler Toledo, SDTA851e) was used at a constant heating rate (10 °C/min) under a nitrogen (N_2) atmosphere, and the waxes were heated in the range of 27 °C to 500 °C. The test was performed by carefully weighing a small wax sample, placing it in a crucible, and then inserting it into the TGA instrument. The process involved gradually applying heat while continuously observing the sample's weight. As the temperature rises, the real-time reduction in weight of the wax sample was recorded, attributable to its thermal decomposition.

The differential thermal analysis test (DTA) was employed to identify phase transitions, endothermic and exothermic reactions, and melting points. In the process, both types of wax and reference material were placed in separate crucibles side by side. The instrument's temperature range and rate were set, and as temperature changes, ΔT was measured.

3.4.3 Fourier Transform Infrared Spectroscopy (FTIR)

Nicolet iS50 FTIR spectrometer as shown in Figure 3.13, was used to analyse the chemical bonds for the two types of wax. The depth of the beam penetration into the sample was about 2 μm and spectra were recorded in the mid-wavenumber range of (4000 to 500 cm^{-1}) (Maia et al., 2013).

Figure 3.13 Nicolet iS50 FTIR spectrometer

3.5 Evaluation Procedure of Dielectric Ceramic Mould Shell Properties

The open-ended coaxial probe method was used to measure the dielectric properties of green mould material. The coaxial probe is attached to the Agilent Technologies vector network analyzer (VNA-85070E), as shown in Figure 3.14. The technique entailed pressing the coaxial probe against the sample material to make the

required measurements. The sample reflected the microwave signal sent by the VNA, and the loss factor (ε'') and loss tangent ($\tan\delta$) are computed using the reflected waves (Barba and D'amore, 2012; Yaw, 2012). It is a simple method to apply, non-destructive, quick, and accurate (5%). The probe device was calibrated before use, with no air gap between the probe and the sample surface and a flat surface. The test was conducted within the frequency range of 0.2-15 GHz and at a temperature of 20 $^{\circ}$C.

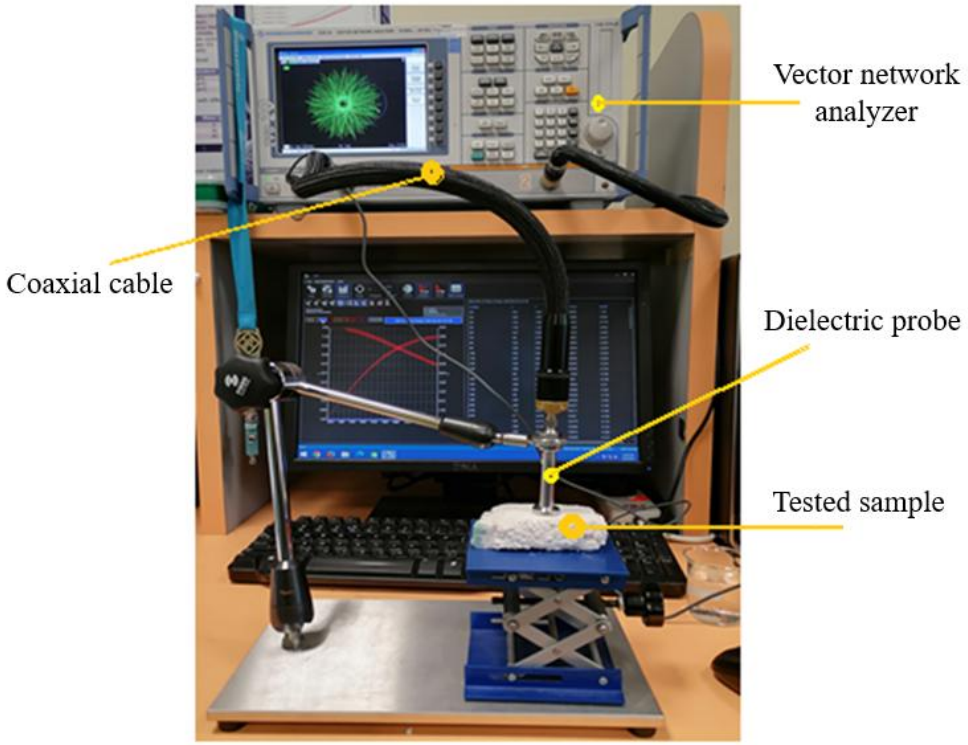

Figure 3.14 VNA apparatus and open-ended coaxial probe method for measuring dielectric properties

3.6 Evaluation Procedure of Ceramic Mould Shell: Physical, Morphological, Thermal, and Mechanical Properties

3.6.1 Density and Porosity Testing Procedure

The assessment of apparent porosity and bulk density of standard and modified green ceramic moulds shells were adhered to the Archimedes method as outlined in ASTM C20-00 (ASTM, 2010). The procedural steps were adhered to as described, and the measurement process for the test is summarized in Figure 3.15.

i. The samples were placed in a desiccator for 24 hours to ensure they were free of moisture.
ii. The dry weight of samples taken from the moulds, Wa (g), using a measuring balance (resolution = 0.01g).
iii. The samples were suspended in water and boiled for 2 hours, avoiding contacting the samples with the container's heated bottom.
iv. The test samples were left to cool in water until they reached room temperature. After 12 hours, the weight of the samples suspended in the water was recorded and labelled as Wb (g).
v. The samples were removed from the water and were gently tumble-dried with a smooth piece of linen. The saturated weight was then determined as Wc (g).

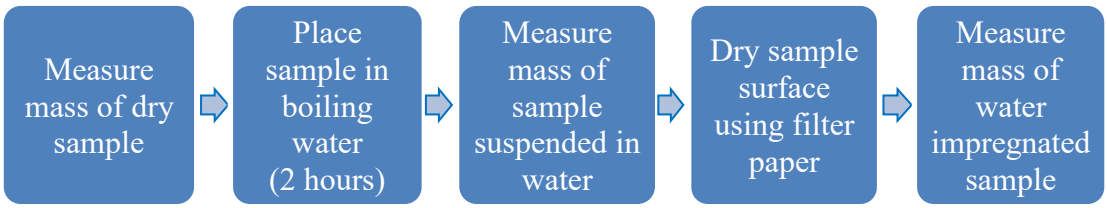

Figure 3.15 Measurement process for Archimedes porosity testing of ceramic mould shell

The bulk density (ρ) and apparent porosity (P) values were then determined using Equation (3.3) and (3.4), respectively (ASTM, 2010).

$$\rho = \frac{W_a}{W_c - W_b} \tag{3.3}$$

$$P = \frac{W_c - W_a}{W_c - W_b} \tag{3.4}$$

3.6.2 Microstructure and Morphology Testing Procedure

Figure 3.16 shows the Scanning electron microscopy (SEM-Zeiss Supra 35VP) associated with energy dispersive X-ray (EDX) was used to identify the layered composition of the ceramic mould shell through cross-sectional imaging for standard mould shell. The morphology of the standard and modified moulds was also analyzed by assessing the pore distribution and pore size on the inner and outer surfaces of the ceramic shell. The key SEM imaging parameters are summarized as follows: for Secondary Electron (SE) mode, Vacc=15kv, Mag= ×500, and a scale bar = 20 µm. For Backscattered Electron (BSE) mode, Vacc=15kV Mag=x10, and a scale bar= 5 µm.

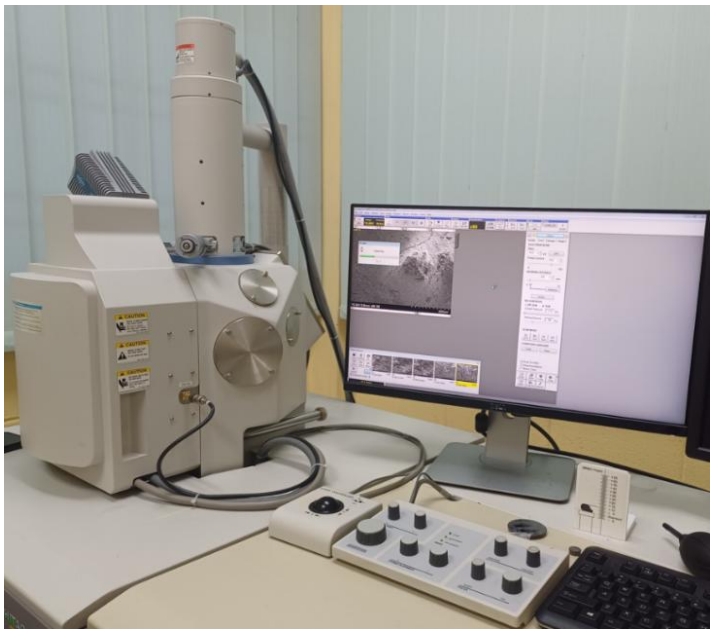

Figure 3.16 Scanning electron microscopy (SEM-Zeiss Supra 35VP)

3.6.3 Thermal Conductivity Testing Procedure

The thermal conductivity of the mould shell material was determined by taking samples from the standard and modified shell. The thermal conductivity (k) of green mould was assessed using the thermal conductivity device (Cussons P5678), as shown in Figure 3.17. The device was equipped with four thermocouples. The heat source was provided by an electric heater positioned at the top of the copper bar, while the heat sink was established by circulating water at the bottom of the copper bar.

The samples were prepared by fabricating a regular rectangular ceramic mould around a polystyrene pattern to facilitate easy manual removal. Next, three circular samples, each with a diameter of 25 mm and matching the thickness of the mould, were taken from different locations on each mould. This approach ensured that the cross-sectional area of each sample precisely matched the cross-sectional area of the copper bar used in the test device. Both surfaces of the green mould samples were flattened to achieve full contact with the surfaces of the two copper bars. A semi-automatic grinding and polishing machine was used for flattening.

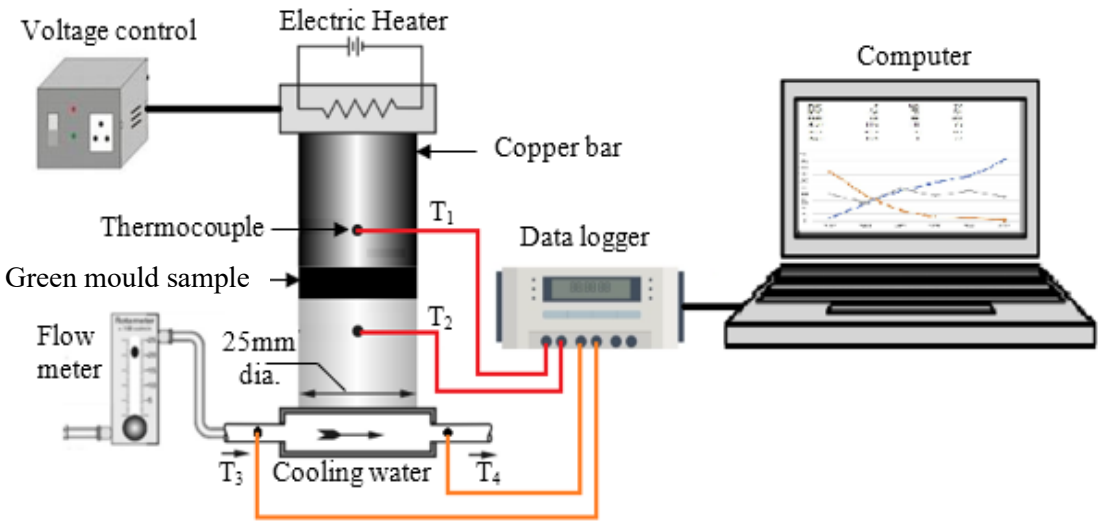

Figure 3.17 Schematic diagram of Cusson P5678 set-up for thermal conductivity measurement

The cooling water flow rate was set to 0.017 kg/s, while the electric heater was adjusted to 50 V. During the heating process, the device was allowed to reach thermal equilibrium. Once the hot end temperature stabilized at 165 ± 5 °C, the temperatures of the green mould sample and cooling water from T1 to T4 (°C) were recorded. The thermal conductivity (k) (W/mK) was calculated using Equation (3.5) and (3.6) (Kumanek and Janas, 2019; Roper et al., 2007; Yahaya, 2016).

$$q = \dot{m} c_p (T_4 - T_3) \tag{3.5}$$

$$k = \frac{q\ dx}{A\ (T_1 - T_2)} \tag{3.6}$$

Where q (J/s) is the heat transfer rate by cooling water, $\dot{m}$ is the mass flow rate of cooling water, c_p is the specific heat of cooling water (4187 J/kg K), T_3 and T_4 are the inlet and outlet temperature of cooling water (°C), dx (m) is the thickness of the sample, A is the sample cross-section area (m^2), T_1 and T_2 are the inlet and outlet temperatures of the tested sample (°C).

3.6.4 Specific Heat Capacity Testing Procedure

Differential scanning calorimetry (DSC) was used to evaluate the specific heat (C_p) of standard and modified green ceramic mould material. DSC measures a heat quantity excessively radiated or absorbed by the sample based on a temperature difference between the sample and the reference material. The temperature was set between 25 to 300 °C (Liu et al., 2019) and applied on 5 mg using Mettler Toledo DSC 1, as shown in Figure 3.18. The heating rate ($dT/d\tau$) used was 10 °C/min, and the heat flux rates ($\delta Q/d\tau$) against temperature were recorded. The specific heat capacity was calculated using the Equation (3.7) (Morîntale et al., 2013; Pop et al., 2001):

$$C_p = \frac{1}{m} \frac{(\delta Q/d\tau)}{(dT/d\tau)} \tag{3.7}$$

Where m is the mass of the sample (g), $(\delta Q/d\tau)$ is the heat flux given by the DSC (J/sec), and $(dT/d\tau)$ is the heating rate (10 °C/min).

Figure 3.18 Mettler Toledo DSC 1 differential scanning calorimeter (DSC)

3.6.5 Flexural Strength Test Procedure

The flexural strength of the standard and modified green ceramic mould shells was evaluated using a three-point bending test following ASTM C1161. Figure 3.19 schematically shows the three-point bending test and the position of the sample relative to the central load applied to it. The samples were prepared by fabricating a regular rectangular ceramic mould around a polystyrene pattern for easy manual removal. The mould shell was then cut into strips to fit the required dimensions of the test specimens using a wire saw method. Three samples were used for each weight percentage of SiC (0, 1, 2.5, 5, and 7.5 wt.%).

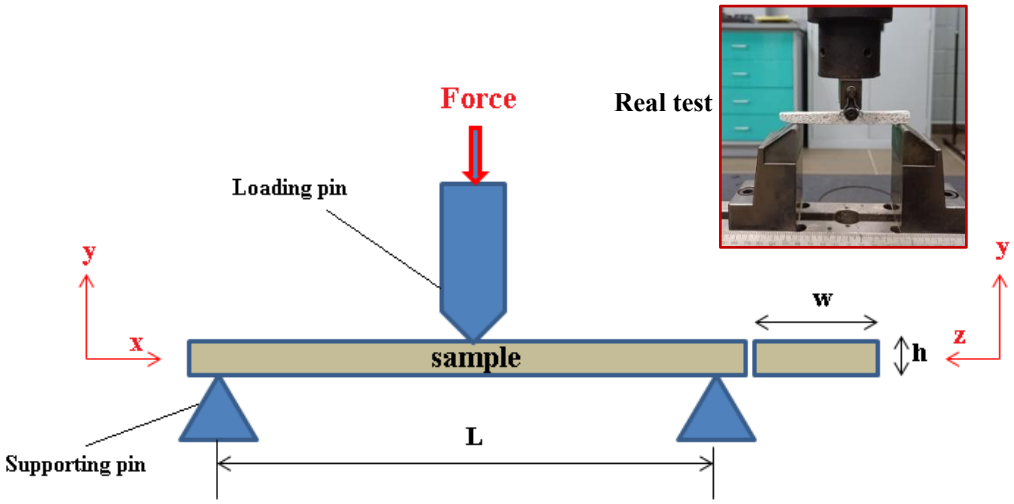

Figure 3.19 Schematic diagram of three-point bending test

The samples were loaded onto a tensile testing machine, and a compression load was applied at a constant rate (1mm/min) until sample failure. The flexural strength (σ_{max}) (MPa) of the sample was calculated using the Equation (3.8) (Pattnaik, 2014).

$$\sigma_{max} = \frac{3F_{max}L}{2wh^2} \tag{3.8}$$

Where; F_{max} is the fracture load applied (N), L, w and h are the length, width and thickness of the test sample (m), respectively. In this study, flat rectangular bars were prepared in dimensional of length (L) of 90mm, width (W) of 10mm and thickness (h) of about 7.5 mm following ISO C1161.

3.7 Dewaxing Test Procedure

3.7.1 Development of Dewaxing Test Apparatus

A multi-mode applicator Samsung microwave oven (model MS28F303TFK) with an internal cavity measuring 357 mm (L) × 357 mm (W) × 255 mm (H) was used to melt the wax pattern from the ceramic mould shell. The experimental set-up of the dewaxing test is presented in Figure 3.20. It consists of a wax collector constructed

from 7.5 mm thick refractory aluminium silicate. The wax collector was equipped with a scale to gauge the percentage of melted wax in the collector (5-100%) over the heating time. A Wi-Fi USB mini camera was mounted on the top of the microwave cavity to monitor the melting process and determine the real-time of dewaxing progress. The percentage of wax melted inside the microwave oven was able to determined accordingly. The surface temperature of the samples during microwave heating was measured using an infrared thermometer, which was positioned through an 8mm hole located at the top of the microwave cavity. The wax collector made of refractory material was equipped with a sample holder to securely fixed the mould. The sample was positioned in a vertical downward direction to facilitate the smooth draining of the melted wax.

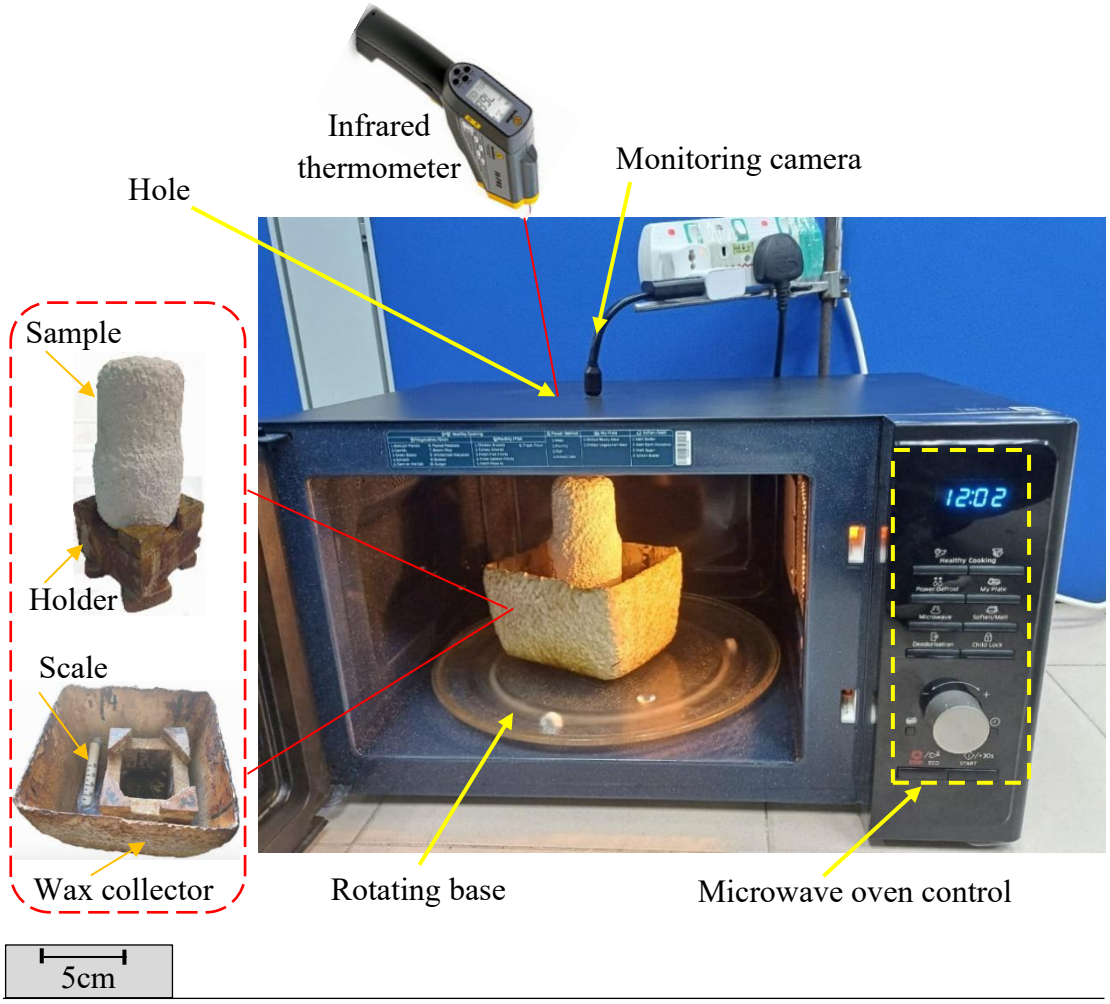

Figure 3.20 Dewaxing test rig set-up

The dewaxing process was performed on standard moulds under ambient conditions, and the process was evaluated at varying microwave power of 300 W, 450 W, 600 W, and 850 W, operating at 2.45 GHz. A comparison was then conducted between the 600 and 850 W on some modified moulds (2.5 and 7.5 wt.% SiC) in terms of mould heating temperature, dewaxing time, and the effect on wax properties. Three samples were used for each weight percentage of SiC.

Subsequently, the most feasible microwave power from the dewaxing process of the standard mould was applied on a modified mould using different percentages of SiC (1 to 7.5 wt% SiC). The minimum time required to completely melt the wax patterns was observed for different waxes used. Each experiment was repeated three times to ensure repeatable and reliable results. ANOVA analysis was conducted to evaluate the contribution of SiC towards the performance of the dewaxing process as compared to the type of waxes used. Two factors are involved, i.e., HYFILL B289 MOD S wax and SIVUCH L1203 wax with different percentages of SiC at a confidence level, $\alpha = 0.05$. The procedure for conducting Two-Way ANOVA with replication using Minitab was explained in detail and is given in Appendix E. The surfaces of the green ceramic moulds were visually inspected for cracks after the dewaxing process.

3.7.2 Strain Gauge Set-up and Installation Procedure

The strain gauge test was conducted to evaluate the thermal stress developed on the mould. Two identical moulds were fabricated using different wax pattern materials. The fabricated moulds were prepared for testing by grinding and flattening a portion of their surfaces close to their nozzle for install the strain gauges, as shown in Figure 3.21(a). The grinding was carried out using the semi-automatic grinding and polishing machine. CEF-3-11 strain gauges were used, their properties are given in Appendix F. The strain gauges were positioned vertically and horizontally on the mould surfaces. The gauges were connected to a data logger through fiberglass insulated cable. The vertical strain gauges were positioned parallel to the cylinder's axis to measure the axial strain, whereas the horizontal strain gauges were positioned

circumferentially to measure the circumferential (hoop) strain. The thermal stress test during the dewaxing process was conducted inside a muffle furnace, heated to 200˚C, instead of using a microwave due to metal-microwave incompatibility, as shown in Figure 3.21(b).

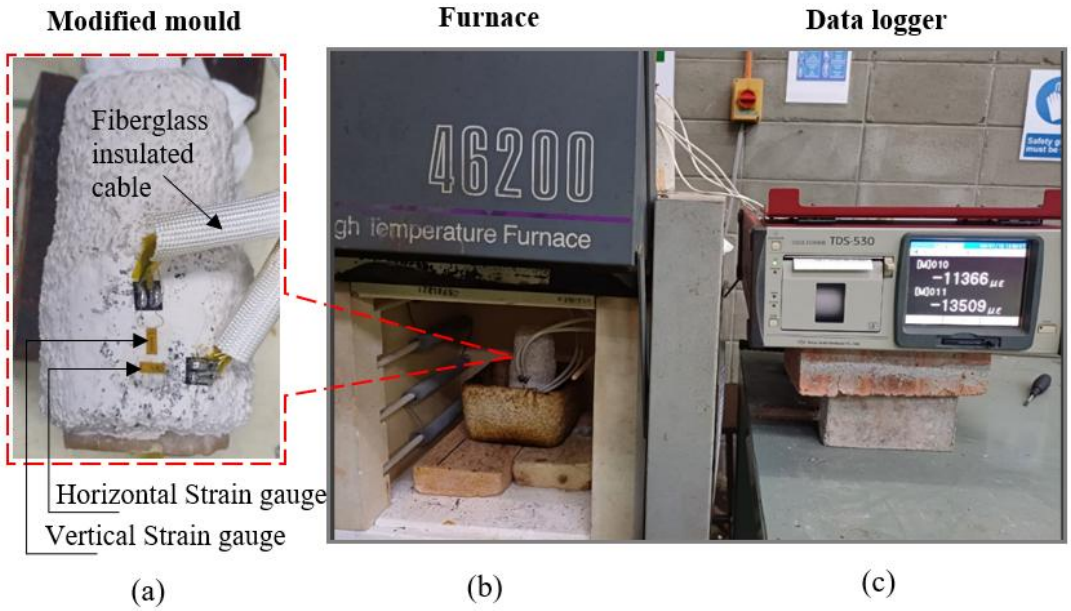

Figure 3.21 Strain gauge set-up (a) close-up view of strain gauges installation on modified mould, (b) overall experimental set-up in furnace, (c) data logger for data capturing

3.8 Evaluation of Microwave Power Absorbed and Analysis of Energy Consumption

3.8.1 Microwave Power Absorbed by Modified Ceramic Mould Shell

The rate of microwave heating is significantly influenced by microwave power. According to the International Microwave Power Institute, the temperature increase of a sample per unit of time can be calculated. In this research, the power absorbed (P_{absorb}) (W/kg) by each sample per unit mass was calculated using the Equation (3.9) (Khraisheh et al., 1997; Houšová and Hoke, 2002).

$$P_{absorb} = \frac{c_p(T_f - T_i)}{t} \quad (3.9)$$

Where c_p is the specific heat capacity at the final temperature of mould (J/kg. K). T_i is the sample temperature before heating (K), T_f is the sample temperature after heating (K), t is the time of sample heating (sec).

3.8.2 Energy Efficiency in Dewaxing

This test was conducted to compare the energy consumption used for dewaxing between a conventional electric firing furnace and a microwave oven. The internal cavity dimensions of the firing furnace used were 1.2 m (L) × 1.45 m (W) × 1.1 m (H).

First, the furnace was pre-heated to 300 ˚C for 15 minutes, and the moulds were heated for 30 minutes. Then, the energy consumption per unit volume, in other words, it is the amount of heat required to melt the wax by the furnace (Q_1) can be calculated using the Equation (3.10) (Yahaya, 2016).

$$Q_1 = Q_r + Q_w + Q_i + Q_{L1} \quad (3.10)$$

Where the four quantities of heat were calculated following formulas (3.11) to (3.14) (Sivanagaraju et al., 2010; Kreith et al., 2011; Yahaya, 2016).

Q_r (J/m^3) is the amount of heat energy needed to raise the moulds' temperature from T_a (ambient temperature) to T_i (furnace internal temperature). ρ_r (kg/m^3) and c_{Pr} (J/kg.K) are the density and specific heat capacity of mould ceramic, respectively.

$$Q_r = \rho_r c_{Pr}(T_\mathrm{i} - T_a) \quad (3.11)$$

Q_w (J/m^3) is the heat energy required to melt out the wax pattern, Q_{LH} (J/m^3) is the latent heat of wax melting (heat transferred at constant temperature, Q_{LH} =$\rho_w L_{Hw}$), T_m the wax melting temperature (K). ρ_w (kg/m^3) and c_{Pw} (J/kg.K) of wax.

$$Q_w = \rho_w c_{Pw}(T_\mathrm{m} - T_a) + Q_{LH} \tag{3.12}$$

Q_i (J/m^3) is the energy supplied to the furnace interior. P_i is the power in watts (W) for a three-phase furnace: ($P_i = \sqrt{3} \times V \times I$), where V(voltage) and I (amperes). t is time of operation (sec), and V_f is Internal furnace volume (m^3) (Fleckenstein, 2017).

$$Q_i = \frac{P_i\ t}{V_f} \tag{3.13}$$

Q_{L1} (J/m^3) is the energy loss from the furnace chamber walls, K_{ins} is the thermal conductivity of the insulating furnace wall (W/mK), A_{ins} is the insulated surface's cross-sectional area (m^2), $L_{ins}$is the insulation thickness (m). t is the required dewaxing time by a furnace (sec).

$$Q_{L1} = K_{ins}(T_\mathrm{i} - T_a)\left(\frac{A_{ins}}{L_{ins}}\right)t \tag{3.14}$$

Secondly, the calculation of the amount of heat needed to melt the wax using a microwave oven (Q_2), was performed using the equation (3.15) (Yahaya, 2016).

$$Q_2 = Q_r + Q_w + Q_i + Q_{L2} \tag{3.15}$$

Q_i (J/m^3) is the interior energy supplied in the microwave was calculated using Equation (3.16), P_M is the microwave power output (W), η_M is the microwave efficiency conversion (%), V_M is the internal microwave volume (m^3) (Meredith, 1998).

$$Q_i = \frac{P_M \ \eta_M}{V_M} \tag{3.16}$$

Q_{L2} (J/m^3) is the heat loss from the mould surface was determined by Equation (3.17) (Kreith et al., 2011; Graham et al., 2014; Yahaya, 2016), considering that; h_{air} is the convection heat transfer coefficient of air (W/m^2 K), A_m is the mould surface area (m^2), T_s is the mould surface temperature (K), t is the required dewaxing time by microwave (sec).

$$Q_{L2} = h_{air} A_m (T_s - T_a) t \tag{3.17}$$

Finally, the proportional relationship (3.18) was used to evaluate the energy saving in dewaxing process.

$$\frac{Q_1 - Q_2}{Q_1} \times 100\ \% \tag{3.18}$$

3.9 Summary

This chapter discussing the methodology employed in conducting the research, detailing the methods, procedures, and analysis to accomplish the outlined objectives. The materials used in constructing the wax patterns and ceramic moulds of the study were characterized. The construction method of standard and modified moulds containing 1, 2.5, 5, and 7.5 wt.% SiC are described. The dielectric, physical, and mechanical properties of the green mould were evaluated, along with an assessment of the thermal properties of the wax pattern. The procedures for conducting microwave experimental dewaxing tests are explained, encompassing measurements of dewaxing time, heating rate, and temperature distribution.

CHAPTER 4

RESULTS AND DISCUSSION

4.1 Introduction

This chapter presents and thoroughly discusses the results of the experimental work obtained to achieve the research objectives. Specifically, the investigation focused on reducing dewaxing time and mitigating crack formation by incorporating SiC content into the outer ceramic mould shell layers and using a novel wax material for the pattern. To begin with, the thermal and chemical properties of the two types of wax patterns used were characterized and systematically compared. Subsequently, the physical, morphological, thermal, and mechanical properties of the green moulds were evaluated. Building upon these evaluations, the chapter discusses the outcomes of microwave experimental dewaxing tests, including measurements of the dewaxing time, the effect of SiC on dewaxing time, wax thermal strain, and temperature distribution. Lastly, attention was given to the assessment of microwave power absorption by the modified moulds, along with an analysis of energy savings achieved through microwave dewaxing.

4.2 Analysis of Wax Pattern Material Properties

Wax properties are primarily influenced by factors such as thermal expansion and melting temperature. Additionally, FTIR analysis is employed to characterize the chemical structure and molecular bonds within the wax, which can help explain variations in these physical properties. In the following sections, all these properties were discussed and analysed for two different wax patterns.

4.2.1 Wax Thermal Expansion Analysis

Table 4.1 presents numerical data of linear thermal expansion values ($\Delta L/L_o$) and thermal expansion coefficients (α) for the types of pattern waxes (HYFILL B289 S Wax, SIVUCH L1203 Wax) across various temperatures (30 to 55 ˚C). Figure 4.1 visually represents the same data at the same temperature range.

Table 4.1 Linear thermal expansion values ($\Delta L/L_o$) and thermal expansion coefficient (α) for pattern waxes

T (˚C)	HYFILL B289 S Wax		SIVUCH L1203 Wax	
	$\Delta L/L_o$ (10^{-4})	α (10^{-6} /˚C)	$\Delta L/L_o$ (10^{-4})	α (10^{-6} /˚C)
30	6.8717	42.4210	0.4107	9.1887
35	12.4523	58.7380	4.1039	43.4067
40	17.9839	68.6437	7.5397	52.1629
45	23.0018	73.7290	9.0605	46.5747
50	23.5872	65.1626	8.2614	33.7855
55	22.4809	54.5684	5.4009	1.8381

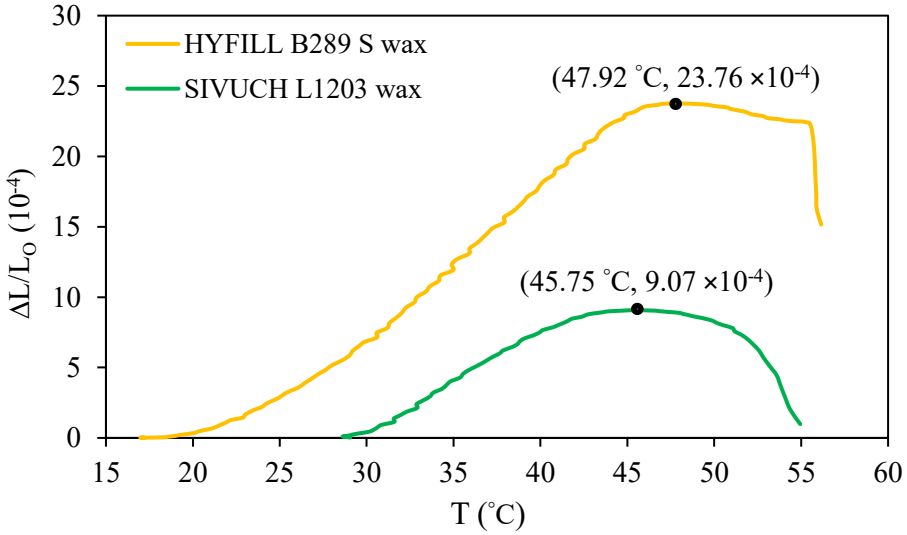

Figure 4.1 Thermal expansion values as a function of temperature for HYFILL B289 S wax, and SIVUCH L1203 wax in the range of (20-55 ˚C).

HYFILL B289 S wax notably expands more significantly at lower temperatures compared to SIVUCH L1203 wax. HYFILL B289 MOD S wax curve shows a gradual upward slope, indicating a progressive increase in strain, such that at about 47.92 °C, HYFILL B289 MOD S Wax reaches its peak ΔL/L0 value of 0.002376. However, as the heating process continued, there was a gradual decrease in the strain rates observed after 55 °C, suggesting a possible complex phase transition or structural change (Wang et al., 2023a). In contrast, SIVUCH L1203 wax showed a smooth, increasing pattern with temperature. The $\Delta L/L_o$ value began at 0.0004 at 30 °C, reaching its peak expansion level at 45 °C where it recorded a maximum thermal expansion rate of only 0.0009, which was three times lower than the thermal expansion rate of HYFILL B289 S wax, thus signifying negligible expansion. This suggests that the SIVUCH L1203 wax possesses a lower and more stable expansion profile compared to the HYFILL B289 S wax, which might make it more suitable for applications where minimal dimensional changes upon heating are desired. The effect of these thermal expansion properties on ceramic mould surfaces is discussed in the 4.5.2 section.

4.2.2 Thermogravimetric Analysis of Wax (TGA & DTA)

Figure 4.2 displays data from thermogravimetric analysis (TGA) and differential thermal analysis (DTA) for HYFILL B289 wax and SIVUCH L1203 wax across a temperature range from room temperature to 550 °C.

The TGA curves (green for HYFILL B289 and yellow for SIVUCH L1203 wax) measure weight changes in the wax samples as they are heated, reflecting weight loss due to melting, vaporization, or decomposition. The decomposition temperatures, where significant weight loss begins, are higher than the melting points, indicating thermal stability up to these temperatures. It is found that the apparent weight loss curve of HYFILL B289 S wax indicates an onset of weight loss at approximately 176 °C and continues until 410 °C as the first stage, with a loss rate of about 40% of the total weight. The sample entered the weight loss stage up to 490 °C. At this point, the entire sample completely burned off due to its organic (Nanda, 2018). On the other hand, the SIVUCH L1203 wax started the weight loss stage at 142 °C (34 °C lower

than HYFILL B289 S wax) and completely burned off at 420 ˚C. Both waxes however showed an identical thermocompatibility and melting peaks, respectively.

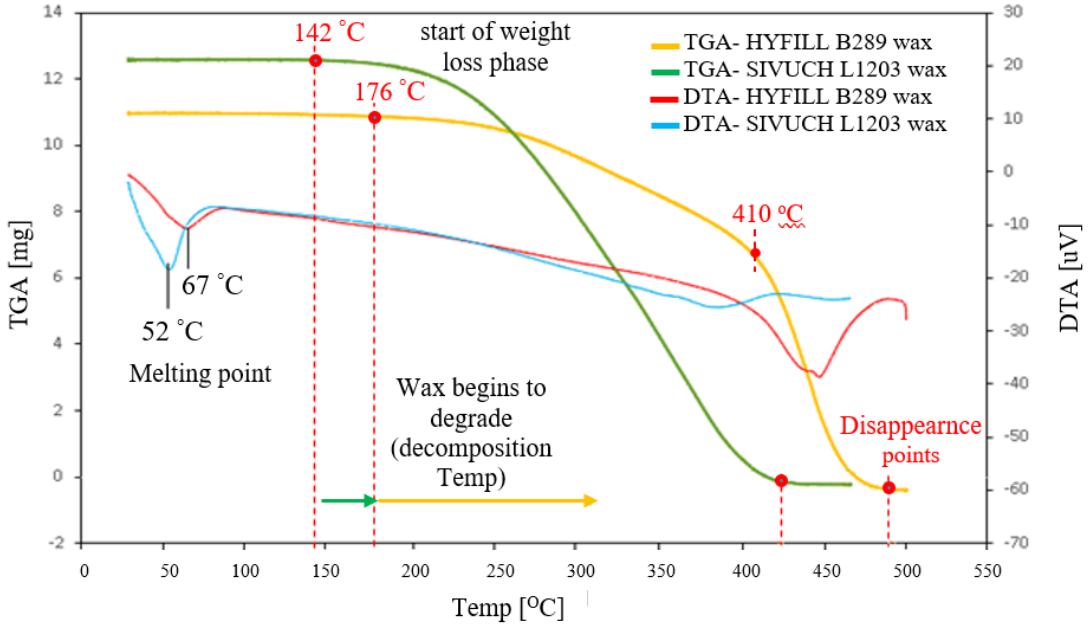

Figure 4.2 TGA and DTA results of the HYFILL B289 MOD S wax and SIVUCH L1203 wax

The DTA curves (red for HYFILL B289 and blue for SIVUCH L1203 wax) measure the heat flow into or out of the wax as it undergoes physical or chemical changes due to heating. It was identified that the HYFILL B289 S wax had two endothermic peaks; the first endothermic peak emerged at 67 ˚C with a fairly low peak value, presumably as a result of HYFILL B289 S wax's phase change (solid to liquid, melting started). The second peak appeared at the end stage of wax decomposition at a temperature of 450 ˚C. SIVUCH L1203 wax, however, only had one sharp endothermic peak at 52 ˚C, indicating that lower melting points are associated with a reduced amount of energy required during the phase change compared to HYFILL B289 S wax. Consequently, it becomes fluid at a lower temperature, which is crucial for processing conditions in applications such as casting. A lower-temperature peak might indicate the melting of a softer or less stable phase, while a higher-temperature peak could represent a higher molecular weight component and more stable, thus

allowing for more uniform and extensive thermal expansion before reaching its melting point (Ronkay et al., 2020).

Based on TGA and DTA, several key insights have been derived to establish boundaries for the dewaxing process. These insights include the range of melting points, the onset of weight loss, and phase transitions. Since the microwave settings are limited to power levels, the aforementioned wax properties were observed during the dewaxing process.

4.2.3 Fourier Transform Infrared (FTIR)

Figure 4.3 shows the absorbance spectra of HYFILL B289 MOD S and SIVUCH L1203 waxes, measured across a range of wavenumbers from 4000 cm^{-1} to 500 cm^{-1} using FTIR to illustrate the chemical interactions.

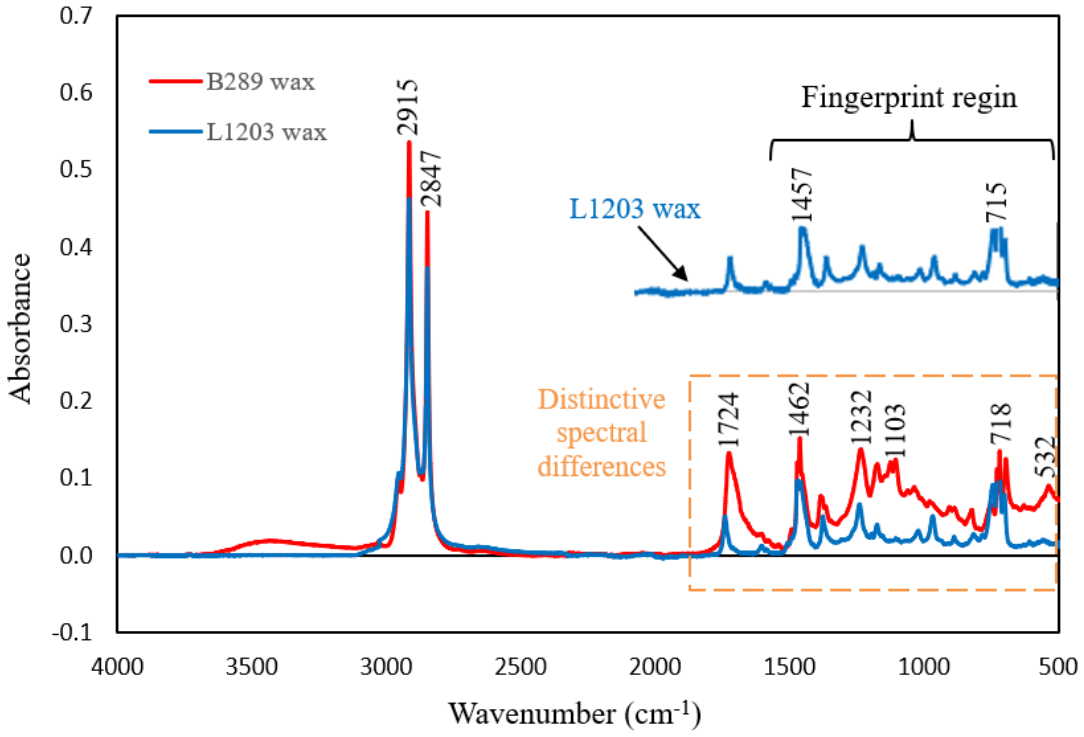

Figure 4.3 Comparison of FTIR spectra of HYFILL B289 MOD S and SIVUCH L1203 waxes

Both waxes show a similar trend from 4000 to 1500 cm^{-1}, indicating the presence of typical aliphatic hydrocarbon that is C-H bands stretched at 2915 cm^{-1} and 2847 cm^{-1}, which, in turn, suggest methylene groups, which are common in paraffin chains. However, HYFILL B289 S wax was observed higher absorption bands than SIVUCH L1203 wax. This indicates that the HYFILL B289 S wax has a higher chemical bond strength between molecules (Smith, 2018). The characteristics of peaks at 1724 cm^{-1} and 1462 cm^{-1} are attributed to the carbonyl in the ester bond (C=O bend) suggested by the glycerol backbone and carbonyl groups. A significant difference in IR spectra was observed ranging from 1200 to 500 cm^{-1}, thus indicating the fingerprint region due to a high number of absorption bands (Brown and Brown, 2000; Cooper et al., 2013). Resins can introduce additional vibrational modes in FTIR spectra due to contained complex chemical functional groups (Chen and Chang, 2020). Therefore, SIVUCH L1203 wax, which contains 27% dammar resin (see Table 3.1), exhibits pronounced vibrational patterns in the fingerprint region, resulting in a spectrum that is richer and more complex than that of HYFILL B289 S wax. Whereas, multiple bands from 1100 to 718 cm^{-1} showed larger aromatic compound bands in HYFILL B289 MOD S compared to SIVUCH L1203. Peaks appearing at 532 cm^{-1} possibly indicate the presence of silica groups (Brown and Brown, 2000; Cooper et al., 2013). This behaviour is confirmed Figure 4.1 which denotes that HYFILL B289 MOD S had larger thermal expansion than SIVUCH L1203. In contrast, substances with stronger chemical bonds (highly absorbent materials) necessitate more energy and time to overcome these bonds and transition from a solid to a liquid state, resulting in higher melting points (67 $^{\circ}C$). Conversely, materials with weaker chemical bonds exhibit lower melting points (52 $^{\circ}C$), as less energy is required to disrupt the bonds (Brown and Brown, 2000; Cooper et al., 2013).

Table 4.2 provides a summary of the thermal and chemical properties of the two types of pattern waxes (HYFILL B289 MOD S and SIVUCH L1203).

Table 4.2 Summary of the analytical results for the wax properties

Type of analysis	HYFILL B289 MOD S wax	SIVUCH L1203 wax
Thermal Expansion	Exhibited higher expansion due to strong intermolecular bonding and a more rigid molecular structure; reached a peak strain of approximately 0.00238. After 55 °C, the strain decreased, possibly due to a phase transition or structural softening.	Showed lower, more stable expansion (peak ≈ 0.0009), approximately three times less than HYFILL, which provided thermal compliance and minimized strain increase.
TGA	Started weight loss at ~176 °C and completely burned off at 490 °C. The delayed degradation was due to its thermal resistance.	started weight loss earlier at ~142 °C, and completely burned off at 420 °C. The earlier decomposition was attributed to its lower thermal stability.
DTA	Had two endothermic peaks at 67 °C and 450 °C.	Had only one sharp endothermic peak at 52 °C, indicating that less energy is required for the phase change and a lower melting point
FTIR	Displayed stronger absorption bands and higher bond density (notably in C-H and aromatic regions), indicating a tightly bonded molecular structure, which corresponds with a higher melting point and expansion.	Displayed additional vibrational modes due to the high resin content and had lower chemical bond strength between molecules, as less energy was required to disrupt the bonds.

4.3 Evaluation of Green Ceramic Mould Shell Properties

The following sections discussed and analysed the green ceramic mould shell with additions of 0, 1, 2.5, 5, and 7.5 wt.% SiC on the dielectric, physical, thermal, and mechanical properties.

4.3.1 Dielectric Properties Analysis

Table 4.3 shows the data on the addition of SiC into the standard, modified ceramic moulds, and their effects on loss factor (ε'') and loss tangent (tan δ) values. The dielectric properties of the waxes were also measured for comparison purposes. The effects of added SiC into ceramic mould shell were plotted as shown in Figure 4.4.

Table 4.3 Dielectric properties of the ceramic moulds shell (standard and modified) and pattern waxes

SiC (wt.%)	Dielectric loss factor (ε'')	No of times improvement: $\frac{\boldsymbol{\varepsilon''}SiC\%}{\boldsymbol{\varepsilon''}unmodified}$	Dielectric loss tangent ($tan\ \delta$)	No of times improvement: $\frac{\boldsymbol{tan\delta}\ SiC\%}{\boldsymbol{tan\delta}\ unmodified}$
Standard (0)	0.0245	0	0.0133	0
1	0.1559	6	0.1007	7
2.5	0.2734	11	0.1394	10.5
5	0.3060	12.5	0.1641	12
7.5	0.3713	15	0.1756	13.5
HYFILL B289 S wax	0.0256	NA	0.0124	NA
SIVUCH L1203 wax	0.0977	NA	0.0435	NA

The blue curve represents the loss factor as a function of SiC wt.%. It increases steadily as the SiC percentage rises, starting near 0 for 0 wt.% SiC and reaching approximately 0.35 at 7.5 wt.% SiC. This indicates the ability of the material to dissipate electromagnetic energy as heat increases with a higher SiC percentage. The red curve represents the loss tangent (tan δ), which measures the ratio of the imaginary

part to the real part of the dielectric constant. Similar to the loss factor, it also increases with SiC content, but at a slower rate compared to the loss factor. Both the loss factor and the loss tangent exhibit a positive correlation with the SiC weight percentage, suggesting that adding SiC enhances the material's ability to absorb and convert microwave energy into heat. This behaviour is likely due to the high dielectric and thermal properties of SiC, which enhance the composite's overall dielectric response (Peng et al., 2013; Singh et al., 2024). Higher SiC content means increased energy dissipation during microwave heating, which could be beneficial in applications like microwave hybrid heating for investment casting moulds.

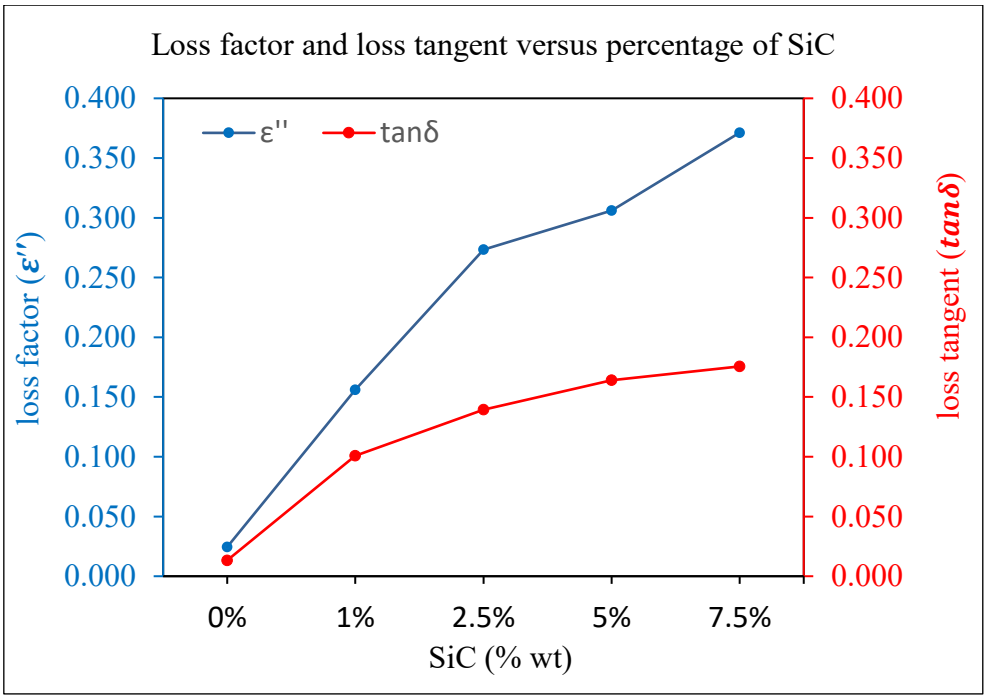

Figure 4.4 Effect of adding SiC on loss factor and loss tangent values

It is noticed that the addition of 7.5 wt.% SiC led to double the dielectric loss factor (ε'') and the loss tangent ($tan\ \delta$) by 15 and 13 times, respectively, compared to the standard mould. This enhancement is attributed to an increased number of polarization sites, which contributed to a significant increase in the dissipation of absorbed microwave energy. From Table 4.3, it can be seen also that SIVUCH L1203 exhibited superior dielectric properties compared to HYFILL B289 MOD S. The higher ε'' (almost four folds) suggests that the conversion of microwave energy into heat will be more efficient if used together with modified ceramic mould.

4.3.2 Bulk Density and Apparent Porosity Analysis

Table 4.4 summarizes the measured weights, apparent porosities, and bulk density of the green ceramic moulds with the addition of various SiC percentages. SiC particles were added to layers 3rd to 6th and their apparent bulk density and apparent porosity of the green mould were measured. These data were plotted into graphs as shown in Figure 4.5.

Table 4.4 Bulk density and apparent porosity of the green moulds

Percentage SiC in the backup layers (%)	Dry sample weight (Desiccator) *Wa (g)*	Suspended sample weight in water *Wb(g)*	Saturated sample weight *Wc (g)*	Bulk density ρ (g/cm^3)	Apparent porosity *P* (%)
0	31.7131	22.1604	33.9794	2.683	19.174
1	37.0425	25.8137	39.6146	2.684	18.641
2.5	33.3974	23.2854	35.6996	2.690	18.544
5	34.2159	23.9380	36.4917	2.725	18.128
7.5	32.9841	22.9307	35.0209	2.728	17.846

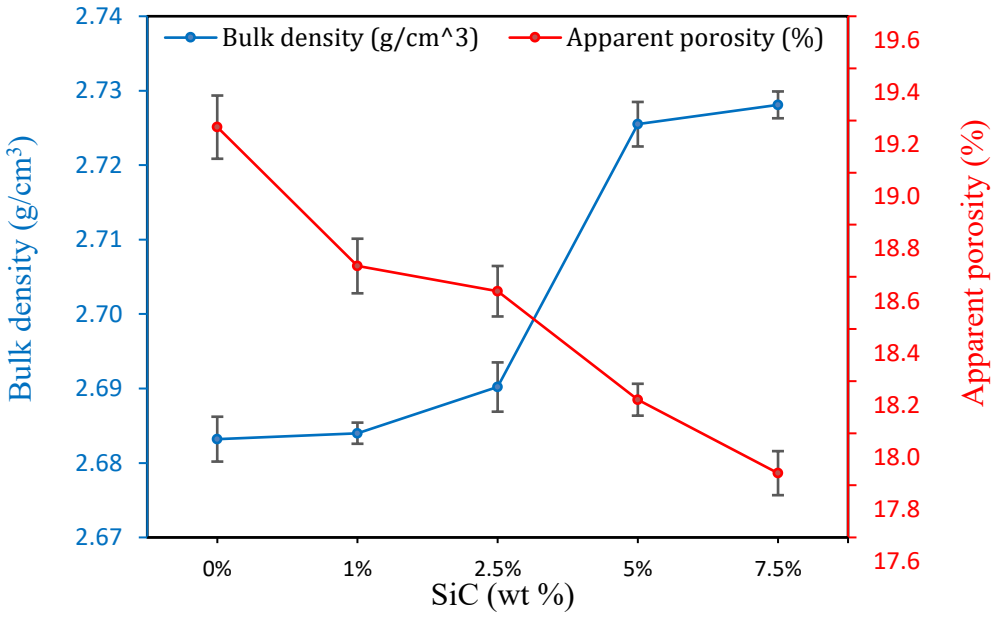

Figure 4.5 Bulk density and apparent porosity standard and modified green ceramic mould samples

Initially, the bulk density increases slightly from 0% to 2.5% SiC wt.%. Beyond 2.5% SiC wt.%, the bulk density increases sharply, peaking at 7.5% SiC wt.%. This behaviour suggests that the densification of the material improves with higher SiC content as the results of better compaction of particles and reduction of voids. These results were in agreement with Kim et al. (2016) in their investigation to improve the mechanical properties of fused silica ceramic core of gas turbine blades by adding SiC particles but at higher percentages (5 to 20 wt.%). Similarly, the addition of 15 wt.% SiC to the backup coat slurry led to a slight increase in the density of the shell moulds compared to the original shell formulation (Wang et al., 2025).

Apparent porosity gradually decreased with increasing silicon carbide content, with the addition of 7.5% silicon carbide reducing the porosity of the ceramic mould shell by 6% compared to the standard mould. These results were also in agreement with Wang et al. (2025), who investigated the effect of adding Al_2O_3 and SiC micro-scale powders to the backup coat slurry of shells for investment casting, where the mould porosity decreased by 13% with the addition of 15 wt.% SiC compared to the standard mould. The reduction in porosity indicates that adding SiC helps reduce void spaces within the material. In contrast, at lower SiC levels, the material seems to have insufficient SiC particles to fill voids, resulting in higher porosity and lower density. A similar finding was reported by Oguntuyi et al. (2023), who studied the effects of SiC on the densification of TiB_2 ceramic matrices using spark plasma sintering.

4.3.3 Microstructure Analysis of Standard Green Ceramic Mould Shell

The microstructural characteristics of materials, including ceramic moulds, play a key role in determining the properties and performance of the final component. Figure 4.6 shows a multilayered stucco structure of the standard ceramic mould shell (0 wt.% SiC) using scanning electron microscopy (SEM). The image shows the cross-section of the ceramic shell from the inner surface (1st layer) to the outer surface (7th layer), highlighting the microstructural differences between layers.

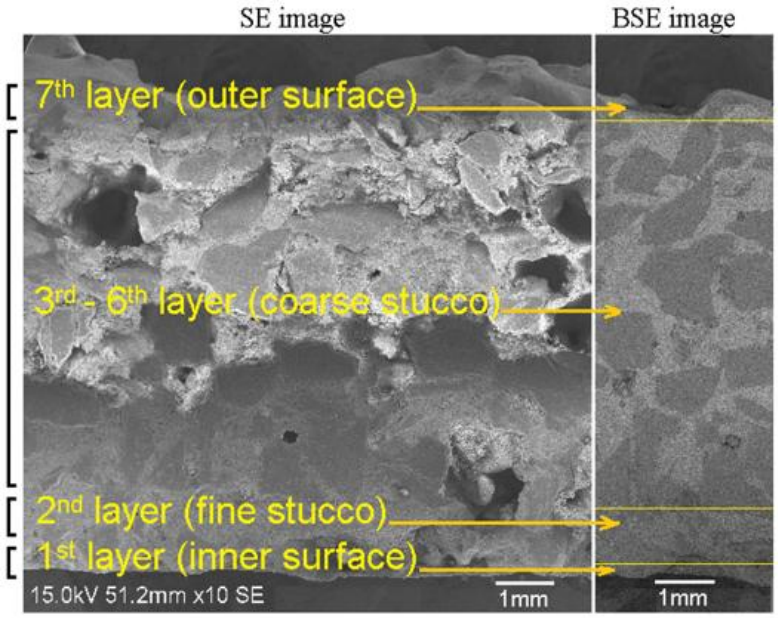

Figure 4.6 The cross-section of the standard ceramic mould shell (0 wt.% SiC)

The secondary electron (SE) image shows the topographical details, highlighting the porosity across different stucco layers. It reveals the transition from fine stucco in the 2nd layer to coarser stucco between the 3rd and 6th layers, and finally to the outermost layer. The backscattered electron (BSE) image shows the variations in stucco grain size, corresponding to fine grain at the bottom and coarse grain at the top across the layers. Finally, the sealing layer was composed solely of slurry.

Figure 4.7 displays SEM images along with EDX analysis of the morphology for two different surfaces of the standard green mould shell. Figure 4.7(a) depicts the primary layer (inner surface), while Figure 4.7(b) illustrates the sealing layer (outer surface) micrograph.

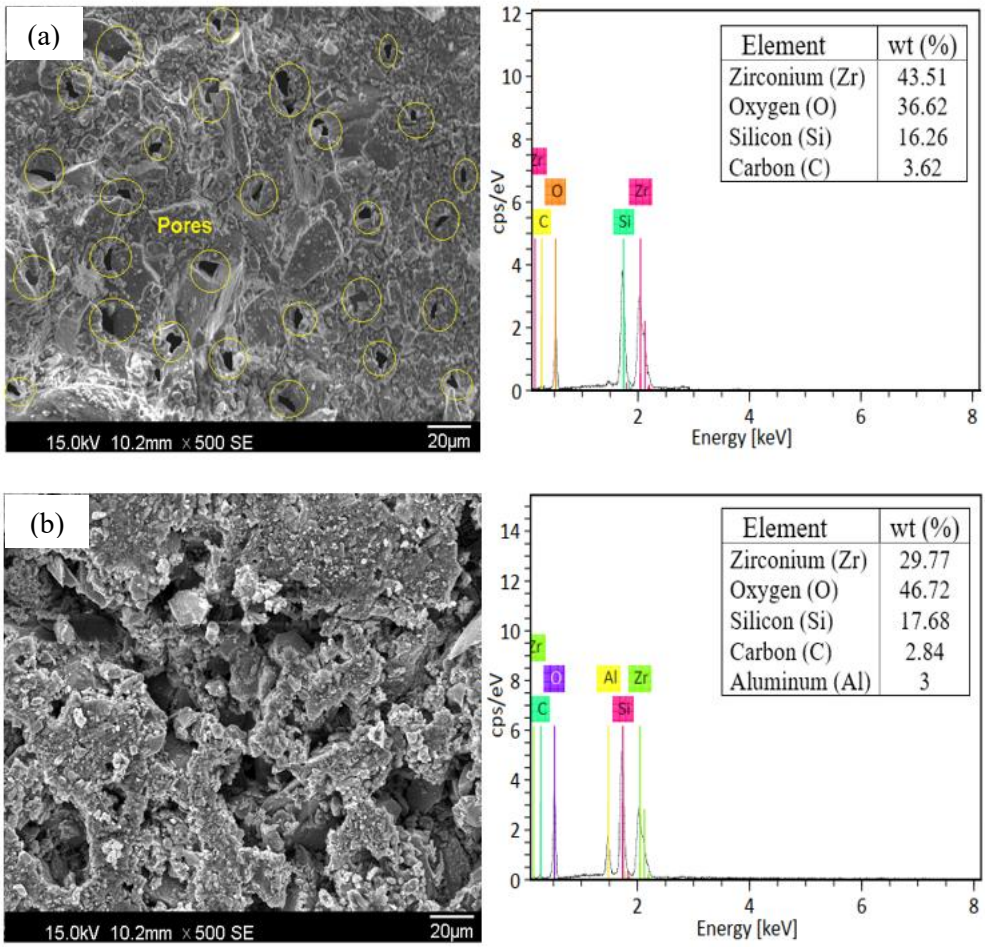

Figure 4.7 SEM image of pores distribution and EDX analysis of the standard green mould shell for (a) the inner surface, and (b) the outer surface

The two figures show a denser pore distribution on both the inner and outer surfaces of the mould. The stucco layers with coarse particles contributed to low density and wider voids, resulting in a highly porous area. The presence of these pores is important for releasing undesirable gases during the dewaxing process in the IC (Nanda, 2018). A notable disparity was observed in the wt.% between the inner and outer surfaces. Specifically, a high zirconium (Zr) weight percentage of 43.51 wt.% is observed in the inner surface, compared to 29.77 wt.% in the outer surface. This can occur through diffusion, adsorption, and reaction with surrounding environments, leading to variation in composition (Zeid and Alnoury, 2023). In contrast, a high weight percentage of about 46.72 wt.% of oxygen is observed in the outer surface, compared to 36.62 wt.% in the inner surface. This variation may be linked to the outer

surface's exposure to the surrounding environment, leading to the formation of oxygen-rich compounds through oxidation processes (Attarzadeh and Ramana, 2021). Notably, Aluminium (Al) is only detected on the outer surface with a weight percentage of 3 wt.%, while it is absent on the inner surface. This is due to stucco residue left in the slurry while constructing mould backup layers. In addition, the distribution of pores and elemental distribution in the standard green ceramic mould shell suggests that it is efficient in preventing gas trapping during the dewaxing process.

4.3.4 Thermal Conductivity Analysis of Green Ceramic Mould Shell

Figure 4.8 displays the thermal conductivity of Al_2O_3-SiO_3-based green ceramic mould shell for standard and modified with various percentages of SiC. The recorded test data are provided in Appendix G.

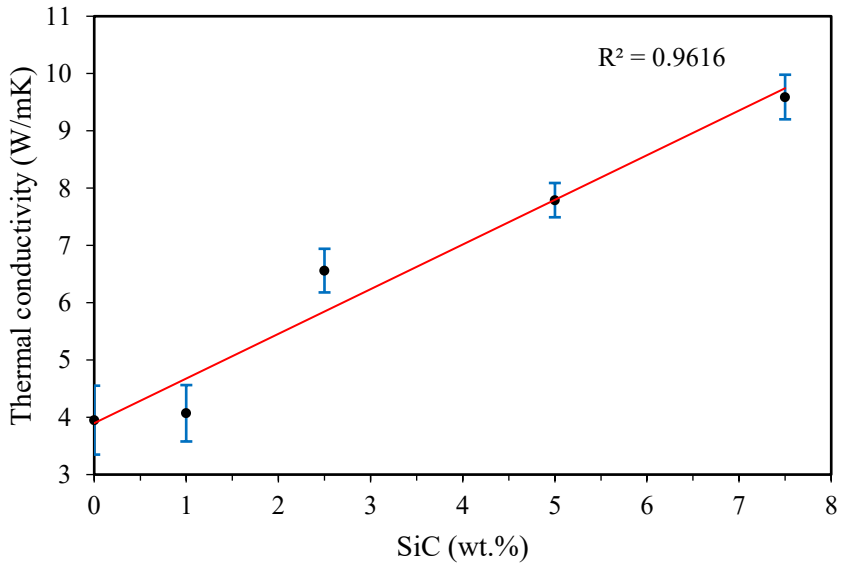

Figure 4.8 Thermal conductivity of ceramic moulds versus percentages of SiC

In fact, the thermal conductivity of the shell mould plays a crucial role in determining the heat transfer rate during both the dewaxing and casting processes. It directly influences the wax removal time, the cooling rate of the casting, the solidification behaviour of the molten metal, and the overall efficiency of the

manufacturing process (Tseng et al., 2023). It was found that a linear increase in ceramic mould thermal conductivity as SiC content increases. Notably, the transition from 0 wt.% SiC to 2.5 wt.% SiC enhanced the mould thermal conductivity by 40% followed by 49% and 59% at 5 wt.% and 7.5 wt.% of SiC addition, respectively. This is supported by a strong and logical reasoning in which SiC is a known heat conductor due to its intrinsic high thermal conductivity properties (130 W/mK at 20 °C) (Kim et al., 2016), and facilitates heat transfer better than Al_2O_3-SiO_2. These results were in agreement with Du et al. (2023) in their investigation to improve the thermal performance of cement-based composite materials (CCMs) by adding SiC in different particle sizes. Furthermore, Wang et al. (2025) observed that the addition of 15 wt.% SiC enhanced the heat transfer coefficient (HTC) of ceramic mould shells from a range of 440–690 W/m²·K to 760–985 W/m²·K. Similarly, Zhang et al. (2022) demonstrated that adding CFs@SiC significantly increased the thermal conductivity of polydimethylsiloxane (PDMS) composites from 0.16 W/m·K to 4.0 W/m·K, confirming the critical role of SiC in improving thermal transport performance. Moreover, an R-squared value of 96.6% indicates a very strong linear correlation between SiC content and increased thermal conductivity suggesting that SiC's proportion in the composite is a reliable predictor of improved thermal performance.

4.3.5 Thermal Expansion of Green Mould Shell

Figure 4.9 displays the thermal expansion curve for a standard ceramic mould shell, showing the relative expansion of the ceramic mould material ($\Delta L/L_o$) across a temperature range of 25 to 600 °C. The corresponding test data can be found in Appendix H.

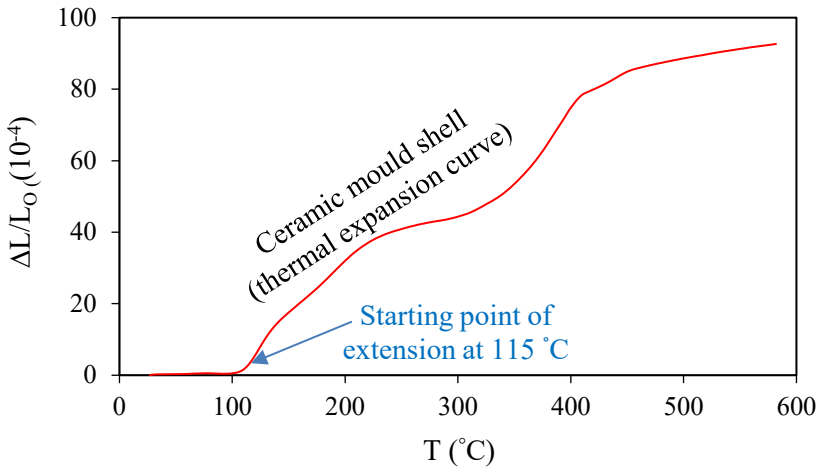

Figure 4.9 Thermal expansion values as a function of temperature for the ceramic mould shell in the range of (25 to 600 ˚C)

The curve remains relatively flat from 25 ˚C to 100 ˚C, indicating minimal thermal expansion in this temperature range. At approximately 115 ˚C, there is a noticeable sudden change point where the expansion rate begins to increase. This point marks the onset of thermal expansion within the ceramic mould material. The curve rises steeply, showing a rapid increase in the thermal expansion as the temperature continues to rise. This behaviour suggests that the ceramic material's crystalline structure becomes more susceptible to thermal stresses as it heats up. This behaviour is consistent with previous findings by Garai et al. (2022), who reported that SiO_2-MgO-Al_2O_3-B_2O_3-K_2O-MgF_2 glass-ceramics exhibited minimal thermal expansion at lower temperatures, with a coefficient of thermal expansion (CTE) of 8.02×10^{-6} C^{-1} in the range of 50–300 ˚C, followed by a significant rise to 9.96×10^{-6} C^{-1} at 800 ˚C. This trend was attributed to increased lattice vibrations and structural relaxation at elevated temperatures, which enhances the material's susceptibility to thermal stresses, supporting the observed behaviour in the current study. Such variation is particularly noteworthy given the potential risk of mould failure (cracking) during the initial phases of the investment casting dewaxing process (Everhart et al., 2013). A more detailed discussion of the thermal expansion behaviour of the ceramic mould shell and its effect on the dewaxing process is provided in Section 4.5.2.

4.3.6 Specific Heat Capacity of Green Ceramic Mould Shell

The raw heat flow data obtained from the DSC experiment are given in Appendix I. Figure 4.10 shows the relationship between power required to heat the sample and the corresponding temperatures of standard and modified green ceramic moulds with varying wt.% of SiC.

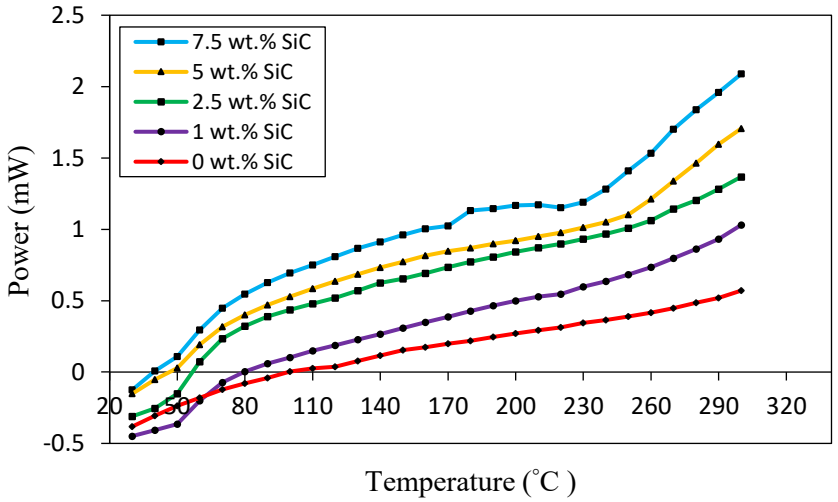

Figure 4.10 Power versus temperature for green ceramic moulds content different percentage of SiC (DSC test)

The negative power readings at the beginning of the curves suggest that the standard and modified green ceramic mould shells absorbed energy. This suggests that an endothermic reaction occurred early in the heating process, with heat absorbed to evaporate moisture or decompose the binders (Stubna and Vozár, 2005; Lombardo and Retzloff, 2020).

The curves also clearly indicate that as the SiC percentages increase, the power required at each temperature point increases. This suggests that SiC enhances the thermal conductivity of the moulds. Higher thermal conductivity means that the material conducts heat more efficiently, but it also implies that more energy (power) is needed to raise the temperature of the material, as it dissipates heat more rapidly. Similar behaviour was reported by Parchovianský et al. (2014) who investigated the

effects of adding SiC to alumina (Al_2O_3) nanocomposites on their thermal and electrical properties.

Figure 4.11 depicts the specific heat capacity (C_p) of green ceramic moulds materials at varying SiC wt.%, measured at three distinct temperatures, 100, 200, and 300 ˚C by using Equation (3.7).

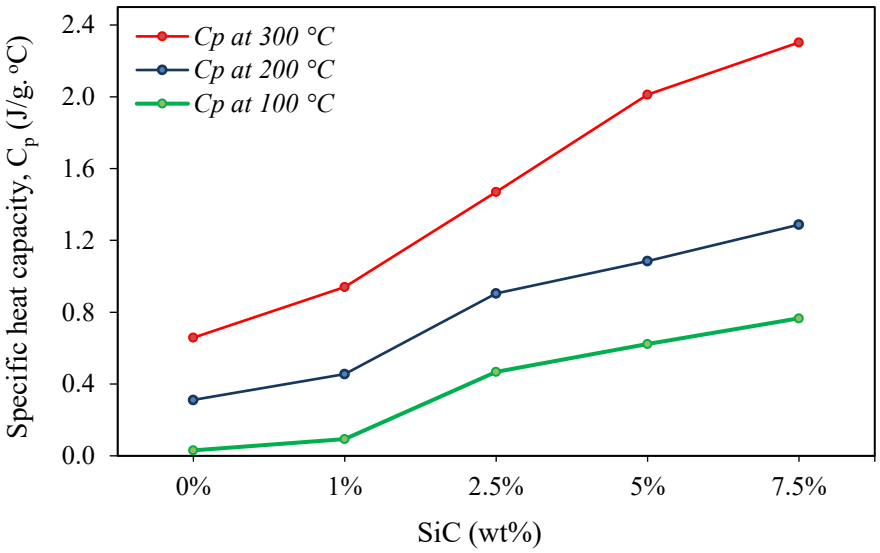

Figure 4.11 Specific heat capacity of green ceramic mould versus SiC wt.% at 100 ˚C, 200 ˚C, and 300 ˚C

The heat capacity of the standard and modified green moulds was calculated using Equation (3.7) (Appendix I) at three different temperature levels to illustrate the effect of temperature on the heat capacity of ceramic samples with varying silicon carbide ratios. The green and blue curves, representing Cp at 100 °C and 200 °C, respectively, show a symmetric and steady rise in specific heat capacity with an increase in SiC content. In contrast, the red curve, depicting Cp at 300 °C, indicates a sharper rise, reflecting the temperature-dependent behaviour of the mould material. This behaviour suggests that at higher temperatures, the interactions between SiC particles and the matrix are more effective, possibly due to enhanced phonon scattering or other thermal mechanisms.

Further analysis reveals a clear and consistent increase in specific heat capacity with an increase in SiC percentages at all temperature cases, highlighting the SiC's role towards improving the thermal absorption capability of the material (Sane et al., 2020). Specifically, at a temperature rise from 200 °C to 300 °C, a considerable increase in specific heat capacity can be noticed, specifically in samples with 5 and 7.5 wt.% SiC, with an improvement of approximately 45% of each. Such a considerable improvement can be attributed to increased temperature enhancing SiC's contribution towards thermal property improvement in the mould material, with increased phonon activity and thermal management in the green ceramic mould shell. These findings are consistent with those reported by Loshchinin et al. (2019) in their study on the thermophysical properties of SiC-based ceramic composite materials across the temperature range of 20–1300°C. The energy absorbed and dissipated per unit mass of the mould increases with SiC content and temperature, indicative of increased absorption and microwave power dissipation, as further discussed in section 4.6.

4.3.7 Flexural Strength Analysis of Green Ceramic Mould Shell

Figure 4.12 illustrates the flexural strength (MPa) of standard and modified green ceramic moulds at varying percentages of SiC from 1 wt.% to 7.5 wt.%. SiC particles were incorporated into the coarse stucco in the four backup layers from 3 to 6.

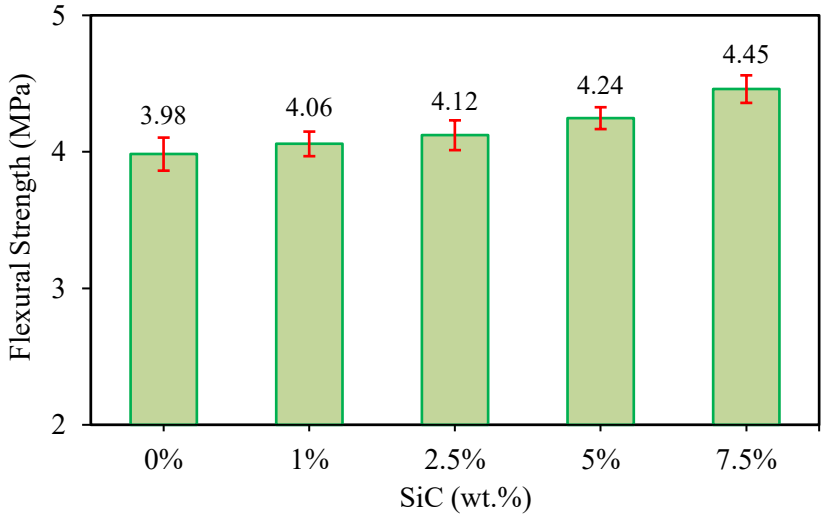

Figure 4.12 Flexural strength of standard and modified green moulds

The above bar plot shows the slight gradual increase in flexural strength of modified green ceramic shells compared to the standard shells. The results reveal that the increase in strength is more pronounced at higher SiC percentages, indicating that the impact of SiC on strength may be more effective at these higher percentages. The addition of 2.5, 5, and 7.5 wt.% of SiC in the 3rd to 6th layers led to an increase in flexural strength by 4%, 7%, and 12%, respectively. These results are consistent with the findings of Kim et al. (2016) and Wang et al. (2025), who reported that the addition of 15 wt.% SiC enhanced the fired flexural strength of ceramic moulds by 33% and 22%, respectively. Additives in ceramic mould don't necessarily produce increased flexural strength in all cases. For example, in the study by Yahaya et al. (2016), the addition of 30% activated charcoal reduced ceramic mould shells' flexural strength by 45%.

4.3.8 Summary of the Influence of SiC Addition on the Dielectric, Physical, Thermal, and Mechanical Properties of Green Ceramic Mould Shells

The incorporation of SiC into ceramic mould shells significantly influenced their dielectric, physical, thermal, and mechanical properties, varying with the percentages of SiC. For instance, adding 7.5 wt.% SiC enhanced the dielectric loss factor (ε'') and loss tangent (tan δ) by 14 times, thereby improving microwave absorption and energy dissipation capabilities—key factors for applications involving microwave hybrid heating. Physically, the addition of SiC had a minor effect, which increased the density of the mould and reduced its porosity. Thermally, the addition of 7.5 wt.% SiC improved the thermal conductivity of the green mould shell by 59%, thereby enhancing heat transfer efficiency. The analysis of specific heat capacity revealed an increase in the heat capacity storage of green ceramic moulds. As the SiC wt.% increased, the enhancement being more pronounced at higher temperatures. Mechanically, the addition of 7.5 wt.% SiC increased the flexural strength of the green mould shell by 12%, offering greater resistance to structural failures during the dewaxing process. These improvements showed that SiC effectively enhances the properties and performance of modified green ceramic moulds, which will greatly help the dewaxing process.

4.4 Analysis of Dewaxing Test Results

The subsequent sections discussed and analysed the effects microwave power and various SiC contents on the dewaxing process in terms of wax pattern melting time and the integrity of the green ceramic mould for two different wax patterns. The contributions of SiC and the type of wax to the dewaxing process were also investigated.

4.4.1 Effect of Various Microwave Power on the Dewaxing Time of Standard Green Ceramic Mould

Figure 4.13 illustrates the effect of different microwave power settings (300, 450, 600, 850 W) on the dewaxing time of green standard moulds using two types of waxes: HYFILL B 289 S and SIVUCH L1203. Each bar indicates the time taken to complete dewaxing at each power level for both wax types.

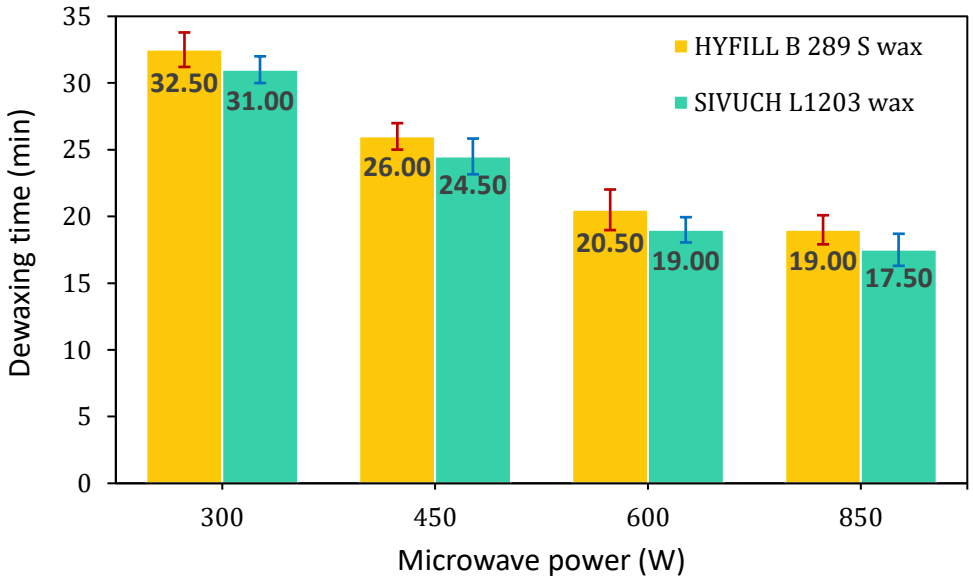

Figure 4.13 Effect of the microwave energy range on the dewaxing time of green standard moulds

The figure shows that as the microwave power increases, the dewaxing time for both types of wax decreases. This trend is consistent across both wax types, suggesting that higher energy inputs lead to faster dewaxing processes. This observation aligns with the findings of Hong et al. (2021), who reported that increasing microwave power significantly enhanced the temperature rising rate of coal powder, thereby reducing the time required to reach target temperatures. The accelerated dewaxing can be attributed to the intensified molecular motion under higher microwave energy, leading to a rapid temperature rise in the ceramic mould shell (Just et al., 2024). Consequently, the wax pattern reaches the phase transformation from solid to liquid much faster. HYFILL B289 S wax requires slightly longer duration to dewax than SIVUCH L1203 wax at all power levels. This could indicate differences in the thermal properties or microwave absorption characteristics of the two waxes, as discussed in the 4.2 and 4.3.1 sections.

Notably, a significant reduction (39%) in dewaxing time was observed when microwave power increased from 300W to 600W. However, there was only a slight difference (~5%) in the dewaxing times for both waxes using a standard ceramic mould composition. It took around 19 minutes to altogether remove the waxes from the mould at 600 W and 850 W.

4.4.2 Analysis of Dewaxing Performance using SIVUCH L1203 Wax at 600W and 850W Microwave Power Settings

The comparison process included exposing two modified moulds, containing 2.5 wt.% and 7.5 wt.% SiC (using SIVUCH L1203 wax) to microwave power levels of 600 and 850 W. The objective was to determine the most feasible microwave power for the dewaxing process. The effect of each microwave power on mould heating temperature, dewaxing time, and wax properties was considered. Three samples were used for each power level.

Figure 4.14 illustrates the surface temperature of two modified moulds, containing 2.5 and 7.5 wt.%, respectively, and the dewaxing times required for each

using two different microwave power settings: 600W and 850W. The image shows wax burning on the inner surface of the shell when using a microwave power of 850 W.

Despite the potential for faster wax removal at higher powers, the reduction in dewaxing time proved marginal beyond 600W, as depicted in Figure 4.14(a). For example, increasing the power from 600W to 850W reduced dewaxing time by only 9% and 10% for the 2.5 wt.% and 7.5 wt.% SiC modified moulds, respectively. Furthermore, using 850 W caused a significant temperature increase on the mould's inner surface, leading to wax burning as the mould temperature exceeded its flash point (>210 °C), as shown in Figure 4.14(b). Accordingly, 600W was selected due to its efficiency and safety. In this investigation, only moulds using SIVUCH L1203 wax were tested, as its flash point is higher than that of HYFILL B289 MOD S wax (see Table 3.1). Consequently, HYFILL B289 MOD S wax is expected to be more susceptible to burning at lower temperatures.

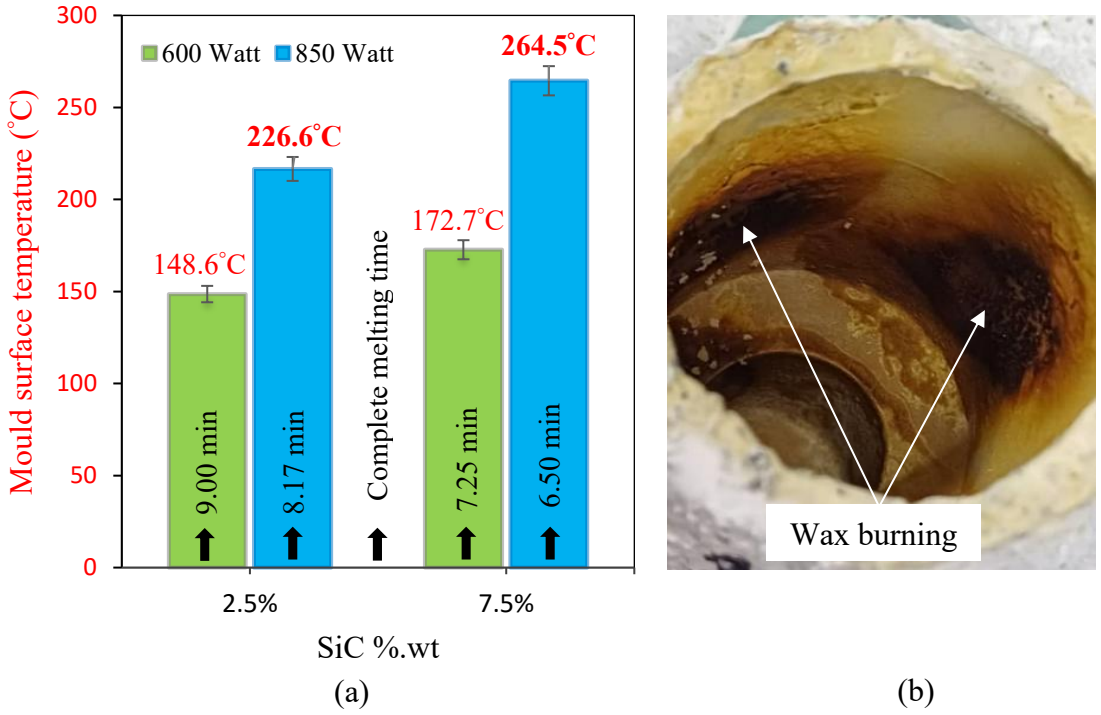

Figure 4.14 (a) Comparison of the effect of 600 W and 850 W microwave power on heating temperature and dewaxing time of green moulds using SIVUCH L1203 wax, (b) Wax burning at 850 W microwave power

Additionally, at high microwave power, rapid heating occurs, causing ceramics to become susceptible to sudden temperature changes, which can result in thermal shock (stress) and fracture (Shang et al., 2019). Conversely, the ceramic material is heated more uniformly at medium power levels. This prevents the hotspots that can occur at high power levels, ensuring that the entire ceramic object or sample reaches the required temperature evenly (Garnault et al., 2021). Another critical factor to consider is the impact of high temperatures on the life and recyclability of the wax. High temperatures that significantly exceed the melting point of wax can lead to its thermal degradation, resulting in the breakdown of its chemical structure, changes in its thermal properties, and linear shrinkage (Grzeskowiak et al., 2015). This degradation reduces the quality and effectiveness of the wax for future use, thereby decreasing its recyclability (Intarapong et al., 2024).

4.4.3 Effect of Microwave Power and SiC (wt.%) Content on the Dewaxing Process of Green Modified Moulds

Figure 4.15 illustrates a schematic diagram of the dewaxing test rig setup for monitoring the percentage of wax pattern melting over time within a microwave cavity.

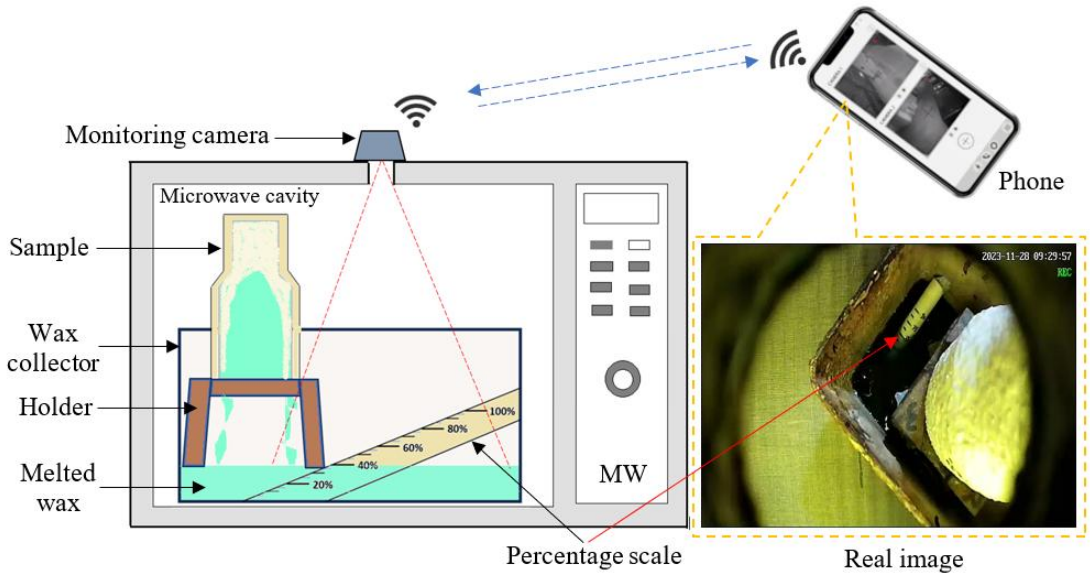

Figure 4.15 Schematic diagram of monitoring the dewaxing process in a microwave

The percentage of melted wax was evaluated by monitoring the wax collector through a Wi-Fi-enabled USB mini camera affixed to a hole at the top of the microwave cavity, as detailed in section 3.7.1. The wax collector is provided with a scale calibrated to indicate the percentage of melted wax in the collector ranging from 5 to 100%, corresponding to the level of melted wax accumulated over time.

Figure 4.16 displays the percentage of wax melted (using SIVUCH L1203 wax as an example) versus microwave heating time at a microwave power of 600W. The vertical axis represents the percentage of wax melted, while the horizontal axis shows the microwave heating time in minutes. The recorded test data is given in Appendix J. Consequently, it is evident that an increase in the SiC percentage in the mould shell results in a faster dewaxing time. In contrast, standard green ceramic moulds shell or those with low SiC percentages exhibited slower wax melting. This indicates that a higher SiC percentage in the mould enhances microwave energy absorption due to SiC's properties as an effective microwave susceptor. Hence, the temperature difference increases, leading to a greater amount of heat generated, as discussed in section 4.4.5. As a result, at a higher mould temperature, less time is required to melt the wax compared to a lower temperature, even with the same microwave power applied. This reduces the dewaxing time and enhances energy saving (Doucet and Laviolette, 2022; Fatykhov and Fatykhov, 2015). Therefore, the time required to melt the wax depends on its SiC percentage. This observation is consistent with several previous studies in the literature. For example, Monzavi et al. (2022) reported that incorporating SiC foam as a microwave susceptor significantly enhanced microwave absorption, leading to faster internal heating and accelerated melting of paraffin wax. Similarly, Cheng et al. (2024) demonstrated that SiC layers within a microwave kiln facilitated rapid temperature rise, achieving over 700 °C quickly, thus promoting faster phase changes. Li et al. (2022) further explained that ceramics with higher dielectric loss factors, such as SiC-based systems, exhibit superior microwave absorption capabilities, efficiently converting electromagnetic energy into heat. This fundamental behaviour aligns with the present findings, where increased SiC content enhanced heat generation within the mould, thereby shortening the dewaxing time, as further validated by ANOVA analysis (section 4.5.1).

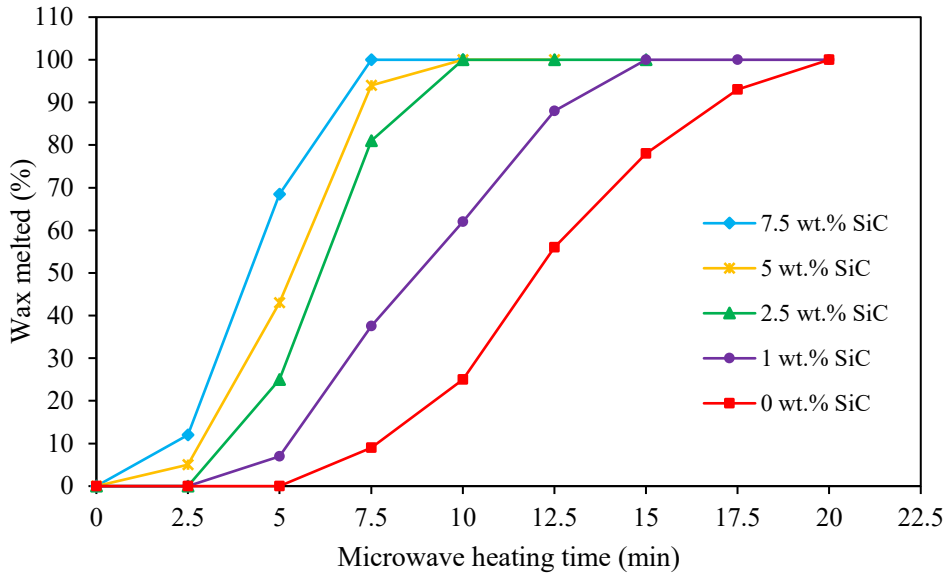

Figure 4.16 Percentage of wax melted versus microwave heating time for different SiC percentages (wt.%)

Table 4.5 presents data on the dewaxing times required for moulds with varying SiC percentages, using a microwave power of 600W for two different wax patterns (HYFILL B289 MOD S and SIVUCH L1203). The table indicates whether each configuration led to mould shell cracking or not. These data were plotted into graphs as shown in Figure 4.17, illustrating the effect of SiC wt.% on the dewaxing time.

Table 4.5 Time required to completely dewax at various SiC percentages in backup stucco using 600W Microwave Power and its effect on mould shell cracking

SiC (wt.%)	HYFILL B289 MOD S wax		SIVUCH L1203 wax	
	Dewaxing time (min)	Crack	Dewaxing time (min)	Crack
0	20.50	Yes	19.00	No
1	14.75	Yes	13.30	No
2.5	10.25	Yes	9.00	No
5	9.20	Yes	8.15	No
7.5	8.80	Yes	7.25	No

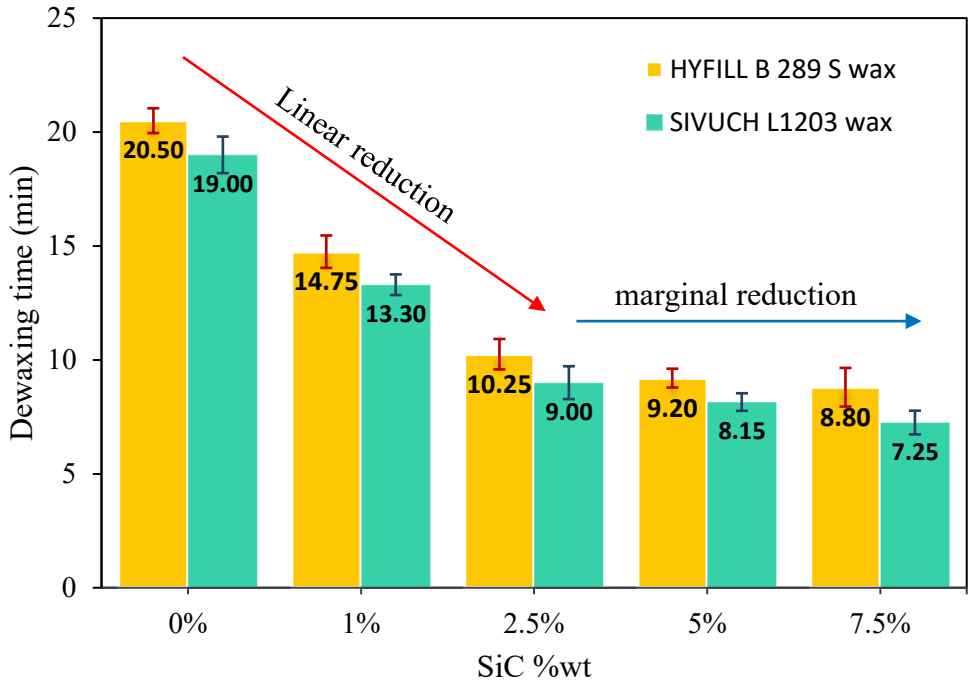

Figure 4.17 Effect of increasing the percentage of SiC on dewaxing time

The graph shows a linear reduction in dewaxing time for both types of wax as SiC content increases from 0 wt.% to 2.5 wt.%, demonstrating that SiC enhances the efficiency of the microwave dewaxing process. The reduction in dewaxing time becomes marginal as SiC wt.% increases beyond 2.5%. It is worth noting that the dewaxing time using a 600 W microwave was successfully reduced by 53%, 57%, and 62% with the addition of 2.5, 5, 7.5 wt.% SiC, respectively. Therefore, the linear reduction in dewaxing time as SiC content increases is logically explained by the synergistic effects of enhanced microwave energy absorption, improved thermal conductivity, and increased heat capacity of the moulds, as was discussed in section 4.3 and Figure 4.16. These factors collectively achieve higher temperatures more quickly and maintain these temperatures more effectively, leading to a faster and more efficient dewaxing process. This indicates that SiC has significant potential to accelerate the dewaxing process in investment casting, thereby enhancing the efficiency and effectiveness of the production process.

Furthermore, the results revealed that no crack was observed with SIVUCH L1203, but this defect was observed across all moulds following the use of HYFILL B289 MOD S, as presented in Table 4.5. This could be due to (i) wax expansion, (ii) differences in thermal gradient between mould and wax, and (iii) mould porosity

(Whitehouse and Dahlin, 2008). A similar trend was reported by Mukhtarkhanov et al. (2024), who demonstrated that waxes with higher thermal expansion forces generate significant internal stresses on the ceramic shell during dewaxing, leading to cracking. Furthermore, Minami et al. (2023) found that the type of wax binder critically influences crack initiation, with paraffin-based binders maintaining structural integrity, whereas other wax compositions led to crack formation. These findings highlight the significant impact of SiC and types of waxes on dewaxing time and crack formation. The reasons for this are further discussed in section 4.5.

4.4.4 Effect of Wax Type and SiC (wt.%) Content on Dewaxing Time: An ANOVA Analysis

Table 4.6 reveals that the type of wax and the percentage of SiC have significant effects on dewaxing time, with the SiC percentage showing an overwhelmingly dominant influence (96.5% factor effect, P-value < 0.0001). This suggests that increasing SiC content significantly reduces dewaxing time, likely due to SiC's properties enhancing microwave energy absorption and heat distribution within the mould. Conversely, the wax type accounts for only a 2.5% effect, though it's statistically significant (P-value < 0.000034), indicating subtle differences in wax formulations that affect their interaction with microwave energy. The interaction between wax type and SiC percentage appears to be statistically insignificant (P-value > 0.98), suggesting that the reduction in dewaxing time afforded by increasing SiC does not depend on the type of wax used. This implies that the primary mechanism through which SiC reduces dewaxing time was through enhanced thermal conductivity and microwave absorption were consistent across different wax types.

Table 4.6 Analysis of variance (ANOVA) table

Source of Variation	*SS*	*df*	*MS*	*F*	*P-value*	*F crit*	Factor effect (%)
Rows (wax type)	14.70	1	14.700	47.96085	0.0034E-06	4.351244	2.5%
Columns (SiC %)	584.01	4	146.003	476.354	1.5934E-19	2.866081	96.5%
Interaction (wax*SiC)	0.12	4	0.03	0.09787	0.981931	2.866081	
Error	6.13	20	0.3065				
Total	604.96	29					

Note that *SS* is the sum of squares, *df* is the degree of freedom, *MS* is the mean of squares *(SS/df),* F-statistic is derived from MS_{factor}/MS_{error}, and *P-value* is the probability value. $P < 0.05$ indicates that the variables have an independent impact on the process while *F crit* is the critical threshold of the analysis. F value > F crit is deemed statistically significant. Factor effect (%) = $(SS_{factor}/SS_{total}) \times 100\%$, respectively.

The residual is defined as the discrepancy between the observed values and the predictions from regression. If the points on the plot fall fairly close to the straight line, then the data are normally distributed. Figure 4.18 (a) illustrates a normal probability plot of residual values and suggests that residuals are normally distributed. Figure 4.18 (b) uses a histogram to display the residuals' distribution across all observations. The figure shows an almost symmetrical histogram, supporting the assumption of normality required for ANOVA (Permana et al., 2024), as analysed using Minitab 22. Figure 4.18 (c), the residual plot versus fitted values shows adequate, albeit not perfect, even spread of residuals, with residuals distributed fairly randomly across the range of fitted values. This pattern supports the model's capacity to maintain consistent error variance across predicted values, which is critical for reliable statistical testing. Meanwhile, the residuals versus order plot shows (Figure 4.18 (d)) no evident patterns of serial correlation, indicating that the residuals are independent of each other as assumed by ANOVA. Consequently, these residual plots are instrumental in regression and ANOVA techniques, offering insights into the effectiveness of a model in capturing the variability observed in the data (Elkady et al., 2022).

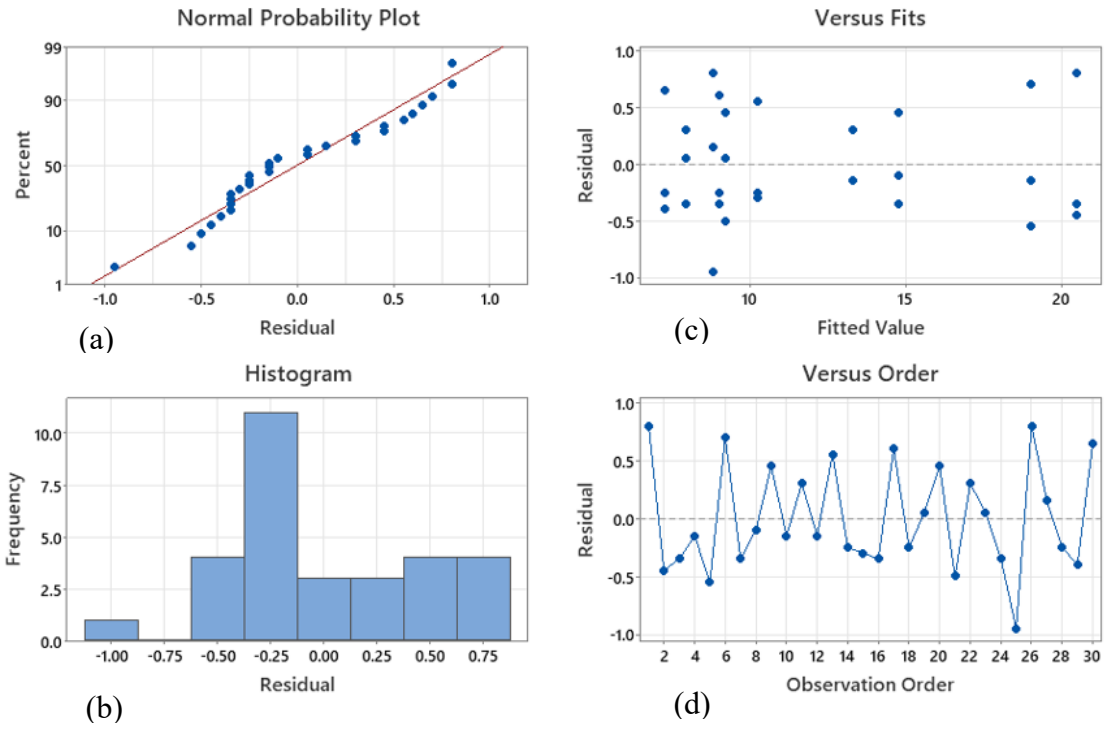

Figure 4.18 Residual plots: the statistical conclusions drawn from the ANOVA (a) normal probability plot, (b) residuals versus fits, (c) histogram of residuals, and (d) residuals versus order

4.5 Analysis of Modified Ceramic Moulds During Dewaxing Process

The following sections investigated the effects of SiC and the type of wax on temperature distribution and crack formation on the ceramic mould surface during the dewaxing process using different methods.

4.5.1 Investigation of Crack Formation on Mould Surfaces

The presence of cracks greatly affects the quality of the green ceramic mould shell, as it can lead to a defect in the final casting. Figure 4.19 shows a comparison of the effect of SiC addition on ceramic shells using two different types of waxes. Axial cracks were observed in all standard and modified moulds when HYFILL B289 MOD S wax was used while no defects were found in any moulds with SIVUCH L1203 wax. This suggests that the mould-wax expansion mismatch led to crack formation, whereas

increasing the SiC percentage contributed to a further increase in crack size, as shown in Figure 4.19(a). It is suggested that during the transition from solid to liquid, the HYFILL B289 MOD S wax molecules expanded slightly and stretched the mould as illustrated in Figure 4.20. This phenomenon helps to explain the mechanism behind crack formation. Crack initiation and propagation in shell structures occur when internal stresses, such as those generated by differential thermal expansion between the wax and the mould, exceed the shell's strength limit. According to Bao et al. (2022), cracks initiate at points of maximum stress concentration and propagate rapidly outward once the stress intensity exceeds the material's critical threshold. The cracks tend to extend along structurally weaker directions, emphasizing the critical role of material toughness and stress distribution in influencing crack behaviour.

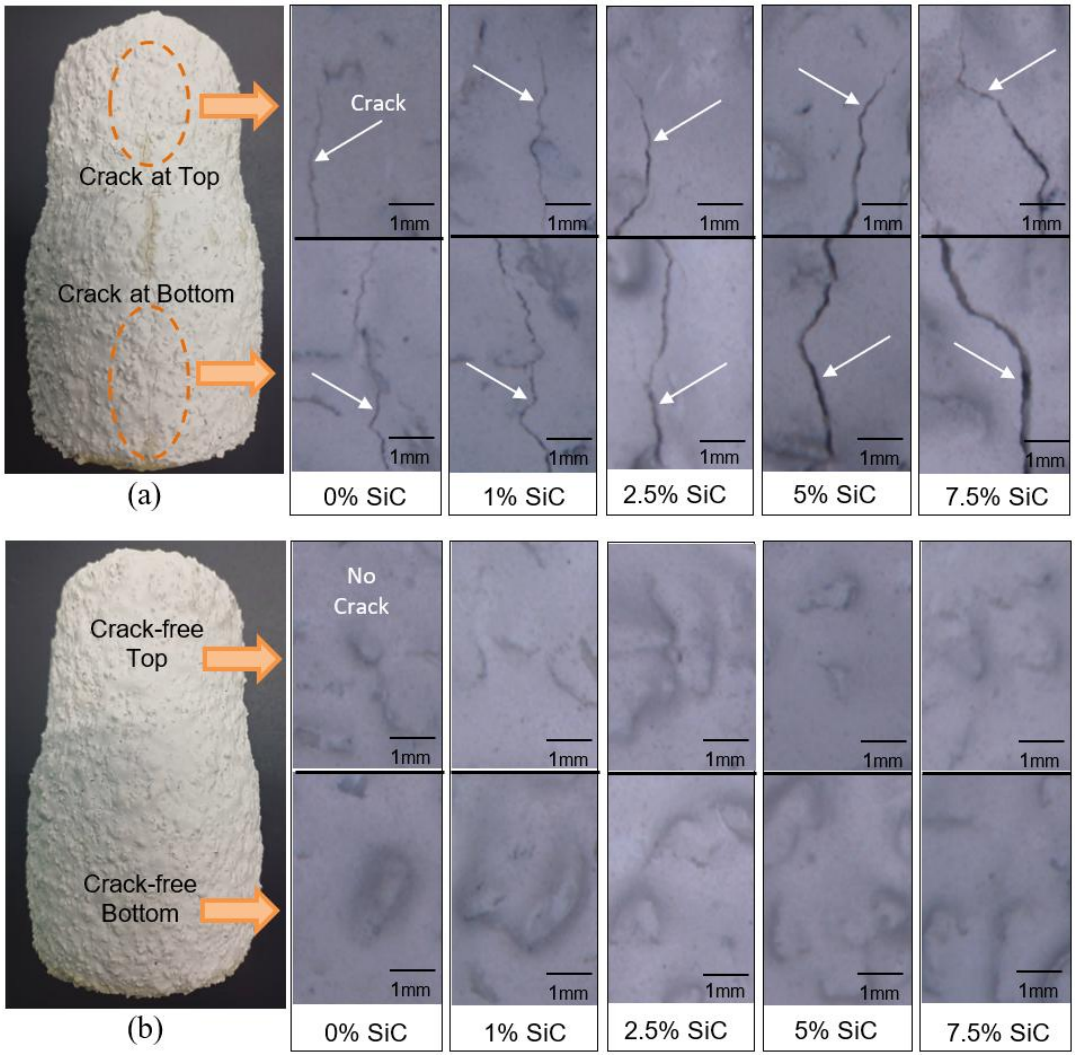

Figure 4.19 Visual inspection of the modified ceramic shell with SiC addition using different types of wax (a) HYFILL B289 MOD S, and (b) SIVUCH L1203, respectively

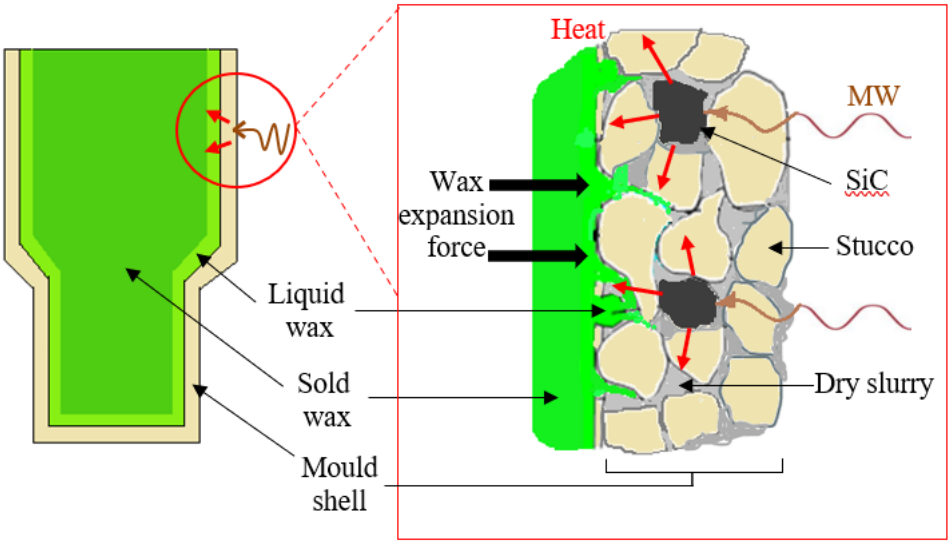

Figure 4.20 The schematic diagram illustrates the expansion force of wax and the heat absorption capacity by a ceramic shell

HYFILL B289 MOD S wax absorbed higher heat for temporary expansion (see Figure 4.1), which further contributed to thermal stress and cracking. Moreover, referring to the linear thermal expansion value ($\Delta L/L_0$) of the HYFILL B289 MOD S wax was 23.58×10^{-4} at 50 °C (see Table 4.1). The green ceramic mould shell, in contrast, showed no thermal expansion at the same temperature (see Figure 4.9). This substantial disparity in the ratio of thermal expansion renders the green mould shell incapable of withstanding the internal pressure generated by the HYFILL B289 MOD S wax during its expansion. Consequently, it has been demonstrated that the mismatch in the thermal expansion coefficients between the mould and the wax leads to crack formation. This finding aligns with evidence that approximately 80% of cracks in manufactured moulds originate during the dewaxing process (Raza, 2015; Lee, 2016). Furthermore, the DTA analysis (Figure 4.2) indicated that HYFILL B289 MOD S wax exhibits a higher-temperature peak, absorbing heat more gradually. Consequently, the gradual increase in temperature allows the material's structure to expand more significantly and consistently. Additionally, the high viscosity of HYFILL B289 S wax (Table 3.1) impedes its penetration into the green ceramic mould shell pores, which would otherwise accommodate the wax expansion. As a result, the internal pressure

inside the mould increases, thereby limiting the relief mechanism and contributing to the formation of cracks (Roach and Ponton, 2013).

As seen in Figure 4.19 (a), the width of the crack was most pronounced at the mouth of the mould and gradually decreased towards the apex, eventually becoming invisible to the naked eye. This behaviour can be attributed to the larger cross-sectional area of the wax near the mouth of the mould compared to the top area. Furthermore, the crack's trajectory was monitored beyond its optical disappearance at the top of the mould using a scanning electron microscope. The analysis revealed that the crack continued to propagate axially, as illustrated in Figure 4.21.

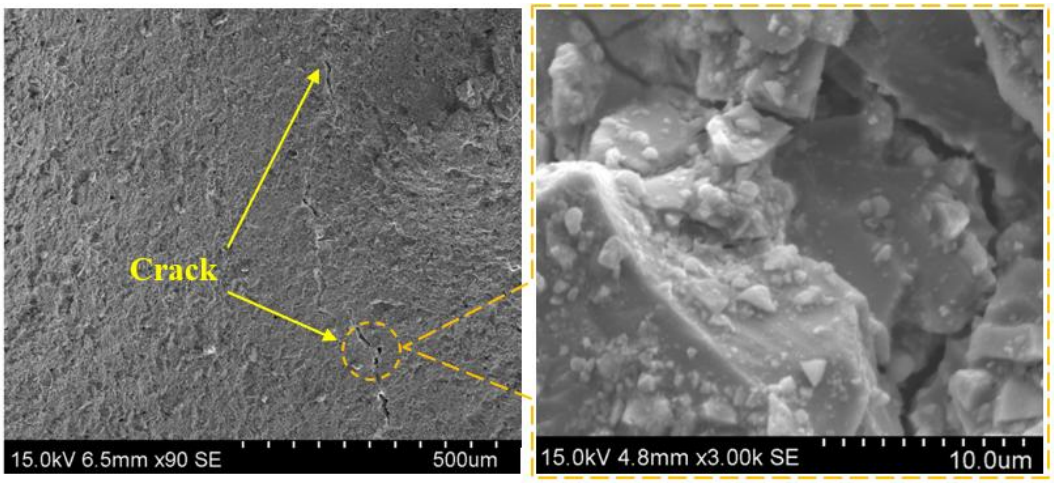

Figure 4.21 SEM image of the outer surface at the top of the HYFILL B289 MOD S wax mould

SIVUCH L1203 wax exhibited low linear thermal expansion (ΔL/L0) (see Fig. 4.1), reaching a maximum of 9.0605×10^{-4} at 45 °C (see Table 4.1). This characteristic allowed the green ceramic mould shell to withstand wax-induced expansion stress, ensuring a successful dewaxing process and producing crack-free moulds in both standard and modified conditions, as shown in Figure 4.19(b). Furthermore, the low melting point of SIVUCH L1203 wax, as confirmed by DTA analysis, required minimal energy for phase transition from solid to liquid, enabling a rapid and efficient melting process. This quick phase change reduced structural expansion stress when the material was in its least plastic state—the wax expansion phase. Additionally, the good dielectric properties of SIVUCH L1203 wax (see Table 4.1) facilitated microwave

energy absorption and conversion into heat, complementing the mould shell's thermal performance. This synergy significantly shortened the wax expansion phase and accelerated melting. Moreover, the wax's low viscosity (see Table 3.1) allows for deeper penetration into the pores of the ceramic veneer, further mitigating the expansion stress of the following wax layers (Bazhenov et al., 2024; Abo-Elmagd, 2017).

The comparison between using the two different wax patterns revealed significant differences in their effects on the shells of standard and modified green ceramic moulds containing varying SiC percentages. Notably, all moulds using HYFILL B289 MOD S wax exhibited axial cracks during the dewaxing stage, where crack size increased as the SiC percentage increased. In contrast, no cracks were observed in either standard or modified moulds when SIVUCH L1203 wax was used. This can be attributed to the superior dielectric properties of SIVUCH L1203 wax compared to HYFILL B289 MOD S (Table 4.3), which required less heat energy for phase transition at similar SiC levels. Moreover, its thermal expansion rate is three times lower than HYFILL B289 S wax. As a result, SIVUCH L1203 melted faster without inducing thermal stress on the ceramic mould. Additionally, its better heat absorption capacity, lower melting point, and moderate viscosity, evidenced by a single heat absorption peak at 52 $^{\circ}$C (Figure 4.2), prevented crack formation under identical conditions (see Figure 4.19(b)). Furthermore, the addition of SiC to the shell enhanced heat conversion for SIVUCH L1203, ensuring efficient melting while minimizing thermal stresses, thereby eliminating crack formation.

4.5.2 Strain Gauge Test Analysis

The visual inspection results of the moulds (see Table 4.5) revealed that cracks were observed in all moulds that used HYFILL B289 MOD S wax. While this defect was absent when SIVUCH L1203 wax was used. To gain a deeper understanding of these crack behaviours, strain gauge measurements were conducted to assess the impact of these waxes on the green ceramic mould shell. Figure 4.22 shows the relationship between strain ($\mu\varepsilon$) and heating time (sec) of the green ceramic mould

shells measured by (a) horizontal and (b) vertical strain gauges with different types of wax at heating temperatures of 200 ˚C.

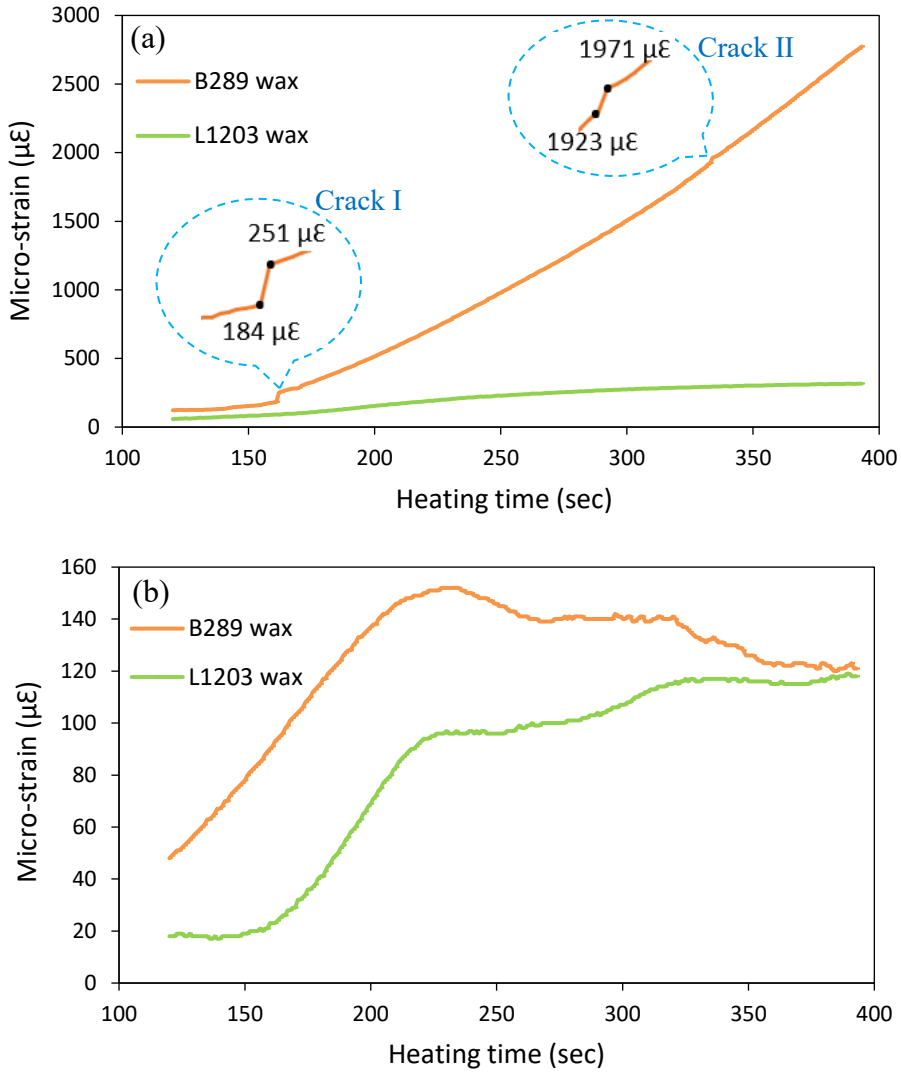

Figure 4.22 Micro-strain changes of green ceramic mould shell as a function of heating time for (a) horizontal and (b) vertical strain gauges

The data in Figure 4.22(a) reveals a noticeable contrast in the behaviour in terms of thermal expansion of the two waxes as heating time progresses. Initially, both waxes exhibited minimal micro-strain and showed slight linear expansion, indicating their stability at the initial heating furnace temperatures (<170 ˚C). However, as heating progressed, a significant divergence was observed. HYFILL B289 MOD S wax showed a sudden jump in strain from 184 to 251 με after nearly 160 sec of heating

time and continued to rise steeply. This suggests that a substantial thermal expansion and potential structural changes occurred. This pattern indicated that internal stress started to develop inside the green ceramic mould shell. This also suggested the initiation of crack formation. As the heating time progressed to 334 sec, the strain curve recorded a sudden increase suggesting the progression of the crack growth as depicted in Figure 4.23(a). In contrast, the green ceramic mould shell with SIVUCH L1203 wax exhibited relatively stable micro-strain changes with a maximum strain of 316 με throughout the heating duration. This is significantly lower compared to the mould shell with HYFILL B289 MOD S wax which reaches a maximum strain of 2733 με. The minimal and stable strain development prevents the crack formation, demonstrating superior thermal stability which makes the SIVUCH L1203 wax more suitable for applications requiring dimensional stability under prolonged heating conditions.

Regarding vertical strain measurement, as shown in Figure 4.22(b), the open-end configuration of the mould plays a significant role, allowing the wax to expand freely towards the open end. This reduces constraint, leading to decreased pressure and strain in the green ceramic mould shell. Initially, both waxes exhibit an increase in micro-strain upon heating, indicative of thermal expansion. Nevertheless, the HYFILL B289 wax shows a steeper and more rapid increase in strain, reaching approximately 150 με compared to SIVUCH L1203 wax at 98 με at 232 seconds. This was in agreement with the thermal expansion result as presented previously in Figure 4.1. However, the rate and magnitude of strain later become plateau as the heating time increases. This strain behaviour enables the green ceramic mould shell to withstand the wax expansions, especially in the vertical position.

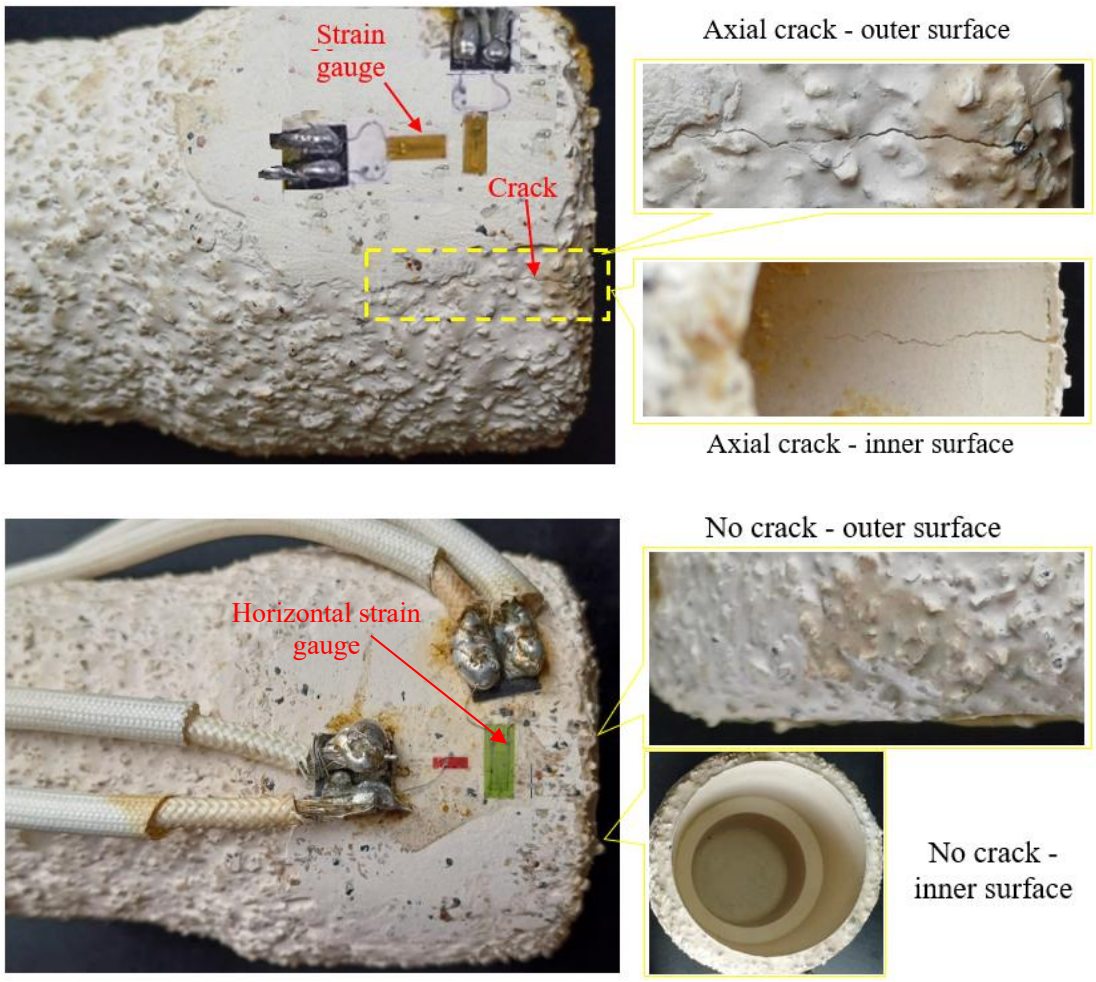

Figure 4.23 Inspection results of the ceramic shell after strain gauges dewaxing test (a) Axial crack observed with HYFILL B289 S wax, (b) No crack observed with SIVUCH L1203 wax

4.5.3 Temperature Distribution Analysis During Microwave Dewaxing

The temperature of the green ceramic mould shell with various SiC percentages was monitored at the top of the mould during the dewaxing process using an infrared thermometer, as shown in Figure 3.20. Table 4.7 shows surface temperature versus dewaxing time using SIVUCH L1203 wax pattern for standard and modified green ceramic mould shell at a microwave power of 600 W. As observed, the temperature increased steadily across all samples with time. The green ceramic mould shell added with 7.5 wt.% SiC exhibited the highest starting temperature of 172.7 $^{\circ}$C, completing the dewaxing after 7.25 minutes. In contrast, the standard green ceramic mould shell

took a longer duration to complete dewaxing (19 minutes) due to a slower rate of temperature increment. This faster dewaxing with higher SiC content is attributed to the enhanced microwave absorption and thermal conductivity of silicon carbide. As a strong microwave susceptor with a high dielectric loss factor, SiC effectively converts microwave energy into heat and distributes it uniformly, accelerating the wax removal process by allowing the mould to reach the wax melting point more quickly.

Table 4.7 Temperature distribution during the dewaxing process at various SiC Contents using 600 W microwave heating – SIVUCH L1203 wax

Dewaxing time (min)	Temperature along the dewaxing process at different SiC percentages (°C)				
	0 wt.% SiC	1 wt.% SiC	2.5 wt.% SiC	5 wt.% SiC	7.5wt. % SiC
1	44.7	52.4	59.7	64.5	69.4
2	51.6	60.5	75.8	87.5	96.5
3	59.8	69.8	96.3	111.6	129.3
4	67.3	81.3	117.8	139.8	158
5	75.5	96	139.4	154.3	170.7
6	84.9	109.4	147.3	158.7	172
7	93.2	119.8	148	157.4	171.8
8	100.7	127.1	149.7	158	172.7
9	106.9	131.8	150	156.4	
10	109	132.4	148.6		
11	112.7	133.9			
12	115	132.4			
13	119.8	131.6			
14	123.4	130.5			
15	125.5		Completed dewaxing		
16	128.6				
17	130				
18	129				
19	129.7				

Figure 4.24(a) shows the thermal infrared camera image of the temperature distribution for the standard green ceramic mould shell during the dewaxing process. The thermal image indicates that the temperature was uniformly distributed on the mould surface. Figure 4.24 (b) shows the plots of temperature versus time during the dewaxing test of the same mould. The experimental results revealed that the maximum temperature reached was approximately 129 °C during 19 minutes of heating (Figure 4.23(b)). This slow heating process was due to the low dielectric properties and

thermal conductivity of the standard green ceramic mould shell, as previously discussed in Sections 4.3.1 and 4.3.4, resulting in prolonged dewaxing times.

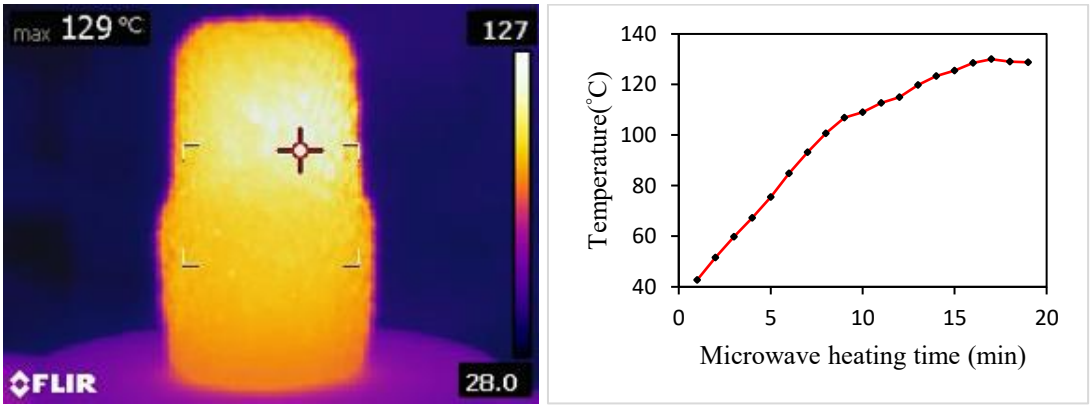

(a) (b)

Figure 4.24 Temperature distribution of standard green ceramic mould shell (a) Thermal image during dewaxing process, (b) Temperature versus time plots during dewaxing process

Figure 4.25 presents the thermal images and temperature distribution in the green ceramic mould shell added with 1 wt.% SiC. It took 9 minutes to reach the maximum temperature of 132 °C. The thermal image also revealed a uniform temperature distribution across the ceramic mould surface. The addition of 1 wt.% SiC not only accelerated the heating time from 19 minutes to 9 minutes but also shortened the dewaxing time to 13 minutes. This improvement suggests that the addition of SiC enhances microwave absorption.

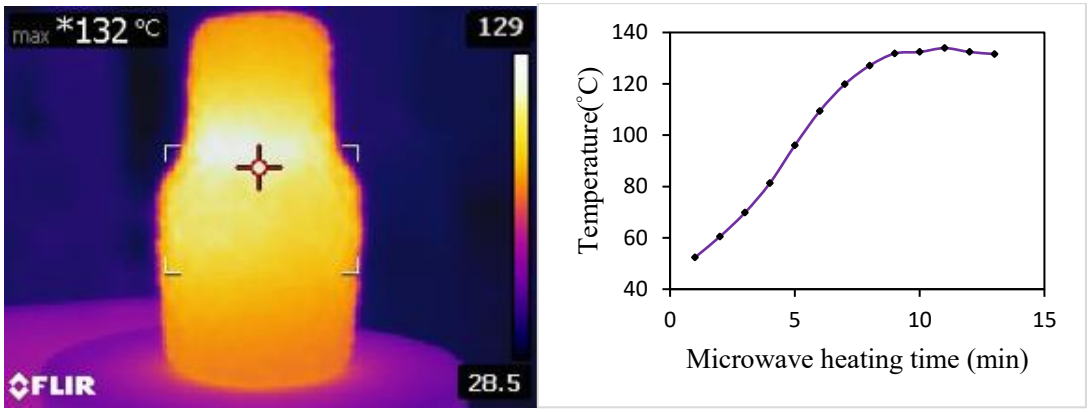

(a) (b)

Figure 4.25 Temperature distribution of green ceramic mould containing 1 wt.% SiC (a) Thermal image during dewaxing process, (b) Temperature versus time plots during dewaxing process

The thermal image and the temperature variation of the green ceramic mould shell with 2.5 wt.% SiC is shown in Figure 4.26. In this case, the time required to reach the maximum temperature of 149 °C was approximately 8 minutes which was 16 °C higher and 4 minutes faster compared to green ceramic mould shell with 1 wt.% SiC. This indicates that a higher SiC percentage has better microwave heat absorption.

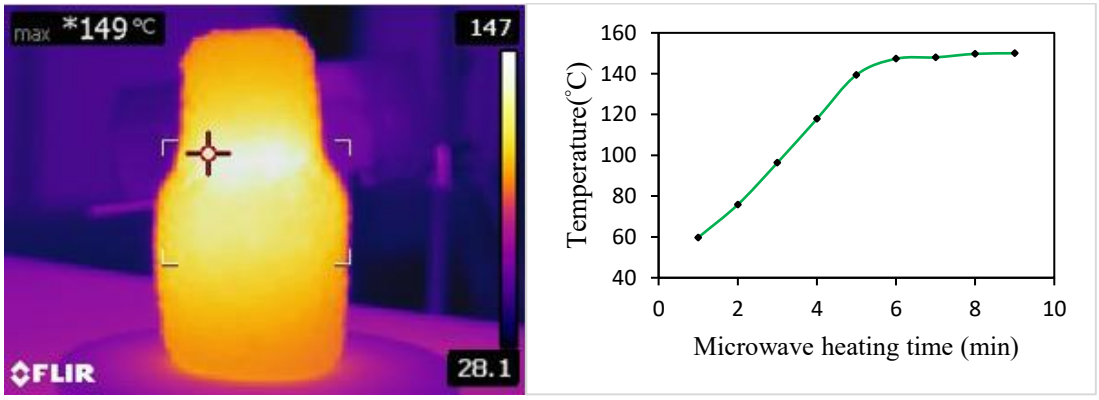

(a) (b)

Figure 4.26 Temperature distribution of green ceramic mould containing 2.5 wt.% SiC (a) Thermal image during dewaxing process, (b) Temperature versus time plots during dewaxing process

Figure 4.27 displays the thermal images and temperature distribution of the green ceramic mould shell containing 5 wt.% SiC. Notably, the maximum temperature

of 158 °C was reached in only 6 minutes, which was 9 °C higher than the green ceramic mould shell containing 2.5% SiC. Moreover, complete dewaxing was achieved just 1 minute faster compared to the 2.5 wt.% SiC mould.

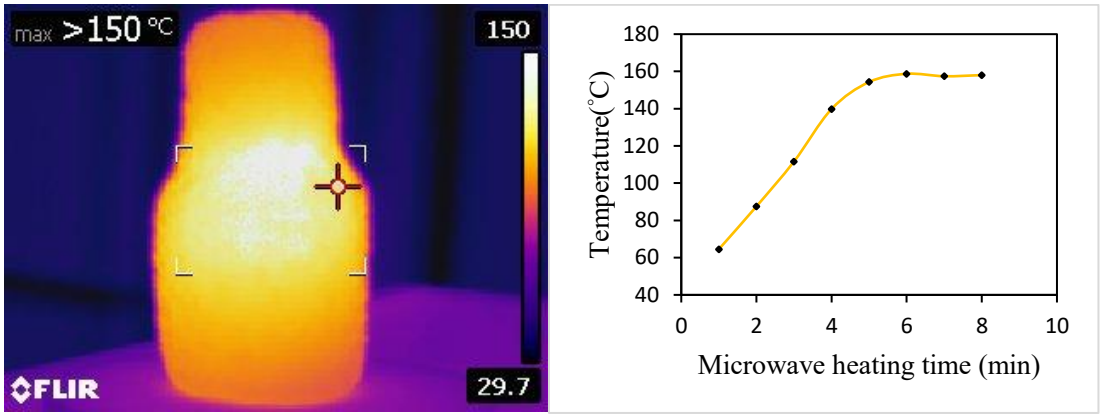

(a) (b)

Figure 4.27 Temperature distribution of green ceramic mould containing 5 wt.% SiC (a) Thermal image during dewaxing process, (b) Temperature versus time plots during dewaxing process

The thermal image and the temperature variation of the green ceramic mould shell with 7.5 wt.% SiC is shown in Figure 4.28. In this case, the time required for this mould to reach the maximum temperature of 172 ˚C was comparable to the 5 wt.% SiC mould trial, approximately 6 minutes. However, it reached a temperature of 14 ˚C higher and only 1 minute faster in completed dewaxing. The thermal images show a similar pattern to that in Figure 4.27.

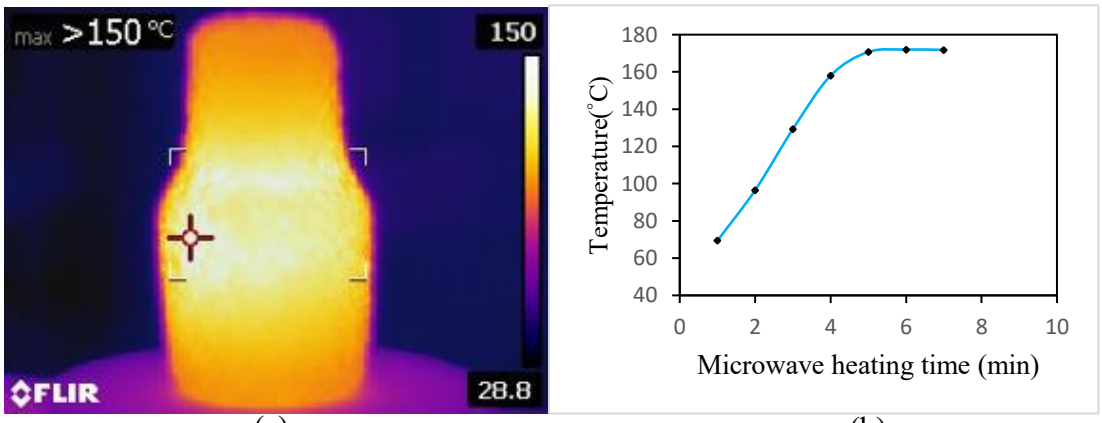

(a) (b)

Figure 4.28 Temperature distribution of green ceramic mould containing 7.5 wt.% SiC (a) Thermal image during dewaxing process, (b) Temperature versus time plots during dewaxing process

From these temperature distribution results, the modification of green ceramic mould shells with higher SiC percentages indeed leads to faster heating rates due to enhanced dielectric properties. These results were in agreement with Ngamkiatpaisan et al. (2023) in their investigation of the effects of different configurations of SiC susceptors and microwave powers on the heating rate and maximum temperature to enhance ceramic sintering. This phenomenon is primarily attributed to the increased microwave absorption and energy dissipation capabilities of the modified moulds. These improvements significantly accelerate the dewaxing process in investment casting.

4.6 Analysis of Energy Saving on Microwave Hybrid Heating-Dewaxing

Table 4.8 shows the microwave power absorbed per unit mass of green ceramic mould shell added with various SiC percentages. As the SiC percentages increase from 0% to 7.5 wt.%, the microwave power absorbed per unit mass progresses significantly from 76.81 W/kg to 382.47 W/kg. This significant 80% increase in microwave energy absorption resulted in a reduction of the dewaxing time from 19 minutes to 7.25 minutes. These trends indicated that higher SiC percentages enhance the efficiency of microwave energy absorption, leading to quicker and more energy-efficient dewaxing processes. This is due to the inherent dielectric properties (ε'' and tan δ) of SiC, which enhanced the green ceramic mould shell's ability to convert microwave energy into heat for rapid and efficient heating (Chiu et al., 2010; Peng et al., 2013; Tamang and Aravindan, 2019).

Table 4.8 Microwave power absorbed during microwave dewaxing

SiC (%)	T_i (°C)	T_f (°C)	Dewaxing time t (minutes)	Microwave power absorbed per unit mass (W/kg)
0	29	129.7	19.00	76.81
1	29	130.5	13.30	102.41
2.5	29	148.6	9.00	156.76
5	29	156.4	8.15	245.86
7.5	29	172.7	7.25	382.47

Table 4.9 presents the energy consumption comparison between electric firing furnace and microwave for the dewaxing process using SIVUCH L1203 wax. The detailed calculations are provided in Appendix K. The results showed approximately 75% energy saving using microwave dewaxing. It only took 7.25 minutes to complete the dewaxing process when a modified green ceramic mould containing 7.5 wt.% SiC was used at 600 W. In contrast, the process was significantly slower when using a firing furnace to dewax a standard mould of the same size. It took 45 minutes to complete the dewaxing process. This duration included 15 minutes of preheating to 300 $^{\circ}$C, followed by 30 minutes for dewaxing. These findings underscore the significant impact of SiC on enhancing the dielectric loss properties (ε'' and tan δ), as previously discussed in Section 4.3.1, thereby improving the microwave absorption and energy dissipation capabilities of the mould. Furthermore, the increased thermal conductivity, as highlighted in Section 4.3.4, facilitated faster and more efficient heat distribution throughout the mould. These enhancements optimized energy transfer within the mould, significantly accelerating the heating process and contributing to a more rapid and efficient dewaxing process. In addition, microwave thermal heating helped microwave energy penetrate through the sample, generating heat inside and beginning at the mould core. This mechanism is contrasted with firing in a furnace, where conventional conduction predominates, and the standard ceramic moulds with low thermal conductivities are preheated. In the furnace process, heat conduction begins at the outermost surface and progresses towards the inner surface of the mould shell, a mechanism that naturally restricts efficiency in heat conduction and significantly extends the dewaxing process (Gupta and Leong, 2008; Bhattacharya and Basak, 2016).

Table 4.9 Comparison of the energy required for the dewaxing process in an electric firing furnace and microwave

Materials & Losses	Energy required (J/m^3)	
	Furnace dewaxing	Microwave dewaxing
Mould	4.78×10^8	4.53×10^8
Wax (SIVUCH L1203)	2.56×10^8	2.56×10^8
Interior heat energy supply	1.02×10^9	5.91×10^3
Insulation losses (Furnace)	$1.07\times10^{9*}$	Not applicable
Convection losses (Microwave)	Not applicable	8.13×10^3
Total	2.83×10^9	7.09×10^8
Microwave energy saving (%)		75.4%

* (Yahaya, 2016)

4.7 Summary

In this research, adding SiC to the outer ceramic mould layers effectively reduced the dewaxing time by employing microwave hybrid heating (MHH) in investment casting. The SiC was incorporated into the mould's coarse backup stucco layers (3rd to 6th) at concentrations of 1, 2.5, 5, and 7.5 wt.%. The study found that increasing SiC content significantly enhances the dielectric and thermal properties of green moulds compared to standard moulds. Adding SiC at concentrations of 2.5, 5, and 7.5 wt.% improved the microwave absorption by 11-fold, 12-fold, and 14-fold, respectively, and thermal conductivity by 40%, 49%, and 59%. This improvement in dielectric and thermal properties resulted in a 62% reduction in dewaxing time at 600 W power compared to direct microwave heating (0 wt.% SiC) and an 84% reduction compared to traditional electric firing furnace heating, saving up to 75% energy. Furthermore, ANOVA statistical analysis confirmed that adding SiC to the ceramic mould composition had the greatest effect on dewaxing time by 92%. The coarse structure of the Al2O3-SiO3 stucco layers (700-800 μm) effectively increased the presence of sufficient pores, facilitating the expulsion of unwanted gases during the dewaxing and mould-casting processes. Conversely, the addition of SiC to the secondary layers (3rd to 6th layers) of the mould shell did not significantly affect the

density or porosity of the moulds. Rather, it contributed to a 12% increase in the green flexural strength of the moulds compared to standard moulds.

The performance of the dewaxing process was also evaluated using two types of pattern wax materials: HYFILL B289 MOD S and SIVUCH L1203 waxes. Moulds using HYFILL B289 MOD S wax exhibited axial cracks due to its high thermal expansion (23.58×10^{-4} at 50 $^{\circ}$C) compared to the ceramic shell (0.3×10^{-4}). Strain gauge experiments further confirmed crack formation in HYFILL B289 MOD S moulds. In contrast, SIVUCH L1203 wax showed better compatibility with the ceramic shell's thermal expansion, preventing cracks.

CHAPTER 5

CONCLUSIONS AND RECOMMENDATIONS

5.1 Introduction

Addressing the challenges of reducing dewaxing time and mould cracking is crucial for enhancing investment casting efficiency and quality. Therefore, this research aimed to investigate and mitigate these issues based on its specific objectives. In particular, it evaluated the effects of SiC on the properties of green ceramic mould shells and microwave dewaxing performance in two different types of pattern wax. This chapter presents the conclusions from the findings of this research and ends with recommendations for future research work.

5.2 Conclusions

Based on the research findings, the following conclusions can be drawn:

1. The influence of incorporating various percentages of SiC (wt.%) as a microwave-absorbing additive into the mould's coarse backup stucco layers on its properties was comprehensively evaluated. The results showed that incorporating SiC significantly enhanced the dielectric and thermal properties of the green ceramic mould shell. Both the loss factor (ε'') and the loss tangent (tan δ) were increased 6-fold with the addition of 1 wt.% SiC to the standard mould, and as the SiC content increased from 1 to 7.5 wt.%, the ε'' and tan δ increased by 58% and 42%, respectively. The thermal conductivity and heat capacity showed a proportional increase, reaching approximately 59% and 76%, respectively, at 7.5 wt.% SiC compared to the standard mould. Moreover, the modified shells exhibited a slight increase in density and flexural strength with a minor reduction in porosity.

2. Most feasible microwave power for the dewaxing process in standard and modified green ceramic moulds was successfully determined through a series of experiments conducted on the standard and modified green ceramic moulds using different waxes and microwave power levels. The microwave power level of 600 W significantly reduced the dewaxing time by up to 64%, whereas the 850 W power level caused the wax to burn, leading to its exclusion. For both wax types, the dewaxing process using the standard green ceramic mould took 20 minutes, while the modified mould completed the process in just 7.25 minutes at 600 W, which is 84% less than the dewaxing time using a conventional electric firing furnace. ANOVA showed SiC addition contributed to a 96% reduction in dewaxing time ($p < 0.0001$), confirming its significant role.

3. The performance comparison of standard and modified green ceramic moulds during the dewaxing process, focusing on crack formation and energy efficiency, was successfully conducted. The thermal expansion properties of waxes played a crucial role in influencing the structural integrity of green ceramic mould shells. While HYFILL B289 MOD S wax exhibited higher thermal stability and a higher melting point; however, its greater thermal expansion led to axial cracks in the moulds, as confirmed by strain gauge tests. In contrast, SIVUCH L1203 wax demonstrated better compatibility with the ceramic shell's thermal expansion, effectively preventing cracks and making it the appropriate choice for pattern production in investment casting. Furthermore, by adding 7.5 wt.% SiC and using microwave power of 600W, the modified mould saved up to 75% of energy in the dewaxing process compared to conventional electric firing furnace heating.

5.3 Recommendations for Future Work

The current research work can be improved further by the following recommendations:

1. Notably, investigations of the dewaxing process were conducted using a commercial microwave oven, and the experimental setup was relatively limited

compared to industrial practices. Therefore, conducting dewaxing tests using an industrial microwave system would provide valuable insights for future improvements.

2. This study demonstrated that dewaxing using microwave hybrid heating is energy-saving. Therefore, future research should investigate the feasibility of integrating this technology into other stages of the investment casting process, such as firing, preheating, and in-situ casting. This could further enhance time and energy saving.

3. Future research should explore the application of microwave hybrid heating for removing rapid prototyping (RP) patterns as a potential alternative to conventional heating methods. This could involve incorporating a susceptor directly into the RP pattern material or applying it externally, which may provide viable and efficient solutions for pattern removal.

4. Due to the high cost and durability of SiC, future research should explore methods, such as centrifugal separation, to recover SiC from spent ceramic moulds. Recycling SiC can help reduce costs and improve the sustainability of the investment casting process.

5. The Al_2O_3-SiO_2/SiC-modified mould shells exhibit decreased porosity with increasing silicon carbide content. To enhance porosity, future research should explore incorporating additional additive materials, such as burnout materials or porous fillers.

6. Further research in this area is recommended to fully realise the potential of using microwave-assisted heating in investment casting processes.

REFERENCES

Abo-Elmagd, A. a. A. 2017. Effect of luting agent viscosity on bond strength and marginal gab of ceramic occlusal veneer restorations. *Egyptian Dental Journal,* 63**,** 1739-1752.

Ahrens, T. J. 1995. *Mineral physics & crystallography: a handbook of physical constants*, Washington: American Geophysical Union.

Andrianov, A., Lee, J., Shynkarenko, O., Simone, D. & Bertoldi, A. E. D. M. 2019. Experimental study of severity level of structural discontinuities in paraffin grains of hybrid propellant rocket. *Acta Astronautica,* 162**,** 256-265.

Astm 2010. *American Society for Testing Materials.* C20-00. West Conshohocken, Pennsylvania, USA: ASTM International.

Attarzadeh, N. & Ramana, C. V. 2021. Plasma electrolytic oxidation ceramic coatings on zirconium (Zr) and zralloys: Part I—Growth mechanisms, microstructure, and chemical composition. *Coatings,* 11**,** 634.

Atwater, J. & Wheeler Jr, R. 2004. Microwave permittivity and dielectric relaxation of a high surface area activated carbon. *Applied Physics A,* 79**,** 125-129.

Atwater, J. E. & Wheeler Jr, R. R. 2003. Complex permittivities and dielectric relaxation of granular activated carbons at microwave frequencies between 0.2 and 26 GHz. *Carbon,* 41**,** 1801-1807.

Ayappa, K., Davis, H., Davis, E. & Gordon, J. 1991. Analysis of microwave heating of materials with temperature-dependent properties. *Aiche journal,* 37**,** 313-322.

Babalola, S. A. 2014. *Characterization and Formulation of Wax Composition for Investment Casting Pattern.* PhD Thesis, University of Nigeria, Nsukka.

Badanova, N., Perveen, A. & Talamona, D. 2021. Concise review on Pattern making process in Rapid Investment Casting: Technology, Materials & Numerical modelling aspect. *Advances in Materials and Processing Technologies***,** 1-13.

Badanova, N., Perveen, A. & Talamona, D. 2022. Concise review on pattern making process in rapid investment casting: technology, materials & numerical modelling aspect. *Advances in Materials and Processing Technologies,* 8**,** 966-978.

Bae, C.-J., Kim, D. & Halloran, J. W. 2019. Mechanical and kinetic studies on the refractory fused silica of integrally cored ceramic mold fabricated by additive manufacturing. *Journal of the European Ceramic Society,* 39**,** 618-623.

Baghel, P. K. 2023. Application of microwave in manufacturing technology: A review. *Materials Today: Proceedings*.

Bai, S., Shen, X., Zhu, G., Zhou, H., Xu, H., Fu, G. & Ye, Z. 2013. Optical Properties and a simple and general route for the rapid syntheses of reduced graphene oxide–metal sulfide nanocomposites. *European Journal of Inorganic Chemistry,* 2013**,** 256-262.

Balanis, C. A. 2012. *Advanced engineering electromagnetics*, 2nd edn. Arizona: John Wiley & Sons.

Bansal, A. & Vasudev, H. 2022. *Advances in microwave processing for engineering materials*, Boca Raton, Florida, USA: CRC Press.

Bao, X., Chen, B., Dai, P., Li, Y. & Mao, J. 2022. Construction and verification of spherical thin shell model for revealing walnut shell crack initiation and expansion mechanism. *Agriculture,* 12**,** 1446.

Barba, A. A. & D'amore, M. 2012. Relevance of dielectric properties in microwave assisted processes. *Microwave materials characterization,* 6**,** 91-118.

Bazhenov, V. E., Ovsyannikov, A. S., Kovyshkina, E. P., Stepashkin, A. A., Nikitina, A. A., Koltygin, A. V., Belov, V. D. & Dmitriev, D. N. 2024. The Numerical Simulation of the Injection Filling of the Fluidity Probe Die with Pattern Waxes. *Journal of Manufacturing and Materials Processing,* 8**,** 213.

Beeley, P. R. & Smart, R. F. 2008. *Investment casting,* Boca Raton, Florida: CRC Press.

Beeley, P. R. & Smart, R. F. 2023. *Investment casting*, CRC Press.

Bemblage, O. & Karunakar, D. B. 2011. A study on the blended wax patterns in investment casting process. Proceedings of the world Congress on Engineering. July 6 - 8, London 2011.

Bhattacharya, M. & Basak, T. 2016. A review on the susceptor assisted microwave processing of materials. *Energy,* 97**,** 306-338.

Bhattacharya, M. & Basak, T. 2017. Susceptor-assisted enhanced microwave processing of ceramics-a review. *Critical Reviews in Solid State and Materials Sciences,* 42**,** 433-469.

Blair, V. L., Raju, S. V., Kornecki, M. & Brennan, R. E. 2018. Single-Mode Microwave Sintering of Traditionally Resistant Materials. US Army Research Laboratory Aberdeen Proving Ground United States.

Borrell, A. & Salvador, M. D. 2018. Advanced ceramic materials sintered by microwave technology. *Sinter. Technol. Method Appl***,** 3-24.

Brodie, G. 2012. Applications of microwave heating in agricultural and forestry related industries. *The development and application of microwave heating***,** 45-78.

Brosnan, K. H., Messing, G. L. & Agrawal, D. K. 2003. Microwave sintering of alumina at 2.45 GHz. *Journal of the American Ceramic Society,* 86**,** 1307-1312.

Brown, R. & Brown, R. 2000. Melting point and molecular symmetry. *Journal of Chemical Education,* 77**,** 724.

Brum, F. J., Amico, S. C., Vedana, I. & Spim Jr, J. A. 2009. Microwave dewaxing applied to the investment casting process. *journal of materials processing technology,* 209**,** 3166-3171.

Butcher, G. 2016. *Tour of the electromagnetic spectrum*, U.S: National Aeronautics and Space Administration.

Chandrasekaran, S., Ramanathan, S. & Basak, T. 2012. Microwave material processing—a review. *AIChE Journal,* 58**,** 330-363.

Chen, L.-F., Ong, C. K., Neo, C., Varadan, V. V. & Varadan, V. K. 2004. *Microwave electronics: measurement and materials characterization*, Hoboken: John Wiley & Sons.

Chen, M., Siochi, E., Ward, T. & Mcgrath, J. 1993. Basic ideas of microwave processing of polymers. *Polymer Engineering & Science,* 33**,** 1092-1109.

Chen, M., Zhu, L., Dong, Y., Li, L. & Liu, J. 2016. Waste-to-resource strategy to fabricate highly porous whisker-structured mullite ceramic membrane for simulated oil-in-water emulsion wastewater treatment. *ACS Sustainable Chemistry & Engineering,* 4**,** 2098-2106.

Chen, Y. Y. & Chang, Y. J. Application of ATR-FTIR spectroscopy for the identification of chemical functional groups in kerogens and fossil resins. EGU General Assembly Conference Abstracts, 2020. 9981.

Cheng, J., Roy, R. & Agrawal, D. 2002. Radically different effects on materials by separated microwave electric and magnetic fields. *Materials Research Innovations,* 5**,** 170-177.

Cheng, S.-C., Kao, M.-S. & Hwang, J.-J. 2024. Advanced Integration of Microwave Kiln Technology in Enhancing the Lost-Wax Glass Casting Process: A Study on Methodological Innovations and Practical Implications. *Journal of Composites Science,* 8**,** 168.

Chhillar, P., Agrawal, D. & Adair, J. 2008. Sintering of molybdenum metal powder using microwave energy. *Powder Metallurgy,* 51**,** 182-187.

Chiu, S.-C., Yu, H.-C. & Li, Y.-Y. 2010. High electromagnetic wave absorption performance of silicon carbide nanowires in the gigahertz range. *The Journal of Physical Chemistry C,* 114**,** 1947-1952.

Clancy, R., Bruton, K., O'sullivan, D. & Keogh, D. 2022. Industry 4.0 driven statistical analysis of investment casting process demonstrates the value of digitalisation. *Procedia Computer Science,* 200**,** 284-297.

Cooper, M. M., Corley, L. M. & Underwood, S. M. 2013. An investigation of college chemistry students' understanding of structure–property relationships. *Journal of Research in Science Teaching,* 50**,** 699-721.

Czarnecka-Komorowska, D., Grześkowiak, K., Popielarski, P., Barczewski, M., Gawdzińska, K. & Popławski, M. 2020. Polyethylene wax modified by organoclay bentonite used in the lost-wax casting process: processing− structure− property relationships. *Materials,* 13**,** 2255.

Dąbrowska, S., Chudoba, T., Wojnarowicz, J. & Łojkowski, W. 2018. Current trends in the development of microwave reactors for the synthesis of nanomaterials in laboratories and industries: a review. *Crystals,* 8**,** 379.

Das, A. & Banik, B. K. 2021. *Microwaves in Chemistry Applications: Fundamentals, Methods and Future Trends*, Amsterdam: Elsevier Science.

Dave, I. & Kaila, V. 2014. Optimization of ceramic shell mold materials in investment casting. *International Journal of Research in Engineering and Technology,* 3**,** 30-33.

Davis, J. R. 1996. *ASM specialty handbook: Cast Irons*, USA: ASM international.

De, A., Ahmad, I., Whitney, E. D. & Clark, D. E. 1992. Microwave (hybrid) heating of alumina at 2.45 GHz: I. Microstructural uniformity and homogeneity. Florida Univ Gainesville Dept of Materials Science and Engineering.

Defonseka, C. 2019. *Flexible Polyurethane Foams: A Practical Guide*, Berlin: De Gruyter.

Dejene, N. D., Lemu, H. G. & Gutema, E. M. 2023. Critical review of comparative study of selective laser melting and investment casting for thin-walled parts. *Materials,* 16**,** 7346.

Dong, R.-Z., Wang, W.-H., Cui, K., Wang, Y.-B., Wang, Z.-C., Kang, K.-Y. & Jiang, R.-S. 2024. An investigation of ceramic shell thickness uniformity and its impact on precision in turbine blade investment casting. *Journal of Manufacturing Processes,* 131**,** 507-522.

Doucet, J. & Laviolette, J.-P. 2022. Catalytic microwave depolymerisation of plastic for production of monomer and waxes. U.S. Patent 11,518,864.

Du, Y., Jiao, K., Huang, W., Jin, J. & Zhang, R. 2023. Influences of silicon carbide fineness on thermal and mechanical properties of cement-based composites. *Journal of Building Engineering,* 74**,** 106907.

E Wong, W. & Gupta, M. 2006. Simultaneously improving strength and ductility of magnesium using nano-size SiC particulates and microwaves. *Advanced Engineering Materials,* 8**,** 735-740.

Ebadzadeh, T. & Marzban-Rad, E. 2009. Microwave hybrid synthesis of silicon carbide nanopowders. *Materials Characterization,* 60**,** 69-72.

El Khaled, D., Novas, N., Gazquez, J. & Manzano-Agugliaro, F. 2018. Microwave dielectric heating: Applications on metals processing. *Renewable and Sustainable Energy Reviews,* 82**,** 2880-2892.

Elkady, E. F., Fouad, M. A. & Mozayad, A. N. 2022. Application of Box-Behnken experimental design and response surface methodology for selecting the optimum RP-HPLC conditions for the simultaneous determination of methocarbamol, indomethacin and betamethasone in their pharmaceutical dosage form. *BMC chemistry,* 16**,** 114.

Everhart, W., Lekakh, S., Richards, V., Chen, J. & Chandrashekhara, K. 2013. Crack formation during foam pattern firing in the investment casting process. *International Journal of Metalcasting,* 7**,** 7-14.

Fatykhov, M. & Fatykhov, L. 2015. Microwave electromagnetic method of melting the paraffin plug in an open coaxial system. *Journal of Engineering Physics and Thermophysics,* 88**,** 724-729.

Fedorov, K., Fayazbakhsh, K. & Ravindran, C. 2022. Surface roughness and dimensional tolerances in A319 alloy samples produced by rapid investment

casting process based on fused filament fabrication. *The International Journal of Advanced Manufacturing Technology*, 1-15.

Fernández, Y., Arenillas, A. & Menéndez, J. Á. 2011. *Microwave heating applied to pyrolysis*, London: InTech Open. .

Fidalgo Fernández, B. & Menéndez Díaz, J. Á. 2013. *Syngas production by CO2 reforming of ch4 under microwave heating–challenges and opportunities*. in Andarto, A., Palguandi,J.(eds.). *Syngas: Production, Applications and Environmental Impact.* New York: Nova Science Publishers, Inc.

Fleckenstein, J. E. 2017. *The effect of fillers on the physical properties of investment casting waxes*, 1st edn. Boca Raton: CRC Press.

Flesoura, G., Monich, P. R., Alarcon, R. M., Desideri, D., Bernardo, E., Vleugels, J. & Pontikes, Y. 2021. Porous glass-ceramics made from microwave vitrified municipal solid waste incinerator bottom ash. *Construction and Building Materials,* 270, 121452.

Fliflet, A. W., Bruce, R., Fischer, R. P., Lewis, D., Kurihara, L., Bender, B., Chow, G.-M. & Rayne, R. 2000. A study of millimeter-wave sintering of fine-grained alumina compacts. *IEEE Transactions on Plasma Science,* 28, 924-935.

Foster, G. H. 1994. Method and apparatus for removing wax from casting mold. U.S. Patent 5,372,177.

Freitag, L., Schafföner, S., Lippert, N., Faßauer, C., Aneziris, C. G., Legner, C. & Klotz, U. E. 2017. Silica-free investment casting molds based on calcium zirconate. *Ceramics International,* 43, 6807-6814.

Gamit, D. N. & Chudasama, M. K. 2020. Size-effect in microwave processing of engineering materials-A review. *Journal of Mechanical Engineering and Sciences,* 14, 6770-6788.

Gangwar, V., Singh, H. & Kumar, S. 2022. Influence of process parameter on microstructure, residual stress, microhardness and porosity of AA-6063 microwave cast. *International Journal of Metalcasting,* 16, 826-841.

Gao, Y., Mao, Y., Song, Z., Zhao, X., Sun, J., Wang, W., Chen, G. & Chen, S. 2020. Efficient generation of hydrogen by two-step thermochemical cycles: Successive thermal reduction and water splitting reactions using equal-power microwave irradiation and a high entropy material. *Applied Energy,* 279, 115777.

Garai, M., Molla, A. R., Reka, A. A. & Karmakar, B. 2022. Wide thermal expansion in Ag0/Au0 nanoparticle doped SiO2-MgO-Al2O3-B2O3-K2O-MgF2 glass-ceramics. *Materials Today: Proceedings,* 50**,** 134-138.

Garnault, T., Bouvard, D., Chaix, J.-M., Marinel, S. & Harnois, C. 2021. Is direct microwave heating well suited for sintering ceramics? *Ceramics International,* 47**,** 16716-16729.

Gebelin, J.-C. & Jolly, M. R. 2003. Modelling of the investment casting process. *Journal of Materials Processing Technology,* 135**,** 291-300.

Gill, Y. Q., Saeed, F., Shoukat, M. H., Irfan, M. S. & Abid, U. 2021. A study on the dewaxing behavior of carbon-black-modified LDPE–paraffin wax composites for investment casting applications. *Arabian Journal for Science and Engineering,* 46**,** 6715-6725.

Gill, Y. Q., Shoukat, M. H., Babar, F., Mehmood, U. & Abid, U. 2022. Fabrication and characterization of PANI-modified LLDPE-paraffin wax blends. *Polymer Bulletin***,** 1-16.

Goyal, H., Chen, T.-Y., Chen, W. & Vlachos, D. G. 2022. A review of microwave-assisted process intensified multiphase reactors. *Chemical Engineering Journal,* 430**,** 133183.

Graham, E. A., Patange, O., Lukac, M., Singh, L., Kar, A., Rehman, I. H. & Ramanathan, N. 2014. Laboratory demonstration and field verification of a Wireless Cookstove Sensing System (WiCS) for determining cooking duration and fuel consumption. *Energy for Sustainable Development,* 23**,** 59-67.

Greenacre, N. R. 1998. *Measurement of the high-temperature dielectric properties of ceramics at microwave frequencies.* PhD Thesis, The University of Nottingham, UK.

Grzeskowiak, K., Czarnecka-Komorowska, D., Sytek, K. & Wojciechowski, M. 2015. Influence of waxes remelting used in investment casting on their thermal properties and linear shrinkage. *Metalurgija,* 54**,** 350-352.

Guan, C. 2016. Rapid and low temperature synthesis of high purity Ti2SC powder by microwave hybrid heating. *Advances in Applied Ceramics,* 115**,** 470-472.

Gude, V. G., Patil, P., Martinez-Guerra, E., Deng, S. & Nirmalakhandan, N. 2013. Microwave energy potential for biodiesel production. *Sustainable Chemical Processes,* 1**,** 1-31.

Guinn, P. A. 2002. Filler material and wax composition for use in investment casting. U.S. Patent 6,485,553.

Guo, Q., Sun, D.-W., Cheng, J.-H. & Han, Z. 2017. Microwave processing techniques and their recent applications in the food industry. *Trends in Food Science & Technology,* 67**,** 236-247.

Gupta, D. & Sharma, A. 2011. Development and microstructural characterization of microwave cladding on austenitic stainless steel. *Surface and Coatings Technology,* 205**,** 5147-5155.

Gupta, M. & Leong, E. W. W. 2008. *Microwaves and metals*, Singapore: John Wiley & Sons.

Haimbaugh, R. E. 2015. *Practical induction heat treating*, USA: ASM international.

Hao, Y., Liu, J., Du, J., Zhang, W., Xiao, Y., Zhang, S. & Yang, P. 2020. Effects of mold materials on the interfacial reaction between magnesium alloy and ceramic shell mold during investment casting. *Metals,* 10**,** 991.

Harsha, A. 2011. An investigation on low stress abrasive wear characteristics of high performance engineering thermoplastic polymers. *Wear,* 271**,** 942-951.

Hodgir, R., Mittal, Y. G., Kamble, P., Gote, G., Patil, Y., Patel, A. K., Bernard, A. & Karunakaran, K. 2022. Mathematical modelling of pattern sublimation in rapid ice investment casting. *International Journal of Metalcasting,* 16**,** 1002-1009.

Hong, W., Xiao, P., Li, Z. & Luo, H. 2014. Microwave radial dielectric properties of carbon fiber bundle: modeling, validation and application. *Carbon,* 79**,** 538-543.

Hong, Y.-D., Lin, B.-Q., Zhu, C.-J., Wang, Z., Saffari, P. & Nie, W. 2021. Temperature rising characteristic of coal powder during microwave heating. *Fuel,* 294**,** 120495.

Horikoshi, S., Sumi, T. & Serpone, N. 2012. Unusual effect of the magnetic field component of the microwave radiation on aqueous electrolyte solutions. *Journal of Microwave Power and Electromagnetic Energy,* 46**,** 215-228.

Hotta, M., Hayashi, M., Lanagan, M. T., Agrawal, D. K. & Nagata, K. 2011. Complex permittivity of graphite, carbon black and coal powders in the ranges of X-band frequencies (8.2 to 12.4 GHz) and between 1 and 10 GHz. *ISIJ International,* 51**,** 1766-1772.

Houšová, J. & Hoke, K. 2002. Microwave heating–the influence of oven and load parameters on the power absorbed in the heated load. *Czech Journal of Food Sciences,* 20**,** 117-124.

Hsieh, C.-H., Lo, S.-L., Chiueh, P.-T., Kuan, W.-H. & Chen, C.-L. 2007. Microwave enhanced stabilization of heavy metal sludge. *Journal of Hazardous Materials,* 139**,** 160-166.

Huang, C.-J., Leu, M.-C. & Richards, V. 2007. Investment casting with ice patterns and comparison with other types of rapid prototyping patterns. *The Minerals, Metals & Materials Society (TMS)*, 2007.Rolla: Missouri University of Science and Technology.

Huang, Z., Gotoh, M. & Hirose, Y. 2009. Improving sinterability of ceramics using hybrid microwave heating. *Journal of Materials Processing Technology,* 209**,** 2446-2452.

Intarapong, P., Preechawong, J. & Nithitanakul, M. 2024. High valuable wax from multilayer film packaging wastes using solid catalyst via pyrolysis process. *Waste Management,* 186**,** 205-213.

Janney, M. A., Calhoun, C. L. & Kimrey, H. D. 1992. Microwave sintering of Solid oxide fuel cell materials: I, zirconia-8 mol% yttria. *Journal of the American Ceramic Society,* 75**,** 341-346.

Jie, X., Gonzalez-Cortes, S., Xiao, T., Yao, B., Wang, J., Slocombe, D. R., Fang, Y., Miller, N., Al-Megren, H. A. & Dilworth, J. R. 2019. The decarbonisation of petroleum and other fossil hydrocarbon fuels for the facile production and safe storage of hydrogen. *Energy & Environmental Science,* 12**,** 238-249.

Jones, M. I., Valecillos, M.-C. & Hirao, K. 2001. Role of specimen insulation on densification and transformation during microwave sintering of silicon nitride. *Journal of the Ceramic Society of Japan,* 109**,** 761-765.

Jones, S. & Yuan, C. 2003. Advances in shell moulding for investment casting. *Journal of Materials Processing Technology,* 135**,** 258-265.

Just, P., Kaczorowski, R., Topola, M., Pacyniak, T. & Rapiejko, C. 2024. Studies of Accelerated Drying of Ceramic Moulds with the use of Microwaves. *Archives of Foundry Engineering***,** 101-108-101-108.

Kääriäinen, P., Tervinen, L., Vuorinen, T. & Riutta, N. 2020. *The Chemarts cookbook*, Otava, Finland: Aalto University.

Kalpakjian, S. 1997. *Manufacturing Process for Engineering Materials Third Edition*, 3rd edn. Boston, USA: Addison-Wesley.

Kanyo, J. E., Schafföner, S., Uwanyuze, R. S. & Leary, K. S. 2020. An overview of ceramic molds for investment casting of nickel superalloys. *Journal of the European Ceramic Society,* 40**,** 4955-4973.

Karwiński, A., Młodnicki, S., Pabiś, R., Robak, I. & Kubosz, G. 2011. New generation of pattern materials for investment casting. *Archives of Foundry Engineering,* 11**,** 53-56.

Kashimura, K., Sato, M., Hotta, M., Agrawal, D. K., Nagata, K., Hayashi, M., Mitani, T. & Shinohara, N. 2012. Iron production from Fe3O4 and graphite by applying 915 MHz microwaves. *Materials Science and Engineering: A,* 556**,** 977-979.

Kaushal, S. 2022. Microstructure and tribological characterization of composite castings developed through in-situ microwave hybrid heating. *International Journal of Metalcasting,* 16**,** 2150-2161.

Kaushal, S., Bohra, S., Gupta, D. & Jain, V. 2021. On processing and characterization of Cu–Mo-based castings through microwave heating. *International Journal of Metalcasting,* 15**,** 530-537.

Kenji, K., Kanuma, Y., Oguro, T. & Harada, A. 1986. The reliability of magnetrons for microwave ovens. *Journal of Microwave Power and Electromagnetic Energy,* 21**,** 149-158.

Khraisheh, M., Cooper, T. & Magee, T. 1997. Microwave and air drying I. Fundamental considerations and assumptions for the simplified thermal calculations of volumetric power absorption. *Journal of Food Engineering,* 33**,** 207-219.

Kim, S., Moon, H. & Kim, J. 2015. Thermal characterizations of the paraffin wax/low density polyethylene blends as a solid fuel. *Thermochimica Acta,* 613**,** 9-16.

Kim, Y.-H., Yeo, J.-G., Lee, J.-S. & Choi, S.-C. 2016. Influence of silicon carbide as a mineralizer on mechanical and thermal properties of silica-based ceramic cores. *Ceramics International,* 42**,** 14738-14742.

Kim, Y. C., Kim, C. H. & Kim, D. K. 1997. Effect of microwave heating on densification and α→ β phase transformation of silicon nitride. *Journal of the European Ceramic Society,* 17**,** 1625-1630.

Kline, D., Lekakh, S. & Richards, V. 2010. Improving investment casting mold permeability using graphite particles. *Transactions of the American Foundry Society,* 118**,** 10-087.

Kline, D. M. 2010. *Controlling strength and permeability of silica investment casting molds.* Master Thesis, Missouri University of Science and Technology, Rolla, USA.

Klinger, J. L., Westover, T. L., Emerson, R. M., Williams, C. L., Hernandez, S., Monson, G. D. & Ryan, J. C. 2018. Effect of biomass type, heating rate, and sample size on microwave-enhanced fast pyrolysis product yields and qualities. *Applied Energy,* 228**,** 535-545.

Komaragiri, S., Li, H., Lekakh, S., Chandrashekhara, K. & Richards, V. Effects of complex geometry, shell thickness and firing regimes on shell cracking in industrial investment casting shells during rigid polymer pattern removal. (2013). *Proceedings of the CastExpo and the Metalcasting Congress*, St. Louis, MO, USA, 2013. 6-9.

Kreith, F., Manglik, R. M. & Bohn, M. S. 2011. Principles of heat transfer. 7th edn. Stamford: Cengage learning

Kumanek, B. & Janas, D. 2019. Thermal conductivity of carbon nanotube networks: A review. *Journal of Materials Science,* 54**,** 7397-7427.

Kumar, B. & Bhardwaj, S. 2015. An Experimental Investigation of Wax Pattern in Investment Casting. *International Journal of Engineering and Management Research (IJEMR),* 5**,** 544-546.

Kumar, R., Bhowmick, H., Gupta, D. & Bansal, S. 2021. Development and characterization of multiwalled carbon nanotube-reinforced microwave sintered hybrid aluminum metal matrix composites: an experimental investigation on mechanical and tribological performances. *Proceedings of the Institution of Mechanical Engineers, Part L: Journal of Materials: Design and Applications,* 235**,** 2310-2323.

Kumar, S. & Karunakar, D. B. 2019. Enhancing the permeability and properties of ceramic shell in investment casting process using ABS powder and needle coke. *International Journal of Metalcasting,* 13**,** 588-596.

Kumar, S. & Karunakar, D. B. 2021. Characterization and properties of ceramic shells in investment casting process. *International Journal of Metalcasting,* 15**,** 98-107.

Kumar, S. & Karunakar, D. B. 2022. Development of wax blend pattern and optimization of injection process parameters by grey-fuzzy logic in investment casting process. *International Journal of Metalcasting,* 16**,** 962-972.

Lee, K. 2016. *Understanding shell cracking during de-wax process in investment casting.* PhD Thesis, University of Birmingham, UK.

Lee, W.-H., Wu, Y.-F., Ding, Y.-C. & Cheng, T.-W. 2020. Fabrication of ceramic moulds using recycled shell powder and sand with geopolymer technology in investment casting. *Applied sciences,* 10**,** 4577.

Lehmhus, D. 2022. Advances in metal casting technology: A review of state of the art, challenges and trends—Part I: changing markets, changing products. MDPI.

Li, D., Jia, D., Yang, Z. & Zhou, Y. 2022. Principles, design, structure and properties of ceramics for microwave absorption or transmission at high-temperatures. *International Materials Reviews,* 67**,** 266-297.

Li, J., Shirai, T. & Fuji, M. 2013. Rapid carbothermal synthesis of nanostructured silicon carbide particles and whiskers from rice husk by microwave heating method. *Advanced Powder Technology,* 24**,** 838-843.

Li, S., Xie, G., Louzguine-Luzgin, D. V., Cao, Z., Yoshikawa, N., Sato, M. & Inoue, A. 2010. Phase transformations in Si-based alloy powder mixtures induced by microwave heating in a 2.45 GHz single-mode applicator. *Intermetallics,* 18**,** 2030-2033.

Li, Y., Zhao, J., Dong, H. & Xi, X. 2021. The role of shearing effect in the evolution of the microscopic behavior of wax crystals. *New Journal of Chemistry,* 45**,** 10418-10431.

Lin, H., Zhu, H., Guo, H. & Yu, L. 2007. Investigation of the microwave-absorbing properties of Fe-filled carbon nanotubes. *Materials Letters,* 61**,** 3547-3550.

Ling, S. J., Moebs, W. & Sanny, J. 2016. *Plane Electromagnetic Waves,* in Electromagnetic Waves. Orlando, FL: University of Central Florida, pp. 278-340.

Liu, C., Wang, F., Jin, S., Li, F. & Lai, X. 2019. Permafrost analysis methodology (PAM) for ceramic shell deformation in the firing process. *International Journal of Metalcasting,* 13**,** 953-968.

Liu, Y. & Xiong, S. 2024. Research progress on thermal conductivity of high-pressure die-cast aluminum alloys. *Metals,* 14**,** 370.

Loharkar, P. K., Ingle, A. & Jhavar, S. 2019. Parametric review of microwave-based materials processing and its applications. *Journal of Materials Research and Technology,* 8**,** 3306-3326.

Lombardo, S. J. & Retzloff, D. G. 2020. Reaction–permeability optimum time heating policy via process control for debinding green ceramic components. *Advances in Applied Ceramics,* 119**,** 150-157.

Loshchinin, Y. V., Lebedeva, Y. E. & Slavin, A. 2019. Thermophysical Properties of Silicon-Carbide-Based Ceramic Composite Materials Obtained by Spark Plasma Sintering (SPS). *Glass and Ceramics,* 75**,** 340-344.

Lü, K., Liu, X.-D., Du, Z.-X. & Li, Y.-F. 2016a. Bending strength and fracture surface topography of natural fiber-reinforced shell for investment casting process. *China Foundry,* 13**,** 211-216.

Lü, K., Liu, X., Du, Z. & Li, Y. 2016b. Properties of hybrid fibre reinforced shell for investment casting. *Ceramics International,* 42**,** 15397-15404.

Luján, R. C., Conesa, I. P., Hernández, F. A. & Pavón, M. M. L. 2025. Microwave technology VS traditional gas systems for Flash Dewaxing in the Art Foundry. *Results in Engineering***,** 105006.

Lv, S., Zeng, Y., Wen, J., Zhao, H. & Su, Z. 2018. Estimation of penetration depth from soil effective temperature in microwave radiometry. *Remote Sensing,* 10**,** 519.

Mahrabi, H., Jolly, M. & Salonitis, K. (2016). Methods of reducing materials' waste and saving energy in investment casting. Shape Casting: 6th International Symposium, 2016. Byczynski (Cham, Switzerland: Springer, 2016), 69-76.

Maia, M., Barros, A. I. & Nunes, F. M. 2013. A novel, direct, reagent-free method for the detection of beeswax adulteration by single-reflection attenuated total reflectance mid-infrared spectroscopy. *Talanta,* 107**,** 74-80.

Mao, Y., Robinson, J. & Binner, E. 2021. Understanding heat and mass transfer processes during microwave-assisted and conventional solvent extraction. *Chemical Engineering Science,* 233**,** 116418.

Martha, R., Mubarok, M., Darmawan, W., Syafii, W., Dumarcay, S., Charbonnier, C. G. & Gerardin, P. 2021. Biomolecules of interest present in the main industrial wood species used in indonesia-a review. *Journal of Renewable Materials,* 9**,** 399-449.

Masin, B., Ashok, K. & Sreemoolanadhan, H. 2022. Microwave hybrid sintering of 0.95 (Mg0. 95Zn0. 05) TiO3-0.05 CaTiO3 ceramics and its microwave dielectric properties. *Journal of the European Ceramic Society,* 42**,** 4974-4979.

Mehta, A., Vasudev, H. & Jeyaprakash, N. 2024. Role of sustainable manufacturing approach: microwave processing of materials. *International Journal on Interactive Design and Manufacturing (IJIDeM),* 18**,** 5283-5299.

Menéndez, J., Arenillas, A., Fidalgo, B., Fernández, Y., Zubizarreta, L., Calvo, E. G. & Bermúdez, J. M. 2010. Microwave heating processes involving carbon materials. *Fuel Processing Technology,* 91**,** 1-8.

Menezes, R. & Kiminami, R. 2008. Microwave sintering of alumina–zirconia nanocomposites. *Journal of Materials Processing Technology,* 203**,** 513-517.

Menezes, R. R., Souto, P. M. & Kiminami, R. H. 2007. Microwave hybrid fast sintering of porcelain bodies. *Journal of Materials Processing Technology,* 190**,** 223-229.

Menezes, R. R., Souto, P. M. & Kiminami, R. H. G. A. 2010. Microwave fast sintering of submicrometer alumina. *Materials Research,* 13**,** 345-350.

Meng, F., Wang, H., Huang, F., Guo, Y., Wang, Z., Hui, D. & Zhou, Z. 2018. Graphene-based microwave absorbing composites: A review and prospective. *Composites Part B: Engineering,* 137**,** 260-277.

Meredith, R. J. 1998. *Engineers' handbook of industrial microwave heating*, London: The Institution od Electrical Engineers.

Metaxas, A. A. & Meredith, R. J. 1993. *Industrial microwave heating*, London: Peter Peregrinus Ltd.

Mills, A., Farid, M., Selman, J. R. & Al-Hallaj, S. 2006. Thermal conductivity enhancement of phase change materials using a graphite matrix. *Applied Thermal Engineering,* 26**,** 1652-1661.

Minami, M., Tatami, J., Iijima, M., Takahashi, T. & Ohji, T. 2023. In-situ investigation on crack-initiation and deformation of Al2O3 green bodies during dewaxing process by combined OCT-TG-FTIR and TMA. *Ceramics International,* 49**,** 15387-15394.

Mishra, R. R. & Sharma, A. K. 2016. Microwave–material interaction phenomena: Heating mechanisms, challenges and opportunities in material processing. *Composites Part A: Applied Science and Manufacturing,* 81**,** 78-97.

Mishra, S. & Ranjana, R. 2010. Reverse solidification path methodology for dewaxing ceramic shells in investment casting process. *Materials and Manufacturing Processes,* 25**,** 1385-1388.

Miyata, T., Gohda, S., Oshita, A., Ono, H. & Kashimura, K. 2023. Synthesis of graphene-like materials from acetylene black, activated carbon, and ketjenblack via separated microwave electric and magnetic field heating. *Materials,* 16**,** 3723.

Mondal, A., Agrawal, D. & Upadhyaya, A. 2010. Microwave sintering of refractory metals/alloys: W, Mo, Re, W-Cu, W-Ni-Cu and W-Ni-Fe alloys. *Journal of Microwave Power and Electromagnetic Energy,* 44**,** 28-44.

Monzavi, M., Chen, Z., Solouki, A. & Chaouki, J. 2022. Microwave-assisted catalytic pyrolysis of paraffin wax. *Fuel,* 320**,** 123886.

Morîntale, E., Harabor, A., Constantinescu, C. & Rotaru, P. 2013. Use of heat flows from DSC curve for calculation of specific heat of the solid materials. *Physics AUC,* 23**,** 89-94.

Mukhtarkhanov, M., Akayev, S., Gouda, S., Shehab, E. & Ali, M. H. 2024. A novel method for evaluating thermal expansion forces during dewaxing of investment casting and 3D-printing waxes. *International Journal of Lightweight Materials and Manufacture*.

Nadolski, M., Konopka, Z., Łągiewka, M. & Zyska, A. 2008. Examining of slurries and production of moulds by spraying method in lost wax technology. *Arch. Foundry Eng,* 8**,** 107-110.

Nanda, I. P. 2018. The Effect of Stucco Sand Size on the Shell Mould Permeability and Modulus of Rupture (MOR). *Journal of Aeronautical-science and engineering-,* 13**,** 5-9.

Naseri, H., Trickett, K., Mitroglou, N., Karathanassis, I., Koukouvinis, P., Gavaises, M., Barbour, R., Diamond, D., Rogers, S. E. & Santini, M. 2018. Turbulence and cavitation suppression by quaternary ammonium salt additives. *Scientific Reports,* 8**,** 7636.

National, R. C. & Stein, D. F. 1994. *Microwave processing of materials*, Washington: National Academies Press.

Neto, R., Duarte, T., Alves, J. L. & Torres, F. 2017. Experimental characterization of ceramic shells for investment casting of reactive alloys. *Ciencia & Tecnologia dos Materiais,* 29**,** e34-e39.

Ngamkiatpaisan, A., Hankoy, M., Kitiwan, M., Keawprak, N. & Tunthawiroon, P. 2023. A study on SiC suscepter configuration for microwave hybrid heating

O'sullivan, N., Mooney, J. & Tanner, D. 2021. Enhancing permeability and porosity of ceramic shells for investment casting through pre-wetting. *Journal of the European Ceramic Society,* 41**,** 411-422.

Oguntuyi, S. D., Shongwe, M. B., Tshabalala, L., Johnson, O. T. & Malatji, N. 2023. Effects of SiC on the microstructure, densification, hardness and wear performance of TiB2 ceramic matrix composite consolidated via spark plasma sintering. *Arabian Journal for Science and Engineering,* 48**,** 2889-2903.

Pal, D. & Ravi, B. 2007. Rapid tooling route selection and evaluation for sand and investment casting. *Virtual and Physical Prototyping,* 2**,** 197-207.

Pal, J., Gupta, D. & Singh, T. P. 2022. Processing and characterization of SS316 based metal matrix composite casting through microwave hybrid heating. *Proceedings of the Institution of Mechanical Engineers, Part C: Journal of Mechanical Engineering Science,* 236**,** 10508-10527.

Panneerselvam, M. & Rao, K. 2003. A microwave method for the preparation and sintering of β′-SiAlON. *Materials Research Bulletin,* 38**,** 663-674.

Parchovianský, M., Galusek, D., Švančárek, P., Sedláček, J. & Šajgalík, P. 2014. Thermal behavior, electrical conductivity and microstructure of hot pressed Al2O3/SiC nanocomposites. *Ceramics International,* 40**,** 14421-14429.

Parthiban, A., Ramesh, A., Suresh, A., Dinesh, D. & Kanishkha, P. 2024. LM6 Aluminium Alloy Processing by Die Casting—A State of the Art. *Advances in Additive Manufacturing Technologies***,** 326-330.

Patterson, M., Apte, P., Kimber, R. & Roy, R. 2011. Batch process for microwave sintering of Si3N4. *MRS Online Proceedings Library (Cambridge University),* 269.

Pattnaik, S. 2014. *Reduction of Shrinkage and Porosity Defects in Investment Casting.* PhD Thesis, Indian Institute of Technology, Roorkee.

Pattnaik, S. 2017a. Influence of sawdust on the properties of the ceramic shell used in investment casting process. *The International Journal of Advanced Manufacturing Technology,* 93**,** 691-707.

Pattnaik, S. 2017b. An investigation on enhancing ceramic shell properties using naturally available additives. *The International Journal of Advanced Manufacturing Technology,* 91**,** 3061-3078.

Pattnaik, S., Jha, P. K. & Karunakar, D. B. 2017. A novel method of increasing ceramic shell permeability and optimizing casting shrinkage and tensile strength of the investment cast parts. *Proceedings of the Institution of Mechanical Engineers, Part B: Journal of Engineering Manufacture,* 231**,** 377-388.

Pattnaik, S., Karunakar, D. B. & Jha, P. K. 2012. Developments in investment casting process—A review. *Journal of Materials Processing Technology,* 212**,** 2332-2348.

Pattnaik, S. & Sutar, M. K. An Effective Way of Reducing the Wax Pattern Shrinkage to Improve the Dimensional Accuracy of the Investment Castings. Asian Conference on Indoor Environmental Quality, 2021. Springer, 131-137.

Pattnaik, S. & Sutar, M. K. 2022. Preparation and analysis of a hybrid ceramic shell for investment casting. *The International Journal of Advanced Manufacturing Technology,* 122**,** 2513-2527.

Peelamedu, R. D., Roy, R. & Agrawal, D. K. 2002. Microwave-induced reaction sintering of NiAl2O4. *Materials Letters,* 55**,** 234-240.

Peng, Z., Hwang, J.-Y. & Andriese, M. 2012. Magnetic loss in microwave heating. *Applied Physics Express,* 5**,** 027304.

Peng, Z., Hwang, J.-Y. & Andriese, M. 2013. Design of double-layer ceramic absorbers for microwave heating. *Ceramics International,* 39**,** 6721-6725.

Peng, Z., Hwang, J.-Y., Mouris, J., Hutcheon, R. & Huang, X. 2010. Microwave penetration depth in materials with non-zero magnetic susceptibility. *ISIJ International,* 50**,** 1590-1596.

Pérez-Conesa, I., Fayos-Fernández, J., Aguilar Galea, J., Monzó-Cabrera, J. & Pérez-Campos, R. 2022. Evaluation of graphite and TiO2 as susceptors for microwave dewaxing in ceramic shell casting processes of artworks. *Journal of Microwave Power and Electromagnetic Energy,* 56**,** 201-215.

Permana, L., Sriprom, P., Manamoongmongkol, K., Phumjan, L. & Assawasaengrat, P. 2024. Optimization of betalain extraction from dragon fruit (Hylocereus undatus) peel and effect of pH on its properties. *Biomass Conversion and Biorefinery***,** 1-12.

Pickles, C. 2009. Microwaves in extractive metallurgy: part 1–review of fundamentals. *Minerals Engineering,* 22**,** 1102-1111.

Pop, V., Chicinas, I. & Jumate, N. 2001. Material physics. Experimental methods. *Cluj-Napoca, Romania: Presa Universitara Clujeana House*.

Prakash, C., Singh, S., Kopperi, H., Ramakrihna, S. & Mohan, S. V. 2021. Comparative job production based life cycle assessment of conventional and additive manufacturing assisted investment casting of aluminium: A case study. *Journal of Cleaner Production,* 289**,** 125164.

Prasad, R. 2012. Progress in investment castings Science and technology of casting processes, in Srinivasan, M. *Rijeka, Croatia: InTech***,** pp. 25–72.

Pundhir, N., Zafar, S. & Pathak, H. 2021. Performance evaluation of HDPE/MWCNT and HDPE/kenaf composites. *Journal of Thermoplastic Composite Materials,* 34**,** 1315-1333.

Rahman Khan, M. M., Rumon, M. M. H. & Islam, M. 2024. Synthesis, Rheology, Morphology, and Mechanical Properties of Biodegradable PVA-Based Composite Films: A Review on Recent Progress. *Processes,* 12.

Rakoczy, Ł., Grudzień-Rakoczy, M. & Cygan, R. 2019. The influence of shell mold composition on the as-cast macro-and micro-structure of thin-walled IN713C superalloy castings. *Journal of Materials Engineering and Performance,* 28**,** 3974-3985.

Ramesh, P. D., Brandon, D. & Schächter, L. 1999. Use of partially oxidized SiC particle bed for microwave sintering of low loss ceramics. *Materials Science and Engineering: A,* 266**,** 211-220.

Rana, K. K. & Rana, S. 2014. Microwave reactors: A brief review on its fundamental aspects and applications. *Open Access Library Journal,* 1**,** 1-20.

Rani, D., Bala, N., Saxena, V. & Saxena, A. 2014. Recycling of Pattern Wax in Investment Casting Process Using Infrared Oven. *MIT International Journal of Mechanical Engineering,* 4**,** p44-48.

Rani, D. & Karunakar, D. 2013. Recycling of pattern wax in the investment casting process using microwave dewaxing. *IOSR Journal of Engineering,* 3**,** 5-10.

Ravi, B., Praveen, V., Selvam, M. P. & Rao, K. 1998. Microwave-assisted preparation and sintering of mullite and mullite–zirconia composites from metal organics. *Materials Research Bulletin,* 33**,** 1527-1536.

Ravi, B., Ramesh, P. & Rao, K. 1997. Microwave assisted preparation and sintering of Al 2 O 3, ZrO 2 and their composites from metalorganics. *Journal of Materials Chemistry,* 7**,** 2043-2048.

Raza, M. 2015. *Process development for investment casting of thin-walled components: Manufacturing of light weight components.* PhD Thesis, Mälardalen University, Sweden.

Razak, S. N. F. B. A. 2017. *Effect of Heating Temperature and Mould Thickness on the Geometry Shape of In-situ Melting Magnesium Investment Casting*. Master Thesis, Universiti Teknologi Malaysia, Skudai.

Reddy, A. C., Murti, V. & Sundararajan, S. 1998. Some aspects of reducing sediments rate of refractory fillers in the investment casting process. *Journal of Engineering Advances,* 10**,** 61-63.

Rezvani, S., Chuo, Y. S., Lee, J. & Park, S. S. 2022. Hybrid sintering of CNT/PZT ceramics using microwave oven. *Ceramics International,* 48**,** 14684-14696.

Richard, C. T. & Kwok, T.-H. Rapid investment casting: design and manufacturing technologies. International Design Engineering Technical Conferences and Computers and Information in Engineering Conference, 2019. American Society of Mechanical Engineers, V001T02A022.

Richards, V. & Mascreen, S. A. 2003. Thermal expansion of investment casting pattern wax. *AFS Transactions,* 111**,** 489–499.

Ripetskiy, A., Khotina, G. & Arkhipova, O. The role of additive manufacturing in the investment casting process. E3S Web of Conferences, 2023. EDP Sciences, 04015.

Roach, P. & Ponton, C. 2013. Aqueous electrophoretic deposition as a method for producing an investment casting shell mould ceramic face-coat. Part 1: formation of a carbon-filled investment casting wax electrode material. *Journal of Materials Science,* 48**,** 7476-7492.

Ronkay, F., Molnár, B., Nagy, D., Szarka, G., Iván, B., Kristály, F., Mertinger, V. & Bocz, K. 2020. Melting temperature versus crystallinity: new way for identification and analysis of multiple endotherms of poly (ethylene terephthalate). *Journal of Polymer Research,* 27**,** 372.

Roper, D. K., Ahn, W. & Hoepfner, M. 2007. Microscale heat transfer transduced by surface plasmon resonant gold nanoparticles. *The Journal of Physical Chemistry C,* 111**,** 3636-3641.

Rutto, H. K. 2011. *Urea-based moulding compounds for investment casting.* PhD Thesis, University of Pretoria, Pretoria, South Africa.

Rydzkowski, T., Reszka, K., Szczypiński, M., Szczypiński, M. M., Kopczyńska, E. & Thakur, V. K. 2020. Manufacturing and evaluation of mechanical, morphological, and thermal properties of reduced graphene oxide-reinforced expanded polystyrene (EPS) nanocomposites. *Advances in Polymer Technology,* 2020**,** 1-9.

Sabau, A. S. & Viswanathan, S. 2003. Material properties for predicting wax pattern dimensions in investment casting. *Materials Science and Engineering: A,* 362**,** 125-134.

Samyal, R., Bagha, A. K. & Bedi, R. 2022. The casting of materials using microwave energy: A review. *Materials Today: Proceedings,* 26**,** 1279-1283.

Sane, A. R., Nigay, P.-M., Pham Minh, D., Toussaint, C., Germeau, A., Semlal, N., Boulif, R. & Nzihou, A. 2020. An investigation of the physical, thermal and mechanical properties of fired clay/SiC ceramics for thermal energy storage. *Journal of Thermal Analysis and Calorimetry,* 140**,** 2087-2096.

Sarcinella, A., Cunha, S., Aguiar, J. & Frigione, M. 2024. Thermo-chemical characterization of organic phase change materials (PCMs) obtained from lost wax casting industry. *Sustainability,* 16**,** 7057.

Sarkar, R. 2020. Binders for refractory castables: an overview. *Interceram-International Ceramic Review,* 69**,** 44-53.

Sebastian, M., Ubic, R. & Jantunen, H. 2015. Low-loss dielectric ceramic materials and their properties. *International Materials Reviews,* 60**,** 392-412.

Shah, M., Monapara, P., Chitroda, Y., Karetiya, D. & Patel, D. Investment casting using additive manufacturing: state-of-the-art and future directions-a review paper. 2023 IEEE 11th Region 10 Humanitarian Technology Conference (R10-HTC), 2023. IEEE, 889-895.

Shang, X., Zhai, D., Zhang, F., Wei, C., Chen, J., Liu, M. & Peng, J. 2019. Electromagnetic waves transmission performance of alumina refractory ceramics in 2.45 GHz microwave heating. *Ceramics International,* 45**,** 23493-23500.

Shen, L., Zhou, J. & Zhang, X. 2024. In situ investigation of the thermal characteristics of microwave resonance-induced focused hotspots in dimers for improving microwave heating uniformity. *Case Studies in Thermal Engineering,* 54**,** 104052.

Shivappa, D., Harisha, K., Prasad, A. & Manjunath, R. 2014. Experimental Studies on Recyclability of Investment Casting Pattern Wax. *Recent Advances in Mechanical Engineering and Mechanics*, 118.

Sindhu, P. 2006. *Fundamentals of Molecular Spectroscopy*, Delhi: New Age International.

Singh, B., Kumar, P. & Mishra, B. 2006. Experimental investigation of wax blends in investment casting process. *Indian Foundry Journal,* 52**,** 29-36.

Singh, D., Singh, R. & Boparai, K. S. 2018. Development and surface improvement of FDM pattern based investment casting of biomedical implants: A state of art review. *Journal of Manufacturing Processes,* 31**,** 80-95.

Singh, S., Bhaskar, R., Narayanan, K. B., Kumar, A. & Debnath, K. 2024. Development of silicon carbide (SiC)-based composites as microwave-absorbing materials (MAMs): a review. *Journal of the European Ceramic Society*.

Singh, S., Gupta, D. & Jain, V. 2021a. Fabricating in situ powdered nickel–alumina metal matrix composites through microwave heating process: a sustainable approach. *International Journal of Metalcasting,* 15**,** 969-982.

Singh, S., Kumar, P. & Singh, J. (2021). An approach to eliminate shell cracking problem in fused deposition modeling pattern based investment casting process. *IOP Conference Series: Materials Science and Engineering*, 2021b. IOP Publishing, 012035.

Siores, E. & Do Rego, D. 1995. Microwave applications in materials joining. *Journal of Materials Processing Technology,* 48**,** 619-625.

Sivanagaraju, S., Reddy, M. B. & Srilatha, D. 2010. *Generation and Utilization of Electrical Energy*, India: Dorling Kindersley.

Smith, B. C. 2018. *Infrared spectral interpretation: a systematic approach*, 1st edn. Boca Raton: CRC press.

Snyder, B., Scott, D. & Snow, J. 2003. A new combination shell strength and permeability test. *Invest. Cast. Inst,* 51**,** 1-26.

Sobol, H. & Tomiyasu, K. 2002. Milestones of microwaves. *IEEE Transactions on Microwave Theory and Techniques,* 50**,** 594-611.

Srinivasan, M. 2012. *Science and technology of casting processes*, Rijeka, Croatia: InTech.

Stubna, I. & Vozár, L. 2005. The influence of the sample size on low-temperature processes in green electroceramics. *Industrial Ceramics(Italy),* 25**,** 110-112.

Stuerga, D. 2006. Microwave-material interactions and dielectric properties, key ingredients for mastery of chemical microwave processes. *Microwaves in Organic Synthesis***,** 1-61.

Suhasril, A. A. 2016. *Hydroxyapatite Coating on Stainless Steel 316L Using Investment Casting Technique.* PhD Thesis, Universiti Teknologi Malaysia, Skudai.

Surendran, A. N., Ajjarapu, K. P. K., Arumugham, A. A., Kate, K. & Satyavolu, J. 2022. Characterization of industry grade soybean wax for potential applications in natural fiber reinforced composite (NFRC) filaments. *Industrial Crops and Products,* 186**,** 115163.

Szabó, L., Deák, G., Nyul, D. & Kéki, S. 2022. Flexible Investment Casting Wax Patterns for 3D-Printing: Their Rheological and Mechanical Characterizations. *Polymers,* 14**,** 4744.

Tamang, S. & Aravindan, S. 2019. 3D numerical modelling of microwave heating of SiC susceptor. *Applied Thermal Engineering,* 162**,** 114250.

Tamta, K. & Karunakar, D. B. Enhancement of Porosity of the Ceramic Shell in Investment Casting Process Using Needle Coke and Camphor. (2014). *Applied Mechanics and Materials*, 2014. Trans Tech Publications, 269-275.

Tamta, K. & Karunakar, D. B. 2019. Enhancing mechanical properties and permeability of ceramic shell in investment casting process. *Materials and Manufacturing Processes,* 34**,** 612-623.

Tamta, K. & Karunakar, D. B. 2021. Development of hybrid pattern material for investment casting process: an experimental investigation on improvement in pattern characteristics. *Materials and Manufacturing Processes,* 36**,** 744-751.

Tayier, W., Janasekaran, S. & Tai, V. C. 2022. Microwave hybrid heating (MHH) of Ni-based alloy powder on Ni and steel-based metals–A review on fundamentals and parameters. *International Journal of Lightweight Materials and Manufacture,* 5**,** 58-73.

Tewo, R. K., Rutto, H. L., Focke, W., Seodigeng, T. & Koech, L. K. 2019. Formulations, development and characterization techniques of investment casting patterns. *Reviews in Chemical Engineering,* 35**,** 335-349.

Thostenson, E. & Chou, T.-W. 1999. Microwave processing: fundamentals and applications. *Composites Part A: Applied Science and Manufacturing,* 30**,** 1055-1071.

Thridandapani, R., Folgar, C., Folz, D., Clark, D., Wheeler, K. & Peralta, P. 2009. Microwave sintering of 8 mol% yttria–zirconia (8YZ): An inert matrix material for nuclear fuel applications. *Journal of nuclear materials,* 384**,** 153-157.

Torgovnikov, G. & Vinden, P. 2009. High-intensity microwave wood modification for increasing permeability. *Forest products journal,* 59**,** 84.

Tran, V. 1991. Applicator Design for Processing Large Quantities of Dielectric Material. *Ceramic Transactions,* 21**,** 683-691.

Travitzky, N., Goldstein, A., Avsian, O. & Singurindi, A. 2000. Microwave sintering and mechanical properties of Y-TZP/20 wt.% Al2O3 composites. *Materials Science and Engineering: A,* 286**,** 225-229.

Tseng, H.-W., Chen, T.-Y., Kao, Y. C., Huang, C.-F., Liu, Y.-C., Lee, S.-C., Wang, C.-C., Chan, C.-W. & Fuh, Y.-K. 2023. Effect of shell mold thickness and insulating wool pattern on internal porosity in investment casting of vortex flow meter. *The International Journal of Advanced Manufacturing Technology,* 127**,** 2371-2385.

Umar, H., Rizal, S., Riza, M. & Mahlia, T. M. I. 2018. Mechanical properties of concrete containing beeswax/dammar gum as phase change material for thermal energy storage. *AIMS Energy,* 6**,** 521–529.

Vaghela, J. R., Valaki, J. B., Thanki, S. J. & Pandey, A. B. 2023. Sustainability Analysis of Rapid Tooling-Based Investment Casting: A Comprehensive Review. *Smart and Sustainable Manufacturing Systems,* 7**,** 54-81.

Valverde, C., Rodríguez-García, M. M., Rojas, E. & Bayon, R. Comparison of Conventional and Microwave Heating. SolarPACES Conference Proceedings, 2023.

Varfolomeev, M. S. & Shcherbakova, G. I. 2021. Interaction of a Ceramic Casting Mold Material of the Al 2 O 3–Al 2 O 3 Composition with a Nickel-Based Superalloy. *International Journal of Metalcasting***,** 1-8.

Venkat, Y., Choudary, K., Das, D., Pandey, A. & Singh, S. 2020. Ceramic shell moulds with zircon filler and colloidal silica binder for investment casting of shrouded low-pressure turbine blades. *Ceramics International,* 46**,** 26572-26580.

Venkat, Y., Choudary, K., Das, D., Pandey, A. & Singh, S. 2021. Ceramic shell moulds for investment casting of low-pressure turbine rotor blisk. *Ceramics International,* 47**,** 5663-5670.

Vijayan, S. & Varma, H. 2002. Microwave sintering of nanosized hydroxyapatite powder compacts. *Materials letters,* 56**,** 827-831.

Vikulova, M., Tsyganov, A., Artyukhov, D., Gorokhovsky, A. & Gorshkov, N. 2023. Dielectric Properties of Composites Based on Ethylene Vinyl Acetate Filled with a Hollandite-Like Ceramic Material K1. 5Co0. 75Ti7. 25O16. *Russian Journal of Physical Chemistry B,* 17**,** 1311-1315.

Viswanathan, S., Apelian, D., Donahue, R. J., Dasgupta, B., Gywn, M., Jorstad, J. L., Monroe, R. W., Sahoo, M., Prucha, T. E. & Twarog, D. 2008. *Casting*, ASM International.

Vyas, A., Pandya, M. & Sutaria, M. Effect of mixing proportion and mixing time on primary slurry retention and surface roughness of investment casting shells. *IOP Conference Series: Materials Science and Engineering*. 10-13 September, 2020 Sozopol, Bulgaria.

Vyzulin, S., Buz'ko, V. Y., Kalikintseva, D., Goryachko, A., Miroshnichenko, E. & Vinokurov, A. 2021. Microwave absorption characteristics of composites based on microdispersed carbon fiber powder. *Bulletin of the Russian Academy of Sciences: Physics,* 85**,** 1019-1021.

Wang, H., Boyer, S. A., Bellet, M. & Dalle, F. 2023a. Effects of Wax Components and the Cooling Rate on Crystal Morphology and Mechanical Properties of Wax–Oil Mixtures. *Crystal Growth & Design,* 23**,** 1422-1433.

Wang, Q., Che, J., Wu, W., Hu, Z., Liu, X., Ren, T., Chen, Y. & Zhang, J. 2023b. Contributing factors of dielectric properties for polymer matrix composites. *Polymers,* 15**,** 590.

Wang, Y.-C., Kao, C.-Y., Chen, C.-M., Huang, C.-F., Liu, Y.-C., Lee, S.-C., Chan, C.-W. & Fuh, Y.-K. 2025. Effects of Al_2O_3 and SiC micro-scale powder addition on mechanical, thermal and physical properties of reinforced shell for investment casting. *Ceramics International,* 51**,** 7217-7228.

Whitehouse, C. & Dahlin, B. 2008. Effects of Wax Viscosity and Shell Permeability on Shell Cracking. *12th World Conference on Investment Casting. October 01, 2008.* Washington, Investment Casting Institute.

Williams, B. A. & Okonek, J. 2018. Wax mold for investment casting and method of assembling a wax mold. U.S. Patent 10,010,930.

Wiśniewski, P. 2021. Polymer binders of ceramic nanoparticles for precision casting of nickel-based superalloys. *Nanomaterials,* 11**,** 1714.

Wisniewski, P., Sitek, R., Towarek, A., Choinska, E., Moszczynska, D. & Mizera, J. 2020. Molding binder influence on the porosity and gas permeability of ceramic casting molds. *Materials,* 13**,** 2735.

Wu, K., Ting, T., Wang, G., Yang, C. & Tsai, C. 2008. Synthesis and microwave electromagnetic characteristics of bamboo charcoal/polyaniline composites in 2–40 GHz. *Synthetic Metals,* 158**,** 688-694.

Wu, Y., Mu, R., Li, G., Li, M. & Lv, W. 2022. Research progress in fluid and semifluid microwave heating technology in food processing. *Comprehensive reviews in food science and food safety,* 21**,** 3436-3454.

Xie, R., Wang, J., Yang, Y., Jiang, K., Li, Q. & Fan, S. 2011. Aligned carbon nanotube coating on polyethylene surface formed by microwave radiation. *Composites Science and Technology,* 72**,** 85-90.

Xie, Z., Yang, J., Huang, X. & Huang, Y. 1999. Microwave processing and properties of ceramics with different dielectric loss. *Journal of the European Ceramic Society,* 19**,** 381-387.

Yahaya, B. 2016. *Effect of Activated Charcoal on Investment Moulds Properties During Microwave Hybrid Dewaxing.* PhD Thesis, Universiti Teknologi Malaysia, Skudai.

Yahaya, B., Izman, S., Idris, M. & Dambatta, M. 2016. Effects of activated charcoal on physical and mechanical properties of microwave dewaxed investment casting moulds. *CIRP Journal of Manufacturing Science and Technology,* 13**,** 97-103.

Yaw, K. C. 2012. Measurement of dielectric material properties. *Application Note. Rohde & Schwarz***,** 1-35.

Yoshikawa, N., Ishizuka, E. & Taniguchi, S. 2006. Heating of metal particles in a single-mode microwave applicator. *Materials transactions,* 47**,** 898-902.

Youn, D. H., Jang, J.-W., Kim, J. Y., Jang, J. S., Choi, S. H. & Lee, J. S. 2014. Fabrication of graphene-based electrode in less than a minute through hybrid microwave annealing. *Scientific reports,* 4**,** 1-8.

Yuan, C. & Jones, S. 2003. Investigation of fibre modified ceramic moulds for investment casting. *Journal of the European Ceramic Society,* 23**,** 399-407.

Yuan, C., Jones, S. & Blackburn, S. 2005. The influence of autoclave steam on polymer and organic fibre modified ceramic shells. *Journal of the European Ceramic Society,* 25**,** 1081-1087.

Yuan, C., Jones, S. & Blackburn, S. 2012. Development of a new ferrous aluminosilicate refractory material for investment casting of aluminum alloys. *Metallurgical and Materials Transactions A,* 43**,** 5232-5242.

Zbigniew, R., Agnieszka, N., Joanna, W. & Danuta, N. 2019. Effect of Different Paraffin's and Microcrystalline Waxes on the Mechanical Properties of Base Plate Dental Waxes. *Saudi Journal of Oral and Dental Research,* 2.

Zeid, S. T. A. & Alnoury, A. 2023. Characterisation of the Bioactivity and the solubility of a New Root Canal Sealer. *International Dental Journal,* 73**,** 760-769.

Zhang, S., Qiu, Q., Zeng, C., Paik, K.-W., He, P. & Zhang, S. 2024. A review on heating mechanism, materials and heating parameters of microwave hybrid heated joining technique. *Journal of Manufacturing Processes,* 116**,** 176-191.

Zhang, Z., Liao, M., Li, M., Li, L., Wei, X., Kong, X., Xiong, S., Xia, J., Fu, L. & Cai, T. 2022. Enhanced thermal conductivity for polydimethylsiloxane composites with core-shell CFs@ SiC filler. *Composites Communications,* 33**,** 101209.

Zhao, C., Vleugels, J., Groffils, C., Luypaert, P. & Van Der Biest, O. 2000. Hybrid sintering with a tubular susceptor in a cylindrical single-mode microwave furnace. *Acta materialia,* 48**,** 3795-3801.

Zheng, X., Zhang, X., Xu, G. & Zhang, R. 2023. Enhancing Performance of Single-Channel SSVEP-Based Visual Acuity Assessment via Mode Decomposition. *IEEE Transactions on Neural Systems and Rehabilitation Engineering,* 31**,** 4203-4210.

Zhou, J., Li, Y., Li, N., Hao, X. & Liu, C. 2016. Interfacial shear strength of microwave processed carbon fiber/epoxy composites characterized by an improved fiber-bundle pull-out test. *Composites Science and Technology,* 133**,** 173-183.

Zhou, Y., Wang, K., Liu, R., Wang, X., Liu, C. & Fang, Q. 2012. High performance tungsten synthesized by microwave sintering method. *International Journal of Refractory Metals and Hard Materials,* 34**,** 13-17.

Zhu, W., Liu, Y., Guan, K., Peng, C. & Wu, J. 2019. Preparation of ZrO2 fiber modified Al2O3 membrane supports with enhanced strength and permeability. *Journal of the European Ceramic Society,* 39**,** 1712-1716.

Zych, J. & Snopkiewicz, T. 2011. Drying and hardening of ceramic moulds applied in the investment casting technology-investigations of the process kinetics. *Metallurgy and foundry engineering,* 37**,** 41-51.

Żymełka, D., Saunier, S., Goeuriot, D. & Molimard, J. 2013. Densification and thermal gradient evolution of alumina during microwave sintering at 2.45 GHz. *Ceramics International,* 39**,** 3269-3277.

APPENDIX A

REMET UK LTD
MATERIAL SAFETY DATA SHEET

1: IDENTIFICATION OF THE PREPARATION AND COMPANY

Product Name:	**HYFILL B289 MOD S**
Application:	INVESTMENT (LOST WAX) CASTING
Company:	REMET UK LTD.
Address:	THAMES ROAD, CRAYFORD, KENT DA1 4QJ, UNITED KINGDOM
	TELEPHONE (24 HOURS) +44 (0) 1322 522500
	FACSIMILE +44 (0) 1322 529770

2: COMPOSITION/INFORMATION ON INGREDIENTS

Composition: A BLEND OF WAXES, RESINS AND POLYMERS

Contains small amounts of free styrene, typically less than 0.5 %.

Refer to Section 8 for exposure limits/standards.

3: HAZARDS IDENTIFICATION

Not classified as Hazardous for Supply according to the Preparations Directive (88/379/EEC) and the Chemicals (Hazard Information and Packaging for Supply) Regulations 1996.

4: FIRST AID MEASURES

EYES: Contact with molten/solid product - Immediately cool with cold, clean, gently flowing water for at least ten minutes, holding eyelids apart if necessary. Obtain medical attention urgently.

SKIN: Contact with molten product - Immediately cool with cold running water for at least ten minutes. Do NOT remove adhering material. Obtain medical attention urgently.

INHALATION: Fume/dust - Remove from exposure, keep warm and at rest. Give oxygen by face mask if there is difficulty in breathing. If respiration stops or shows signs of failing give artificial respiration. If heart beat absent give external cardiac massage.

INGESTION: Solid product - Wash out mouth with water. Do NOT induce vomiting. If patient develops pain or feels unwell obtain medical attention.

5: FIRE-FIGHTING MEASURES

SUITABLE EXTINGUISHING MEDIA: Carbon dioxide, foam or water fog - Do NOT use water jets.

SPECIAL EXPOSURE HAZARDS: Irritant/toxic fumes - complex hydrocarbons.

SPECIAL PROTECTIVE EQUIPMENT: Self-contained breathing apparatus.

6: ACCIDENTAL RELEASE MEASURES

PERSONAL PRECAUTIONS: Solid product None.
Molten product Risk of slip and thermal burns. Wear suitable protective clothing including boots.

ENVIRONMENTAL PRECAUTIONS: Prevent entry into drains, sewers and water courses.

DECONTAMINATION PROCEDURES: Allow molten product to solidify. Dispose of solid as waste.

7: HANDLING AND STORAGE

HANDLING: Do not eat, drink or smoke whilst using this product. Use only in well ventilated areas. Avoid breathing fumes/dust. Avoid skin and eye contact. Do NOT heat above 100°C.

STORAGE: Store in a cool, well ventilated area out of direct sunlight. Do not expose to temperatures above 30°C.

8: EXPOSURE CONTROLS/PERSONAL PROTECTION

OCCUPATIONAL EXPOSURE LIMITS - The following substance(s) will be released from the molten product. Avoid overheating - 100°C max.

Substance information	8 hr. TWA	STEL	Source	Other
PARAFFIN WAX FUME (OES) 8002-74-2	2 mg/m^3	6 mg/m^3	EH40/2000	CAS #:
STYRENE (MEL) 100-42-5	430 mg/m^3	1080 mg/m^3	EH40/2000	CAS #:

ENGINEERING CONTROL MEASURES:
Use in well ventilated areas only. Efficient local exhaust ventilation, to minimise exposure to fume/vapour from molten product, is strongly recommended, especially in wax melting and pattern assembly areas. Local exhaust ventilation is recommended when breaking slabs/handling pastilles to minimise exposure to product dust. Mechanical methods to minimise exposure must take precedence over personal protective measures.

PERSONAL PROTECTIVE EQUIPMENT:
Safety glasses. Impervious gloves (eg PVC). Dust masks. A high standard of personal hygiene is essential. Change contaminated clothing and launder before re-use.

9: PHYSICAL AND CHEMICAL PROPERTIES

PHYSICAL STATE:	Waxy solid	FLASH POINT (OPEN, °C)	>200
COLOUR:	Green	VAPOUR PRESSURE (kPa @ 20°C)	Negligible
ODOUR:	Characteristic	RELATIVE DENSITY @ 20°C	1.05
MELTING POINT RANGE (°C)	70 - 84	WATER SOLUBILITY	Insoluble
VISCOSITY @ 100°C (cPs)	400 - 600		

10: STABILITY AND REACTIVITY

STABILITY: Stable up to 100°C under normal usage conditions. Extended exposure to temperatures above 90°C may cause thermal degradation of the product. Do not let molten product stand unused in melt tanks and injection machines. Stir molten product at all times.

CONDITIONS TO AVOID: Temperatures above 100°C

MATERIALS TO AVOID: Strong oxidising agents

11: TOXICOLOGICAL INFORMATION

HEALTH EFFECTS;

ON EYES: Fumes from molten product may cause irritation. Contact with molten product may produce severe thermal burns and permanent injury.

ON SKIN: Solid material may cause skin sensitisation and allergic dermatitis. Contact with molten product may produce severe thermal burns and permanent injury.

BY INHALATION: Product dust may cause respiratory tract irritation/sensitisation. When heated releases fume/vapour that may cause irritation/sensitisation of the respiratory tract. Further exposure of a sensitised person may produce symptoms of asthma - tightness of the chest, wheezing and coughing.

BY INGESTION: Low order of acute systemic toxicity.

OTHER: None known

12: ECOLOGICAL INFORMATION

ENVIRONMENTAL ASSESSMENT: When used and disposed of as intended, no adverse environmental effects are foreseen.

MOBILITY: Solid. Insoluble in water.

PERSISTENCE AND DEGRABILITY: Not readily biodegradable.

BIOACCUMULATIVE POTENTIAL: Not determined

ECOTOXICITY: Not expected to be ecotoxic to fish/daphnia/algae

13: DISPOSAL CONSIDERATION

Disposal must be in accordance with local and national legislation.

UNUSED PRODUCT: Dispose of through an licensed contractor to a licensed site.

USED PRODUCT: May be reclaimed. Dispose of through a licensed waste contractor to a licensed site.

PACKAGING: Must be disposed of through a licensed waste contractor. May be recycled.

14: TRANSPORT INFORMATION

The product is NOT classified as Hazardous for Transport.

15: REGULATORY INFORMATION

NOT classified as Hazardous for Supply according to the Preparations Directive (88/379/EEC) and the Chemicals (Hazard Information and Packaging for Supply) Regulations 1996.

16: OTHER INFORMATION

The information provided in this Safety Data Sheet has been compiled in accordance with the Preparations Directive (88/379/EEC), the Safety Data Sheet Directive (91/155/EEC) and the Chemicals (Hazard Information and Packaging for Supply) Regulations 1996 and is based on the present state of our knowledge.

This data is intended to enable safety assessments to be made and should not be construed as guaranteeing specific properties. Users are recommended to consult technical information sheets for advice on specific applications.

The data and advice given apply when the product is sold for the stated application or applications. The product is not sold as suitable for any other application. Use of the product for applications other than as stated in this sheet may give rise to risks not mentioned in this sheet. You should not use the product other than for the stated application or applications without seeking advice from us.

If you have purchased the product for supply to a third party for use at work, it is your duty to take all necessary steps to ensure that any person handling or using the product is provided with the information on this sheet.

If you are an employer, it is your duty to tell your employees, and others who may be affected, of any hazards described in this sheet and of any precautions which should be taken.

Further copies of this Material Safety Data Sheet may be obtained from REMET UK Ltd.

APPENDIX B

LIANG LINN ENTERPRISE CO., LTD.

Safety Data Sheet

SIVUCH

SECTION 1 - Identification of the substance/mixture and of the company/undertaking

1.1 Product Identifier

Precision Investment Casting Wax for Industrial use

Further trade names

Item No.: L1203

1.2 Relevant identified uses of the substance or mixture and uses advised against

Relevant identified uses of the substance or mixture

Waxes for lost-wax casting

Uses advised against

No data available.

1.3 Details of the supplier of the safety data sheet

Company name: LIANG LINN ENTERPRISE CO., LTD.

Address: 1F, NO.1-32 DONGSHIH, DONGCHENG VILLAGE, DONGSHAN DISTRICT, TAINAN CITY 73343, TAIWAN.

Telephone: +886-6-6803988

Fax: +886-6-6803569

Email: liang-linn@sivuch.com

Website: https://www.sivuch.com

SECTION 2 – Hazards identification

2.1 Classification of the substance or mixture

Classification information

This product does not meet the classification and labelling criteria given in the Regulation (EC) No 1272/2008 (CLP).

This product does not meet the classification and labelling criteria given in Dangerous Preparations Directive (1999/45/EC; DPD)

2.2 Label elements

Not relevant

2.3 Other hazards

PBT assessment

No data available.

vPvB assessment

No data available.

Current Version: 2.0.6 Revision Date: 01.06.2022

SECTION 3 – Composition/information on ingredients

3.1 Substances

Not applicable. The product is not a substance.

3.2 Mixtures

Chemical characterization

Paraffin wax.....40% Dammar resin....27% Eva polymer....11% Ceresine Wax...8% Synthetic resin....7% Carnauba Wax 3%

Bees Wax.....3% Microcrystalline Wax....1%

CAS No.

Paraffin Wax: 8002-74-2

Microcrystalline Wax: 63231-60-7

Carnauba Wax: 8015-86-9

Bees Wax: 8012-89-3

Dammar resin: 9000-16-2

Eva polymer: 24937-78-8

Ceresine Wax :8001-75-0

Synthetic resin: 64742-16-1

SECTION 4 – First aid measures

4.1 Description of first aid measures

After inhalation

Inhalation of product is unlikely. No special measures necessary.

After skin contact

In case of contact with skin wash off with water.

After eye contact

Remove contact lenses, irrigate copiously with clean, fresh water for at least 15 minutes, holding the eyelids apart and seek medical device.

After ingestion

Rinse mouth thoroughly with water. Never give anything by mouth to an unconscious person. Let plenty of water be drunk in small gulps. Call a doctor immediately.

4.2 Most important symptoms and effects, both acute and delayed

No data available.

4.3 Indication of any immediate medical attention and special treatment needed.

No data available.

SECTION 5 – Firefighting measures

5.1 Extinguishing media

Suitable extinguishing media

Carbon dioxide; Extinguishing powder; Foam

Unsuitable extinguishing media

Water

5.2 Special hazards arising from the substance or mixture

In the event of fire, the following can be released: Carbon monoxide and carbon dioxide

5.3 Advice for firefighters

Use self-contained breathing apparatus. Product itself does not burn. Adapt extinguisher and fire-fighting measures to fire in the environment. Wear protective clothing.

SECTION 6 – Accidental release measures

6.1 Personal precautions, protective equipment and emergency procedures

For non-emergency personnel

Refer to protective measures listed in sections 7 and 8.

For emergency responders

No data available. Personal protective equipment (PPE)- see Section 8.

6.2 Environmental precautions

Do not discharge into the drains/surface waters/ground water. Do not discharge into the subsoil/soil.

6.3 Methods and material for containment and cleaning up

Take up mechanically. When picked up, treat material as prescribed under heading "Disposal considerations".

6.4 Reference to other sections

No data available.

SECTION 7 – Handling and storage

7.1 Conditions for safe storage, including any incompatibilities

Further information on storage conditions

Protect from sunlight. Keep in a cool place.

SECTION 8 – Exposure controls/personal protection

8.1 Exposure controls

Protective and hygiene measures

Wash hands before breaks and at the end of work.

Hand protection

Caution! Hot molten mass. Avoid contact with skin.

SECTION 9 – Physical and chemical properties

9.1 Information on basic physical and chemical properties

Physical state: solid
Colour: Various colours
Odour: Odourless
Flash point: > 210°C (Cleveland Open Cup , ASTM D92)
Melting Point: 60~70 °C
Density: 0.931 g.cm^-3 (solid)
Water solubility: Insoluble
Auto Ignition Temp: Not applicable.
Boiling Point: Not applicable
pH: Not applicable.

SECTION 10 – Stability and reactivity

10.1 Reactivity

Dangerous reactions are not expected if the product is handled according to its intended use.

10.2 Chemical stability

Stable under recommended storage and handling conditions (See section 7)

10.3 Possibility of hazardous reactions

None, if handled according to order.

10.4 Conditions to avoid

None, if handled according to intended use.

10.5 Incompatible materials

None known.

10.6 Hazardous decomposition products

No hazardous decomposition products known.

APPENDIX C

Properties of Aluminium-Silicate (Al_2O_3-SiO_3) Stucco

ALUMINA SILICA

Refractories for Ceramic Shell Casting

PRESICO
METAL.CASTING.TITANIUM
President Co., Ltd.
Taiwan Headquarters, No.57, Fu-Hsing N. Rd., Taipei City, Taiwan, R.O.C.

○ Choice of Chemistry and Sizes in Grains and Flours

MULGRAIN™ 47 Grain Size Specifications (% Retained)

Screen Grade	8 2.38mm	12 1.70mm	14 1.40mm	16 1.18mm	20 0.85mm	30 0.60mm	40 0.425mm	50 0.30mm	70 0.212mm	100 0.15mm	140 0.106mm	200 0.075mm	325 0.045mm	PAN*
10×18	0-3	10-25			60-82	0-15								0-5
14×28		0	1 max		30-55	35-45	10-25	5 max						1.5 max
16×30				0-3	65-75		4 max							1 max
22S				TR	15-25	32-47	27-37	4-10					3max	TR
35S				TR	1-5	21-38	40-54		9-19		2-8			3 max
50S					0	1-8	22-37	26-40	12-22	6-16	0-6			3 max
60S						0	0-5	30-48	30-44	9-22	2-7			3 max
20×50				TR	0-8	20-50		50-72					2 max	TR
25×80					0-5	Eyen distribution		80-93	7-12					2 max
50×100							TR	5-20		70-86	0-15	3 max	1 max	TR
60×200								0	0-6		58-88	12-25		1max
3000	0-2					30-40						18-30		35-45
2001C-C										TR		15-25		75-85
3251C-C										TR			5-15	85-95

"PAN" designates the percentage of material passing last report screen for each sizing

MULGRAIN™ 60 Grain Size Specifications (% Retained)

Screen Grade	8 2.38mm	12 1.70mm	14 1.40mm	16 1.18mm	20 0.85mm	30 0.60mm	40 0.425mm	50 0.30mm	70 0.212mm	100 0.15mm	140 0.106mm	200 0.075mm	325 0.045mm	PAN*
22S				TR	15-25	32-47	27-37	4-10					3 max	0-5
35S				TR	1-5	21-38	40-54		9-19		2-8			1.5 max
60S						0	0-5	30-48	30-44	9-22	2-7			1 max
20×50				TR	0-8	20-50		50-72					3max	TR
2001C-C										TR		15-25		75-85
3251C-C										TR			5-15	85-95

"PAN" designates the percentage of material passing last report screen for each sizing

Typical Physical Analysis			
Specific Gravity gm/cc	2.60	2.70	2.85
P.C.E. Temperature Value	3200°F	3310°F	3390°F

Typical Chemical Analysis				
		M-47	M-60	M-70
Alumina (%)	Al_2O_3	47-52	58-62	68-72
Silica (%)	SiO_2	44-49	33-38	22-28
Titania (%)	TiO_2	≦ 3.0	≦ 3.0	≦ 3.5
Ferric Oxide (%)	Fe_2O_3	≦ 1.3	≦ 1.4	≦ 1.5
Calcium Oxide (%)	CaO	≦ 0.25	≦ 0.4	≦ 0.3
Magnesium Oxide (%)	MgO	≦ 0.1	≦ 0.2	≦ 0.2
Sodium Oxide (%)	Na_2O	≦ 0.2	≦ 0.3	≦ 0.3
Potassium Oxide (%)	K_2O	≦ 0.25	≦ 0.2	≦ 0.2

MULGRAIN™ 70 Grain Size Specifications (% Retained)

Screen Grade	100 0.15mm	200 0.075mm	325 0.045mm	PAN*
2001C-C	TR	15-25		75-85
3251C-C	TR		5-15	85-95

"PAN" designates the percentage of material passing last report screen for each sizing

Products Include:

Ceramic Shell Refractories
Fascote® Refractory
Ranco-Sil® Fused Silica
Alumina Silica
Zircon

Binders
Fascote® Binder
Primcote™ Binder
Nyacol® Colloidal Silica

E-mail : presico@presico.com.tw / Tel +886-2-2741-1190 / Fax 02-2741-2378

APPENDIX D

Properties of SiC (additive material)

荣盛集团 RONGSHENG GROUP **Zhengzhou Rongsheng Refractory Co., Ltd. 1/1**

Silicon Carbide SiC

Reference No.: RSQ22051201
Date: 12th May. 2022
From: Zhengzhou Rongsheng Refractory Co., Ltd.
Add.: Litang Industrial Dist., Laiji Town, Ximmi, Zhengzhou 450000, Henan Prov., China.

Technical Information

Color	Granularity Range	Chemical Component %				Density g/cm³
		mm	SiC	F.C	Fe_2O_3	
Black	F8 ~ F10/P8 ~ P12	1 ~ 0.85	≥ 98.2	≤ 0.2	≤ 0.4	≥ 3.21
	F12 ~ F14/P12 ~ P16	0.8 ~ 0.7	≥ 98.2	≤ 0.2	≤ 0.45	
	F16 ~ F24/P8 ~ P12	0.65 ~ 0.4	≥ 98.1	≤ 0.2	≤ 0.45	
	F30 ~ F60/P40 ~ P80	0.35 ~ 0.2	≥ 98.0	≤ 0.3	≤ 0.5	≥ 3.12
	F100 ~ F150/P120 ~ P150	0.15 ~ 0.1	≥ 98.0	≤ 0.3	≤ 0.5	
	F180 ~ F220/P180 ~ P220	0.08 ~ 0.06	≥ 97.2	≤ 0.3	≤ 0.55	
	F230 ~ F280/P240 ~ P360	0.063 ~ 0.04	≥ 97.2	≤ 0.3	≤ 0.55	≥ 3.10
	F320 ~ F500/P400 ~ P1000	0.045 ~ 0.02	≥ 97.0	≤ 0.35	≤ 0.6	
	F600 ~ F800/P1200 ~ P1500	0.025 ~ 0.013	≥ 96.5	≤ 0.4	≤ 0.6	
	F1000 ~ F1200/P2000 ~ P2500	0.013 ~ 0.005	≥ 95.5	≤ 0.5	≤ 0.7	

SiC **F12~F14** Test Report

ITEM		UNIT	Standard	Test result
Chemical Analysis	SiC	%	≥ 98.2	98.53
	F.C	%	≤ 0.2	0.13
	Fe_2O_3	%	≤ 0.45	0.27
Physical Properties	Bulk Density	g/cm³	3.21	3.21
	Hardness		9.5	9.5
	Melting Point	°C	2700	2700

E-mail: inquiry@rsnewrefractory.com / Tel +8616838759011

APPENDIX E

Procedure for Conducting Two-Way ANOVA with Replication Using Minitab 22

Step 1: Open Minitab and Prepare Data:

Load the dataset into Minitab worksheet, ensuring that the response variable and factor variables are in separate columns as in the table below.

C1	C2	C3	C4	C5	C6
Type of wax	0 wt.% SiC	1 wt.% SiC	2.5 wt.% SiC	5 wt.% SiC	7.5 wt.% SiC
B289 wax	21.3	14.4	10.8	9.25	7.85
B289 wax	20.05	14.65	10	9.65	9.6
B289 wax	20.15	15.2	9.95	8.7	8.95
L1203 wax	18.85	13.15	8.65	8.25	7
L1203 wax	18.45	13.6	9.6	8	6.85
L1203 wax	19.7	13.15	8.75	7.6	7.9

Step 2: Access the Two-Way ANOVA:

Go to "Stat" > "ANOVA" > "General Linear Model" > "Fit General Linear Model".

Step 3: Specify Response and Factors:

- In the "Responses" field, enter the name of your response variable (0 wt.% SiC, 1 wt.% SiC, 2.5 wt.% SiC, 5 wt.% SiC, 7.5 wt.% SiC)
- In the "Factors" field, enter the names of your factor variables (SiC, Wax).

Step 4: Model Selection:

- Click on the "Model" button.
- In the "Factors and Covariates" window, select the factor variables to include in the model.
- Note: By default, Minitab uses 95% confidence intervals, corresponding to a significance level of $\alpha = 0.05$. Therefore, statistical significance is determined based on p-values less than 0.05

Step 5: Run the Analysis:

Click "OK" in each dialogue box to run the two-way ANOVA.

Home > Strain gauge > High and low temperature strain gauge

High and low temperature strain gauge

CEF series High and low temperature strain gauge

CEF series high and low temperature strain gauges utilize polyimide resin for the backing and a special alloy for the element. They feature a wide range of operating temperature from －269 t

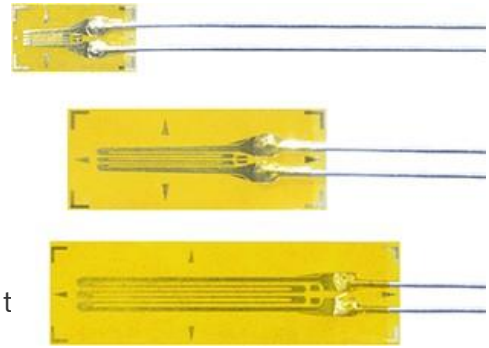

Applicable specimen	Metal, Ceramics
Operational temperature (℃)	-269 to +200°C
Temperature compensation range (℃)	-196 to +80°C
Applicable adhesive	C-1, EA-2A, CN
Backing	Polyimide

Element	Special alloy foil
Strain limit	1% (10000 x 10^{-6} strain)
Fatigue life at room temperature	1 x 10^{6} (±1500 x 10^{-6} strain)

– High and low temperature Use

Gauge pattern	Type	Gauge length (mm)	Gauge width (mm)	Backing length (mm)	Backing width (mm)	Resistance (Ω)
Single element (G.F. 2.1 approx.)  CEF-1-11	CEFLA-1-11 CEFLA-1-17 CEFLA-1-23	1	0.5	4	2.2	120
	CEFLA-3-11 CEFLA-3-17 CEFLA-3-23	3	0.6	6.9	2.8	120
	CEFLA-6-11 CEFLA-6-17 CEFLA-6-23	6	1.0	10.6	3.1	120

APPENDIX G

Table F1 Thermal conductivity test data & results

Silicon carbide contents (wt.% SiC)	0	1	2.5	5	7.5
Mass flow rate of cooling water ($\dot{m}$) [*Kg/s*]	0.017	0.017	0.017	0.017	0.017
Specific heat capacity of cooling water [*J/Kg K*]	4187	4187	4187	4187	4187
Sample thickness (dx) [m]	0.0073	0.0070	0.0074	0.0071	0.0066
Sample cross sectional area (A) [m^2]	0.00049	0.00049	0.00049	0.00049	0.00049
Inlet sample temperature (T_1) [˚C]	162.67	160.58	168.44	163.26	157.39
Outlet sample temperature (T_2) [˚C]	66.09	78.26	88.16	91.82	99.44
Inlet cooling water temperature (T_3) [˚C]	29.12	29.23	28.94	28.96	28.90
Outlet cooling water temperature (T_4) [˚C]	29.48	29.56	29.43	29.50	29.48
Heat transfer rate (q) [*J/s*]	25.624	23.489	34.877	38.436	41.283
Thermal conductivity of the sample	**3.955**	**4.076**	**6.560**	**7.795**	**9.595**

Example for thermal conductivity calculations of standard mould sample (0 wt.% SiC).

The calculation occurred in two steps. Initially, the heat gain q (J/s) by the cooling water was determined using Equation (A1).

$$q = \dot{m} c_p (T_4 - T_3) \quad \text{(F1)}$$

$$q = 0.017 \times 4187 \times (29.48 - 29.12) = 25.624 \text{ J/s}$$

Then the thermal conductivity was calculated using Equation (A2).

$$q = kA\frac{dT}{dx} \longrightarrow k = \frac{q\,dx}{A\,(T_1 - T_2)} \quad \text{(F2)}$$

Where; $A = \pi r^2$ is the sample cross-section area (m^2), r = 0.0125m, dx is the thickness of the sample (m).

$$k = \frac{25.642 \times 0.0073}{0.00049\ (162.67 - 66.09)} = 3.955 \text{ W/mK}$$

APPENDIX H

Table G1 Data of thermal expansion test for the ceramic mould shell

T (°C)	$\Delta L/L_0$ (10^{-4})	T (°C)	$\Delta L/L_0$ (10^{-4})	T (°C)	$\Delta L/L_0$ (10^{-4})
26.87982	0.054991996	211.163208	35.05545413	401.999786	75.64186245
31.804171	0.222084019	216.113388	36.1817390	406.89563	77.50948403
36.600601	0.265443238	221.040436	37.17582923	411.864075	78.78593921
41.414879	0.278391768	225.880157	38.04936064	416.912598	79.49449355
46.276558	0.29705056	237.405762	39.63779125	421.913452	80.19458809
51.065849	0.310838356	242.432495	40.18454149	426.897552	80.92112006
55.919121	0.332068011	247.417511	40.64986013	431.907288	81.70793303
60.730381	0.371197327	252.277313	41.10143104	436.897461	82.58463633
65.573227	0.455800814	257.337158	41.5297364	441.910248	83.52267756
70.373367	0.490700226	262.325226	41.92208541	446.918518	84.41630156
75.200745	0.542519253	267.249207	42.28270797	451.776978	85.11428006
79.976006	0.544634205	272.23645	42.59362538	456.751831	85.65151247
84.782417	0.472721511	277.246948	42.88021922	461.711487	86.03751554
89.638458	0.425132388	282.18631	43.14460553	466.682739	86.41188692
94.456215	0.414556546	287.019043	43.39418608	471.550781	86.7809693
99.308578	0.511850827	291.890076	43.70087359	476.540192	87.13313097
104.149208	0.756143464	296.687347	44.06678408	481.600677	87.4493363
108.902901	1.385382239	301.579163	44.50672221	486.626678	87.79198124
113.753281	2.728462193	306.51474	44.98473165	491.716797	88.11241647
118.603188	4.764233808	311.317535	45.56849517	496.697845	88.41804705
123.456673	7.271668917	316.223419	46.30348803	501.722656	88.70675584
128.269897	9.76535738	321.088531	47.11462457	506.723511	88.99652265
133.096024	11.99571647	326.000854	48.00296065	511.654755	89.26090895
137.957153	13.90035241	330.884918	48.86380126	516.680176	89.51366139
142.812988	15.50676174	335.859558	49.83885686	521.689636	89.81294711
147.671066	16.90694864	340.725891	50.94504705	526.727722	90.09848293
152.539032	18.2257061	345.736694	52.26380343	531.817932	90.3660422
157.363022	19.53705962	350.592255	53.69994777	536.886475	90.62831247
162.256836	20.83149351	355.600983	55.28309045	541.861633	90.85039649
167.111008	22.13121425	360.5336	56.9413188	546.847839	91.102092
171.993362	23.45208666	365.513184	58.74125867	551.788879	91.33898177
176.856888	24.83535287	370.471832	60.71569235	556.759216	91.5748146
181.759659	26.31591444	375.448303	62.85827607	561.79248	91.81064634
186.654617	27.84089216	380.337555	65.17746856	566.755981	92.00734986
191.561401	29.39653939	385.308197	67.60770414	571.869019	92.22731892
196.449738	30.924689	390.274445	70.01044317	576.79187	92.41873452
201.366669	32.4063075	395.265869	72.4639443	578.448792	92.48853226
206.196442	33.79803568	400.275848	74.92167534	581.845581	92.64293349

APPENDIX I

Table H1 Raw data of differential scanning calorimetry (DSC) for ceramic moulds between 30 to 300 °C

Temp (°C)	Power (mW)				
	SiC (wt.%)				
	0	1	2.5	5	7.5
30	-0.38227	-0.44884	-0.31046	-0.15211	-0.12546
40	-0.30682	-0.40616	-0.25572	-0.05342	0.00746
50	-0.23752	-0.3638	-0.15258	0.02755	0.10801
60	-0.1807	-0.19992	0.07321	0.19176	0.29444
70	-0.12257	-0.07343	0.23392	0.31707	0.44753
80	-0.07888	0.00322	0.32105	0.40062	0.54607
90	-0.04265	0.05901	0.38901	0.46934	0.62705
100	0.00293	0.10286	0.43604	0.52785	0.69489
110	0.02639	0.14842	0.47949	0.58339	0.75015
120	0.03692	0.18689	0.51994	0.63549	0.80952
130	0.07689	0.22677	0.57004	0.68618	0.86609
140	0.11563	0.26555	0.62549	0.73286	0.91158
150	0.15311	0.30747	0.65396	0.77348	0.96109
160	0.17383	0.34803	0.69248	0.81554	1.00461
170	0.19733	0.38623	0.73411	0.84634	1.02333
172.7	0.19923	0.39881	0.74560	0.85228	1.050
180	0.21777	0.42618	0.77304	0.86952	1.13191
190	0.24532	0.46519	0.80537	0.89762	1.14472
200	0.27002	0.49836	0.84206	0.92065	1.16791
210	0.29224	0.52826	0.87199	0.95069	1.17287
220	0.31355	0.54538	0.89877	0.97707	1.15211
230	0.34411	0.59737	0.93273	1.01204	1.19022
240	0.36415	0.63484	0.96859	1.05116	1.28061
250	0.38982	0.68318	1.00876	1.10222	1.40863
260	0.41566	0.73473	1.06229	1.21249	1.53281
270	0.44788	0.79781	1.14223	1.33706	1.70012
280	0.48541	0.86196	1.20243	1.46366	1.83799
290	0.52006	0.93238	1.28224	1.59499	1.95859
300	0.57067	1.03029	1.36808	1.70662	2.08862

Table H2 Weight of tested samples

Sample mass (mg)	SiC (wt.%)				
	0	1	2.5	5	7.5
	5.200	6.573	5.581	5.089	5.440

Example for specific heat capacity calculations of modified mould sample (2.5 wt.%) SiC.

$$C_p = \frac{1}{m}\,\frac{(\delta Q/d\tau)}{(dT/d\tau)} \qquad \text{(H1)}$$

Where m is the mass of the sample (g), $(\delta Q/d\tau)$ is the heat flux given by the DSC (J/sec), and $(dT/d\tau)$ is the heating rate (10 °C/min).

at 100 °C: $C_p = \frac{1}{0.005581(g)}\,\frac{0.43604 \times 0.001\ (\frac{J}{sec})}{0.1667\ (°\frac{C}{sec})} = 0.4686$ J/g. °C

at 300 °C: $C_p = \frac{1}{0.005581(g)}\,\frac{1.36808 \times 0.001\ (\frac{J}{sec})}{0.1667\ (°\frac{C}{sec})} = 1.4705$ J/g. °C

Table H3 Specific heat capacity of 2.5 wt.% SiC moulds at different temperatures

Temp (°C)	Specific heat capacity (J/g. °C)				
	SiC (wt.%)				
	0	1	2.5	5	7.5
100	0.0304	0.0938	0.4686	0.6222	0.7662
150	0.1766	0.2806	0.7029	0.9117	1.0598
172.7	0.2298	0.3639	0.8014	1.0046	1.1578
200	0.3115	0.4548	0.9051	1.0852	1.2878
300	0.6583	0.9403	1.4705	2.0117	2.3032

APPENDIX J

Table I1 Wax melting analysis data in percentage versus microwave heating time for different SiC content (wt.%).

SiC (wt.%)	Pattern wax percentage (L1203 wax)	Microwave heating time (minutes)								
		0	**2.5**	**5**	**7.5**	**10**	**12.5**	**15**	**17.5**	**20**
0	Left (%)	0.0	0.0	0.0	9.0	25.0	56.0	78.0	93.0	100
	Remained (%)	0.0	100	100	91.0	75.0	44.0	22.0	7.0	0.0
1	Left (%)	0.0	0.0	7.0	37.5	62.0	88.0	100	100	100
	Remained (%)	0.0	100	93.0	62.5	38.0	12.0	0.0	0.0	0.0
2.5	Left (%)	0.0	0.0	25.0	81.0	100	100	100	100	100
	Remained (%)	0.0	100	75.0	19.0	0.0	0.0	0.0	0.0	0.0
5	Left (%)	0.0	5.0	43.0	94.0	100	100	100	100	100
	Remained (%)	0.0	95.0	57.0	6.0	0.0	0.0	0.0	0.0	0.0
7.5	Left (%)	0.0	12.0	68.5	100	100	100	100	100	100
	Remained (%)	0.0	88.0	31.5	0.0	0.0	0.0	0.0	0.0	0.0

APPENDIX K

Table J1 Comparison of energy required for the dewaxing process

Furnace dewaxing	Microwave dewaxing
Energy required to raise mould temperature (Q_r) [J/m^3]	
Standard mould (0 wt.% SiC) $Q_r = \rho_r c_{Pr}(T_\mathrm{i} - T_a)$ ρ_r=2683.2 kg/m^3 (from Table 4.4) c_{Pr}= 658.3 J/kg.K (from Appendix I) T_i=300 ˚C, T_a= 29 ˚C Q_r= 4.78 ×10^8 J/m^3	Modified mould (7.5 wt.% SiC) $Q_r = \rho_r c_{Pr}(T_\mathrm{i} - T_a)$ ρ_r=2728.1 kg/m^3 (from Table 4.4) c_{Pr}= 1157.8 J/kg.K (from Appendix I) T_i=172.7 ˚C, T_a= 29 ˚C Q_r= 4.53 ×10^8 J/m^3
Energy required to melt the wax (Q_w) [J/m^3]	
$Q_w = \rho_w c_{Pw}(T_\mathrm{m} - T_a) + Q_{LH}$ $Q_{LH} = \rho_w L_{Hw}$ For SIVUCH L1203 wax ρ_{wax}= 931 kg/m^3 (from Appendix B) $c_{P(wax)}$=1846 J/kg.K (by Calorimeter) L_{Hw}= 200 ×10^3 J/kg T_m=70 ˚C, T_a= 29 ˚C Q_w= 2.56 ×10^8 J/m^3	$Q_w = \rho_w c_{Pw}(T_\mathrm{m} - T_a) + Q_{LH}$ $Q_{LH} = \rho_w L_{Hw}$ SIVUCH L1203 wax ρ_{wax}= 931 kg/m^3, $c_{P(wax)}$=1846 J/kg.K L_{Hw}= 200 ×10^3 J/kg T_m=70 ˚C, T_a= 29 ˚C Q_w= 2.56 ×10^8 J/m^3
Energy supplied to the furnace interior (Q_i) [J/m^3]	
$Q_i = \frac{P_i\ t}{V_f}$ $P_i = \sqrt{3}\ \times V \times I$ [W] V = 415 Voltage I= 100 A t= 45min × 60 = 2700 sec $V_{furnace}$= 1.914 m^3 Q_i= 1.02 ×10^9 J/m^3	$Q_i = \frac{P_M\ \eta_M}{V_M}$ $\dot{q}_M = \frac{Q_r V_{mould}}{t}$ [J/sec] $\eta_M = \frac{\dot{q}_M}{P_M}$ V_{mould}= 0.000184m^3 P_M= 600 W t= 7.25min × 60 = 435 sec V_M= 0.0325 m^3 Q_i= 5.91 ×10^3 J/m^3

<table>
<tr><td colspan="2">Energy loss from the heat system walls (Q_{L1}) [J/m^3]</td></tr>
<tr><td>$Q_{L1} = K(T_i - T_a)\left(\frac{A}{L}\right)t$
Q_{L1}= 1.07 ×10^9 J/m^3*</td><td>Not applicable</td></tr>
<tr><td colspan="2">Energy loss from mould by convection (Q_{L2}) [J/m^3]</td></tr>
<tr><td>Not applicable</td><td>$Q_{L2} = h_{air}A_m(T_i - T_a)t$
A_m= 0.0173m^2
To evaluate h_{air} for loss in a vertical cylinder as the mould was placed in the furnace;
Grasshof No: $G_{r_L} = \frac{\beta\ g\ \Delta T\ L^3}{\nu^2}$
Reynolds No: $R_{a_L} = G_{r_L}.P_r$
Nusselt No: $N_{a_L} = \frac{hL}{K} = 0.148R_{a_L}^{0.333}$
Prandtl No: $P_r = \frac{C_P\,\nu}{K}$
T_i=172.7 ˚C, T_a= 29 ˚C
Film temperature $T_f = \frac{T_i + T_a}{2}$ = 374 K
For air and at 374 from properties of air table : (ρ_{air}= 1.036 kg/m^3, ν_{air}=2.04×10^{-5}Pa.s , K_{air}= 0.029W/m.K, C_P = 1003J/kg.K)
From that:
P_r= 0.706, G_{r_L}= 1.3 × 10^7,
R_{a_L}= 9.18 ×10^6, N_{a_L}= 30.824,
h= 8.126 W/m^2.K
Q_{L2}= 8.13 ×10^3 J/m^3</td></tr>
</table>

*(Yahaya, 2016)

LIST OF PUBLICATIONS

Ahmed Omar Aswaye Amhamed, Izman Sudin, Wan Fahmin Faiz Wan Ali, Najlaa Nazihah Mas'ood, Najib Meftah Almukhtar Omar. (2024). Role of silicon carbide in enhancing microwave hybrid heating and reducing dewaxing time in investment casting. Journal of Materials Today Communications, Vol. 39 (2024): 108842. https://doi.org/10.1016/j.mtcomm.2024.108842 (Q2, IF: 3.7)

Ahmed Omar Aswaye Amhamed, Wan Fahmin Faiz Wan Ali, Izman Sudin, Najlaa Nazihah Binti Mas'ood, Najib Meftah Almukhtar Omar, Mohd Azlan bin Suhaimi. (2024). Evaluating thermal and dielectric properties of wax patterns and their effects on ceramic mould during the microwave dewaxing process. Journal of Materials and Engineering, Vol. 03, Iss. 3 (2025) 301-313. DOI:10.61552/JME.2025.03.005. (ICI, COBISS, SJIF, ASCI Indexed)

Ahmed Omar, Wan Fahmin Faiz, Najla Nazihah, Izman Sudin. (2024). Understanding the role of susceptors in hybrid heating and the properties of waxes for enhanced dewaxing in investment casting. The Engineer Story, UTM. Vol. 12 (2024) 17-21: https://theengineerstory.com/resources/paper/vol-12/TES-12-17-21.pdf

Najib Meftah Almukhtar Omar, Mohd Hafiz Dzarfan Othman, Zhong Sheng Tai, **Ahmed Omar Aswaye Amhamed**, Mohamad Fairus Rabuni, Mohd Hafiz Puteh, Juhana Jaafar, Mukhlis A. Rahman, Tonni Agustiono Kurniawan. (2024). Overcoming challenges in water purification by nanocomposite ceramic membranes: A review of limitations and technical solutions. Journal of Water Process Engineering. Vol. 57 (2024): 104613. https://doi.org/10.1016/j.jwpe.2023.104613 (Q1, IF: 7.340)